UNIVERSITY OF SOUTHAMPTON

Characterising the flash flood potential in the arid Red Sea coast region of Egypt

Eman Mohamed Ghoneim

A thesis submitted for the degree of Doctor of Pholosophy

Department of Geography
Faculty of Science

June 2002

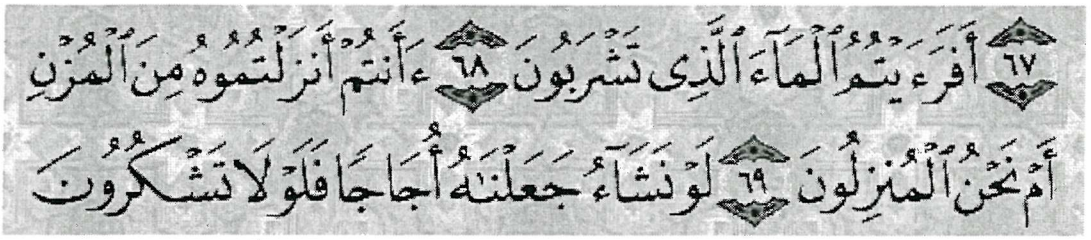

The above are three verses from the Noble Qur'an and could be interpreted as follows:

In the name of Allah

"Then tell Me about the water you drink. Is it you who cause it from the rain-clouds to come down, or We the Causer of it to come down? If We willed, We verily, could make it very salty (and undrinkable): why then do you not give thanks (to Allah)."

UNIVERSITY OF SOUTHAMPTON

ABSTRACT

FACULTY OF SCIENCE
GEOGRAPHY
Doctor of Philosophy

CHARACTERISING THE FLASH FLOOD POTENTIAL IN THE ARID RED SEA COAST REGION OF EGYPT

by Eman Mohamed Ghoneim

This study presents an integrated approach to estimating the risk of flash floods in arid wadis. Flash floods impact seriously on the infrastructures and development of Egyptian desert towns, such as Marsa Alam, and their surrounding areas. The study developed a method using the example of the wadi El-Alam, which has an area of approximately 407 km^2. The method has three stages. First, the construction of a Digital Elevation Model from which morphometric properties of the basin were calculated. In particular, representing the flat areas and the sharp junctions between badland slopes and the adjacent wadi system (which generally characterised arid landscapes), were among the major issues facing this study. Second, the derivation of land cover from satellite remote sensing data which were rigorously pre-processed with the aid of aerial photographs and fieldwork measurements. Third, the application of a hydrological model, incorporating the basin morphometry and land cover data, to transform rainfall into runoff and route the floodwater through the sub-catchments of the wadi.

The hydrological model system (HMS) was run to simulate discharge at the main wadi outlet (where the town of Marsa Alam is located) and at each sub-basin intersecting the Idfu-Alam highway that runs through the wadi. From these results, sites vulnerable to flash flood and their risk classes were identified. The sites judged to have the highest flood hazard along the highway were exactly the sites damaged in the 1991 flash flood. Thus, as an outcome of this study, the first digital database that includes information on land cover, geomorphology and hydrology of wadi El-Alam was developed. This database can be used to highlight regions vulnerable to flood damage.

To my great Mum and Dad,
To my beloved husband Essam,
To my sweet daughters Salma and Didi.

ACKNOWLEDGEMENT

Before all and above all thanks to Almighty Allah for giving me the strength, and making this possible. Although, the degree of PhD is awarded to only one person, it is the result of the efforts of many people who support, encourage and help in many different ways. I would like to thank everyone who helped me during my research over the last few years. First, I wish to express my special thanks to my supervisor Professor Nigel Arnell, for being a shoulder to lean on and encouraging me to believe in my ideas, additionally, his valuable contribution to my scientific research view and understanding, which will always guide me in my future academic life. I also extend my grateful thanks to my co-supervisor Professor Giles Foody for his indispensable advises and pushing me forward during my research project and sparing no effort to make the remote sensing enjoyable science. I would also like to thank Professor Mike Clark and Dr. Ted Milton for their very useful advises at the beginning of this research. Huge thanks go to Essam (my husband) who sacrificed a considerable amount of time for helping and supporting me. Next, I wish to acknowledge the Egyptian Government for the generous financial support, which made this study possible.

Thanks as well go to Professor Abd El-Salam and my friend Zenab (Tanta Univ.) for their help during my fieldwork in Egypt. My gratitude go also to Professor Ashmawy (Tanta Univ., Egypt) for his advice regarding the most suitable and available map sheets for the study area and its sheet numbers. Thanks also go to my professors, colleagues and friends in the Geography department, Tanta University for their emotional support. Many thanks to the Geography postgraduate community at Southampton University and to all my friends including, Sally, Tatiana, Islam, Nick, Sarah, Matt, Reno, Mohammed, Michael, Richard, Garry, Marie, Sally, Valeria, Iles and all others who, with their friendship, mad life fun and fruitful in Southampton. My gratitude goes also to Southampton University Cartographic Unit's members of staff for being helpful and friendly. Finally, a very special thanks to my Mum and Dad for everything they have done for me.

CONTENTS

LIST OF FIGURES

LIST OF TABLES

CHAPTER 1

Introduction and study area

1.1 INTRODUCTION

Flash floods are a world-wide problem, from the tropics to the sub-polar regions. Virtually by definition, a flash flood is a hydro-meteorological event: an event that depends on both hydrological and meteorological factors. Flash floods are distinguished from "ordinary" floods by the time scale of the event. Whereas floods may occur over periods of several days and it maybe possible to attempt damage mitigation (like sandbagging), flash floods occur much too rapidly for such preparations. The worst of the event can develop in periods of hours or less, which makes flash floods particularly dangerous in terms of human casualties. In arid regions flooding represents a major hazard to human life and well being as well as to the infrastructure of the societies dwelling in such regions. Drylands experience occasional very heavy short-duration rainfall. These storms create flash floods which run rapidly along the network of wadis (Arabian term for dry river channels cut into the terrain) draining the mountains, frequently causing severe flooding, which cause damage to desert towns, linear structure and property. Desert wadis regularly continue to take human life despite the fact that they are non-functional for most of the time.

Whilst flash flooding has been recognised as an environmental hazard throughout most of this century, many aspects of the processes leading to it and controlling its attributes remain uncertain or, at least, less than adequately documented. The reasons for this lack of scientific understanding stem from the fact that a typical desert flood is usually very short-lived. Also, the probability of an adequately equipped scientific team being able to document a complete desert flood on-site is very small, given the complex logistics typical of working in the world's deserts (Schick *et al.,* 1997). The wadi forms an inconvenient environment for instrumentation especially at sites with high relief.

It is, however, important to emphasise that the destructive power of a flash flood is not related completely to the strength and the velocity of the flood-water but it is also related to the human mistakes: many of the towns and road network have been built at the outlets of the desert wadis or located inside the wadis itself. The rarity of flood events in such areas and the long dry periods between rainfall events are probably the reasons why many engineers do not take the desert floods risk sufficiently seriously.

Since flash flood phenomena are considered among the biggest natural disasters that threaten and maybe hamper the development in arid areas, there is a need to gain a quantitative understanding of this phenomenon and more comprehensive study urgently needed to be achieved. This is one of the primary motivations of the current study, which uses the Wadi El-Alam, one of the Egyptian eastern desert basins, to develop and test a method for estimating flash flood risk in arid environments.

Wadi El-Alam is characterized by its rugged terrain nature and its occasional experience of heavy short duration rainstorms. The Eastern desert is becoming one of the most popular places in Egypt for tourism, and several international cities have been built in the region for this purpose along the Red Sea coast, such as Hurgada and many cities are now prepared to enter the field of tourism. Marsa Alam is one of these small cities (towns) which is catastrophically located at the main outlet of Wadi El-Alam. This town has its own airport (Alam Airport) to facilitate transportation to and from it. Tourism activities are mainly dependent upon diving in the Red Sea, which is characterised by its unique coral reefs as well as the safari tour in the background attractive mountain zone. Unfortunately, the town of Marsa El-Alam has been hit strongly twice, in 1991 and 1994, by flash floods which ruined the town and its serving highway network that runs across the Wadi El-Alam itself. Moreover, in the winter of 1996 the town was hit by a moderate flood that damaged part of the coastal highway at the Wadi El-Alam outlet (oral communication with local members of Marsa Alam towns). The Figures 1.1, 1.2 and 1.3, display some photos for this flooding event acquired by one of the local resident in 1996.

Figure 1.1 The Flash flood of 1996 at the outlet of Wadi El-Alam (Photos were acquired after a few hours from the main flood event of 1996).

Although Wadi El-Alam may stay dry for many years, sudden rainstorms cause severe flash flooding which as the town of Marsa Alam continues to grow will only get worse especially as the flood-vulnerable sites are unknown. As the risk of significant flooding increases, concerns about flood damage within the town and its associated linear structure rise. Therefore, it was vital to embark on the current study to understand the rainfall-runoff aspects of the terrain. The ability to predict the velocity and magnitude of the flood peaks as they move through the town is extremely valuable. Information about flash flood peak discharge and the time to peak are needed, e.g. to correctly design various hydraulic structures such as spillway, dams lévées and culverts to alleviate the effects of the flood during its occurrence. Hydrological and historical flow data are necessary to conduct flood frequency analysis. This type of analysis enables the prediction of flow rates with certain returned periods. In cases where the historical flow records and flow data are not available, as is the case in the current study, it has become necessary to resort, as an alternative, to hydrologic modelling. A literature survey, found that research projects concerned with the flooding phenomena in the Egyptian Red Sea coastal area in general and in particular in Wadi El-Alam, are very scarce and limited in their scope. If any, they tackle the subject qualitatively from just the geomorphological point of view (such as El-Etr and Ashmawy, 1993; NARSS, 1997), without paying any attention to the hydrologic and climatic factors that mostly drive the floods in such arid regions. Besides, virtually none of the catchments in this area are provided with rainfall or runoff measuring gauges.

Paradoxically, if the gauging stations are there, the strength of the floods, in general in such arid region, are so intense that the measurements would be inaccurate. In short, one has to start building a digital database for the region from scratch.

Figure 1.2 Dead vegetation carried by the flash flood of 1996, indicates how high the level of the floodwater was.

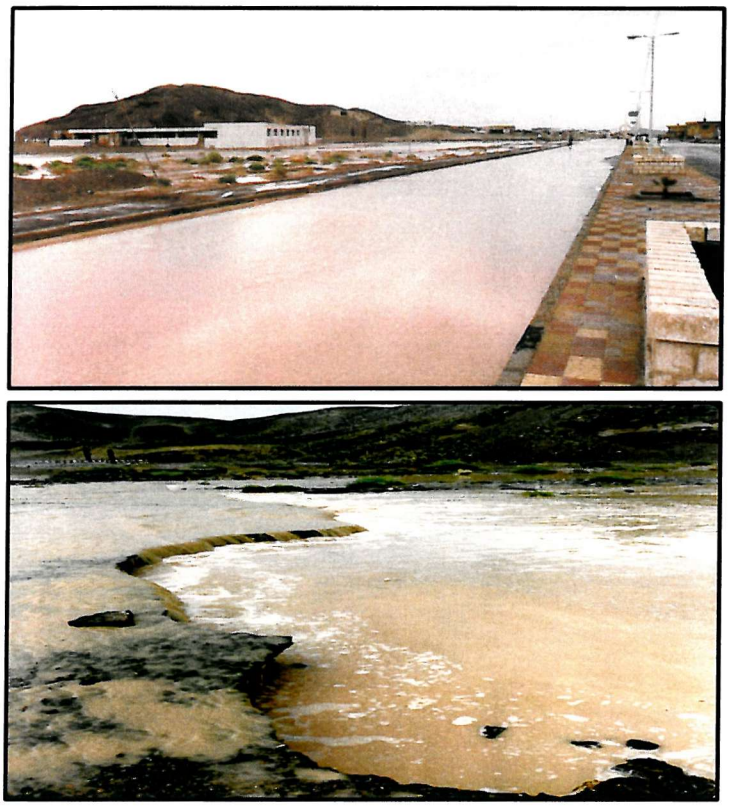

Figure 1.3 Damage of part of the coastal highway by the1996 flood event.

1.2 THESIS AIM

The ultimate aim of this research is to develop and test a method for estimating flash flood risk in the arid watershed of Wadi El-Alam. The research pursued in this thesis was conducted in order to meet this aim, with four specific objectives:

- To construct a digital database for Wadi El-Alam using the GIS methods to derive the geometric parameters that are assumed to affect flash flood generation.
- To derive a land cover and soil property map for the basin under study from Landsat TM images.
- To apply and test a hydrological model.
- To run this hydrological model to identify locations at risk of flooding in Wadi El-Alam basin.

1.3 THESIS STRUCTURE

The research presented in this thesis provides a realistic view of the applicability of integrating GIS analysis and display capabilities with hydrologic modelling tools for basin delineation, visualization and risk assessment. This thesis contains 8 chapters (Figure 1.4). The next section of this chapter provides an introduction and description of the physical environment of the study area. Flash flood key dimensions and factors affecting their generation in arid areas are addressed in Chapter 2. Chapter 3 outlines the procedures followed for the construction of the Digital Elevation Model (DEM) of the study basin and the delineation of its sub-catchments along with the drainage network. It also discuses the technical obstacles and their solutions. In Chapter 4, the geomorphometric parameters of the concerned basin that are related to the flood risk are extracted from the derived DEM and then used to estimate merely the main parameters characteristics of the response of the basin to rainfall events (hydrograph). By making use of remote sensing techniques, the land cover/use of the basin has been derived from a TM digital image for the basin and the key features of each cover have been addressed in Chapter 5. The DEM and land cover/use of the basin constitute the main input parameters that are needed for running the Hydrological Modelling System (HMS) modeler to better

estimate the basin response to rainfall event. The underlying principles of this model and the resulting basin hydrograph are described in Chapter 6. In Chapter 7, the flood vulnerable sites within the basin and along the highway that runs through it have been located. Finally, the main findings of this research are summarized in Chapter 8 with recommendation for further study.

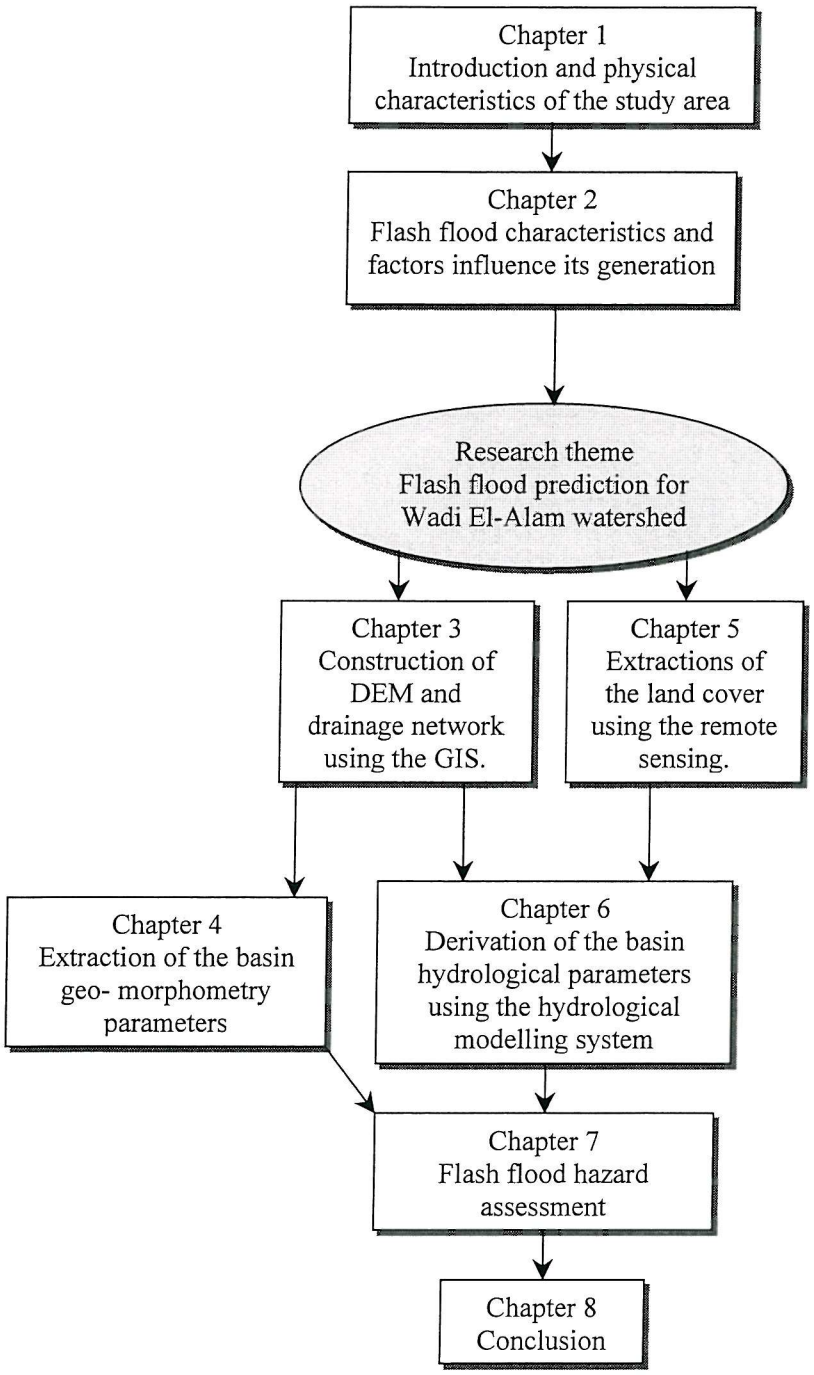

Figure 1.4 Schematic representation of the structure of the thesis.

1.4 STUDY AREA

As a prerequisite to the following chapters 4-7, a preliminary overview of the study area, from the physiographic, climatic and geologic points of view, will be provided in this section.

1.4.1 Location and Physiography

El-Alam basin spans approximately 407 square kilometers, between longitudes 34° 33′ - 34° 53′ and latitudes 24° 50′ - 25° 04′. Figure 1.5 shows a general location map of the study area, which is a part of the Red Sea high mountain region.

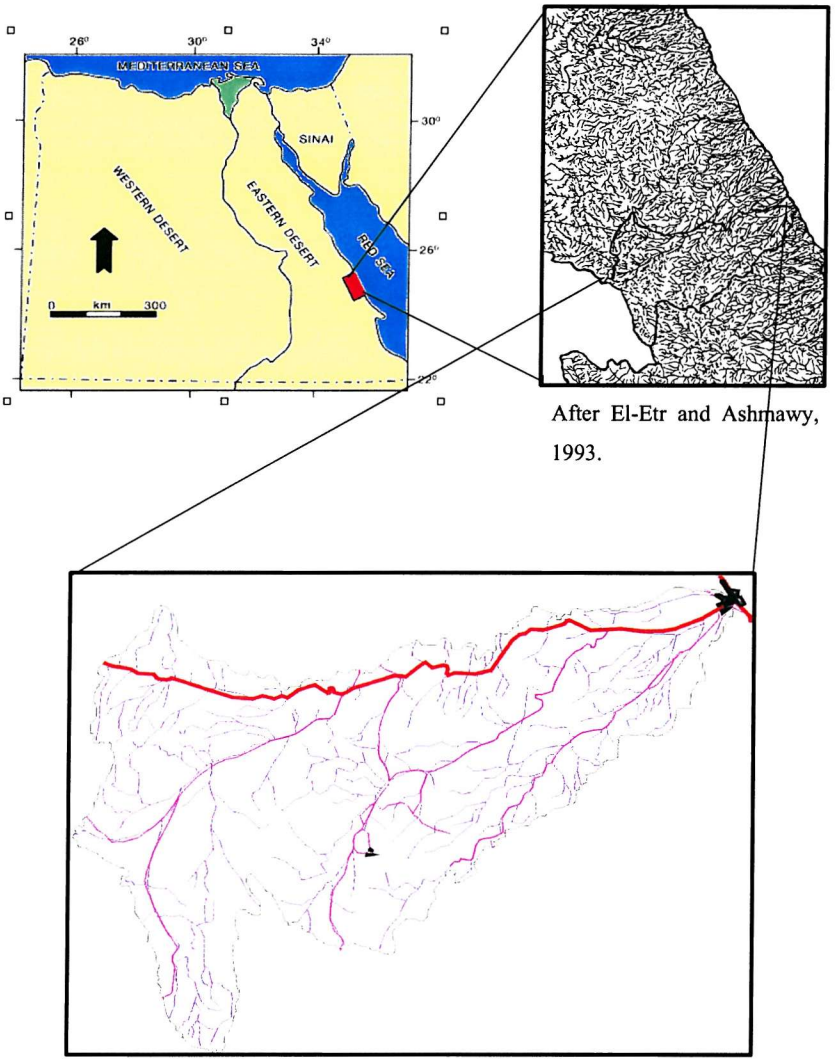

Figure 1.5 Location map of the study area.

The study area comprises essentially the backbone of high and rugged mountains built up of a series of mountainous ranges, more or less coherently trending parallel to the Red Sea coast with maximum elevations of about 1200 m above sea level. These mountains are dissected by many wadis running from west to east toward the Red Sea. The channels of these wadis are very steep and narrow - with V shape – upper stream area (Figure 1.6), while they are of gentle slope, wide and flat in the downstream area (Figure 1.7).

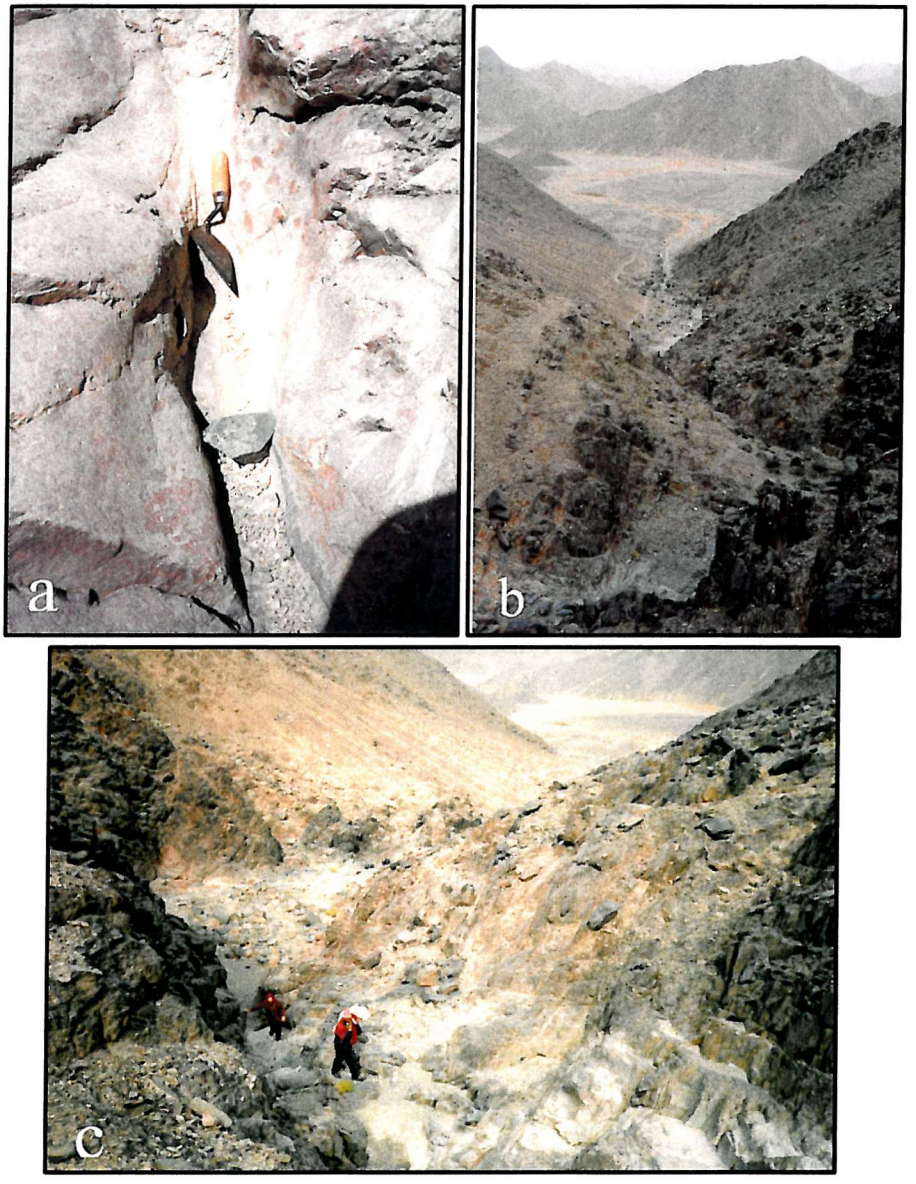

Figure 1.6 Wadi El-Alam channels Upper-stream area. (a) Shows a small rill that represents the head of the channel eroded on a basement rock, (b and c) Show the narrow wadi of V shape (photos were acquired during the fieldwork of this research).

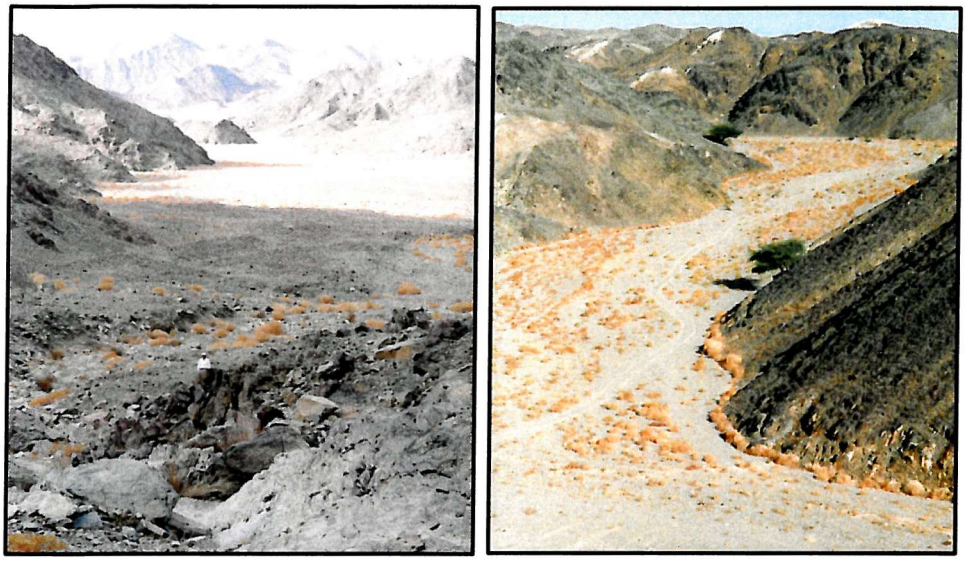

Figure 1.7 Shows the wide, flat and gentle slope of Wadi El-Alam channels.

The water divide line, which runs over the high peaks of these mountains, separates the short steeply-sloping basins draining towards the Red Sea and those long and wide basins that drain towards the Nile valley. The study basin is extremely poor in fresh water resources. It is supplied by water from the Nile River through a pipeline. Recently Marsa Alam town has been supplied by a desalination water station.

1.4.2 Climate

The area under study lies in the middle part of the Egyptian Eastern desert region. The location of the area influences its climatic characteristics, where the Red Sea mountains in the west of the area affect and increase the amount of rainfall. Wadi El-Alam is located between two meteorological stations, the El-Quseir station in the north and Ras-Benas station in the south along the Red Sea coast. These stations are about 70 km distant (north and south) from the basin, which is internally void of any meteorological stations. The temperature and rainfall data acquired from these two meteorological stations over a period of 30 years from 1968 up to 1998 (The Egyptian Meteorological Authority) are represented pictorially in Figure 1.8 and 1.9 respectively.

The extremely arid climate of the region of the Wadi El-Alam is reflected in high temperatures and meagre rainfall events. The hottest period starts from May to the

end of September, where the temperature ranges from 30° to 40° in daytime and from 20° to 25° in night-time. The average minimum temperature during the coldest months of January and February ranges between 12° and 14° while the average maximum temperature during the hottest months of July and August ranges between 32.9° and 38.6° in El-Qusier and Ras-Benas respectively (Figure 1.8).

The long-term mean annual rainfall of about 5-10 mm (RIGW, 1988) is highly variable. Years with just a few millimetres are not infrequent, as are years with more than double the mean annual amount. The rainfall is not uniformly distributed and it may precipitate the whole amount in one day or in just a few hours and the area may stay dry for many years (Figure 1.9). The rain events mainly occur in autumn and mostly originate in local convective cells associated with an incursion of the Red Sea trough (Abu-Hassen, 1994). In contrast, the winter rains, which are less frequent, originated from Mediterranean depressions.

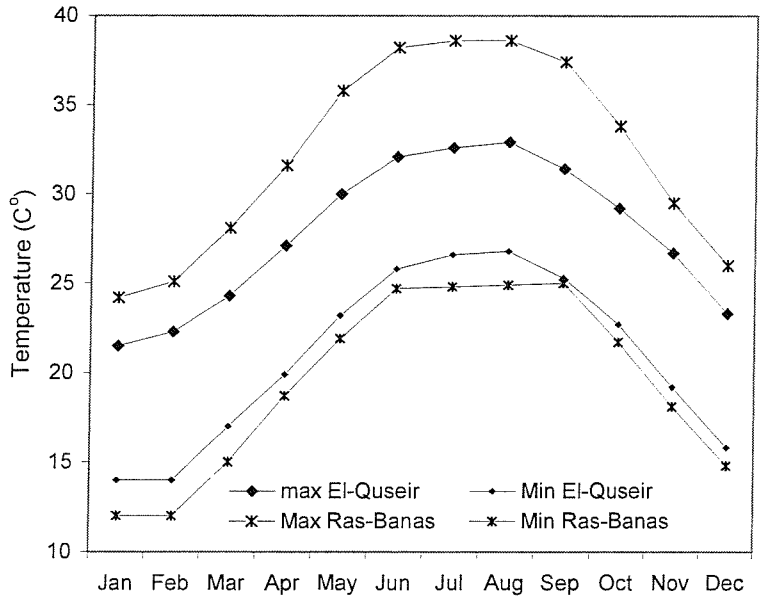

Figure 1.8 Maximum and minimum temperature of El Quseir and Ras Benas (adapted from Atia, 1999).

1.4.3 Geology

The intense tectonic processes at the coastline of the Red Sea trough have resulted in steep terrain of magmatic and metamorphic rocks. The basement rocks cover most of the study area, while the sedimentary rocks cover only a small part of the coastline (Figure 1.10). The basement rocks include metavolcanic rocks

(intermediate and acidic), which are the dominant rock type in the study basin (NARSS, 1997), the metasediments, serpentines, granite and metagabbro-diorite. The sedimentary rocks include three sequences, the Miocene, the Pliocene and the Pleistocene. Lithologically, most of their formations are made of coarse-grained sandstone with occasional limestone and marls. The sandstone is mainly arkosic and calcareous. It is formed of sub-angular quartz and feldspar grains (Atia, 1999).

The floor of Wadi El-Alam is covered with thick debris derived from the weathering of adjacent Red Sea Mountains. In the upper-stream area of the Wadi, the rills and the small tributaries are covered almost entirely with blocks and big boulders. At the mouths of these tributaries the boulders give place to gravel and sands. The flat floors of the lower reaches of these wadis are mostly covered by mixture of gravel, sand and relatively rich in fine sand and silt. Along the coastline there are the recent raised beaches and coral reefs. They form three levels (3, 7, 12 metres) above the mean tide Red Sea level and they are present at Marsa Alam town area. They are composed mainly of sand and gravel and are strewn with plenty of shells, which are still living in the modern Red Sea (El-Etr and Ashmawy, 1993, Atia, 1999).

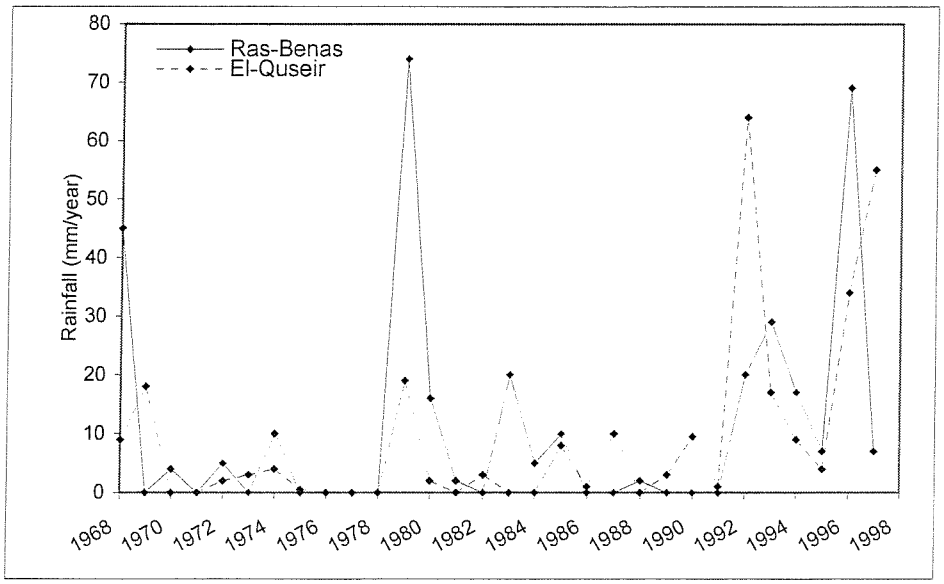

Figure 1.9 Rainfall mm in Ras Benas Station and El-Quseir (1968-1997), Mohamed M. Eissa, Egyptian Meteorological Authority (personal communication).

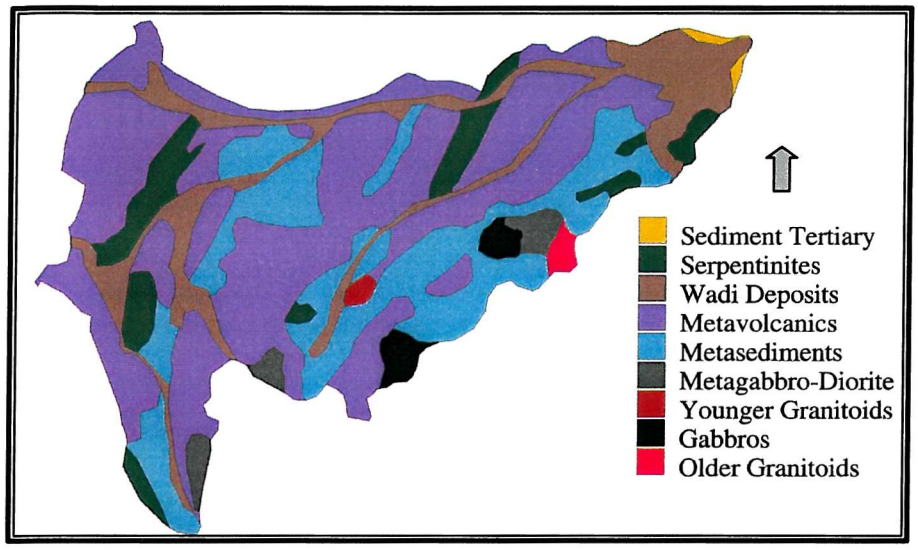

Figure 1.10 Geological map of Wadi El-Alam Basin (adapted from El-Etr and Ashmawy, 1993).

CHAPTER 2

Flash flood generation

2.1 FLOOD GENERATION IN ARID REGIONS

Perhaps the most remarkable feature of the arid region is the high rainfall intensity of the storm events. During these events Hortonian overland flow accumulates on the ground surface, concentrates quickly and induces episodic floods in wadi channels (Pilgrim *et al.,* 1988). While, especially in large desert wadis, a huge amount of floodwater is lost by transmission losses into dry channel beds, direct runoff contributions from underground storage are negligible (Lange and Schick, 2000).

This chapter specifically deals with the climatic, hydrologic, geomorphological factors that influence the flooding phenomenon, in particular, in the arid regions with emphasis on the role played by each of them in making the flooding phenomenon significant.

2.1.1 Key dimensions of floods in arid areas

The most distinguishing features of the flash floods are their variability in space and time, the rapid rise and fall of its hydrographs, which mainly happens due to the high rainfall intensity and negligible interception capacities. They are also characterised by runoff of high velocity, with large amount of sediment load.

Desert storms are characterised by their high variability in space and time. Precipitation is spatially very varied and only partial areas of large catchments will contribute to a given runoff. This can be observed from the flood frequency curve of arid and semi-arid lands. The high slopes of these curves are related to the large variation from event to event due to variation in rainfall amount and location. Arnell (2002) noted that the flood frequency curves of dry lands are generally much

steeper than those in temperate regions, because storm rainfall totals are much more variable (Figure 2.1).

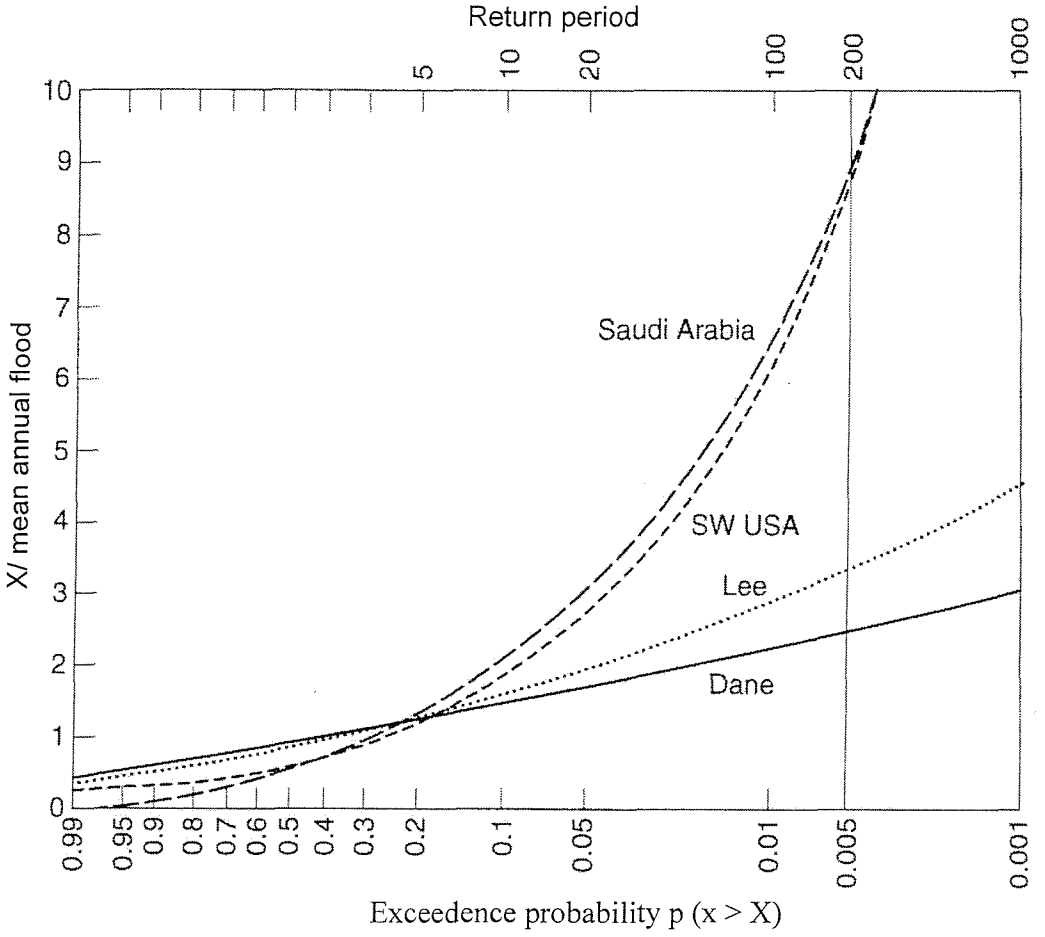

Figure 2.1 Flood frequency curves: the Lee and Dane are in south-east and north-west England, respectively (Arnell, 2002).

Greenbaum *et al.*, (1998) recorded a noticeable difference between stations spaced only 150 m apart. Most rainfall in drylands generally occurs as a result of the passage of low pressure or from small convective cells producing intense storms of short duration. These intense storms are characterised by rainfall of high intensity of normally 1 mm min^{-1} (Cooks *et al.*, 1982), an abrupt fall in temperature and gales with hail of different sizes (Abu-Hassan, 1994; Greenbaum *et al.*, 1998).

Within a very short time (normally few minutes) flow over an initially dry bed rises to depths of several tens of centimetres (Schick, 1971, 1988). Laronne *et al.*, (1994a) recorded a series of increases in river depth to a maximum depth of 2.5 m.

These increases in flow depth were accompanied by the appearance of floating vegetation and other organic debris suggesting inputs from individual tributaries. Hjalmarson (1984) reported that according to the Arizona Daily Star " the water rose faster than the youths could react, two feet in 15 seconds, four feet in less than a minute, and still it comes". Hassan (1990) reported that in the flood of 6 January 1987 in the Judaean desert, water depth changed so rapidly- from zero to 32 cm over a distance of only 3.5 m. Laronne *et al.,* (1994) recorded a very quick flow rise, which reached a depth of 90 cm in less than 3 minutes.

The flooding processes involved are markedly different from those operating in humid environments. Time to peak tends to be very short; specific peak discharge of the high magnitude events is very high; and the supercritical flow provides high values of stream power that manifest themselves in pulsating flows (Graf, 1988). The flow in most arid regions is characterised by a typical hydrograph form with an instantaneous rise sharp peak and steep initial recession limb (Cooke *et al.*, 1982), Figure 2.2. The steep rising limb indicates a short time to peak often in the form of bores advancing on a dry bed (El-Hames and Richards, 1998). The rising limb of the hydrograph is ranges from 2 to 58 minutes with a median time of rise of 10 minutes (Reid *et al.,* 1998). The very sharp peak results from the high and dissected relief and the dense of the network in both first and second channel orders besides the high rainfall intensity, which characterises most of the arid areas. With respect to the peak discharge of flood in arid areas it normally does not last for a long time. Schick *et al.* (1987) reported a peak discharge of 1.07 $m^3 s^{-1}$ that lasted for only 8 minutes in Nahal Yael watershed. Similar to the quick peak, there is also a quick or near-immediate abrupt recession for the flood hydrograph of the arid lands. Laronne *et al.,* (1994) illustrated that the flood receded almost as quickly as it had come. After reaching a depth of 2.5 m, within just 48 hours the wadi bed was once again completely dry. The quick recession can be ascribed to the transmission loss factor, as much of the flood water is normally absorbed in the thick alluvial fill that exist along the beds of most of the high channel orders and at the arid basin's outlets (alluvial fans). The transmission loss has a significant effect, as it steepens the flood-wave front (Thorne, 1976), decreases the flood rise time (Cooke *et al.*, 1982) and decreases flow downstream. It also helps in merging successive small

peaks, increases relative sediment load and decreases stream width as bankfull discharge in drylands is normally unusual (Renard, 1970).

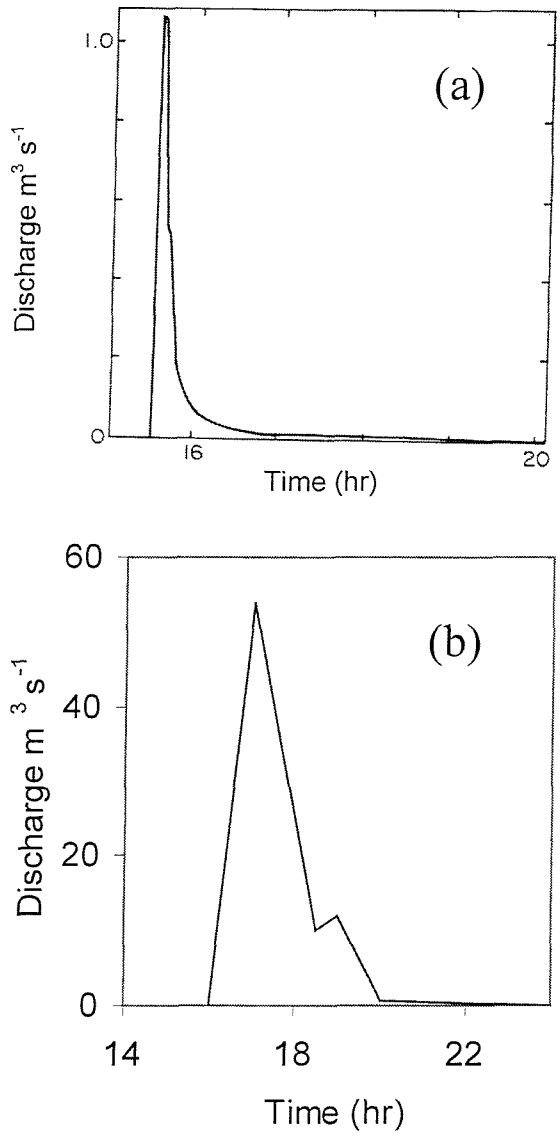

Figure 2.2 Typical arid region hydrographs, (a) Negev desert (Schick *et al.*, 1987), (b) Saudia Arabia (Abdulrazzaq *et al.*, 1989).

One of the most important characteristics of arid floods is the high values of water surface slope of the flood bore, which is as a result of frictional retardation by the rough bed of desert wadis. Leopold and Miller (1956) found that, in Canada Ancha Arroyo, the mean velocity of the flow exceeded 1.5 m s^{-1} within five minutes of

bore arrival. Reid *et al.,* (1998) reported a bore velocity of 2 m s^{-1} in Eshtemoa Wadi (West Bank, Palestine). They related this comparatively slow nature of a bore's advance in large part to the high flow resistance that arises from the roughness of the gravel bed.

Hassan (1990) recorded an average flow velocity of 1.0 m s^{-1} in the flash flood of 1987 (Israel), but he showed that this velocity is related to both the channel geometry and the wadi bed condition (whether the bed was wet or dry). Reid *et al.,* (1998) reported a flow velocity of 2 m s^{-1} while it exceeds in some cases 3 m s^{-1} (Allam and Balkhair, 1987) as shown in Table 2.1. Field measurements revealed that the advance rate of the flood bore is much less than the velocity of the flow that prevails within a minute or so of its passage (Reid *et al.,* 1998). The arrival of the flood bore is heralded by the sound of rushing water. In gravel bed wadis such as the Eshtemoa, the sound of gravel clasts being thrown against each other is distinctly audible from 100 m (Reid *et al.,* 1998). Laronne *et al.,* (1994B) reported a strong noise with the bore arrival and related this noise to the particle movement over the wadi bed. It also may be as a result of friction between the floodwater and the bed (Hassan, 1990).

Table 2.1 Some climatological and hydrological characteristics of wadi flash floods in Saudi Arabia (Allam and Balkhair, 1987).

Wadi	Date of event	Rainfall depth (mm)	Runoff depth (mm)	Peak discharge ($m^3 s^{-1}$)	Peak velocity ($m^3 s^{-1}$)
Jawf	04/05/85	40.00	1.70	100	2.10
	04/23/85	34.00	1.67	93	2.00
	05/17/85	14.40	0.73	41	0.90
	05/22/85	27.00	0.67	83	1.80
Khat	05/12/84	25.50	1.58	205	3.00
	05/21/84	16.75	1.05	177	2.70
	08/19/84	14.50	1.67	133	2.30
	11/17/84	7.00	0.81	80	1.52
	04/05/85	34.45	4.05	290	3.10
	04/11/85	11.50	1.12	100	1.70
	04/22/85	14.00	0.69	75	1.50
	09/21/85	9.80	0.68	35	0.90

The barren slopes typical of arid environments provide little protection from sub-aerial erosion, and the general lack of a continuous cover of riparian vegetation

presents the opportunity for very large amounts of bed material to be transported by strong floods (Sckick *et al.,* 1987). Flood flow always carries a high volume of sediment, which increases the destructive strength of the flood. For example, the flood of 1991 in Wadi El-Alam basin (Egypt) has left behind about 20000 m^3 of sediment at the Marsa-Alam town (Egyptian Geological Survey Authority, 1994). In Eshtemoa Wadi, the bedload flux was found to be high, on average 2.67 kg s^{-1} m^{-1}, during the period that the channel carries flow (Reid *et al.,* 1998). Laronne *et al.,* (1994A) reported that analyses of bed sediment indicate no vertical differentiation of bed material by size. Consequently, structural constraints on sediment entrainment are less pronounced than in armoured perennial streams and result in greater bed mobility and sediment availability. Not only the high volume of sediments but also the large size of material that can be carried as bedload are due to the high velocities encountered especially in desert mountains and mountains front. Cooke *et al.,* (1985) have reported that the flood of March 1982 in Saudi Arabia was so strong that it carried boulders up to 2 metres in diameter. Cairns (1997) also mentioned that the flash flood of 17 August 1995 in Morocco moved boulders the size of lorries and created a 'wall' of water and rock 6 m high.

Many wadis in the arid regions contain deep alluvial deposits characterised by high infiltration capacities and great water storage potential and the loss of flash flood water into this alluvial material is well known. A study undertaken by Brunsden *et al.,* (1982) to measure the transmission rates along the channels of Wadi Dhamad (Saudi Arabia) has illustrated that water loss into the soil is high (Table 2.2). Despite the existence of permeable alluvial materials that form wadi fans and pediment surfaces, bare rock slopes cover a higher proportion of drylands. These bare surfaces are mainly impermeable and have near-zero infiltration rates and hence contribute a quick runoff. Coarse fragments cover wide areas of the arid basins, which may be ascribed to the physical erosion. Many studies assumed the size of these coarse fragments are positively related to the runoff production. In most hot drylands the capillary rise of water in surface sediments is very common and leads to the concentration of the salt crystals on the surface (Cooke *et al.,* 1982). This phenomenon which is known as soil crusting is considered also as one of the important factors that influence the generation of runoff in desert lands.

Table 2.2 Transmission loss rates in desert channels, Saudi Arabia (after Brunsden *et al.*, 1982).

Location	Transmission Loss Rate (cm s^{-1})	Notes
Wadi Dhamad	0.007 - 0.008	sand/gravel
Wadi Jizan	0.038 – 0.056	gravel
Sabya	0.00625	gravel
Wadi Dhamed	0.000024	silt
	0.00011	sandy silt
	0.000098	silty sand
	0.000079	fine sand
	0.00016	med. sand

2.2 FACTORS AFFECTING RUNOFF GENERATION IN ARID LANDS

Flood magnitude is controlled by many interrelated factors. These factors are often separated into two main categories, transient and permanent. Transient factors mainly involve the temporal and spatial distribution of rainstorm input, whereas permanent factors include the physical characteristics of the basin itself (Baker, 1977). There are a number of factors controlling runoff generation from hillslopes and headwater catchments in arid regions. These controls include steep slopes, absence of dense vegetation, antecedent rainfall and soil moisture, the absence of permeable detritus, cemented and compacted mantles, thin soil, and poor water-storage capacity.

Patton and Baker (1976) and Costa (1987) indicated that drainage basin characteristics must play an important role in determining flash flood peaks in some basins. They tried to study flood peaks and their relationships to the morphometeric characteristics of basins in an attempt to find what factors contribute to flooding. However, other researchers, such as Benson (1964), deduced that basin characteristics have a small effect on floods and that the magnitude of the flood's peak discharge may have little relation to basin characteristics, and may depend entirely on volume and intensity.

2.2.1 Basin physiographic and morphologic characteristics

One of the most startling paradoxes of the world's drylands is that although they are lands of low precipitation, the details of their surfaces are mostly products of the action of water (Graf 1988). Some of these topographic details are absolute such as area, length, perimeter, relief, basin magnitude (total number of first order), and some are obtained by combining two absolute measurements as in relief-ratio, density, frequency, basin shape, and Ruggedness number. All these factors constitute the basin physiographic and morphologic characteristics. The first hydrological applications of quantitative studies of drainage basin morphology were illustrated by Horton (1945) and Langbein *et al.* (1947). Many investigators have extended Horton's morphometric work, but only a small percentage of them have been aimed at the practical problem of relating flood hydrograph properties to permanent hydrogeomorphic control.

2.2.1.1 Basin area

Basin area, which can be extracted from the available topographic maps, is the area of the land that drains water, sediment, and dissolved materials to a common outlet some point along a stream channel. The term is synonymous with watershed in American usage and with catchment in the UK and other countries (Dunne and Leopold, 1978). Perhaps it is the most frequently employed variable in the estimation of stream discharge, and it has been used with runoff in both humid (Benson, 1962) and arid areas (Burkham, 1966). Agnew and Anderson (1992) indicated that most basins within the arid zone have few, if any, raingauges. Therefore, the basin area may be the only variable from which a forecast of flow and possibly flood can be made. Average and peak discharge increase with increasing the catchment area (Morisawa, 1962), and there is a relationship between the maximum flood discharge and the drainage area (Patton, 1988)

As the larger the size of the basin, the greater the amount of rain it intercepts and the higher the average peak discharge that results (Chorley, 1969; Renard, 1970). In an investigation of factors affecting the occurrence of floods in the American Southwest, drainage area was found to be the most important variable affecting peak discharge (Benson, 1964). A similar result was found by Nouh (1990), who

indicated that the size of the basin in arid region is the most effective catchment characteristic affecting the accuracy of the flood hydrograph model. Ward and Robinson (2000) illustrated that basin area is fundamentally important in the sense that the larger the basin, the greater the flood product. However, they emphasised that when the rainstorm covers only part of the basin, the attenuation of the resulting flood hydrograph as it moves through the channel network to the basin outlet is greater in a large catchment than in a small one.

However, there are a number of other factors that are partly dependent on basin area in drylands. For example, it is not easy for a large catchment to be covered by a single storm. Cooke *et al.* (1982) indicated that in larger catchments in arid regions, only a part of the system might be functioning in a given storm. Ben-Zvi and Shentsis (2000) stated that, in a study conducted at the Sinai, Negev, Arava and the Dead Sea, the maximum observed depth of runoff event declines as catchment area increases. For catchment of 30 km^2 in area, the maximum observed depth is 63 mm, whereas, for 3000 km^2 catchments it is only 17 mm.

In large basins, runoff sometimes covers only one tributary of the whole catchment, and as a result, runoff is unlikely to reach the main basin outlet. In 1971 a flood occurred exclusively in the tributary Wadi Mikeimin of area 13 km^2 which is located in the main drainage artery of south-eastern Sinai-Wadi Watir, of an area of 3513 km^2. Further, Schick and Lekach (1987) reported that this small tributary deposited overnight a 6200 m^3 alluvial fan that completely obstructed the channel of Wadi Watir at their confluence. Accordingly, small catchments exhibit a more rapid concentration of overland flow and shorter time-to-peak flood than larger catchments.

In summary, rapid flash floods of small magnitude but possibly of catastrophic effects are more likely in small basins. This conclusion was supported by Baker (1977) and Cooke *et al.* (1982), who declared that there are several reasons that make small size basins give possibly catastrophic flash flood effects in arid regions. Firstly, slope length is generally short, and slope angles are steeper than in larger catchments. Secondly, soil cover is thin, and time to saturate is short. Thirdly, small

catchments can be covered by a single storm. Also as basin size increases, the channel storage effect becomes increasingly dominant (Chorley, 1969). For these reasons the storm hydrograph for small catchments may display high peak hydrographs in contrast to larger catchments which may display lower and flatter peaks and hydrographs.

2.2.1.2 Basin shape and orientation

Basin shape is of an obvious importance in influencing peak flow and other hydrograph characteristics (Chorley, 1969). It influences runoff through its effects on flood intensities and on the mean travel time of a drop of water from its point of impact on the surface of the catchment to its point of exit in the main stream. The basin shape can be assessed by the *Elongation ratio* (Schumm, 1956), which is the ratio between the diameter of a circle with the same area as the basin and the basin length. Basin shape tends to be circular when the Elongation ratio approaches 1.0, whereas, it become long and narrow when this ratio approaches 0.

Ward (1975) indicated that generally in square or circle-like basin, the tributaries often tend to come together and join the main stream near the basin outlet. Consequently, the separate runoff peaks generated by a heavy rainfall are likely to reach the main stream in approximately the same locality at nearly the same time, thereby resulting in a larger and rapid increase in the discharge of the main stream. So in general, equidimensional basins tend to have greater flash-flood peaks (Strahler, 1964). Conversely, if the catchment area is long and narrow, the tributaries will tend to be relatively short, and are more likely to join the main stream at different points. This means that, after a heavy rainfall over the area, the runoff peaks of the lower tributaries will have left the catchment before those of the upstream tributaries that have moved very far down the main stream. Elongated catchments are, thus, less subject to high runoff peaks. This is besides the fact that an elongated basin has generally higher bifurcation ratio than the circular one. This high bifurcation ratio in the former shape tends to reduce the velocity of the surface flow and hence increase the infiltration rate (see section 2.4.2.1.3 and Figure, 2.6).

Basin orientation in relation to the direction of the storm progress is also a major factor, which affects the flood peak discharge (Ward, 1975; Martiez and Goytre *et*

al., 1994). As shown in Figure 2.3, when the storm is moving in an upstream direction, the flood peaks from the lower tributaries will pass the gauging station at x before those from the middle and upper tributaries. Conversely, when the storm moves downstream, the flood peak from the individual tributary channel is more likely to arrive at the gauging station at approximately the same time with the result that the maximum runoff at this point will be considerably higher than in the case of the storm moving upstream.

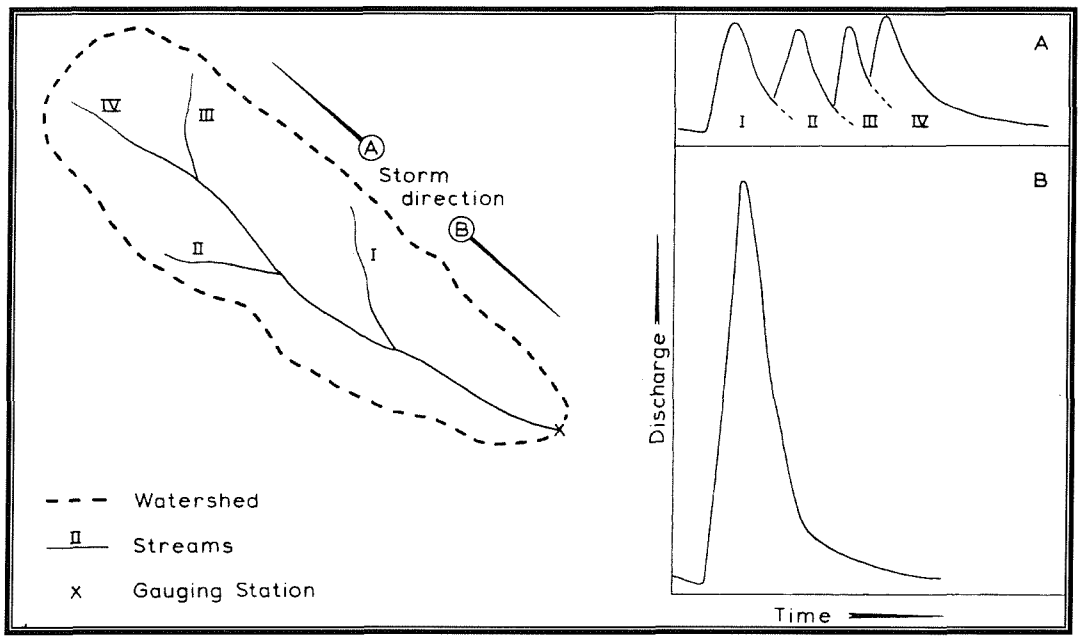

Figure 2.3 Diagram showing the probable runoff hydrographs resulting at gauging station x from two storms of equal rainfall amount moving in opposite directions over a hypothetical catchment (after Ward, 1975).

2.2.1.3 Drainage basin density, frequency, ordering and bifurcation

Drainage density, or what can be thought of as the texture of topography, is regarded as the most important areal measure of network geometry in that it expresses the degree of basin dissection by surface streams. It reflects, in particular, basin efficiency in removing excess precipitation inputs (Patton and Backer, 1976). Horton (1932) defined drainage density as the average length of stream channel per unit area within a drainage basin or area. For a given valley network, the closer channel heads are to the drainage divides, the greater is the total length of channel and therefore the drainage density (Knighton, 1998). Thus drainage density can

be approximated by $1/L_s$, where L_s is the mean length from channel heads to divides (Montgomery and Dietrich, 1989).

Patton (1988) demonstrated that the flood runoff has a positive correlation with drainage density that reflects the increased drainage network efficiency and more rapid hydrograph response associated with increasing drainage density. Smith and Stopp (1978) stressed the importance of drainage density in hydrological studies, as it is one of the factors that controls the speed of runoff following a period of precipitation. Water moves relatively slowly through a soil cover, if compared to its movement in an active stream channel. The greater the drainage density the faster the runoff. Therefore, with a high drainage density the stream hydrograph for runoff responds more rapidly to precipitation and becomes more peaked. Hence, flooding for a given quantity of rainfall becomes more likely to occur in a region with higher drainage density. At the same time basin lag time decrease as drainage density increase, reflecting the shorter path length of overland flow (Patton, 1988). Drainage density is controlled by numerous variables, such as lithology and rock structure (Morisawa, 1968), infiltration capacity of the terrain, resistance of the land to erosion (Horton, 1945), relief ratio (Schumm, 1956), climatic factors (Chorley, 1957), soil and vegetation (Smith and Stopp, 1978), basin relief and slope. Lithology, rock structure and soil type are important factors in flood generation, since they determine the resistance of the surface to erosion. A basin underlain by clay or shale, which can be easily eroded, generally has a high drainage density and stream frequency in relation to one underlain by sandstone. In a rugged region, drainage density and channel frequency are generally assumed to be high. Channel length tends to be longer in flat lying resistant beds and in areas of prominent coarse grains. On the contrary, it becomes much shorter and steeper in areas of fine grains and folded sediments and also where channels cut across resistant strata (Morisawa, 1968). Drainage density is a direct reflection of the relationship between the input of precipitation to the surface of a drainage basin and the transmission of infiltrated water through the subsurface materials (Ward, 1975). High drainage density values indicate the lower infiltration capacity, while the low value, especially in basins with intermediate relief, probably indicates the greater infiltration capacity of thicker soils and the increased vegetative cover.

Drainage density is broadly correlated with mean annual precipitation. The drainage density attains maximum values is semi-arid areas (Figure 2.4), where surface runoff rates are high because of intense rainfall over surfaces with sparse vegetation cover and limited soil development (Knighton, 1998). Positive correlations have been obtained between drainage density and both basin relief and slope (Roberts, 1978), suggesting that densities will be highest in steep headwater areas and when incision is at a maximum during landscape development (Knighton, 1998).

Channel frequency defined as the total number of channels per unit area within a drainage basin of area. More streams per unit area enable runoff to proceed faster, as the channel network can carry a large amount of water and discharge it quickly. A large number of channels also means more rainfall conducted out of the watershed by stream flow, rather than by infiltration through the soil (Morisawa, 1962).

Channel order was put forward by Horton (1945) and later modified by Strahler (1957). Strahler channel ordering can be described as the following: the smallest streams of the network, which have no tributaries, are called first-order streams. When two of these first-order streams coalesce they form a second-order stream, and further along its course this stream may join another second-order channel to form one of the third order, and so on. When a low-order stream, such as one of first order joining another of higher order, it does not alter the rank of the latter (Figure 2.5).

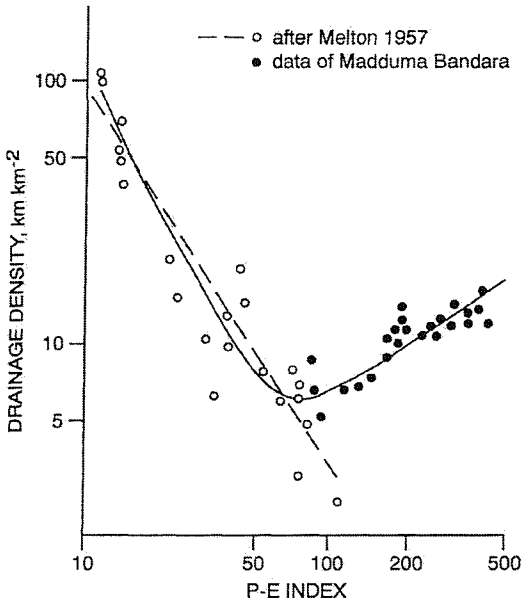

Figure 2.4 Variation of drainage density as a function of precipitation-effectiveness (P-E) (Knighton, 1998).

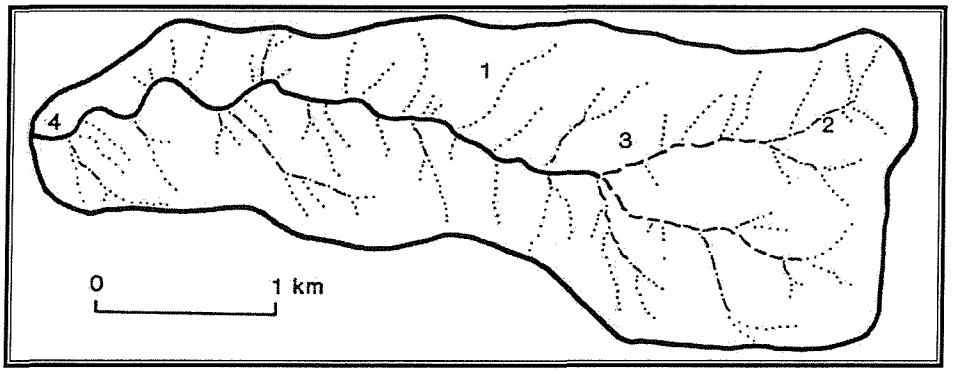

Figure 2.5 Designation of stream orders (Patton, 1988).

Basin discharge is found to be highly correlated with stream order, which is apparently related to the high correlation between drainage area and order for basins in similar climatic and geologic settings (Patton and Baker, 1976; Patton 1988). Numerous first-order tributaries can conduct stream flow out of a basin in a short time. These small mountainous upstream tributaries in extremely arid catchments tend, as a rule, to unite into lager channels with a continuous alluvial cover somewhere during their growth from third to fifth order. These alluvial fills form an infiltration trap for flood waters that flow into them either through the orderly tributaries system or directly from adjoining slope.

Ghosh and Scheidegger (1970) argued that channel length increases with stream order, and they attributed this increase to an increase in channel meandering with order, but oppositely Smart (1970*b*) criticised this note as he found that length in some cases increases and decreases with order. It is clear that basins characterised by large numbers of short, lower order channel that flow from many small basins into a few large sub-basins will have a flashy hydrograph response. Conversely, basins characterised by a relatively few, long, lower order channels and a more conservative increase in the number and size of basins will have a more sluggish hydrograph response (Patton, 1988).

Bifurcation ratio is the ratio of number of segments of a given order to the number of segments of the higher order. El-Shamy (1992) indicated that basins of low bifurcation ratio are more susceptible to floods than those of high bifurcation ratio, as high bifurcation ratio gives a slow surface flow, which means high infiltration rate and hence big chance for increasing the groundwater feeding (aquifer). Strahler (1964) proposed that basin shape and bifurcation ratio would produce noticeable changes in stream hydrograph. He suggested that rounded basins with low bifurcation ratios and nearly equal path lengths of water flow would have sharp hydrograph peaks, while elongate basins with high bifurcation ratios and greatly unequal flow path lengths would have lower hydrograph peaks (Figure 2.6).

In the measurements of channel length and calculating drainage density, frequency and orders, one must depend on recent topographic maps, as during rainstorms the stream network will expand into formerly dry gullies. Also one has to use large-scale maps, as Leopold and Miller (1956) surprisingly showed that the size or drainage area of the smallest, or first-order, stream on a smaller-scale map became a fifth-order stream in the study area.

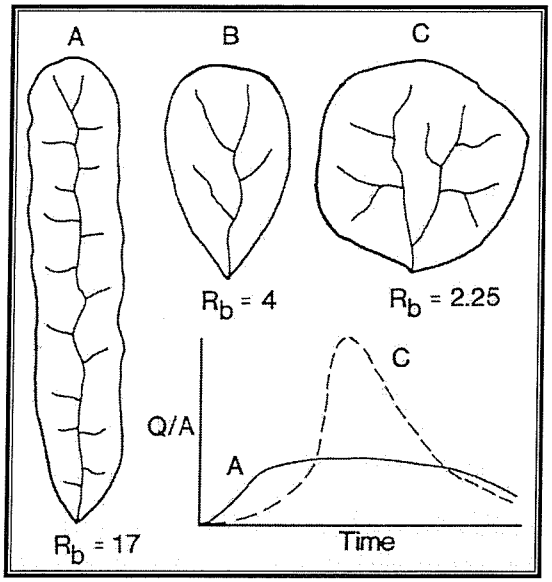

Figure 2.6 Hypothetical runoff hydrographs as a function of basin shape and bifurcation ratio (Strahler, 1962).

2.2.1.4 Basin relief, Relief ratio and Ruggedness number

Basin relief is the elevation difference between the highest point on the drainage divide and the mouth of the watershed. The importance of basin relief as a hydraulic parameter has been noted by Horton (1945) and Strahler (1958). Relief may indirectly affect total runoff through its direct orographic influence on precipitation amount (Ward, 1975). Differences in basin relief have several important effects on the hydrology of arid regions. The most obvious effect is that in regions with low relief, there is often no integrated drainage network. Also, it has been noticed that basin relief becomes higher in the flash flood prone regions than in the low potential ones. Accordingly, high basin relief combined with high drainage density forms steep short hillslopes, minimising the length of overland flow and again more rapidly concentrating the runoff. Abrahams (1977, 1984), demonstrated that both drainage density and frequency decrease as basin relief is erosionly reduced. While channel abstracted by relief reduction, new ones develop as relief increased by stream incision processes. In a comparison of morphometric parameters from basins of differing hydrologic response and diverse physiographic regions, two dimensionless measures of relief were significant variables in regression analysis with the maximum flood of record (Patton, 1988).

Relief ratio, is defined as the ratio between total basin relief and basin length (Schumm, 1956). Relief ratio allows comparison of relief in basins of varying size. The relief ratio, generally, indicates the overall slope of the watershed surface (Strahler, 1957). With increasing relief ratio, steeper hillslopes, and higher stream gradients, time of concentration of runoff increases, thereby increasing flood peaks, (Patton and Backer, 1976). So the greater the relief ratio of a basin, the greater the rate of hydrograph rise. Morisawa (1962) reported that more resistant beds result in basins with decreased relief ratio and drainage density as well as basins with increased area, length and stream gradient.

Ruggedness number is the dimensionless product of drainage density and relief. Areas of high drainage density and low relief can be as rugged as areas of low drainage density and high relief (Melton, 1957). Relative peak discharge increases with increasing drainage basin ruggedness (Parker, 1977). The increased peak discharge is the result of the improved efficiency of the network caused by the increased relief and drainage density (Patton, 1988).

Areas of potential flash flooding might be expected to have the highest ruggedness numbers incorporating a fine drainage texture (dense channel number), with minimal length of overland flow across steep slopes, and high stream channel gradients. All these factors together might lead to higher flood peaks for an equivalent rainfall input than for basins having a low ruggedness number (Patton and Baker, 1976).

2.2.1.5 Slope and channel gradient

Slope of catchment is considered as a very important topographical factor that may affect both the vertical (infiltration) and the lateral (overland flow) movement of water. The former tends to be more important in flat areas, while the latter in steeply sloping areas (Ward, 1975). The influence of surface slope is shown by the development of parallel rills, gullies or channels on steep surface slopes. Yair and Lavee (1985) emphasised that semiarid and arid areas are characterised by rugged landscape and steep rocky slopes that are covered at their bases by scree. This phenomenon can be explained by the fact that physical weathering predominates

over chemical processes in arid regions. Cooke *et al.* (1982) indicated that such steep slopes cover a higher proportion of drylands than any other type, and are characterised by their short length, sharp angle and hydrological features that strongly influence the infiltration, storage and runoff characteristics. Slope may indirectly influence the total runoff from a catchment through its effect in delaying water movement after a rainfall event, thereby possibly affecting the amount of evapotranspiration (Ward, 1975).

Runoff reaches stream channels quickly in steeply sloping areas, as the speed of water movement will tend to increase with slope. After a rainfall event in a small mountain basin, or the upper part of a large basin, runoff tends to exceed the infiltration rate and the storage capacity within the channel alluvium. The result is that there is a rapid increase in discharge for every comparatively small increase in catchment area. While in the downstream, or the lower part of the basin, rainfall is likely to be less (according to its relative low relief), runoff is less and channel storage capacity is greater. As a result, major increases in the catchment area have little effect upon the discharge while increasing in slope angle has high effect on basin discharge. Nouh (1990), in his model, emphasised the importance of catchment slope in the flood hydrograph as the soil of the catchment become more permeable when the slope decrease, and thus the effect of infiltration becomes more significant.

Channel gradient may be as important as catchment slope and has frequently yielded more significant correlation with runoff characteristics. Some researchers illustrated that streams, with steep gradients, are generally shorter and carry less water than stream with low gradient, which are long and deep and, thus, have greater channel storage. It has been pointed out that tributaries affect the gradient of a mean stream, since they add volume and load. Leopold and Maddock (1953), showed that increase of depth in channel overcompensates for decreased gradient and tends to provide a net increase in stream velocity at mean annual discharge stations. Hence, if precipitation conditions are equal, a stream with steeper gradient will have a smaller mean annual runoff and lower peak flow than a stream with low gradient (Morisawa, 1962). However, Langbein (1947) determined that channel

gradient is one of the most effective determinants of flood flow. The runoff hydrograph shape depends not only on the speed with which water gets into the stream channel but also on the speed with which it moves down the channel to the outlet of the catchment. The steeper the angles of any channel the faster the water flows down it according to the effect of gravity. Patton (1988) indicated that with steeper hillslope and higher channel gradient time of concentration of runoff decreases, thereby increasing flood peaks.

2.2.2 Soil cover

Arid regions are characterised by a low annual precipitation that cannot support significant amount of vegetation, thus exposing the native soil complexes to severe erosion by wind and high rain intensity. For desert areas and a large percentage of most arid basins, the surface soil is largely the first point of contact by rainfall. Therefore, soil type and its surficial properties play a primary role in runoff production.

Infiltration capacity refers to the rate at which water can penetrate into the soil. It depends upon numerous factors, but in particular is affected by the soil's physical characteristics of structure and texture. The infiltration capacity controls the rate at which rainwater can be taken into the soil and thus influences the point at which overland flow occurs (Briggs, 1977). Soil infiltration shows a temporal and spatial variation from one part to another in desert landforms, according to some essential factors, such as, different surface character, the nature of the surface material that covers its parts, slope angle, antecedent soil moisture and vegetation cover.

Soils in deserts are as variable as, if not more variable than, their temperate counterparts (Abrahams and Parsons, 1994). Hillel and Tadmoor (1962), in a comparison of four desert soils in the Negev, showed that sandy soils wetted deeply, have the largest storage, the highest infiltration rates, and the lowest evaporation when compered with rocky slope soils and loessic and clay soils. The latter have high storage as a result of surface crusting, poor absorption, and high evaporation rates. As a result the plant growth capabilities were markedly different. The very slow chemical and physical weathering rates in desert areas coupled with

a relative high efficiency of wash processes, due to the general sparseness of vegetation, result in more widespread occurrence of slopes with little or no regolith than in areas with humid climate (Abrahams and Parsons, 1994).

One might think that as soil is unlikely to become saturated in arid areas (because of its low precipitation) hence no overland flow should be expected in such areas. But there are several studies in arid regions indicating that runoff does occur (Yair and Lavee, 1976; Greenbaum *et al.,* 1998). This phenomenon can be ascribed to the existence of the *rocky slopes*, which cover a higher proportion of drylands than any other type (Cooke *et al.* 1982). This steep bare rock slope owes its existence to the decreased average annual rainfall that helps the physical weathering to be predominated over the chemical processes as it has a negligible absorption capacity. Abrahams and Parsons (1994), mentioned that the bare soil surface was often characterised by impermeable, hydrophobic, algal crusts, which in laboratory experiments required two hours to soften and allow absorption of water.

Given the widespread occurrence of bedrock outcrops on many desert hillslopes, an important control of infiltration and runoff is the ratio of bedrock to soil. Figure 2.7 shows the infiltration curves for rocky and soil-covered surfaces at Sede Boquer and the Hovav plateau in the northern Negev, Israel (Yair and Shachak, 1987). From this figure, it appears that the infiltration capacity is lower for the bedrock than for the soil-covered surface at both sites. Yair (1983) indicated, by using data from natural rainfall events at Sede Boquer, that the threshold level of daily rainfall necessary to generate runoff in rocky areas is 1 to 3 mm, whereas it is 3 to 5 mm for the colluvial soils, as the frequency and magnitude of runoff events are both much greater on the rocky than on the soil-covered areas.

Evenari *et al.* (1971), illustrated that with increasing stone cover percentage and fragment size, runoff yield will decrease. This is because the stone cover is assumed to limit the area of bare soil, which contributes to runoff by sealing the pore space, through the impact of the raindrops on the topsoil. However, the existence of deep incised gullies in such arid parts clearly indicates that runoff does occur, despite the coarseness of the material. In contrast, Yair and Lavee (1976),

assumed that the size of coarse fragments (gravel, cobble and boulder) is to be positively related to runoff production. This can be explained by the assumption that over a uniform lower layer big blocks allow a higher concentration of water above limited patches of the lower layer than does small gravel, (Figure 2.8). This conclusion was supported later by Poesen *et al.* (1990), who argued that this positive correlation between infiltration and stone cover depends on whether the rocks are partially buried or resting on the surface. They clearly indicated that rock fragment position in topsoil, susceptible to surface sealing, has a significant effect on water intake rate and on runoff generation. Rock fragments, if they rest on the top of the soil, increase water intake rate and the time of runoff concentration and in turn decrease the runoff volume. But if these rock fragments are well embedded in the topsoil they reduce infiltration rates and, hence increase runoff generation.

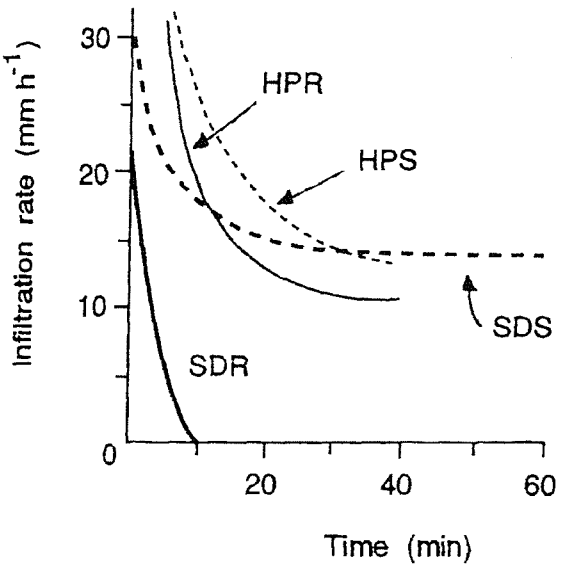

Figure 2.7 Infiltration curves for rocky and soil-covered surface in the northern Negev: Sede Boqure massive limestone (SDR), Sede Boqure stony colluvium soil (SDS), Hovav Plateau densely jointed and chalky limestone (HPR), and Hovav Plateau stoneless colluvial soil (HPS) (after Yair,1987).

In more detailed research by Lavee and Poesen (1991), with some laboratory measurements of overland flow on stone-covered soil surface, it has been established that under certain conditions of rainfall, soil properties and slope gradient, the stone size, stone spacing, and stone position are dominant factors in

controlling the overland flow yield. They concluded that stone cover usually activates overland flow relative to bare soil. Small stones, however, especially in low cover percentage and when in an 'on top' position, produce less overland flow than bare soil. Overland flow is positively related to stone size but negatively to distance between stones.

Yair and Lavee (1985) found that runoff generation in badlands in arid regions can be ascribed to the difference in composition and structure of the material forming the bottom of gullies and adjoining interfluve. Gullies are characterised by large blocks of rock embedded in a dense, compact, and thick mixture of fine grained material deposited by many flows. These large blocks respond rapidly to rainfall as they have a negligible absorption capacity. Water flowing from the blocks concentrates on the limited patches of the compact fine-grained material. Since the water delivery rate from the blocks is higher than the infiltration rate of the dense and compacted material, runoff can develop in the gullies shortly after the onset of rainfall. In contrast, the adjoining interfluve areas are quite different. They are composed of a thin surficial gravely layer, underlain by loose, coarse material with a small amount of fines and a high void ratio. The capacity of such porous material is so high that runoff is unlikely to occur even under extreme rain conditions (Yair and Lavee, 1976).

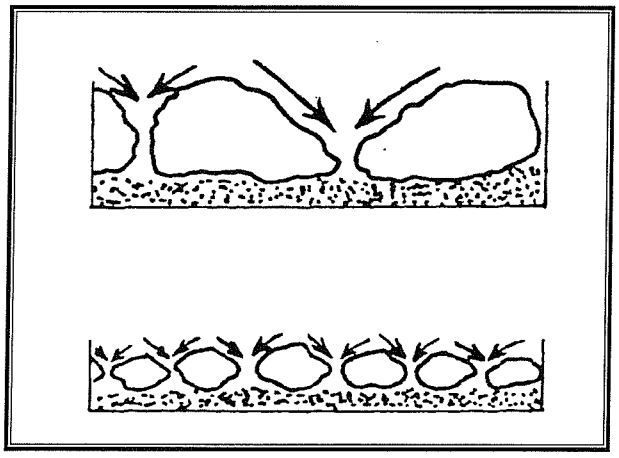

Figure 2.8 The influence of stone size on water concentration and runoff yield (Yair and Lavee, 1976).

The time to peak in desert floods is counted in minutes (Schick, 1988), despite the high infiltration rate that characterises the wadi bed deposits. Lekach *et al.,* (1998) indicated that infiltration rates in the wadi deposits are at least two orders of magnitude lower than the observed down stream flood front progression rate. They have suggested that alluvial fill in an arid wadi need not be fully saturated before the flow progresses downstream. The amount of water absorbed by the alluvial and the lateral and vertical components of the infiltrating water are dependent on flow duration and sedimentary structure of the wadi bed deposits (Lekach *et al.,* 1998).

There are some other factors affecting infiltration processes in desert land such as crusting processes that generally reduce the infiltration rates due to the concentration of salt crystals in the upper parts of the soil profiles. This phenomenon can be explained on a climatic basis as drylands are of very high potential evaporation and evapo-transpiration. Consequently, capillary rise of water in surface sediments becomes very pronounced leading to the concentration of these salt crystals on the surface (Cooke *et al.* 1982).

Moreover, an often-neglected factor influencing infiltration and runoff in desert hillslopes is the presence of cryptogamic crusts. Such crusts may be composed of algae, lichen, and moss. They are surprisingly common on desert surfaces and help to stabilise such surfaces. Some workers claim that the crust, by limiting the impact of raindrops on a bare soil, actually prevents the development of a true rainbeat crust and thus the algae increase infiltration. A contrary view, however is that the biological crusts have a strong water repellencey that results in generating runoff during relatively light showers of short duration. For example, Yair (1990a), in the Nizzana sand field, southern Israel, found that less than 1 mm of rainfall was sufficient to initiate runoff at a relatively low rainfall intensity of 18.4 mm hr^{-1}. They concluded that some runoff could be expected over the crusted surface during any rainstorm exceeding 2 to 3 mm. (Abrahams and Parsons, 1994).

Chemical properties of surficial material may also play an important role in runoff generation or inhibition, particularly in clay-rich soils. Yair *et al.,* (1980, 1985) reviewed the role of chemical processes in arid regions. They showed that there is a

correlation between the formation of a soil crust caused by clay dispersion and the percentage of exchangeable sodium ESP and electrolyte concentration. This is because high ESP values with low electrolyte concentration enhance the clay dispersions that form the soil crust which reduce the soil permeability and infiltration rate and in turn increase the probability of surface runoff.

2.2.3 Vegetation cover

Infiltration rate is strongly influenced by vegetation cover. In arid regions, indeed, vegetation is sparse and absent in many areas. It generally contains xerophytes, ephemeral grasses and small leafy plants. At a given location, the density of vegetation may be very different after a wet period than after a prolonged dry period. Even in more favourable locations plant cover may not reach 50%, giving an impression of the predominance of bare ground. The lack of available water is the most important limit to vegetation growth in desert area.

Abrahams and Parsons (1994) indicated that in the arid zone, where precipitation falls below about 100 mm, vegetation cover contracts to the drainage lines, leaving the interfluves and pediments bare. In hyperarid areas where annual precipitation may be less than 25 mm, perennial vegetation is concentrated in the main wadis and depressions which have high water tables or receive substantial amounts of run-off from surrounding areas or from sources outside the desert region. Perennial vegetation also occurs in areas with high mist and fog inputs. Opportunistic plants may still germinate and grow following rainfall. The relative absence of organic matter and litter on the surface of the ground has a significant effect on many processes including interception, infiltration, evapotranspiration and runoff. In general, infiltration rates increase with litter and organic matter content of soils. Most plants located along stream channels have a significant effect on ground water recharge and presumably on channel transmission losses. One of the earliest investigations, by Lyford and Qashu (1969), showed that infiltration rates decrease with radial distance from shrub stems. The infiltration rate near the stem of the plant was nearly three times greater than that for the area between plants. This can be explained by the fact that under the plant cover soil bulk density is lower than in the interplant areas and the organic matter content of the soil is significantly higher

under the plant than in the open area. This result was supported later by Stark (1973) who found that infiltration rates were eight to ten times greater under shrubs than in the open on desert soils with a high clay fraction. Later, Rostagno *et al.* (1991) found that mean infiltration rates, after 35 minutes of simulated rainfall applied at a rate of 70 mm hr^{-1}, were significantly higher beneath the plant (3.3 cm hr^{-1}) than in the intervening unvegetated areas (0.5 cm hr^{-1})

Micro-topography may have, in areas of low relief, a profound influence on vegetation, and runoff. Pilgrim *et al.* (1988) illustrated that small acacia trees in central Australia, grow in linear groves that are clearly visible from the air. The infiltration capacity of the soil within these groves is typically higher than in the intergrove areas. These intergrove areas play an important role in collecting rainfall water to supply those groves, and without it, the trees would not survive.

2.2.4 Climatic variation

Arid zones are often in a delicate hydrological balance. The whole nature of the hydrology may be changed by a prolonged wet or dry sequence. Climate, indeed, controls the basin mophometry (Chorley, 1957). Patton and Backer (1976) stated that in a region where intense rainfall is an infrequent and random event, a feedback process enhancing the rapid drainage response can be recognised as the infrequent rainfall does not promote vegetation or soil development and, therefore, increase the overland flow that leads to hillslope rills or gullies. These newly formed first-order channels increase the response of the drainage system. In contrast, in a region where rainfall is temporarily and spatially more uniform feedback processes dampen the basin response by aiding the development of thick soils and dense vegetation, thereby increasing infiltration rate and retarding surface runoff.

2.2.4.1 Rainstorms

In the sense that precipitation forms the raw material of streamflow, meteorological factors are obviously of great importance and their variation with time tends to be closely related to similar variations of runoff (Ward, 1975).

The most characteristic features of desert storms are their unpredictability and their high variability in space and time (Yair and Lavee 1985). Storms typically occur suddenly, are brief and spatially very varied. Individual storm totals can be very high even though the number of rainy days and the annual total are very low (Cooke, 1985). Precipitation, generally, is limited to the winter season in many arid areas (Yair and Lavee, 1985). Rainfall in desert environment known with its long sequences, the long dry periods between these sequences may cause changes in the vegetation and soil surface structure that have an appreciable effect on infiltration and the production of runoff.

Although the rainfall amount in most arid areas is limited to less than 50 mm per year (Schick, 1971), many desert areas suffer strongly from catastrophic high magnitude floods; exemplified by the flash flood of Israel in October 1991 (Greenbaum *et al.* 1998) and of Egypt in November 1994 (Egyptian Geological Survey Institution, 1994). These floods are the result of intense rainfalls from severe thunderstorms created by unstable weather conditions and the orographic effect of these regions.

Two distinct storm types were recognised in arid areas, convective and frontal storms. The convective storm type occurs under unstable weather conditions at the end of the winter season. These storms are characterised by high rain intensity and short duration and hence tend to give larger volumes of quickflow with most sudden and short-lived streamflow. Sharon (1972) illustrated that half to two thirds of the rainfall in the hyperarid extreme south of Israel occurred in convective cells approximately 5 km^2 in diameter that were mainly associated with synoptic scale low pressure systems in winter. They are often of 1-hour duration or less and are virtually always less than 4 hours unless associated with a large storm system (Sabol and Stevens 1990). These storms can account for up to 50 % or more, of the average-annual precipitation for a specific location during a single one to three-hours time period (Zeller, 1990). For example, Yuma, Arizona experienced an extreme precipitation event on August 9, 1989. In this event 130 mm of precipitation fell in approximately two hours, while the average-annual

precipitation for Yuma, is only 67 mm. According to Byers (1959) a convective cell's life span may vary from a few minutes to nearly an hour and usually occurs in irregular cells of 3-10 km in diameter (Sharon, 1972,1981). These localised convective rainstorms are the major rain source of rainfall in subtropical desert (Sharon, 1974).

With regard to frontal rainstorms, they are of large systems that are often associated with frontal activity and develop in humid areas, and extend into adjoining semi-arid and arid areas. They are characterised by low to medium rainfall intensity, long duration (several hours to few days) and cover very large areas (Yair and Lavee, 1985).

With respect to the Red Sea region, rainstorms are often cellular and follow discrete tracks. As a result, the pattern of these rainfalls can be extremely patchy (Sharon, 1972; Wheater *et al.*, 1991) affecting only a fraction of the catchment (Figure 2.9). Sharon and Kutiel (1986) indicated that the Red Sea trough, which is characterised by the development of convective rain systems, occurs mainly in autumn (September – November) and spring (March – May). These rainstorms are characterised by short duration but yield high intensities of up to 60 mm hr^{-1} with peak values of 120 mm hr^{-1}. This indication has been supported later by the rainstorm that crossed the hyperarid catchment of Nahal Zin (Israel) in October 1991. In this rain event a short period of 15 minutes of rainfall has been reported with high intensity of up to 130 mm hr^{-1} (Greenbaum *et al.*, 1998). Moreover the results of five stations in the Negev showed that 65% of the high-intensity rains (> 30 mm hr^{-1}) occurred in the afternoon time when surface temperature is high whereas less than 15% occurred in the early morning, (Sharon, 1972).

Abu-Hassen (1994), in his study on the effect of the Red Sea trough and its effect on Jordan climate, indicated that the effect of the Red Sea trough begins when the area of the cold air (from the north of the Mediterranean) with the warm air (from the Arabian Peninsula) move toward the north. This gives the chance to the Red Sea trough to extend along the Red Sea. But he mentioned that this is not enough to create the unstable weather conditions, as it must be combined with a cold front in

the upper trough that increases the upward motion which, then, creates an unstable zone that produce dark cloud (cumulonimbus) with thundery heavy rain that was sometimes combined with hail.

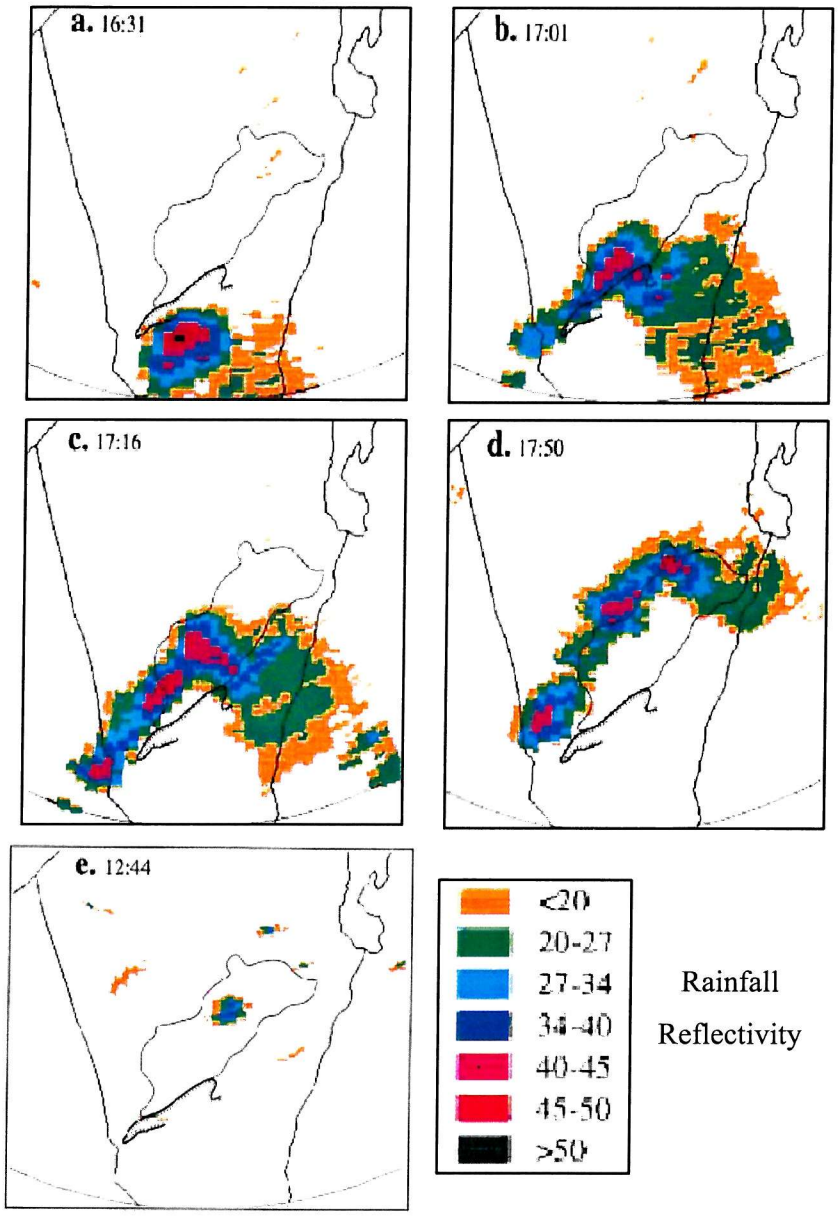

Figure 2.9 (a to d) Progression of the storm structure towards and over the Nahal Zin catchment, as scanned by radar at designated time intervals, 13 October. Map (e) shows the convective cell over a small part of the catchment on the following day (Greenbaum *et al.*, 1998).

2.2.4.2 Evaporation

In desert areas the potential evaporation rate reaches its highest value, compared to other climatic zones, due to high temperature, dryness of air, open surface and minimum vegetation cover (Saleh, 1989). Many studies, in general, suggested that there is a high negative correlation between runoff and both evaporation from the surface and transpiration from plants. Renard (1969) for example, found that evaporation and evapotranspiration from Walnut Gulch is about 85% to 90% of the incoming rainfall. Potential evaporation in extreme deserts may be around 10 mm per day. In southern Israel, for example, it varies from 4.7 to 16.0 mm per day for class A pans, and from 110 to 330 mm per month for large water surfaces (Schick *et al.*, 1987). In spite of its importance, there are several factors that reduce the role played by evaporation as a factor in controlling flash floods in deserts. These factors include, the short rainfall and runoff duration, the small area of desert watersheds, limited or absence of plant cover that means a decrease in evapotranspiration processes, the extent of the cloud cover during desert rainstorm, and the tendency of most arid regions to have predominantly winter rainfall when temperature and potential evaporation are low. An abrupt 8 °C fall in temperature with hail has been reported in the flash flood events of 1991 in Israel (Greenbaum *et al.*, 1998). To sum up, evaporation is a negligible factor for rainfall-runoff modelling in arid lands. Yair and Lavee (1985) excluded potential evaporation from their model, as the data obtained clearly indicated that during a storm, when cloudiness is high and air temperature quite low, the potential evaporation for 1 minute is insignificant.

2.3 SUMMARY

The flash floods processes in the arid regions are infrequent, usually they are years apart and different from those which are often taking place in the humid areas. They occur in short time scale with very sharp peak discharge. The typical barren slopes in the arid regions that are lacking the vegetation cover and liable to areal erosion present the opportunity for high volumes of sediment to be transported

downstream by the tremendous power of the flow of a high velocity resulting in substantial reworking of the channel's geometry.

Magnitudes of flash flood events depend not only upon meteorological factors but also upon physiographic features of the arid catchments. The physical characteristics of the catchment either absolute such as the area, length, elevation, or derived such as drainage density, bifurcation ratio, basin shape and ruggedness all play a significant role in the flood lag time, peak and magnitude. The unpredictable patchy (cellular) rainstorms that characterise the arid regions are very variable in space and time and in the Red Sea area occur in the winter season. They deliver a huge amount of precipitation in a short period of time leading to quick flood of short life.

CHAPTER 3

DEM generation and channel network derivation

3.1 INTRODUCTION

One of the basic tasks in hydrological analysis is to extract drainage basins and stream networks, which can then be used in various applications, such as the prediction of flooding and studies of stream flow hydraulics. From the time when the methodology of basin analysis was first developed, it has been known for its tediousness and labour intensity. Mostly the measurements were made manually from topographic maps, and the measurement of morphometric parameters, such as channel length, gradient of different orders, density, frequency, mean basin elevation and slope, were hampered by the amount of work involved.

The use of Geographical Information Systems (GIS) to store and manipulate data has become increasingly widespread. The wide range of functions that the GIS is capable of performing are summarised by Maguire and Dangermond (1991), (Table 3.1). Not all the functions are necessarily employed in any single GIS implementation and some functions that are required may not be available, but most GIS have a macro language in which new functions can be programmed.

With the advent of GIS, Digital Elevation Models (DEM) have been used to derive drainage basins and channel networks, which have obvious applications in hydrological models and geomorphology. The delineation and analysis of channel networks can be automatically achieved by using the DEM and computers instead of measuring directly from hardcopy maps, thus minimising the analyst's time.

A DEM is an ordered array of numbers that represents the spatial distribution of elevations above some arbitrary datum in a landscape (Moore *et al.*, 1991). These data are commonly stored in one of three data structures: contours, grids, and

triangulated irregular network (TINs). Grid terrain models are the most widely available data structure, terrain analysis methods using grid models are simple, and the grid structure is compatible with remote sensing techniques. Although they were introduced in the late 1950s (Miller and Laflamme, 1958) their potential was not fully realised until the early 1980s.

Table 3.1 The functional components of GIS (After Maguire and Dangermond, 1991)

Function	Description
Capture	Primary data collection (e.g. Scanning, radar, GPS, field survey). Secondary data collection (e.g. digitising, scanning, stereo plotting).
Transfer	Moving previously collected data into the GIS.
Validate & Edit	Checking accuracy of primary or secondary data.
Store & Structure	Data stored as, usually, either raster (grid-based) or vector (line-based) data structure.
Restructure	Changing data structure (e.g. vector-raster conversion or *vice versa*).
Generalise	Smoothing and aggregation feature (e.g. simplifying or aggregation grid cells (pixels)).
Transform	Define transformations, e.g. scaling, rotation, translation, inversion), curvilinear, transformation (e.g. changing map projection).
Query	Retrieve attribute data about spatial features using operations such as, spatial searching (buffering or proximity analysis) and overlay (comparing two or more data layers).
Analyse	Similar to query, also involves relating features on different data layers using map processing (or map algebra) and spatial operators (e.g. adjacency, nearest neighbour, overlap, direction etc), logical and mathematical operators.
Present	Presenting results in the form of maps, tables, reports and lists.

DEMs can be used to derive a wealth of information about the morphology of the land surface. Watershed and channel network derivation is considered as one of the fundamental uses of DEMs. It is used to calculate slope characteristics, to enhance distributed hydrologic models and to produce flow paths of surface runoff (O'Callaghan and Mark, 1984; Hogg *et al.*, 1993). Recent studies have illustrated

that the accuracy of the basin network parameters extracted from DEMs is comparable to those obtained by manual methods while the processing time is much less. For example, Garbrecht and Martz (1993) derived a network for a low relief drainage basin of 84 km² from a 1: 24,000 resolution DEM. They compared the DEM's network parameters with those derived from the topographic maps and found that the DEM's parameters including drainage area and density were in general within 5% of those measured manually from the hardcopy. However, they illustrated that the largest differences were found for channel slope. Eash (1994) compared 24 basin's characteristics measured from 1: 250,000 DEMs and 1: 100,000 DLG (digital line graph) hydrologic data with those measured manually from the topographic maps of the same scale for 10 basins. Of the 10 primary parameters including total stream length, total drainage area, mainstream length and basin slope, only the basin slope was significantly underestimated by the DEMs. They found that measurement differences for basin slope ranged from -8.9 to -66.1 percent, with an average underestimation of -40.4 percent.

The procedures followed in generating the DEM of Wadi El-Alam, from digitised contour lines and spot heights, along with its sub-basin boundaries and channel network are schematically illustrated in Figure 3.1 and detailed in the following sections. The Arc/Info package (ESRI, 1993) was used for implementing these procedures.

3.2 CONSTRUCTION OF THE DEM

A DEM is generated by fitting a mathematical surface to a set of data points of known elevation. The quality of the resulting DEM depends mainly on the accuracy, density and distribution of the input data points as well as the method of interpolation used. The resolution of the DEM sets the step at which elevation data points are interpolated from the mathematical surface. The elevation data required for DEM generation are usually provided by photogrammetric methods or field surveys. Contour maps are also a common source of elevation data that can be used for generating DEMs. In this study, the contour maps of Wadi El-Alam were the only source of data available for generating its DEM. These contour maps were

first converted into digital formats through lengthy digitisation processes explained in the following section.

3.2.1 Contour line digitisation

The four topographic map sheets of Wadi El-Alam, held by the Egyptian Military Survey, First edition 1989 (Figure 3.2), were originally derived from aerial photographs at 1: 50,000 scale with a 20 m contour interval. There is no doubt that the complete digitisation of these maps is a very labour intensive task. To get this task achieved properly with less effort, the possibility of digitising not every contour line was first necessary to be checked.

First a subset from one of the topographic map sheet was chosen and digitised twice, respectively, at contour intervals of 20 m and 100 m, Figure 3.3 (a1, b1), starting from zero meter as a base contour. Then, a DEM was generated, Figure 3.3 (a2, b2), from each resulting contour map using the ARC TOPOGRID command. As a test for the quality of these DEMs, new contour lines were generated from them at every 40 m, Figure 3.3 (a3, b3), by making use of the GRID CONTOUR command. A visual inspection of the resulting contour lines revealed that the lines generated from the DEM which was initially derived from the digitised contour map of 100 m interval were lacking the topographic details, Figure 3.3 (a3, b3), that were further needed for automatic delineation of the channel network and in turn the sub-watersheds boundaries. Therefore, it was decided to digitise the original topographic maps of Wadi El-Alam with the complete inclusion of all the contour lines of an interval of 20 m.

The topographic map sheets covering the whole study area and named as Marsa Alam, Jabal Al-Aswad, Jabal Ghadir and Jabal Nuqrus, were manually digitised into twelve coverages (automated map layers) using the ARCEDIT module of the ARC/INFO package. The digitised features were the contour lines, spot-heights, and watershed boundary. The digitisation process was, in the literal sense, formidable and time-consuming tasks; three months were needed for digitising only the contour lines. The twelve coverages were then transformed from the digitiser

units into the Transverse Mercator (TM) projection of the Egyptian zone (36). By using the ARC APPEND command, the small four coverages for every topographic feature (e.g. contour lines) were joined together into one coverage. The contour lines were built as a line coverage, spot-heights as a point coverage and watershed main boundary as a polygon coverage (Figures 3.4 and 3.5). These three coverages were then cleaned using the CLEAN command to construct the topology and to add the feature attributes. The resulting coverages were afterwards checked for errors to make sure that there were no unconnected, duplicate and intersection arcs in the contour line coverage, there was a node at each intersection of more than two arcs, the boundary polygon was closed and there were no gaps between the edges. All these checks were made automatically in the cleaning processes but the errors that exceeded the tolerances set for the CLEAN command (e.g. undershot and overshot arc) were flagged and corrected by manual editing. As the manual editing and correction for the digitising errors in the coverages always alter the topology, it was necessary to reconstruct again the correct topology for establishing the spatial relationships. By making use of the ARC JOINITEM command, the INFO data files were then linked to their corresponding elevation cods in the feature attribute tables.

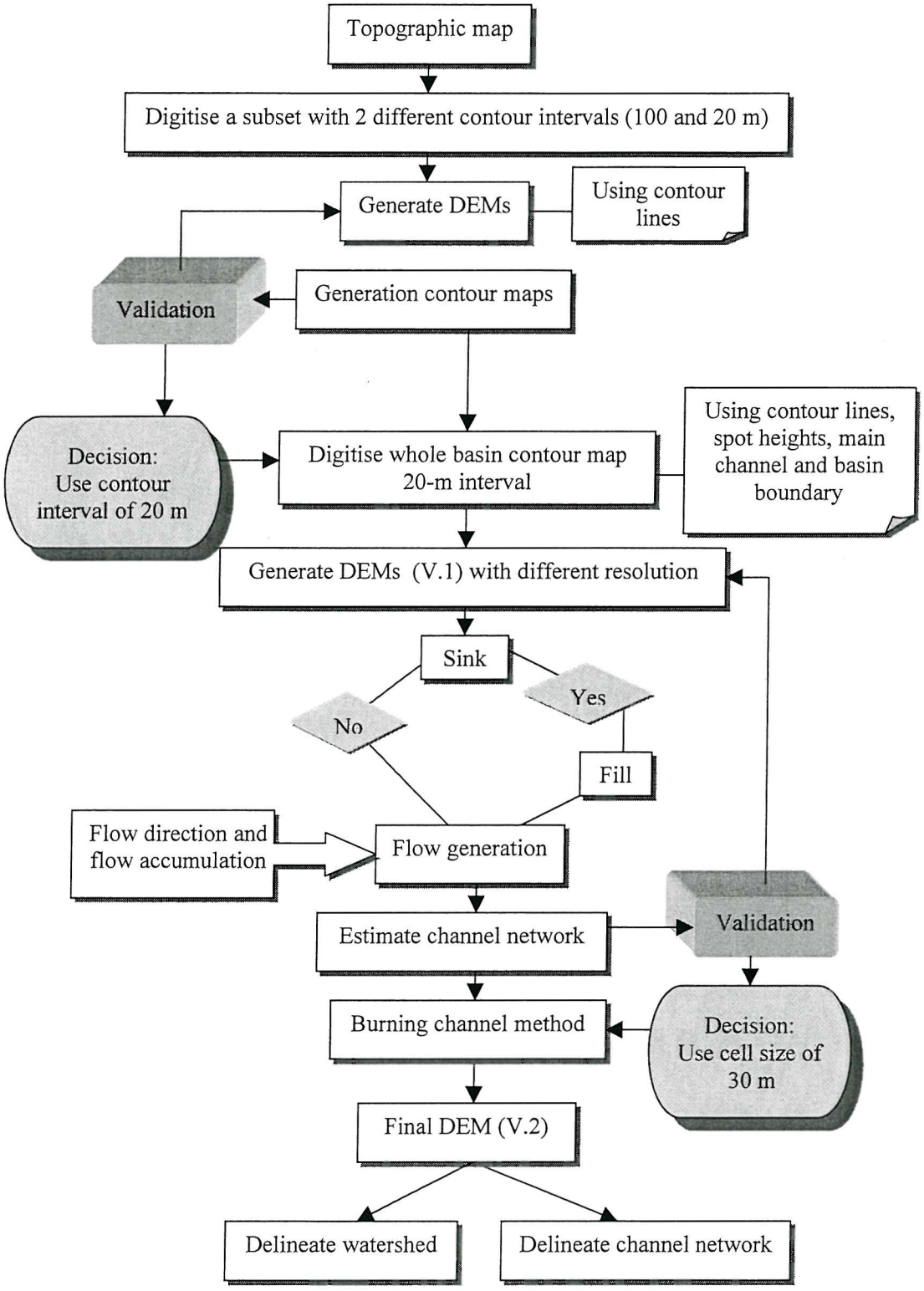

Figure 3.1 Flowchart shows the generation process of the sub-watersheds and the channel network of Wadi El-Alam.

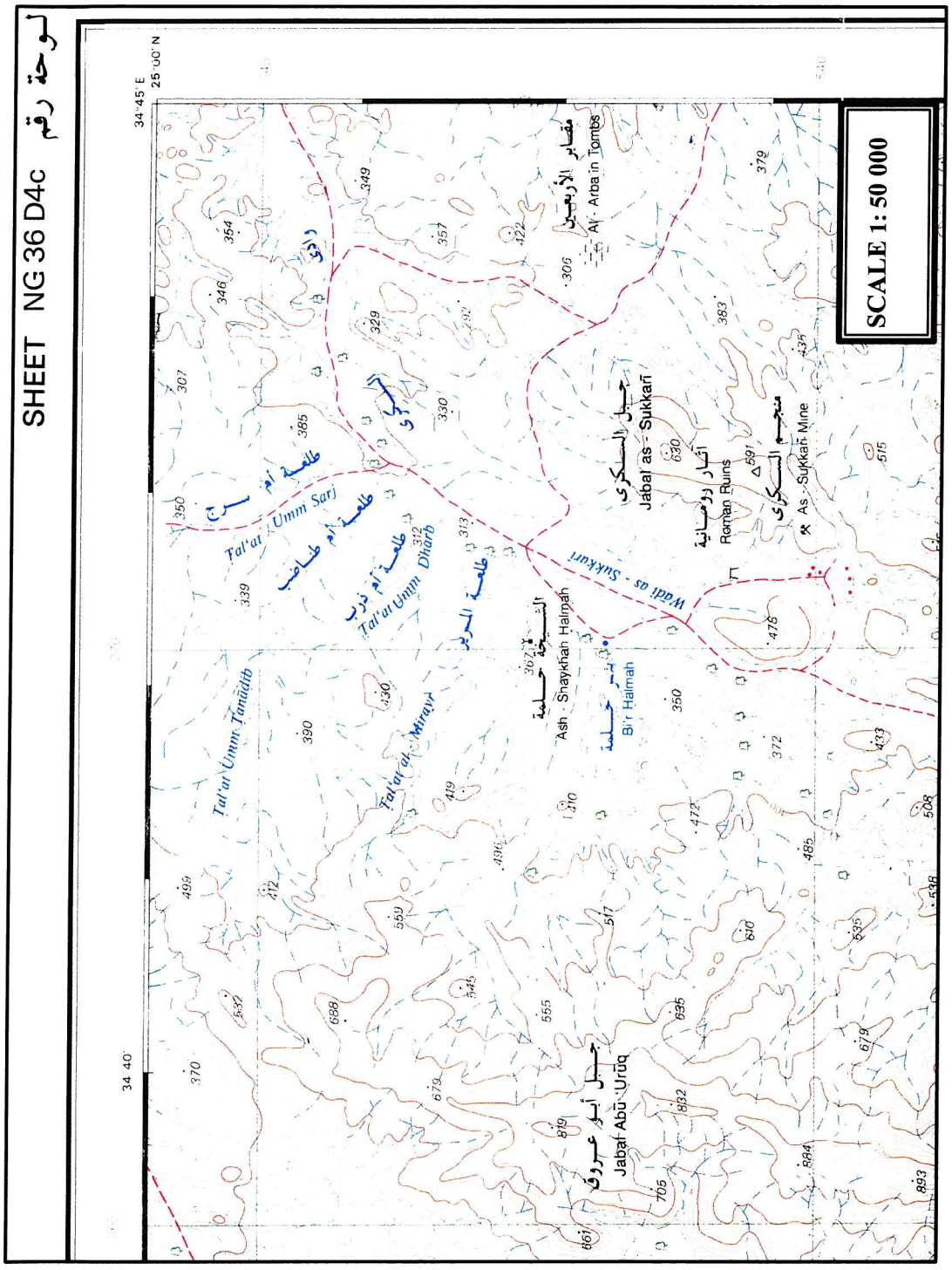

Figure 3.2 Part of the topographic map sheet of Jabal Nuqrus.

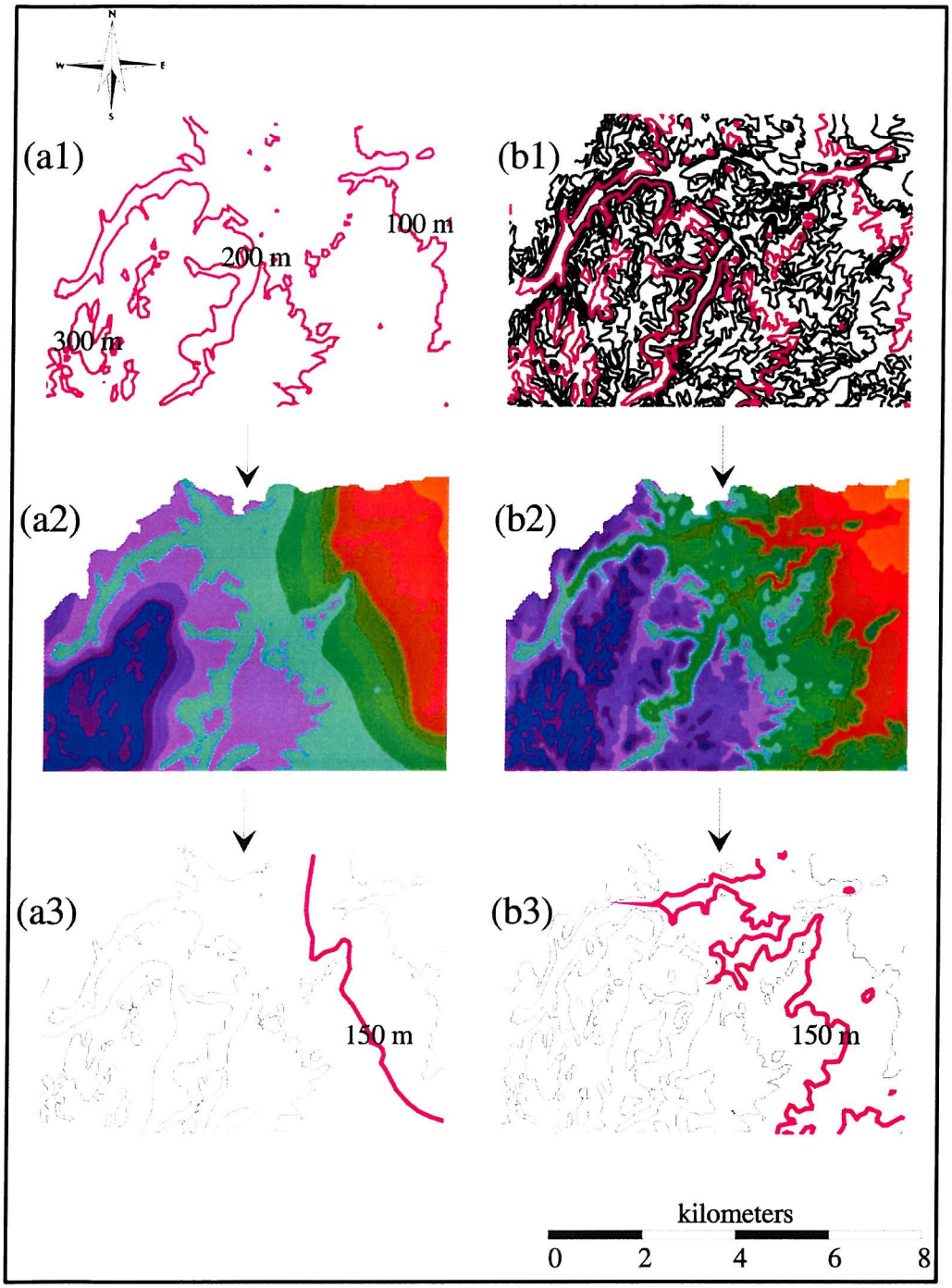

Figure 3.3 Comparison between resulted contour maps derived from DEMs generated from maps of 20 m (b) and 100 m (a) contour intervals.

3.2.2 Generation of the DEM (V1)

A DEM was generated from the digitised maps using the ARC command TOPOGRID, which is an interpolation method designed for the formation of

hydrologically correct digital elevation models from comparatively small but well selected elevation and stream coverages (ESRI, 1993). The coverage of contour lines and the spot heights were used in the interpolation processes together with the basin boundary coverage to clip later the excess parts of the resulting DEM.

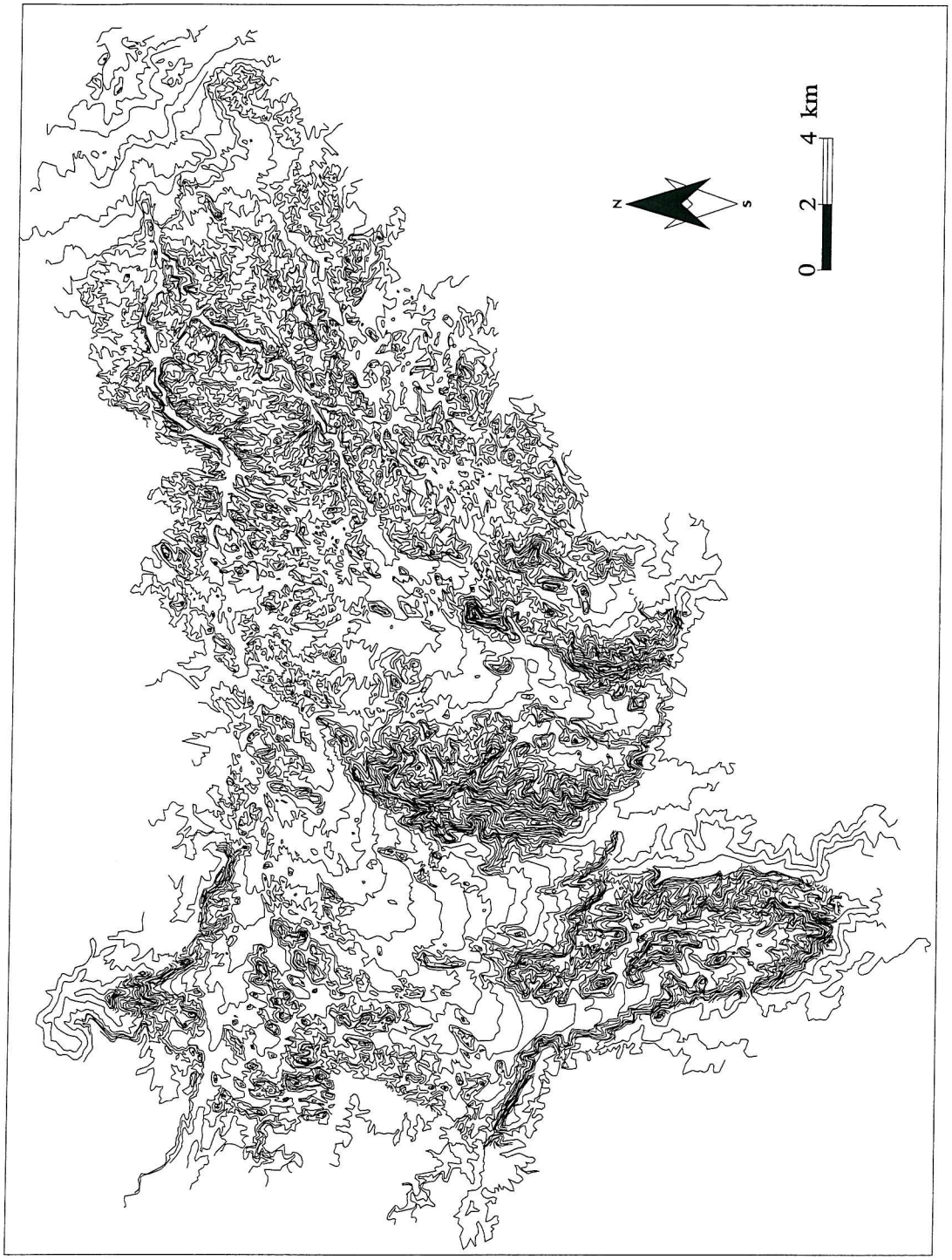

Figure 3.4 Digitised contour lines of Wadi El-Alam.

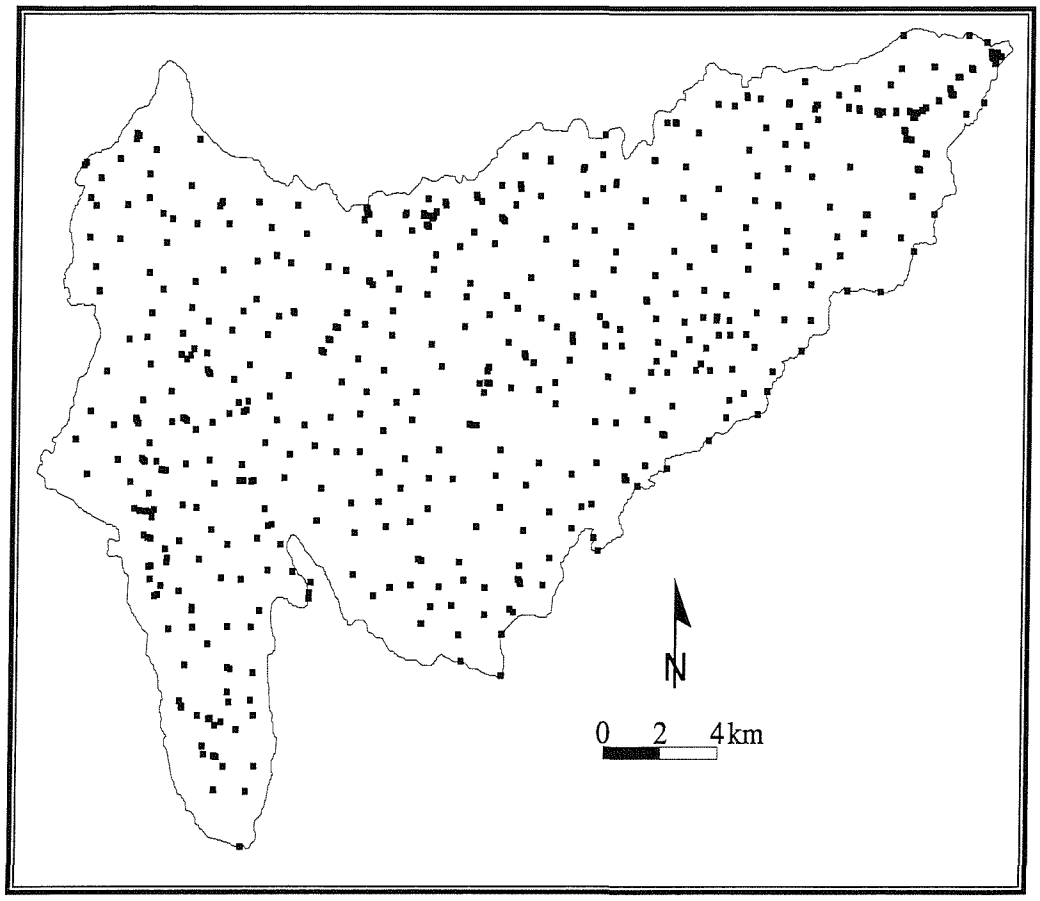

Figure 3.5 Digitised spot heights and basin boundary.

To enable accurate enforcement of the drainage channel network in the generated DEM, the topographic map layer of the channel network of the Wadi was needed to be provided as input as well to the TOPOGRID command. The mainstream channel (and not the whole channel network) was digitised by tracing only the centre of the double blue lines in the topographic maps (Figure 3.6). This was followed by the application of the ARCEDIT FLIP and the ARCPLOT TRACE commands, respectively, to flip the direction of the channel network as the maps were not digitised according to downstream direction as required.

Before generating a working DEM for Wadi El-Alam in the raster domain, it was necessary to decide upon the optimum grid cell size, which defines the resolution of the DEM. To this end, the DEM was generated a number of times using different cell sizes (120, 100, 80, 60 and 30 m). A delineation process was then applied on

each ensuing DEM to derive a channel network. Upon contrasting the resulting channel networks with the digitised one, Figure 3.7, it was found that the smaller the DEM's cell size; the better is the derived channel network. The channels delineated from a 30 m DEM perfectly matched the digitised one. Therefore, the grid cell size of 30 m was used in the present study for generating the DEM (V1) of Wadi El-Alam, Figure 3.8. This resolution was identical to the resolution of the TM satellite image of Wadi El-Alam (which was used in chapter 5) and, thus, made a good base for a raster database that would have included both the map layers and remotely sensed data. Moreover, it has been shown by Quinn *et al.,* (1993) that at resolutions finer than 50 m, the widely used concept of single flow path along the steepest flow direction could be applied without any significant error.

The validity of the resulting DEM was initially checked by the ability of regenerating all the original contour lines and comparing the result with the original contour map. As shown in Figure 3.9 there was a good match, in general, between the two sets of contours. The relative differences between contour lines in the flat areas (Figure 3.9b) were mainly due to the low density of the original contour lines.

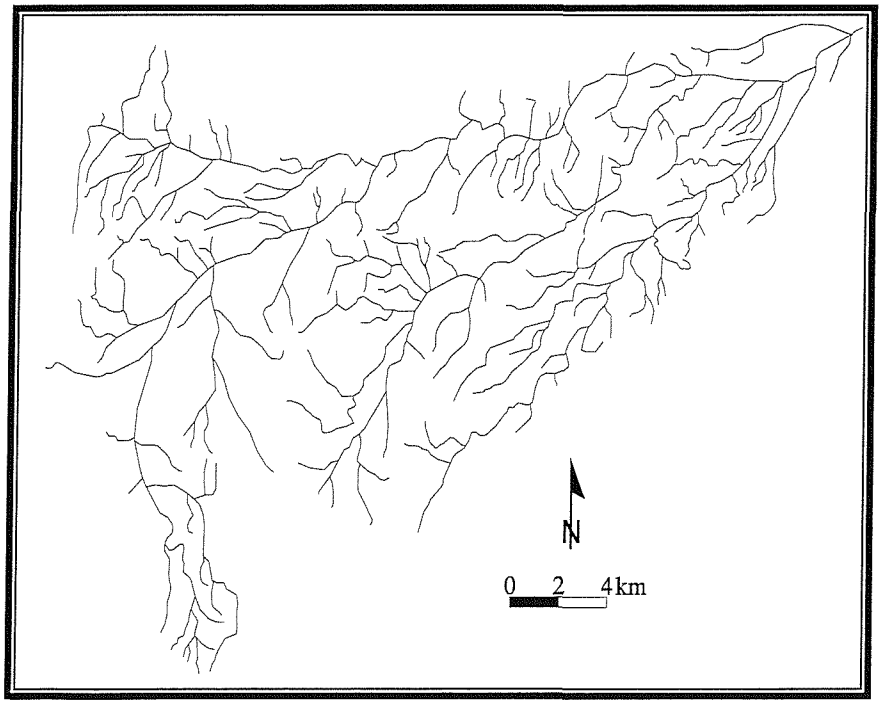

Figure 3.6 Digitised main channel network.

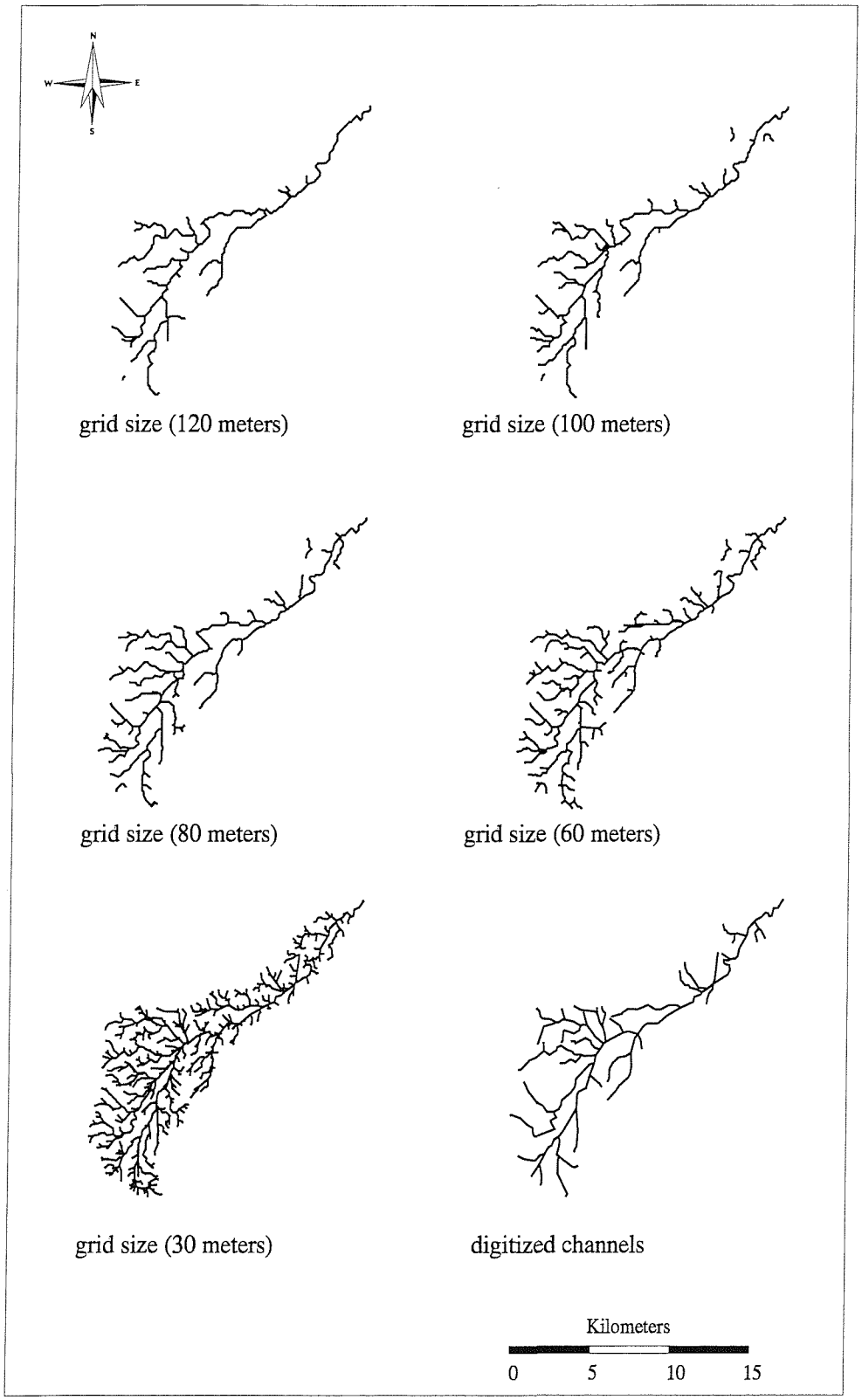

Figure 3.7 Extraction of El-Sukkari sub-basin drainage network at different grid cell sizes.

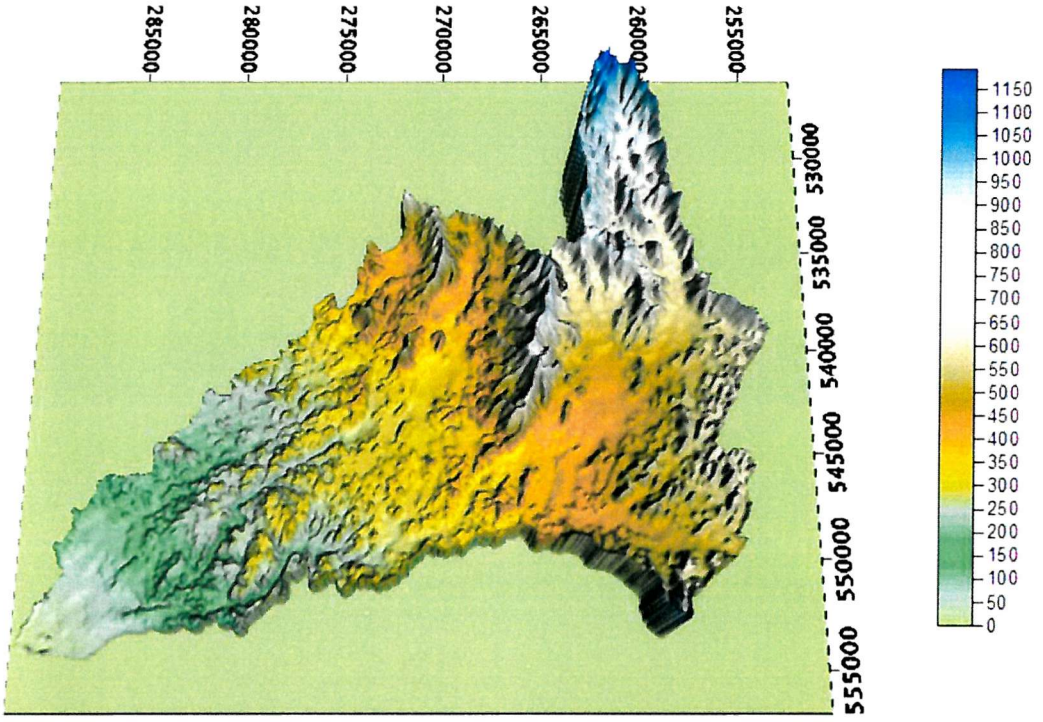

Figure 3.8 Interpolated DEM of Wadi El-Alam watershed.

3.3 DELINEATION OF THE FLOW NETWORK

The shape of a terrain determines the movement of water across the terrain surface. DEM values form the basic data layer for surface flow routing from which other layers can be derived by the calculation of topographic attributes, such as flow direction, slope, aspect, upslope area, slope curvature and others (Moore *et al.*, 1991). In ARC/INFO, the GRID module contains a suite of surface flow routing functions that enable stream flow to be derived from a DEM for a surface topography (ESRI, 1993). The very first step consists in determining depressions (known as pits or sinks), and filling them to ensure proper delineation of the basin and its channels as described in the subsequent section.

3.3.1 Sink Filling

As the study catchment is void of any real depressions, it was necessary to fill any pits (sinks) in the elevation grid before computing the flow direction grid; flow

directions would be undefined for all unfilled pits. A pit forms when a grid cell is lower than its entire neighbouring grid cells (Figure 3.10), and thus receives flow but does not have any outflow. These sinks are considered as errors in the DEM as a result of errors in the input elevation data or, in most of the cases, as a result of manipulating integer elevation data. By using the grid FILL SINK command all single pixel pits are raised to the level of their lowest neighbour pixels to create a seamless elevation grid. The procedure for gridding elevation data consists of an iterative interpolation technique coupled with a drainage enforcement algorithm. The interpolation technique uses an iterative method for calculating elevation at regularly spaced grid points from a set of input elevation-data points. The procedure begins with a grid at a coarse resolution and proceeds with successively finer resolution grids until the user-specified resolution is reached. At each grid resolution the drainage enforcement algorithm is applied to remove any spurious sinks found at this resolution.

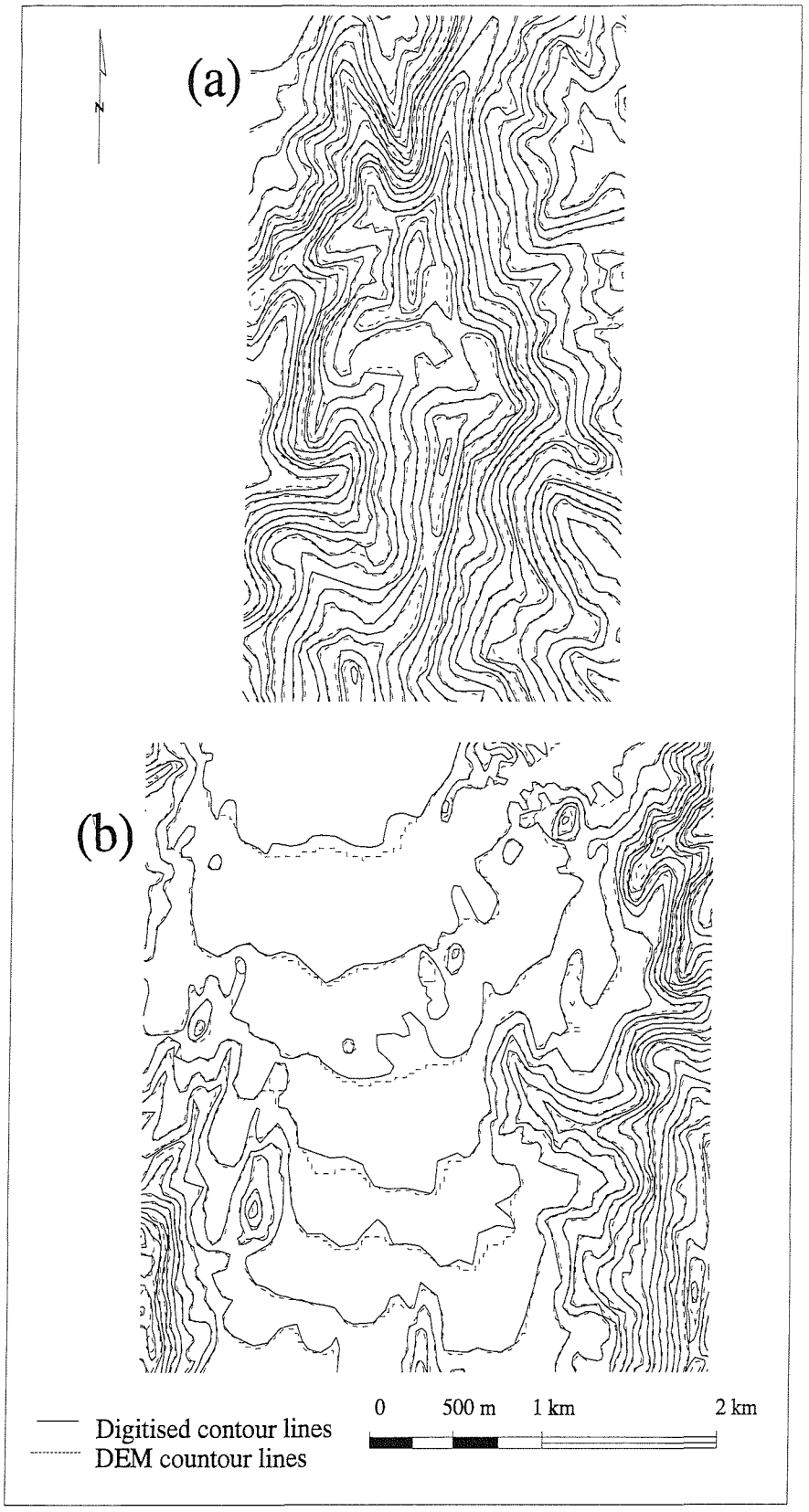

Figure 3.9 Comparison between the contour lines generated from the DEM and the original digitised contour lines (a) in a steeply sloped area, (b) in a gentle gradient area.

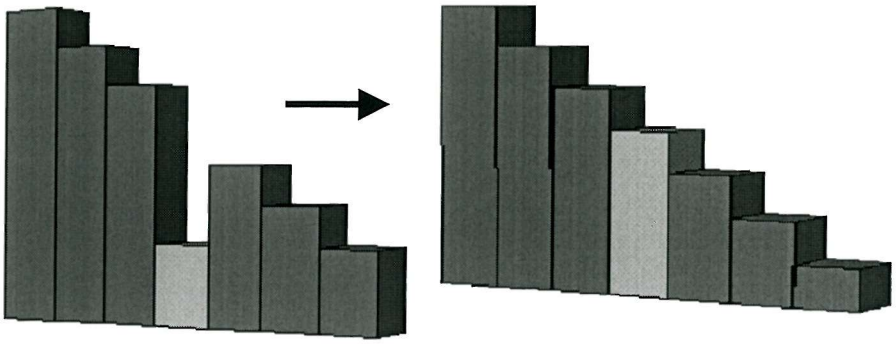

Figure 3.10 Fill Sinks Algorithm

The algorithm of drainage enforcement proceeds by first signalling as a sink any grid point of elevation that is equal to or lower than the elevations of its immediate neighbouring points in a 3 by 3 window. Each sink is assumed to have at least one saddle point in its vicinity. A saddle point is defined as the grid point that 'has at least two immediate neighbour points strictly higher than itself interleaved by a neighbour point no higher than itself' (Hutchinson, 1989). The algorithm associates saddle points with sink points by searching in the downslope direction out of each saddle point until reaching a sink point or the grid boundary. This is illustrated in Figure 3.11 where saddle points A, B, C, D and E are associated with the sink point S1. Chains are then inserted to link between the sinks. These chain links start at a high elevation sink and continue through the associated saddle point until reaching a lower elevation sink channel link or intersecting with another channel link.

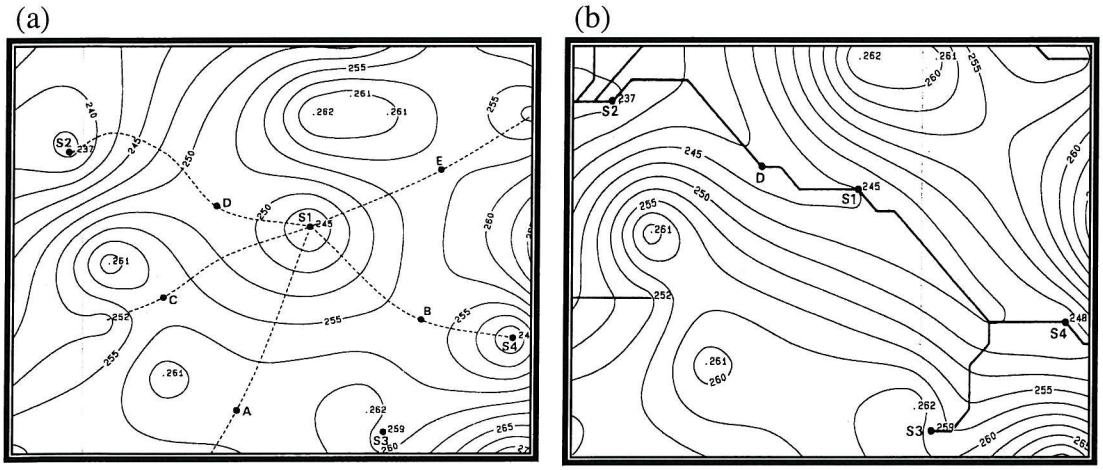

Figure 3.11 (a) Associating sinks with saddle points via flow lines (indicated by dash lines), (b) results of the drainage enforcement (After Hutchinson, 1989).

Figure 3.11 shows two channel links, the first between S1 and S2 via the saddle point D, while the other one starts at S3 and joins the chain linking S1 and S4. The final step in the process of drainage enforcement consists of opening the flow path between the sinks along their joining chains. Eventually, this implies that either the sink will be raised to a certain elevation that allows water to flow out of the sink or the saddle point blocking the passage will be cleared. The action taken depends on whether the sink or the saddle point is verified by an elevation data point.

There are four possible cases, the first case when the sink is associated with a data value but the saddle is not, then the saddle will be cleared. In the opposite case, when the saddle point is associated with elevation data but the sink is not, then the sink will be raised to a higher elevation than the saddle point. The third case occurs when neither the sink nor the saddle point is associated with an elevation data value, then both of them will be adjusted so that the flow can pass. The fourth case, when both of the sink and the saddle point are associated with elevation data values, then a choice has to be made: whether to open the passage or to maintain the sink. With any adjustment made, whether to the sink or the saddle, elevations of all the points along the chain in between will be linearly adjusted. The process of clearing the sinks is controlled by tolerances set by the user. These tolerances define the maximum depth of sinks that can be filled or the maximum height of saddles that can be cleared to open the flow path. Sinks of depths beyond the tolerance will remain in the DEM and will be flagged as sinks.

3.3.2 Flow directions

Once the DEM pits have been filled, a flow direction can be assigned to each cell in the elevation grid. Numerous algorithms have been proposed to determine flow directions from gridded elevation data. The simplest and most widely used method (often referred to as the D8 method) is described by O'Callaghan and Mark (1984) and Jenson and Domingue (1988). In the D8 method it is assumed that flow follows the path maximum descent and that each cell can only flow out in one direction, which known as the single flow algorithm. To assign a flow direction value to a cell, "the distance weighted drop" to each of the eight neighbouring cells is

computed by taking the difference in elevation values and dividing by $\sqrt{2}$ for a diagonal cell and one for a non-diagonal cell. The formula used is as follows:

$$S = \frac{\Delta z}{d} \tag{3.1}$$

Where

S : slope,

Δz : change in elevation between cells,

d : distance between cells.

The distance between cells is given as follows

$d = 1$ * cell size for the orthogonal cells

$d = \sqrt{2}$ * cell size for the diagonal cells

The flow direction grid has one of eight values for each grid cell. The direction of the flow from each cell flows to its nearest neighbour along 1 of 8 compass directions labelled in ARC/INFO as East = 1, Southeast = 2, South = 4, Southwest = 8, West = 16, Northwest = 32, North = 64 and Northeast = 1. The outflow grid for the elevation lattice was created by using the FLOWDIRECTION command, which is one of the grid hydrological functions. To provide an example, Figure 3.12 shows the outflow values used by ARC/INFO and the eight cardinal directions for outflow. Figure 3.13 shows part of Wadi El-Alam elevation grid, the numerical values assigned to cells in the flow direction grid and the flow directions symbolically with arrows.

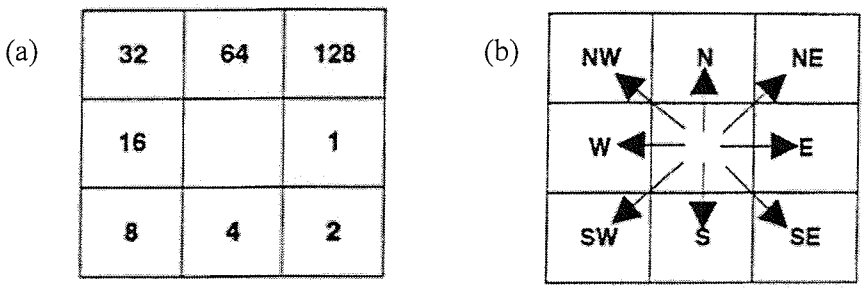

Figure 3.12 Surface flow routing based on a DEM using the 8-cell neighbourhood approach. (a) is the outflow values used by ARC/INFO (b) is the Eight cardinal directions for outflow.

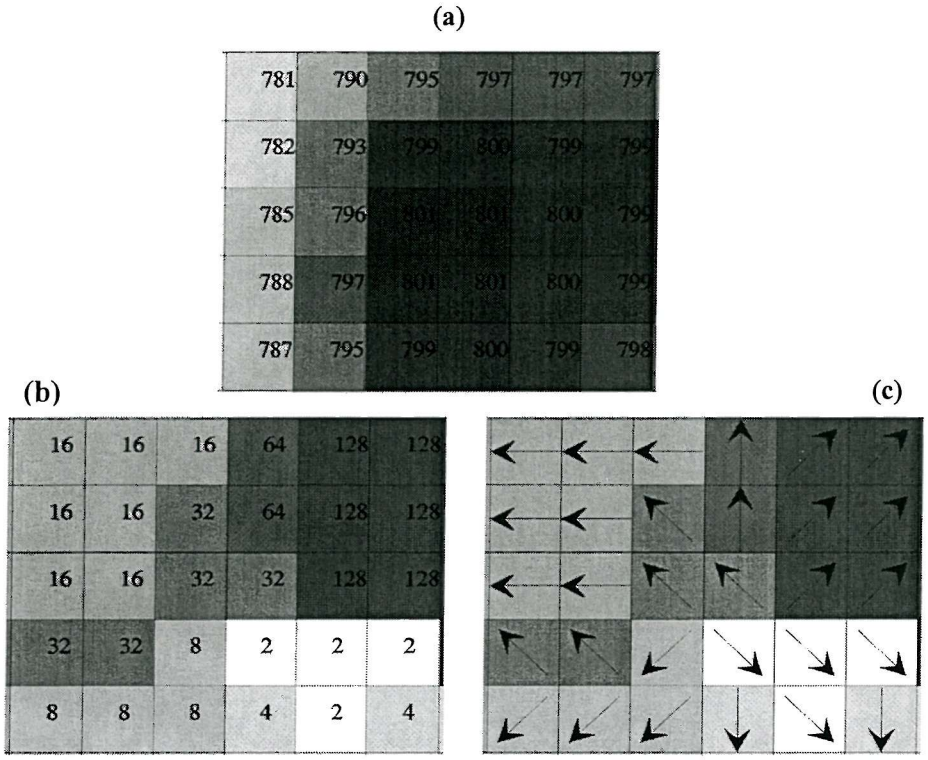

Figure 3.13 Assignment of flow directions of Wadi El-Alam basin by using the D8 model. (a) elevation, (b) flow direction grid value, (c) symbolic representation of flow directions.

3.3.3 Flow accumulation and deriving a stream network

Once the direction of flow out of each cell is known, it is possible to calculate the flow accumulation grid. The computation of the flow accumulation was carried out by using the GRID FLOWACCUMULATION function, which calculates the accumulated number of cells upstream (and hence, the upstream area). In other words it counts all the cells upstream of a given cell, so the flow accumulation values increase correspondingly as more and more cells join. Flow accumulation values range from 0 at topographic highs (ridges) to very large numbers (on the order of millions of cells) at the mouths of large rivers.

With the flow-accumulation grid, the stream network can be defined by specifying a threshold value above which water is said to become permanent flow. In other

words, all cells receiving flow from the threshold number of cells or above are said to be streams (Figure 3.14).

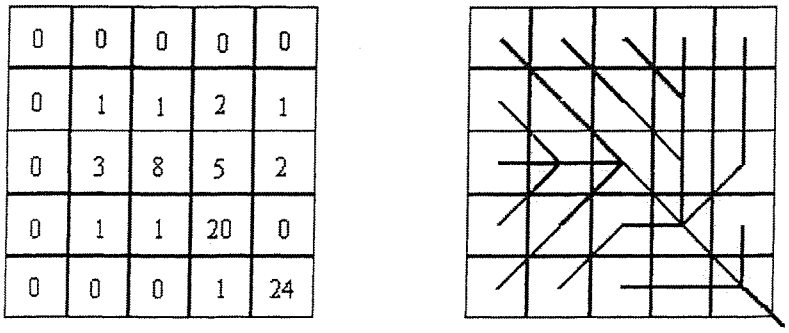

Figure 3.14 Raster-based functions for network delineation.

An important issue here was to decide at which threshold the channels should be delineated. For the Wadi Alam watershed a threshold of 30 cells (900 m^2) was chosen after a number of attempts. It was noticed that a threshold of a number less than or equal to 20 gave rise to a poor stream network of parallel straight lines, Figure 3.15 that do not reflect the reality. On the other hand, a threshold greater than 30 (e.g. 100, 200) resulted in an extremely low channel frequency and density. It has been pointed out by Huggins and Burney (1982) that the overland flow could only exist for the first 100 m along the flow path before the flow starts to concentrate into smaller rills. With the assumption that the contributing area could be idealized as a semi-circular area, 30 cells of 900 m^2 result in a maximum overland flow distance of 185 m. Thus, when a threshold of 30 cells (as a channel selection criterion) was applied on the flow accumulation grid, an output grid was generated in which cells with a number of cells upstream equal to or greater than that threshold were formed into a gridded network and those below it were given the Nodata value.

Ultimately, it is the channel network that is considered as one of the critical items in landscape delineation because it is the channel that carries the flood's water. Having the stream network grid generated, the Strahler drainage orders approach (Strahler, 1957) was used to create a new stream network grid with stream order (needed in watersheds delineation in the following section). This was accomplished

by using the grid STREAMORDER function, in which the channel order increases by one only when two tributaries with the same order meet at the confluence.

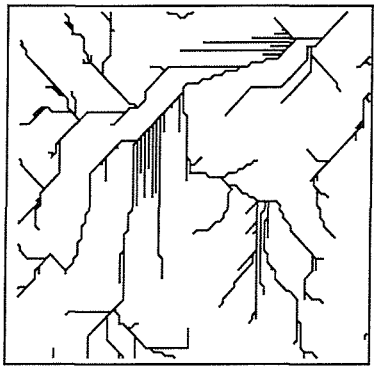

Figure 3.15 Parallel straight lines of the DEM-derived channel network.

The topic of stream order will be discussed in detail in chapter 4 but at this point it suffices to mention that for Wadi El-Alam the highest stream order is six. The stream order approach of Strahler was chosen as it can be easily applied and has been used in many previous studies (e.g. Patton and Baker, 1976; Ashmawy and Nassim, 1999) giving the opportunity to compare between the morphometric results. For a more realistic display, the grid representing the raster linear stream order network was converted to line coverage using the original cell centre. The STREAMLINE function was used instead of GRIDLINE command, as by the STREAMLINE it was possible for two adjacent linear features of the same value to be vectorised as two parallel lines instead of being lumped into a single line.

3.3.4 Watershed delineation

A watershed is the area from which water drains to a common pour point (outlet) as a concentrated drainage. For any selected point, the watershed contributes stream flow and/or runoff to that point. The automatic delineation of watershed boundaries relies mainly on defining all the cells that contribute flow to a given cell. Delineation process requires a flow direction grid and a set of pour points (outlets). Using a GIS, pour-points may be (1) selected interactively with a mouse, (2) selected automatically at the downstream end of each link in the drainage network created using an area threshold, or (3) identified using a co-ordinate file. An

example of the second method, which is automatically delineating a watershed for each link in a drainage network, is illustrated in Figure 3.16. This figure shows cells tagged as stream cells (a) based on the arbitrary criterion that a stream cell has flow accumulation greater than two, (b) is a grid in which each stream link is assigned a unique integer value and (c) shows same grid divided into six sub watersheds. Cells in the same sub-watershed are assigned the same grid-code.

Figure 3.16 (a) channel cells, (b) channel link grid, (c) sub watersheds.

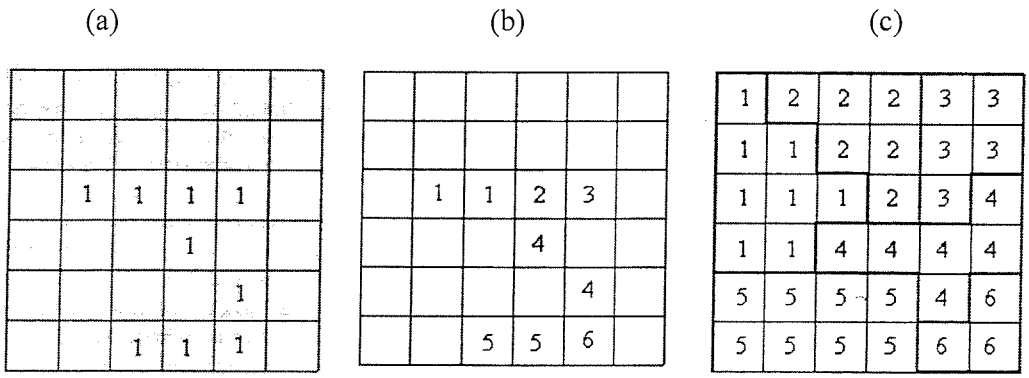

The sub-watersheds of Wadi El-Alam were delineated according to the following steps:

First: A new channel network was created with a threshold of 20000 cells in order to delineate only the sub-watersheds of stream orders equal to or greater than five. On using the STREAMLINK function, the resulting channel network grid was then separated into different zones of cells; each zone was assigned a unique value.

Second: the maximum flow accumulation in each zone was assigned as the value of all cells in the zone by using the GRID ZONALMAX function. Then the outlets were pinned down as those cells for which the flow accumulation was maximised in each reach by using the GRID CON function.

Third: The WATERSHED function was used to delineate the drainage basin and its main sub-basins by using both the outlet cells (which have been derived in the second step) and the flow direction grid. As a result, four sub-basins were produced in addition to the main basin trunk, which was found better to be further subdivided

into two smaller sub-watersheds. The sub-watersheds were converted to a vector coverage using the GRIDPOLY function.

3.4 VALIDATION OF DEM (V1) AND CONSTRUCTION OF A BURNED-IN DEM (V2)

3.4.1 Validation of DEM (V1)

The quality of the DEM depends on the quality of the original data used in its construction and the errors introduced by the interpolation method. In addition, the resolution at which the DEM was originally constructed controls the resolution of any hydrological features extracted from it.

Although the DEM lattice was filled to remove pits (depressions), some of the streamlines were found to be discontinuous (Figure 3.17 a), and some of the tributaries changed their channel directions near their outlets (Figure 3.18 1a). In fact, these faults represented a major issue facing this project. These faults were, firstly, due to the existence of some flat areas in the study catchment (Figure, 19). These flat areas were present as a number of contiguous cells of the same elevation in the DEM. Wadi El-Alam catchment contains very flat areas surrounded by mountains from most of the directions (Figure 3.19). The flat areas may exit in places of geological contact lines, which are considered as weak sites that can be eroded easily. They also may be considered as places of old lakes which were generated in previous humid periods (Ghoneim, 1995). Although the TOPOGRID function offers the LAKE sub-command, which can be used in flat areas, this sub-command can not be used in the present case. This is due to the fact that the flat areas that exist in the study basin are not only totally flat but also somewhat inclined towards the downstream direction. Secondly, the study area is characterised by sharp junctions between badlands slopes and adjacent alluvial surfaces, (Figure 3.20). These sharp junctions presented a difficulty to the used standard interpolation procedures. The sharp junctions are probably created by erosion concentrated at the base of the slope (a type of lateral planation), re-emergence of interflow, and changes of flow regime at the slope-alluvial-surface

junction (Hodges, 1982). In spite of the good agreement between the delineated channel network of Wadi El-Alam and the digitised one, the former is shorter and denser than the latter, Figure 3.18 (2).

To rectify the faults in the delineated channel network, a number of artificial spot heights, in all the flat and low relief areas, were added to the digitised point coverage (Figure 3.5). A new DEM was, then, generated and all the sinks were filled. The addition of more spot heights and the DEM generation process were needed to be repeated many times until the resulting channel network matched the digitised one. Although this approach was successful in improving the channel network, it was very time consuming, manual and more importantly not a systematic method. Therefore, it was found to be more reliable to rely on the so-called 'burning-in' method to delineate a correct channel network for Wadi El-Alam. This method is well established, systematic, reliable and easy to apply as explained in the following section.

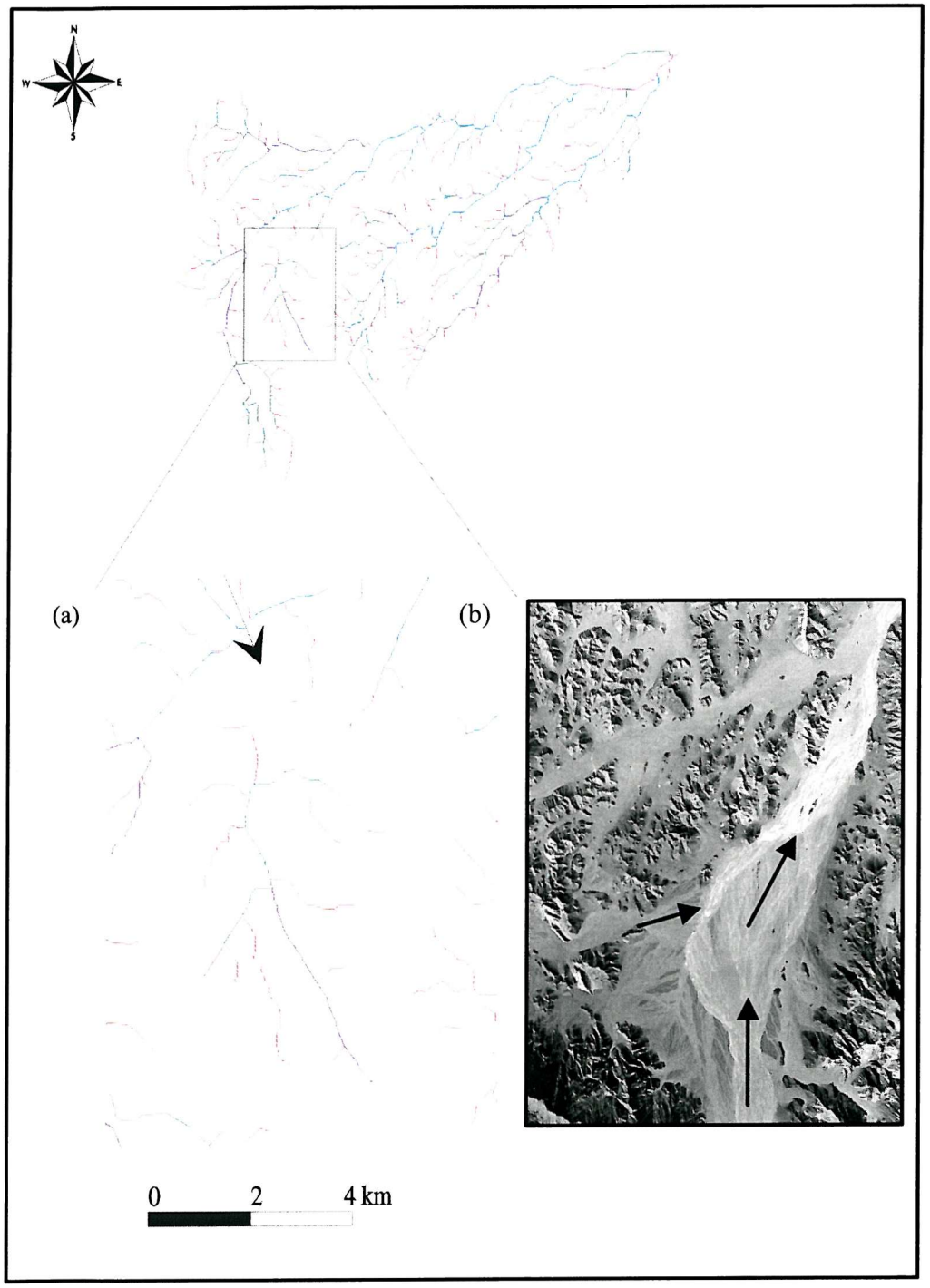

Figure 3.17 Channel discontinuous in area of complexity (a) DEM derived network, (b) aerial photo of the study area, (the arrows indicates the runoff direction).

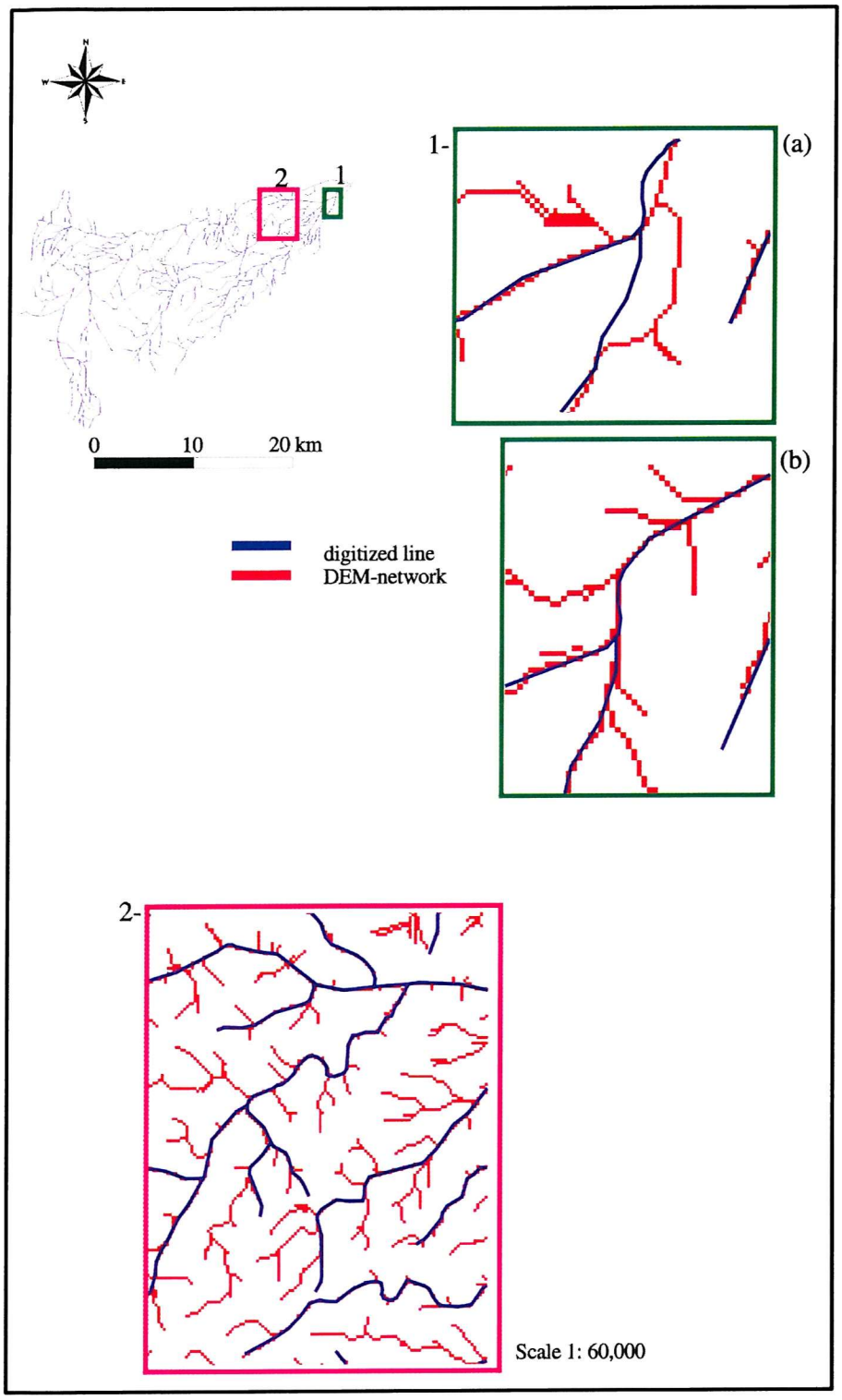

Figure 3.18 (1a) DEM derived channel network (1b) derived channel after adding the spot heights, in area of low relief. (2) Shows the derived network and the digitised one in an area of high relief.

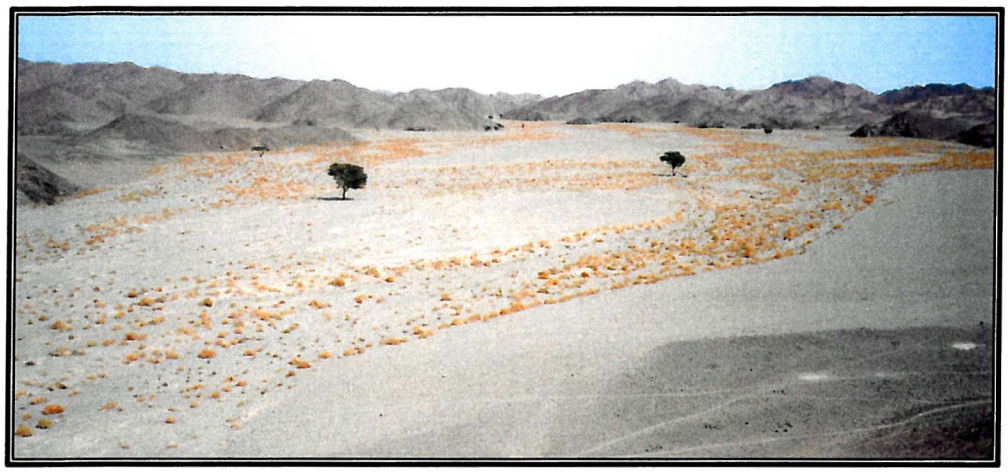

Figure 3.19 Typical flat area in Sukkari sub-basin, woody vegetation indicates the changing in the flow direction, as there is no detailed water body for the flow to follow.

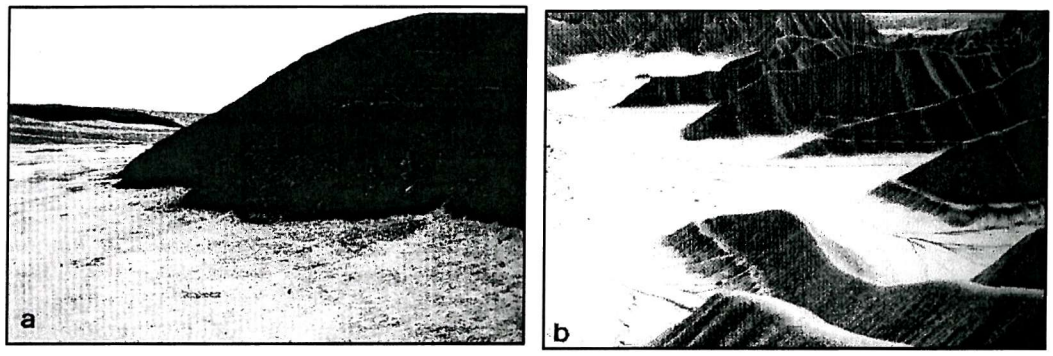

Figure 3.20 Sharp junction between steep badland slopes and Alluvial surface (a) and (b), (After Abrahams and Parasons, 1994).

3.4.2 Construction of a burned-in DEM (V2)

It was clear from the above section that the initial attempts at determining the stream network based on the DEM (V1) alone resulted in an improper channel network. Accordingly, it was found necessary to construct a new DEM (V2) good enough for delineating a correct channel network. One commonly used procedure of correcting for the channel direction error is a process known as "burning-in" developed by the University of Texas-Austin's Department of Civil Engineering. This method forces the computer model to follow a known stream path by raising the elevation of all the cells but those that coincide with the digitised channels. By doing so water is forced to remain in the streams once it gets there; however, it is not forced to flow towards them. This method accomplishes two things. First, it

ensures that a more accurate stream network will be created from the DEM. Second, it guarantees that once water has entered a part of the stream network, it will stay within the network and eventually flow off the DEM. Practically, the burn-in method consists of:

- Converting the line coverage of the digitised channel into a grid (with value of 1 in the channel cells and NODATA elsewhere). This grid must present continuous channels (no gaps), and does not involves short circuits.
- Adding a constant value to the DEM (in this case 200 m was used). Merging the two grids together, keeping the channel grid on top of the modified elevation grid, to obtain the burned DEM.

This was done in GRID module of the Arc/Info package using a macro due to Francisco Olevira 1996. Although, the "Burning in" method significantly improved the derived channel network and the sub-basins boundaries, it generated unreal infinite slopes surrounding the water bodies as a consequence of altering the landscape by digging the trenches.

3.5 SUMMARY

The main aim of this chapter was the construction of a Digital Elevation Model and a correct channel network for Wadi El-Alam. A DEM (v1) was generated from digitised contour lines and spot heights using a contour interval of 20 m and a grid cell size of 30 m. All the identified spurious pits were filled to ensure that the DEM was able to produce an uninterrupted movement of water across its surface. The 8D method was used to calculate the flow direction grid. Once the direction of flow out of each cell was known, it was possible, through the creation of a flow accumulation grid, to delineate the drainage network of Wadi El-Alam and consequently its main sub-watersheds.

Producing a correct channel network for the study basin was one of the major issues facing this project. Firstly, this is due to the existence of number of flat areas in the study catchment. Secondly, the study area (arid mountainous desert) contains

sharp junctions between badlands slopes and adjacent system. These sharp junctions presented a difficulty to the standard interpolation procedures. Some channel lines were found to be discontinuous and others changed their directions. To overcome these deficiencies a new DEM (V2) was constructed using the "Burning in" method. This method is equivalent to digging a trench wherever a water body exists. The trenches will not force the water to flow towards the streams, but will keep it from leaving the water bodies once it gets into them. This process improved the automated derived channel network for the study basin and the sub-basin boundaries. The "Burning in" method was found to be the simplest and quickest method of making a realistic digital channel network. Moreover, this method made less change to the original DEM. One of the drawbacks of this method is that it generates unreal infinite slopes surrounding the water bodies.

CHAPTER 4

Prediction of flash floods in arid lands using watershed characteristics

4.1 INTRODUCTION

According to Schick (1971), in desert regions a major flow happens nearly every three years, a widespread destruction event about every ten years, and a catastrophic one every 50 years. According to that the flash flood protection has to be considered as a most urgent necessity for many arid and semiarid countries. The protection against the hazards of the floods has to be based on quantitative grounds which need, apart from suitable analytical techniques, physiographic and climatic data, which are usually inadequate if not absent in most of the arid regions. As a result designers in such places have to resort to relatively crude methods, which predict hydrograph characteristics from measured morphometric parameters. Unit hydrographs, which are the hydrographs of one inch of direct runoff resulting from rainfall uniformly distributed over the catchments and of uniform intensity throughout a specified period of time, are computed from derived flow data for some gauged watersheds. The lag time, flow peak, and duration of these hydrographs are related to their geomorphic parameters, such as drainage area, density, frequency, slope and channel gradient. The Synthetic Unit Hydrograph (Dunne and Leopold, 1978) in a catchment can then be estimated from its physiographic features. This chapter summarises some empirical relationships between basin morphometry and hydrograph characteristics, and applies them in the Wadi El-Alam catchment using morphometric indices calculating using the DEM described in chapter 3.

4.2 MORPHOMETRIC PARAMETERS

The drainage basin has been the focus of research aimed at understanding the geometric characteristics of the master channel and its tributary network. Increasingly, studies have used the patterns of basin morphometry to predict or

describe geomorphic processes. For example, Patton and Baker (1976) and Costa (1987) indicated that drainage basin characteristics must play an important role in determining flash flood peaks in some basins. They tried to study flood peaks and their relationships to the morphometeric characteristics of basins in an attempt to find what factors contribute to flooding.

Every basin possess a quantifiable set of geometric properties (known as the basin morphometry), which define the linear, areal, and relief characteristics of the basin. Two general types of numbers have been used to describe basin morphometry or network characteristics (Strahler, 1957 and 1964). Linear scale measurements allow size comparisons of topographic units. The parameters may include the length of the stream of any order, the relief, the length of basin perimeters, and other measurements. The second type of measurement consists of dimensionless numbers, often derived as ratios of length parameters that permit comparisons of basins or networks. Length ratios, bifurcation ratios, and relief ratios are common examples. Table 4.1 shows the most commonly used linear, areal, and relief equations, and the numerical values derived from these relationships for Wadi El-Alam basin and sub-basins are tabulated in Table 4.2.

Once the stream network grid was generated and the main sub-basin boundary has been delineated (Figure 4.1) from the derived DEM (Chapter 3), the hydro-geometric information for Wadi El-Alam were extracted, and the geometric characteristics were quantified using GIS procedures.

From the morphometric analysis of Wadi El-Alam basin (Table 4.2), it is obvious that the study basin has a relatively large area of 406.9 km^2 and length of 37.29 km from its outlet to the most remote point on the divide. The value of the elongation ratio of 0.62 indicates that the basin is of a shape nearly close to the circular, which is characterised by short runoff distance compared with the other basin shapes.

The drainage basin network is in general well developed and highly integrated with total channel number of 1,759 and total channel length of 1,082 km. The drainage density is of moderate value of 2.6 km/km^2 with constant of channel maintenance

of 0.38. The drainage density of the study basin is not as high as it would be expected for an arid region basin, for two reasons. Firstly, the basin is underlain by hard rocks (Metamorphic and Igneous) highly resistant to the stream erosion and only relatively large channels can maintain themselves. For that reason, the network channels are of relative high frequency value of 4.32 especially in the first-order channel (basin magnitude) of value of 1333, see Table 4.3. Secondly, the network runs, in some places, over highly permeable materials (alluvial fans and coarse wadi bed), which enhances the infiltration process into the subsurface. As a consequence of the short time needed for the infiltration to occur, little water becomes available as surface runoff to maintain channels.

Table 4-1 Drainage basin characteristics and morphometric relationships.

Linear Morphometry	
Bifurcation Ratio	R_b = NO / NO+1
Channel length	C_L = maximum length form outlet to divide
Channel slope	MC_s = (elev85 - elev10) / 075 (C_L)
Channel sinuosity Ratio	$C_s = C_L / B_L$
Basin magnitude	B_M = total number of first-order streams
Areal Morphometry	
Drainage Density	$D = \sum L / A$
Constance of channel maintenance	$CC_M = 1 / DD$
Basin width	$B_W = A / B_L$
Basin shape factor	$S_F = B_L / B_W$
Elongation ratio	E_R = 1.13 (1/S_F) 0.5
Basin length	BL = line length from outlet to the divide
drainage area	A
Stream Frequency	$Fs = \sum N / A$
Relief Morphometry	
Basin Relief	B_R = Max Elev - Min Elev
Relief Ratio	$Rh = H / B_L$
Ruggedness Number	$R = D * B_R$
Basin slope °	S = rise / run
Hypsometric integral	HI = area under the Hypsometric curve

Table 4-2 Morphometric characteristics of Wadi El-Alam basin and its sub-basins.

MORPHOMETRIC RELATIONSHIP	Khirayjah	Sukkari	Aswad	Mb1	Mb2	Alam	W. El-Alam
Linear Morphometry							
Bifurcation Ratio	3.52	3.38	2.79	2.92	3.12	3.13	3.58
Main channel length (km)	30.06	29.27	18.86	11.69	19.17	27.53	55.34
Main channel slope (%)	0.20	0.19	0.29	0.45	0.28	0.20	0.11
Channel sinuosity Ratio	1.43	1.28	1.51	1.18	1.38	1.19	1.51
Basin magnitude	454	287	125	114	133	220	1333
Total channel length (km)	320	239	131	88	111	194	1082
Total channel number	598	382	171	143	175	290	1759
Areal Morphometry							
Drainage Density (km/km^2)	2.62	2.54	2.97	3.01	2.57	2.60	2.66
Constant of channel maintenance	0.38	0.39	0.34	0.33	0.39	0.39	0.38
Basin width (km)	5.80	4.09	3.54	2.95	3.11	3.23	11.08
Basin shape factor	3.62	5.60	3.53	3.35	4.47	7.15	3.31
Elongation ratio	0.60	0.47	0.60	0.62	0.53	0.42	0.62
Basin length (km)	21	22.95	12.49	9.87	13.90	23.09	36.71
Drainage area (km)	121.87	93.96	44.19	29.08	43.18	74.61	406.89
Stream Frequency	4.91	4.07	3.87	4.92	4.05	3.89	4.32
Relief Morphometry							
Basin Relief (m)	883	811	664	246	332	721	1196
Relief Ratio	0.04	0.04	0.05	0.04	0.02	0.03	0.03
Ruggedness Number	2.32	2.06	1.97	0.74	0.85	1.87	3.18
Average basin slope (°)	7	8.70	7.90	2.50	7	6.90	7.70
Hypsometric integral	0.49	0.41	0.54	0.32	0.61	0.37	0.34

According to the stream ordering approach of Strahler, the main trunk of Wadi El-Alam, (Figure 4.2), assumes the 6th order. The longest flowpath of Wadi El-Alam measured along the main channel from the basin outlet to the intersection of the main channel and the basin boundary has a length of 55.34 km. The longitudinal profile of Wadi El-Alam main channel, which is the plot of elevation versus distance along the channel, displays a strongly concave-upward shape that is steep near the source and gentle near the lower reach (Figure 4.3). Since stream discharge typically increases in a downstream direction, slope must decrease in order to minimise stream power. The decrease in slope in a downstream direction results in the concave-up longitudinal profile. Main channel gradient along the longitudinal

profile has a relatively high degree of 0.11% with low sinuosity value of 1.51 that may have no impact on channel gradient. The first and second order channels constitute alone 73.4% of the total basin channels with length of 786.6 km and bifurcation ratio of 3.58 (see Table 4.2).

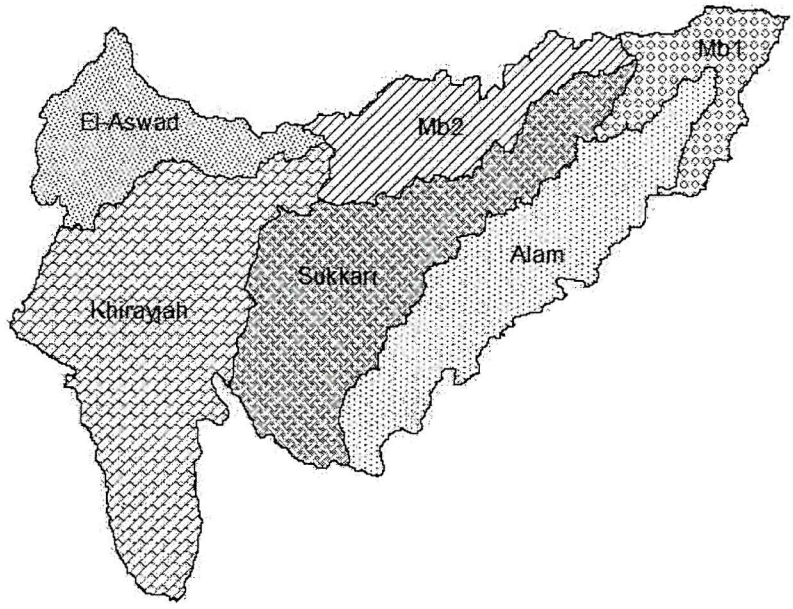

Figure 4.1 Main sub-basins of Wadi El-Alam.

Table 4-3 Network channel segments of Wadi El-Alam basin and its sub-basins.

Strahler order		Khirayjah	Sukkari	Aswad	Mb1	Mb2	Alam	W. El-Alam
order/1	total number	454	287	125	114	133	220	1333
	total length (km)	156.06	115.79	50.33	33.54	54.64	91.11	501.47
order/2	total number	104	74	35	22	34	55	324
	total length (km)	79.45	56.30	50.33	15.92	28.71	54.37	285.08
	bifurcation 1/2	4.37	3.88	3.57	5.18	3.91	4	4.11
order/3	total number	30	17	8	5	6	11	77
	total length (km)	47.32	35.19	14.37	15.08	7.87	17.70	137.52
	bifurcation 2/3	3.47	4.35	4.38	4.40	5.67	5	4.21
order/4	total number	7	3	2	1	1	3	17
	total length (km)	20.14	12.84	8.15	15.08	2.53	18.52	77.25
	bifurcation3/4	4.29	5.67	4	5	6	3.67	4.53
order/5	total number	2	1	1	0	0	1	5
	total length (km)	8.28	18.71	7.95	0	0	12.09	47.03
	biforcation4/5	3.50	3	2	0	0	3	3.40
order/6	total number	1	0	0	1	1	0	1
	total length (km)	8.66	0	0	8.05	17.32		34.03

The direction of channels in several places of the basin is greatly affected by geological structure (Figure 4.4). Faults strongly modify and control the courses of many tributaries. The rose diagram representing the characteristic orientation of the faults in the studied area is shown in Figure 4.4b. From Figure 4.4a, it is apparent that the channel network is in the directions of the East, North and Northeast with a ratio of approximately 49.5% relative to the other directions. These channel directions match to a marked degree the widespread trends of the area faults implying that the fractures commonly control substantial parts of the courses of the channel as well as their sharp bends making them of anomalous angle of junction (EL-Etr and Ashmawy, 1993).

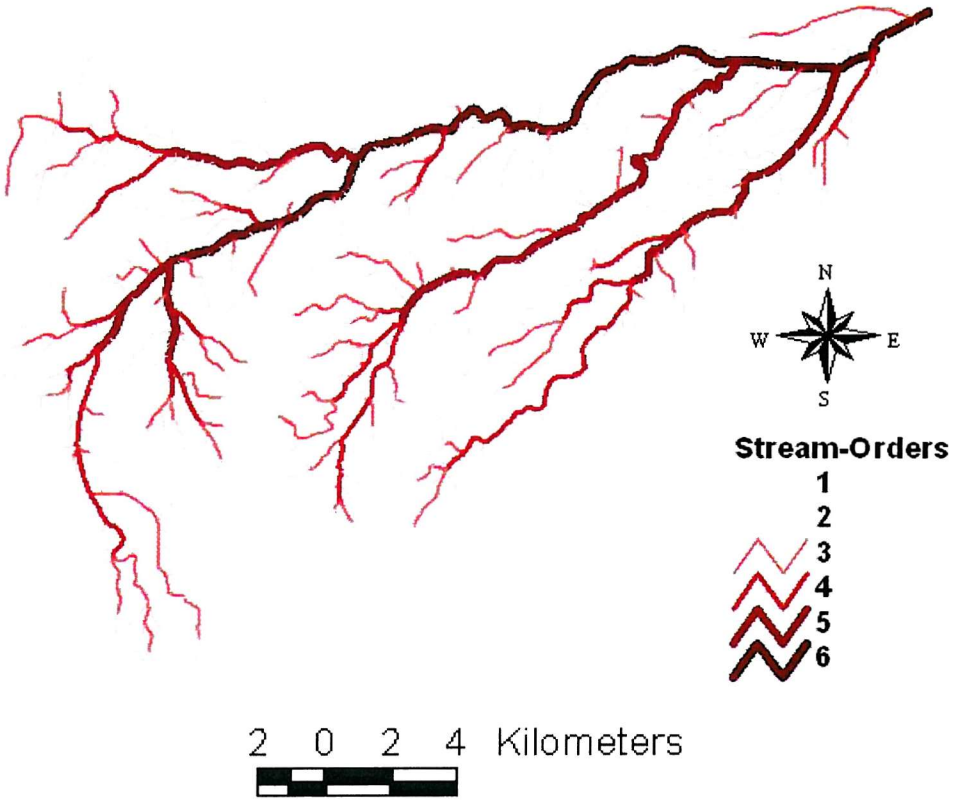

Figure 4.2 DEM-derived channel network orders (Strahler approach).

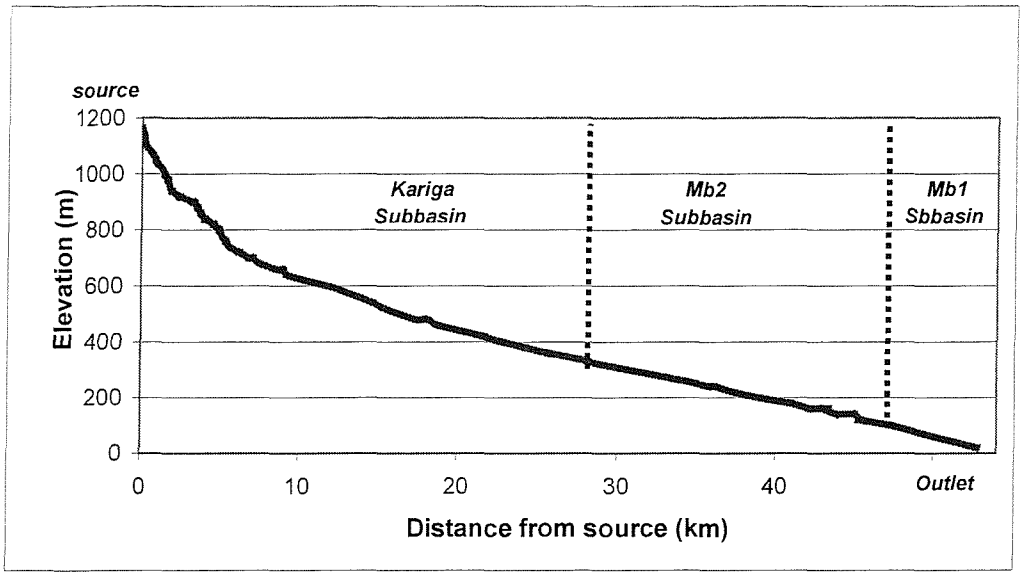

Figure 4.3 Longitudinal profiles of Wadi El-Alam basin.

Wadi El-Alam displays a steep valley-side slopes of 49° classified as a precipitous angle (Young, 1978), with average of 7.7°. This steep slope of the Wadi catchment, may be attributable to the resistance of the metamorphic rocks, which covers most of the basin area. For the sake of simplicity, different slopes in the studied basin have been grouped into five categories (Figure 4.5). The steep and very steep slopes are mainly concentrated in the upstream area. However, there are two other areas along the main channel coarse approximately 9 km far away from the basin outlet, They are relatively narrow of 100 meters in wide and have very steep sides giving them the gorge appearance.

The basin has relief of height up to 1196 m (Figure 4.6) and relatively high relief ratio of 0.032 km/km^1, which indicates overall slope of the basin surface, and short time of runoff concentration. Ruggedness number is relatively high with a value of 3.18 reflecting the fine-texture of the relief of highly dissected surface connected with the prevalence of first-order channels of total number of 1333. Because of the rocky nature of the Wadi surface, the feedback processes are retarded and instead of increasing the channel length, they conversely increase the number of the first-order channels. The ruggedness of the basin is also manifested in channel average hillslope gradients (see Table 4.2). The high ruggedness number of Wadi El-Alam

is associated with more youthful terrain of high relief with greatly dissected surface and deeply incised, narrow valleys and broad upland areas. This conclusion could be evidenced by the Hypsometric Curve, which graphically depicts the distribution of basin area relative to height, and the Hypsometric integral, that depict the area under this curve which by definition lies in the range 0 to 1. The Hypsometric curve of the Wadi under study is characterised by its concave-convex form with Hypsometric integral value of 0.34 (Figure 4.7), which indicates moderate stage of surface erosion, which marked by a high degree of uplands dissection.

Wadi El-Alam is a basin composed of six interlocking sub-basins. The most conspicuous sub-basins are Wadis Khirayjah, Sukkari and Alam, which discharge on the southern side of the main channel. These three sub-basins constitute 71.4% of the total basin area. They are of total channel number of 1270 and of total channel length of 753 km and stream order of five and six.

Highly contrasted morphometric parameters can be distinguished among the sub-basins of Wadi El-Alam. The elongation ratio varies from 0.42 (for the long and narrow sub-basin of Alam) to 0.60 (for the nearly equidimensional sub-basin of Khirayjah). The sub-basins are generally characterised by large numbers of short channels, which can be noted from the moderate density value and high frequency and bifurcation values. Values of drainage density are ranging from moderate (2.54 for Sukkari) to slightly high (3.0 for Mb1), see Table 4.2. This variation in the drainage density is greatly related to the rock type of the sub-basins. The sub-basin of Mb2, for example, runs over resistant rocks of Metavolcanics, Metasediments and Serpentines types, while that of Mb1 is underlain by weak sediment of limestone and quaternary deposits which can be easily eroded by the feedback process and, thereby, increasing the total channel length.

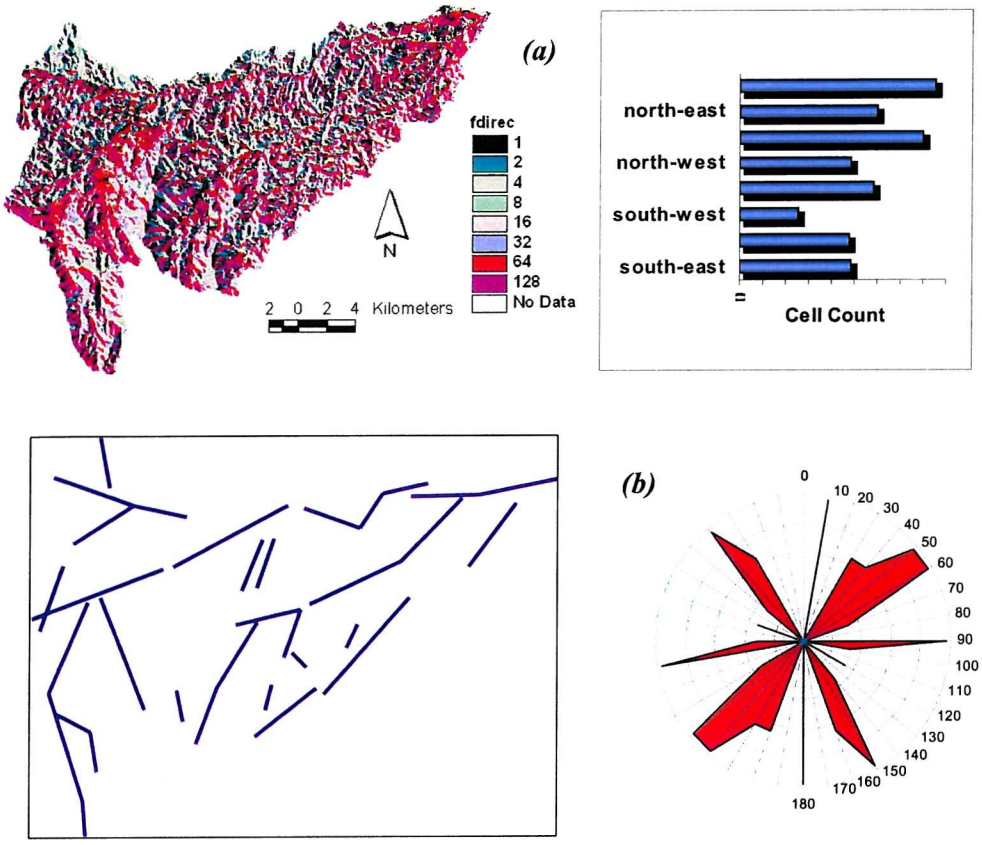

Figure 4.4 (a) The derived flow directions grid, and (b) The faults map with rose diagram of the fault directions of Wadi El-Alam.

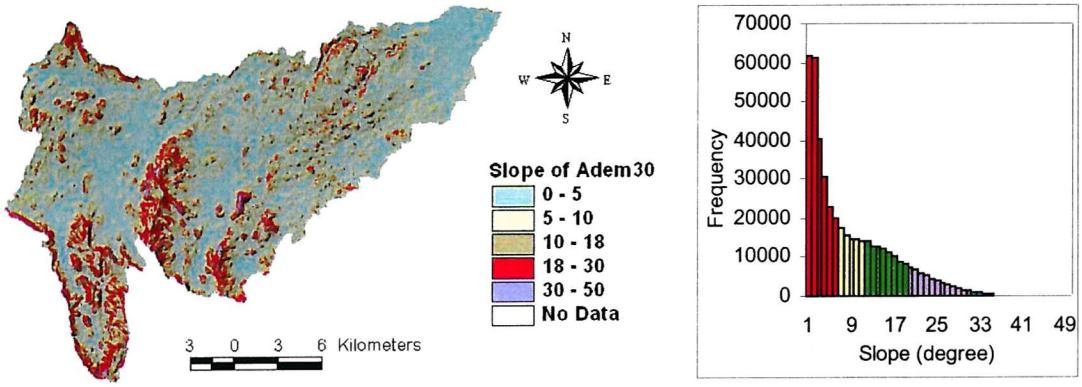

Figure 4.5 Slope categories with degrees.

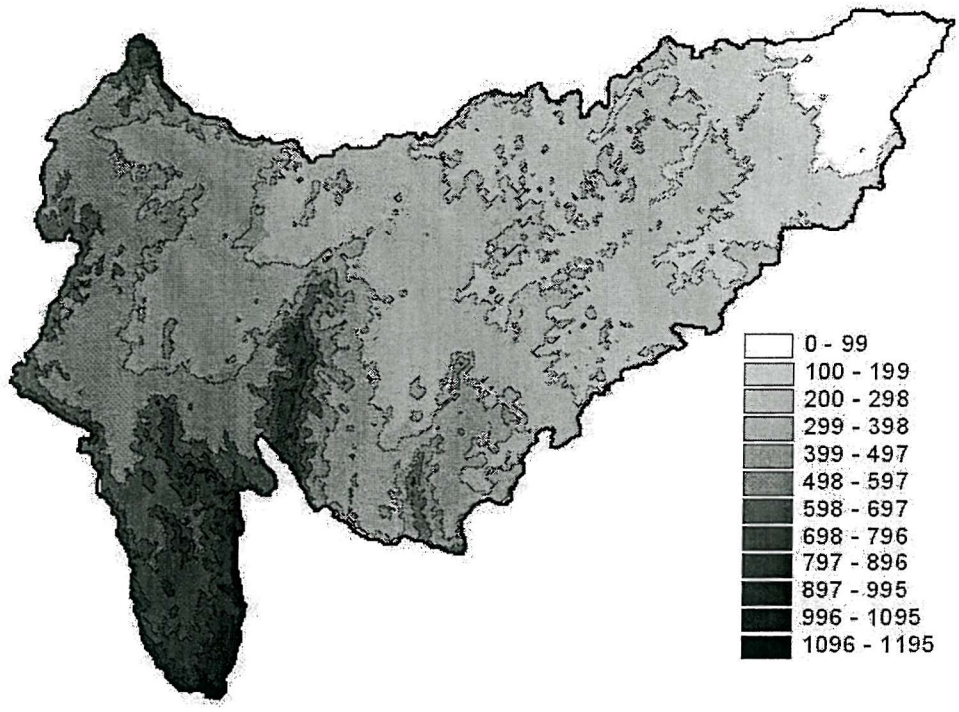

Figure 4.6 The DEM-derived elevation map of Wadi El-Alam basin.

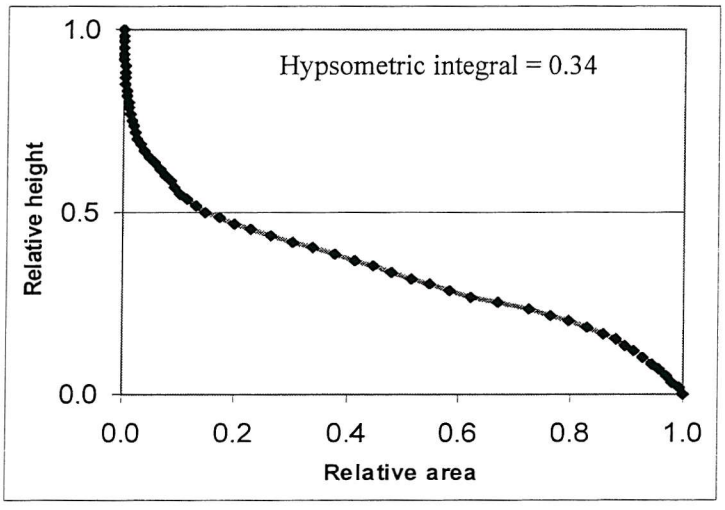

Figure 4.7 Hypsometric Curve of Wadi El-Alam.

The Wadi sub-basins have different Ruggedness numbers, which are relatively low in MB1 sub-basin of value of 0.74 and high in the rest sub-basins, such as Khirayjah of a value of 2.32. This means that high relief of dissected surface is predominated in the main tributaries (except Mb1) supporting the viewpoint that

the studied area is associated with more youthful terrain marked by deeply incised, narrow channels and broad upland areas which is characterised by the dominance of the active vertical channel erosion over lateral one, and hence more dissected badlands. As a further piece of evidence, three of the Wadi sub-basins (Khirayjah, Aswad and Mb2) are characterised by convex hypsometric curves (Figure 4.8) and by high hypsometric integral values of 0.50, 0.54, and 0.61 respectively. The high integral value of the three sub-basins indicates that the majority of their areas lie at comparatively high relief and are associated with an early stage of downward erosion and slope wall development.

The Mb1 and El-Aswad sub-basins are characterised by high gradient of the main channel (longest flowpath) of 0.45 and 0.29 m/km respectively. These high values relate to its short length from the sources to the outlets, which can be illustrated in its straight longitudinal profile (Figure 4.9). It also can be due to the straight shape of the main channels for the Mb1 sub-basin with low channel sinuosity ratio of 1.18. Low sinuosity indicates steeper channel gradient, while high sinuosity is associated with less steep gradient. On the other side, the Sukkari has relative low channel gradient with highly concave-up longitudinal profile, which may relate to its long distance from the source.

Basin relief is consistently intermediate in all sub-basins with relief ratios, of the range of 0.02 – 0.05. However, it is relatively higher for El-Aswad sub-basin of value of 0.49, due to the resistant Metavolcanic rocks, which cover a great part of its area, and gives rise to sharp mountain peaks that reach up to 937 m in height.

To sum up, Wadi El-Alam is a basin of a shape close to the circle (elongation ratio of 0.62) characterised by relatively dense channel network of value of 2.7 km/km^2 and total channel length of more than 1.759 km. It has a large number of short channels of low order discharge either in its sub-basins or directly in its main trunk giving rise to overland flow of short path length. The channels of the first three orders constitute 98.5 % of the total channel numbers and 85.4% of total channel length. The first order channels contribute alone by 46.3 % to the total length indicating that the basin surface is a highly dissected, of fine drainage texture, high

relief (up to 1196 m) and of high ruggedness number of value of 3.18. All these features indicate that during the rainfall event the runoff in El-Alam basin is assumed to reach the stream channels quickly across steeply surface with the result of flashy hydrograph response.

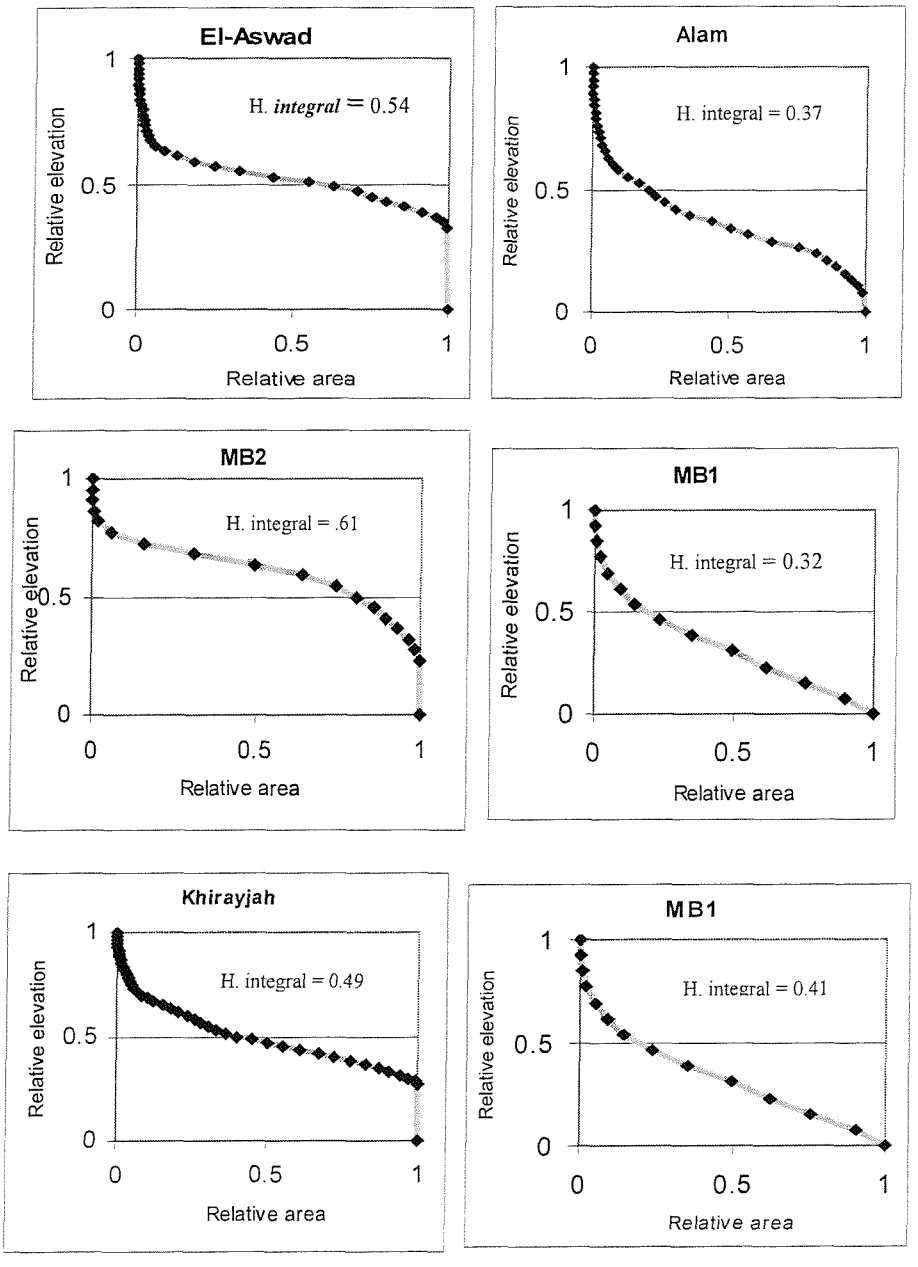

Figure 4.8 Hypsometric curves of the main channel of Wadi El-Alam sub-basins.

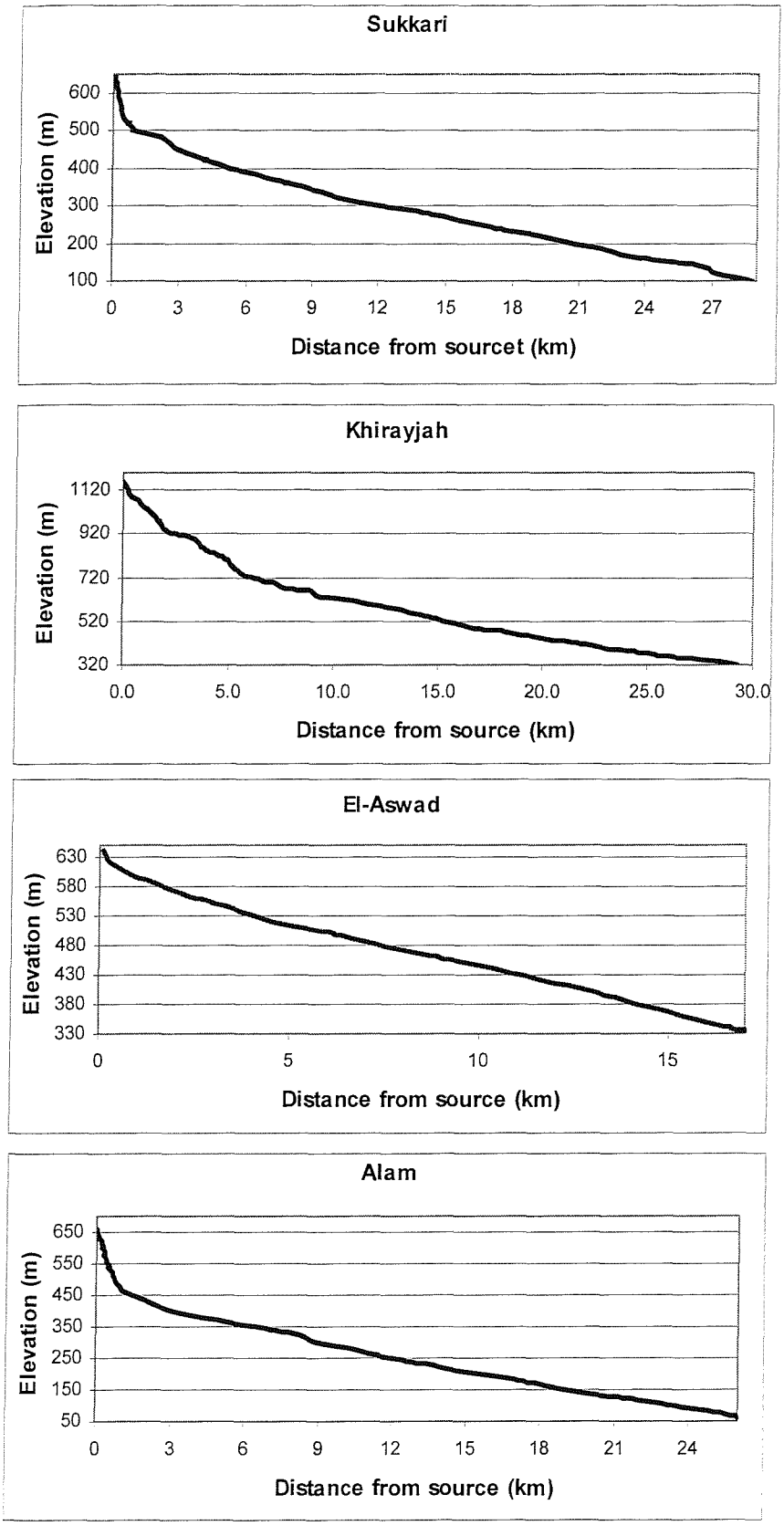

Figure 4.9 Longitudinal profiles of the main channel of Wadi El-Alam's subbasins.

4.3 HYDROLOGICAL PARAMETERS

There are numbers of traditional formulae that predict hydrograph characteristics of a drainage basin depending on its physiographic features. Three common empirical formulae have been applied to help understanding the hydrological response of the basin and sub-basins under study.

4.3.1 Lag time

Snyder (1938), who introduced the Synthetic Unit Hydrograph method, based an equation to predict lag time on data from the Appalachian Mountains. Snyder's method was developed for modelling areas ranging from 10 to 10,000 mile^2 (26 to 26,000 km^2). Snyder related the lag time (time from beginning of runoff to the peak, also termed as lag to peak) to the drainage basin length by:

$$T_p = C_t \left(L \times L_c\right)^{0.3} \qquad (4.1)$$

where

T_p = lag to peak (hours),

L = "Hydraulic length", flow path length from the basin outlet to hydraulically farthest point (miles).

L_c = "Centroid length" flow path length from the outlet to the basin centroid (miles),

C_t = coefficient varying from 0.3 to 8.0

The C_t is a lag factor coefficient that ranges from 0.3 for mountainous regions to 8.0 in lowland areas (Dunne and Leopold, 1978). A value of 0.4 was selected to represent the study basin, as used in other studies of mountainous basins (http://www.civil.mtu.edu/projects/watershed/other_river/.../north_gis_4.htm). The centroid of the basin is determined with the ZONALCINTROID Grid function.

Another empirical formula for determining basin lag time is introduced by Hickok *et al.* (1959), which correlates the lag time to the basin slope and drainage density as follows:

$$T_l = K_1 \left(\frac{A^{0.3}}{S_a \sqrt{DD}} \right) \quad (4.2)$$

where

T_l = lag time (minutes),

K_1 = coefficient dependent on units used (106),

A = catchment area (acres),

S_a = average slope of catchment (percent),

DD = drainage density.

Hickok indicated that the steeper portion of the watershed might control the time to peak of the hydrograph.

4.3.2 Peak discharge

The peak of a hydrograph depends on the amount of flow in the channel which depends on the amount of rainfall of the basin area, and the time to peak. Snyder (1938) developed the following empirical formula:

$$Q_{pk} = \frac{C_p A}{T_p} \quad (4.3)$$

where

Q_{pk} = peak discharge (cubic feet per second)

C_p = coefficient ranging from 370 to 440 with average value of 405,

A = catchment area (miles)

T_p = lag time (hours)

The coefficient C_p clearly depends highly on the rainfall and hence the range of coefficient values quoted by Snyder is not appropriate for calculating the absolute peak flow value outside the Appalachians. However, this equation has been used in this chapter with an arbitrary coefficient number of 1000 in order to extract the relative peak flow for the Wadi sub-watersheds.

4.3.3 Time of concentration

The time of concentration was defined by McCuen (1982) as the measure of the time for a particle of water to travel from the hydrologically most distant point in the watershed to the point where the design estimate is to be made. It is the time after which the runoff rate equals the excess rainfall rate. Chow (1988) showed that the time of concentration is the time at which the entire watershed begins to contribute: this is the time of flow from the farthest point on the watershed to the outlet. It can be approximated by applying the empirical formula of Kirpich (1940).

$$T_c = 0.0195\, L^{0.77}\, S^{-0.385} \qquad (4.4)$$

Where

T_c = time of concentration in minutes,

L = maximum length of flow in metres.

S = basin gradient in metre per metre.

The S can be determined by dividing difference in elevation between the outlet and the most remote point on the basin by the maximum flow length.

It is apparent that difference between the time to peak and the time of concentration depends highly on the geometry of the catchment and its channel network. However, the basin-channel geometry has less effect on the peak discharge, which rather depends mainly on the rainfall event.

4.4 FLOOD POTENTIAL

El-Shamy (1992) has introduced two hydrogeomorphometric geographical relations to differentiate between basins in terms of their flood potential. He used three of the basin morphometric parameters, the bifurcation ratio, the basin density and the channel frequency, to submit a simple management system, which would be suitable for all arid mountainous areas with scarce precipitation. This system enables categorising each basin to one of three types. The first type is basins of low

flooding possibilities and hence good groundwater potentialities; the second type is basins of moderate flooding possibilities and groundwater potentialities; and the third one is of basins of high flooding (high peak flow and not channel overbank flow) possibilities and low groundwater potentialities. This predicted system is used in this study in order to get a broad view of the character of the basin under study. The quantitative hydrogeomorphometric analysis reveals that the Alam basin and its all tributaries occupy domain B (Figure 4.10), indicating high flooding possibilities.

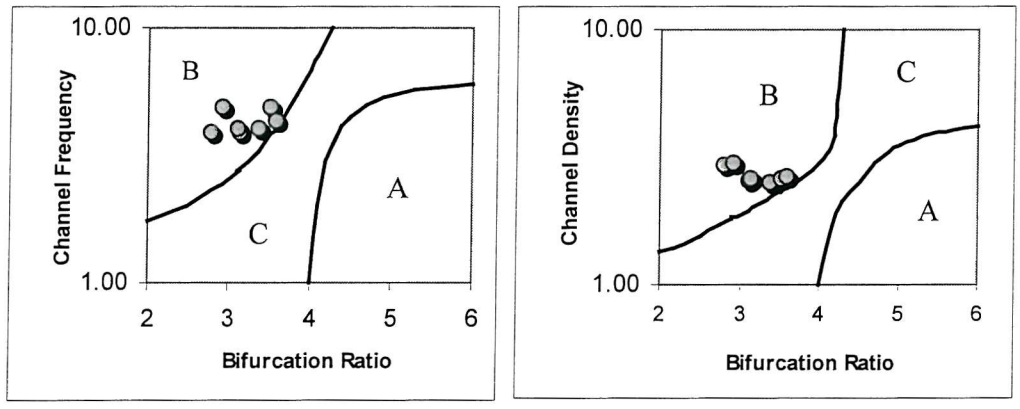

Figure 4.10 The quantitative Hydrogeomorphometric analysis of Wadi El-Alam basin and its sub-basins. A = low flooding possibilities and good groundwater potentialities, B = high flooding possibilities and low groundwater potentialities, C = moderate flooding possibilities and groundwater potentialities.

4.5 HYDROLOGICAL CHARACTERISTICS

By making use of some of the derived morphometric results some empirical formulae have been used to determine the hydrological aspects for the basin under study. Three hydrological empirical formulae (Table 4.4) have been used to estimate the basin hydrologic response of the flash flood on the assumptions that the rainstorm is of uniform intensity and covers all its sub-watersheds.

The calculated hydrologic parameters are presented in Table 4.5. It is apparent from Table 4.5 that the major contributions of flow are from the sub-basins of Khirayjah and Sukkari. The latter two sub-basins alone discharge about half (49%) of the total amount of the discharged water. The value of the lag time (calculated by using

equation 4.1), which is defined as the time elapsing between the peak of the rainfall and that of the runoff, indicates that the discharge hydrograph of Wadi El-Alam is a single peak hydrograph (Ghoneim *et al.* 2002). Within about 1.5 hours from the peak of rainfall, the peak discharge occurs more or less at the same time in each sub-basin. This result supports the finding that Wadi El-Alam is a basin of shape closer to the circle than to the rectangle. The huge peak discharges especially of Khirayjah and Sukkari sub-basins shed light on the vulnerability of destructive flood at these sites. From the dependence of lag time upon the basin area, it would be expected that the sub-basins of Khirayjah and Sukkari with the largest basin areas are of lag time markedly different from that of the other sub-basins. However, it is the high slopes of these sub-basins that give them lag times comparable to those of the other sub-basins of smaller areas.

Table 4-4 Empirical formulae for determining the basin hydrograph characteristics.

Time of concentration (min)	$T_c = 0.0195 * L^{0.77} * S^{-0.385}$	Kirpich formula, 1940
Lag Time (hr)	$L_t = C_t * (LL_{ca})^{0.3}$	Snyder formula ,1938
Peak Discharge (cfs)	$Q_p = C_p A / L_t$	Snyder formula ,1938

Table 4-5 Hydrologic aspects of Wadi El-Alam basin and its main sub-basins.

Basin name	Lag time (hr)	Time of concentration (hr)	$^{*}\Delta t$	Relative contribution to peak flow
Mb1	1.0	1.57	0.37	0.100
Mb2	1.29	3.00	1.31	0.119
aswad	1.26	2.18	0.52	0.124
sukkari	1.56	3.32	1.36	0.209
alam	1.50	3.28	1.38	0.180
khirayjah	1.54	3.34	1.40	0.283
Wadi El-Alam	2.36	6.20	3.44	1.0

$^{*}\Delta t$: The time between the lag time and the time of concentration.

From the values of the time of concentration in Table 4.5 it is clear that the runoff water originating in the most remote portions in the sub-basins of Khirayjah, Sukkari and Alam takes the longest time to reach the basin outlets. The difference between the lag time and the time of concentration for a given basin indicates how

late the runoff from the most distant parts of that basin reaches its outlet to contribute to the basin's peak discharge. The values of this difference Δt, see Table 4.5, in particular, for the sub-basins of Khirayjah and Alam indicate that the distant portions these basins contribute less to their peak flows. On the contrary, in the sub-basin of Mb1 of a high channel density of 3 km^{-1}, the runoff peaks as soon as the rainfall reaches its maximum indicating the synchronised contribution of all its parts to the peak flow. Although the contribution of the different parts of a basin to the peak flow is a complex function of various morphometric parameters, for the basin under study, one may conclude that it is somewhat dependent on the elongation ratio and the slope of the constituent sub-basins.

4.6 SUMMARY

With the aid of geomorphometrical relationships, the linear, areal and relief characteristics of Wadi El-Alam were calculated. The hydrological parameters such as the time of concentration, lag time, and peak discharge were roughly estimated. Through a geographical hydrogeomorphometric analysis incorporating morphometric parameters such as bifurcation ratio, channel density and frequency, initial estimations of the flood potential in Wadi El-Alam and its sub-basins have been determined.

CHAPTER 5

Land cover of Wadi El-Alam basin: A remote sensing study

5.1 INTRODUCTION

Hydrological models often require the basin loss rate as an important input parameter, which means the need for a detailed soil map for the whole area of study. Due to the unavailability of soil maps for Alam basin, the Soil Conservation Service (SCS) runoff curve number (CN) method can be used to predict water abstraction (losses) by infiltration. A CN is a value (ranging from 0-100) that represents the ability of the land surface to capture water. A low CN means that water easily infiltrates into the soil, leaving less for run-off. The CN method has been widely used in calculating water loss in arid and semi-arid regions (Sorman *et al.,* 1990, Eissa *et al.,* 1999, Gheith and Sultan, 2002). Because of its relative ease of use and reliance on easily acquired parameters, the runoff CN method is most useful in areas where intensive field studies are not feasible as in arid and semi-arid regions. This method estimates runoff using hydrological soil group, land cover and hydrological condition data. CN can be taken from published sources and tables produced by the Soil Conservation Service from which one can look up the appropriate CN value.

Since the CN is a function of both land cover and soil, a land cover map for the study basin must first be derived before modelling the basin runoff. This aim can be achieved if one uses remote sensing techniques for the following reasons.

- Remotely sensed images cover large areas and can be acquired rapidly with a spatial resolution that matches the degree of detail required for the study.
- Satellite sensor images eliminate the problems of surface access that often hamper ground surveys, and provide a perspective that is lacking for these ground surveys.

- Over large areas, interpretation of satellite images is faster and less expensive than conducting ground surveys (Floyd, 1987).

5.2 IMAGE PRE-PROCESSING

ERDAS IMAGINE package (Version 8.4) has been used in this study for data processing, modeling and analysis. The image data used to carry out this study was extracted from a Landsat 4 Thematic Mapper TM image recorded in 26th of March 1988 and additionally a 1: 50,000 scale topographic map (held by the Egyptian Military Survey – First edition 1989), and 1: 40,000 black and white aerial photographs. TM bands 1 to 5, and 7 with 30m resolution were used for the analysis, the thermal band (band 6) was excluded because of its coarser spatial resolution of 120 m.

When remotely sensed data are received from the imaging sensor on the satellite platforms they contain flaws and deficiencies. Basic transformations (pre-processing or image restoration) have to be applied on the raw image to recover the ground leaving radiance before performing data analysis reliably. To make physically based interpretations from remotely sensed data, a series of processing steps must be carried out. The approach used is based on five main steps: (1) geometric rectification of the TM image, (2) conversion from image Digital Number values to radiance, (3) correction for atmospheric and topographic effects, (4) supervised classification of the corrected image, and (5) accuracy assessment for the classified image (Figure, 5.1).

5.2.1 Geometric correction

Geometric registration involves precise transformation of the image from the sensor-based projection to an Earth surface-based projection. The image was geometrically corrected, see Figure (5.2), and geo-coded to the Transverse Mercator (TM) coordinate system (same as the projection of the produced GIS layers in chapter 3) by using 1: 50 000 scale topographic maps. Fourteen ground control points (GCPs) dispersed over the test site were selected both on the topographic maps and the TM image. Resampling was done by using a nearest

neighbour method to maintain the image Digital Numbers. The transformation had a root mean square error (RMS) of 0.7 indicating that the image was accurate to within one pixel.

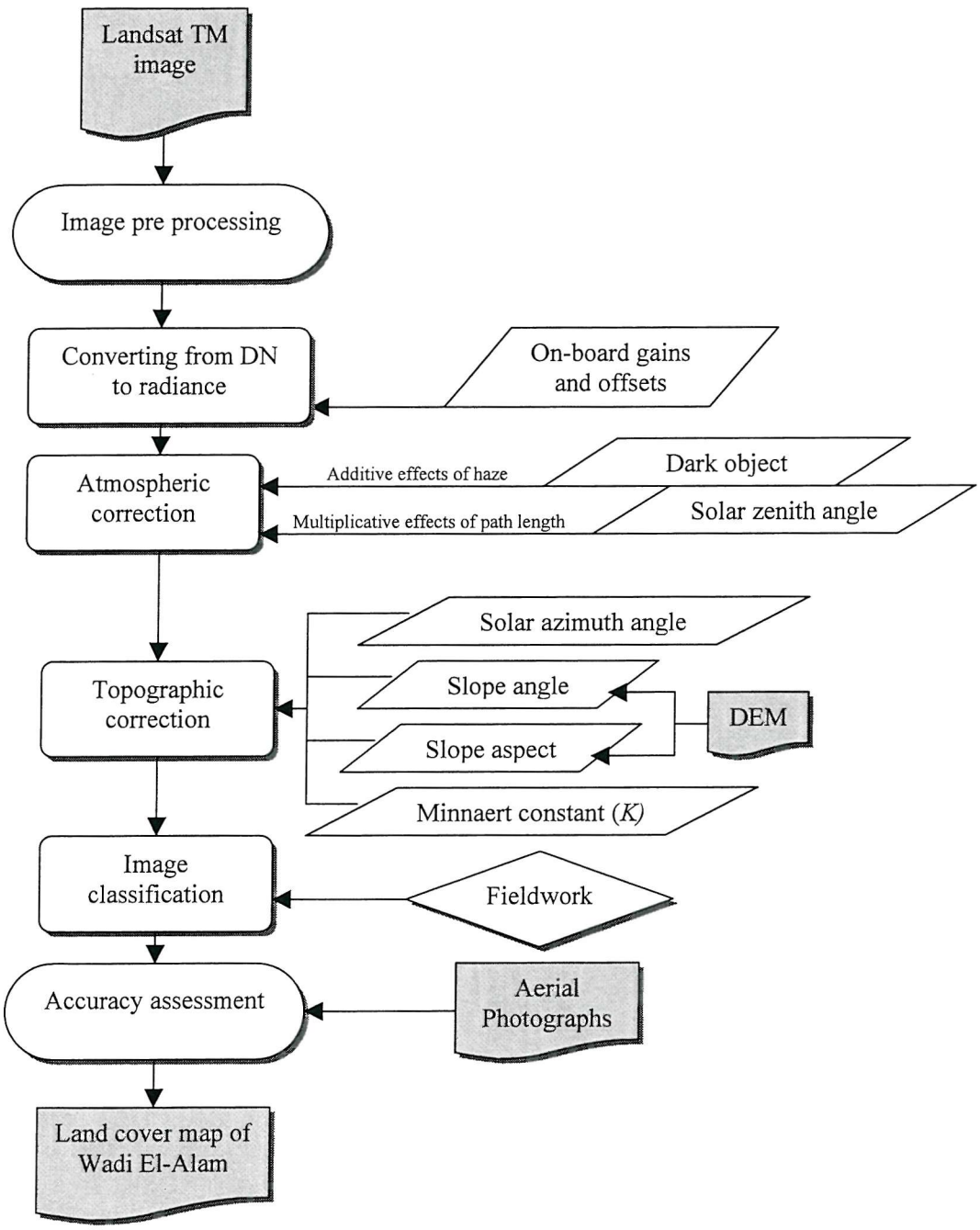

Figure 5.1 Schematic representation of the structure of this chapter.

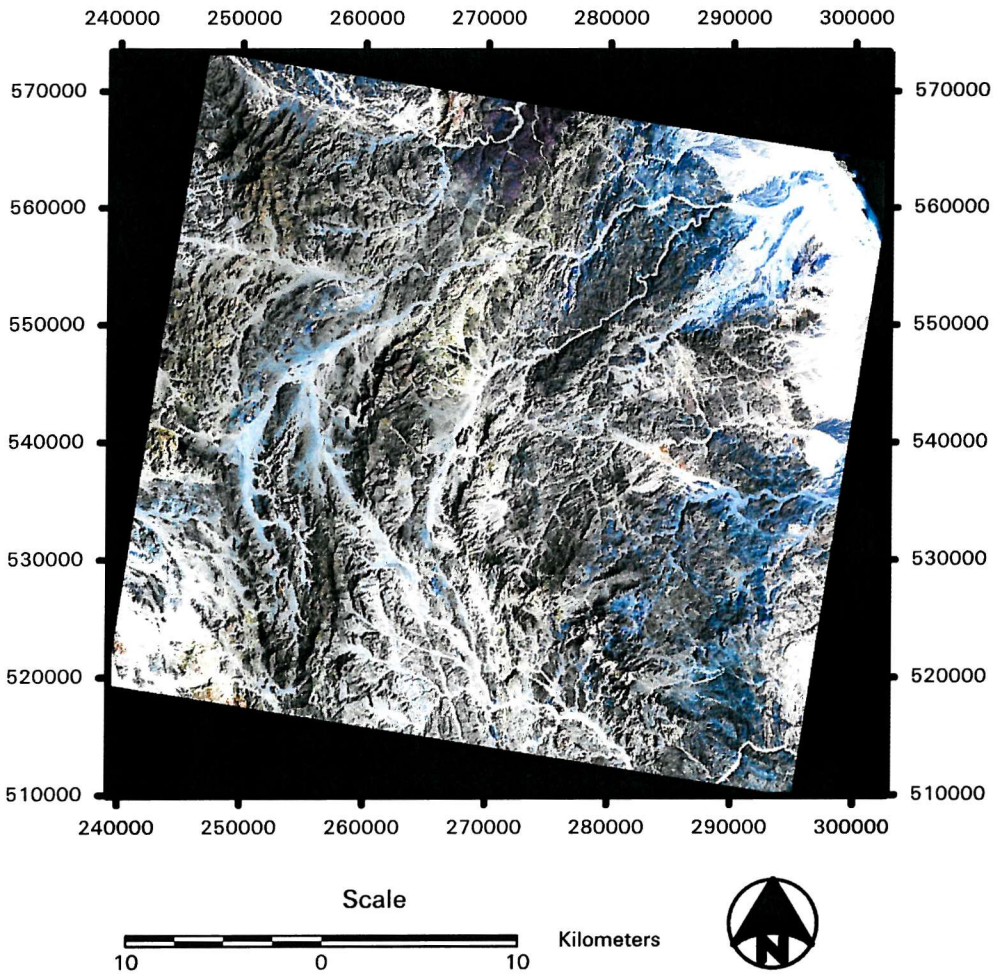

Figure 5.2 A subset of Landsat-4 TM (26 March 1988), with false colour composite RGB band 1,3,4 at sensor radiance (geo-coded to TM coordinate system).

An unsupervised classification was applied to the geo-referenced image to get general view about the surface classes and their distribution along the study area. This classification was based on the ISODATA algorithm. After studying the derived classes it was noticed that there is a class among these classes representing sites affected by relief shade (Figure 5.3). To calculate the total area of this false class, the entire study catchment has been clipped out from the image using the mask function and the total cells of this class have been counted. Since this shade class covers 4.2 % (with total cell number of 18874) of the total catchment, it was, therefore, found necessary to correct the image topographically before any further processing.

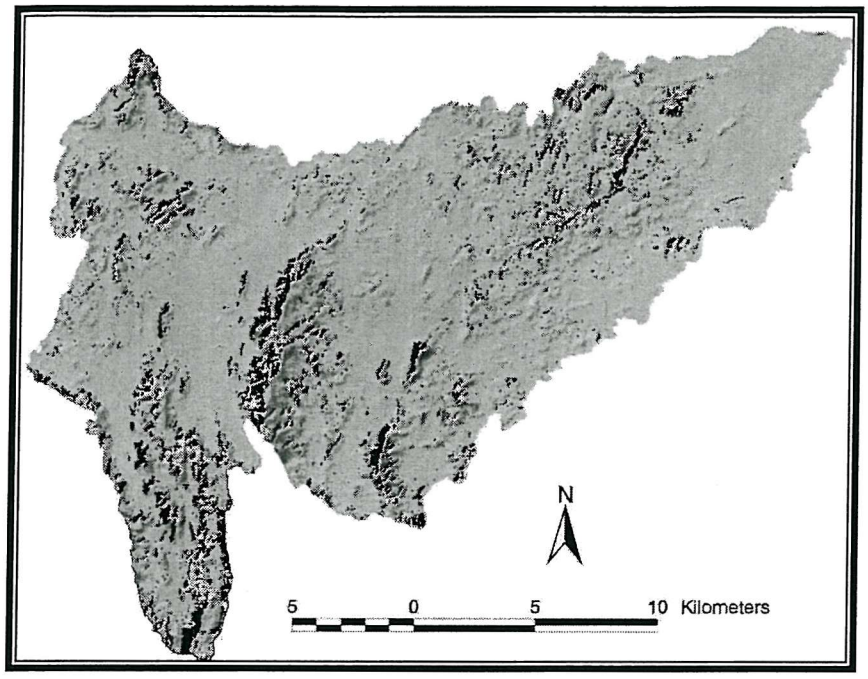

Figure 5.3 Cells affected with shade (cells are in black colour).

5.2.2 Radiometric correction

There are different levels of radiometric calibration. The first converts the sensor digital number (DN) to at-sensor radiances which requires sensor calibration information. The second is the transformation of the at-sensor radiances to radiance at the Earth's surface. That level requires information about the atmospheric conditions at the time and location of the image. The third is the topographic correction to get rid of the shade effect.

5.2.2.1 Sensor calibration

Typically, sensor calibration can be done by converting the received DN values (ranging from 0 to 255) into radiance. Conversion of DN to absolute radiance values is a necessary procedure for comparative analysis of several images taken in different dates or by different sensors. DN-radiance conversion can be done by correcting for gain and offset values of the particular spectral band and satellite used to record the data. Gain and offset values are normally given in the header file of the image.

Although the sensor gain and offset are often assumed to be constant throughout the sensor's life, they can and usually do change over time. Typical degradation in sensor performance with time is attributed to material deposition on the sensor optics due to out gassing from the system in vacuum. Several studies have attempted to quantify this degradation in TM sensitivity over time (Moran *et al.* 1995, Thome *et al.* 1997). A simple linear formula using calibration gain and offset, was used as follow:

$$L_{sat} = a * DN + b \qquad (5.1)$$

Where,

L_{sat} = Apparent at satellite radiance $W\,m^{-2}\,sr^{-1}\,\mu m^{-1}$

DN = Image Digital Number

a = Gradient of the transfer function, calculated from $(L_{max} - L_{min}) / DN_{max}$, where L_{max} is radiance value at DN 0, and D_{max} is 255.

b = Intercept of the transfer function with L_{sat} axis, L_{min}.

5.2.2.2 Atmospheric correction

The atmosphere influences the amount of radiance measured by a sensor. The atmospheric effects are wavelength-dependent so they vary between each waveband. The atmosphere will both scatter and absorb light reflected from the ground surface and, therefore, the atmospheric effect can be classified into multiplicative effects and additive (scatter) effects.

The dominant effect of the atmosphere is the scattering of incident radiation, which is an additive component effectively, a proportion of incident radiation is scattered back to the sensor without having interacted with the ground surface. This component of the measured radiance, therefore, carries no information and hence must be removed. The second effect, is the selective absorption of reflected radiation by the atmosphere, which is a multiplicative effect.

There are a variety of methods available to calculate the additive component of the atmosphere. However they require independent atmospheric data that are almost

never available for any given image. A robust approach to the problem is to estimate atmospheric parameters from the image itself.

The image-based procedure of removing additive effects, which has been used in this study, is often called dark object subtraction (DOS) (Chavez, 1988). This (DOS) method determines the dark pixel in the image with the lowest radiance value, which assumed to have a zero ground reflectance especially in the near infrared. Possible dark objects are deep, clear water, shadow and asphalt paving. In the present study, the deep water of the Red Sea was considered as the dark object. Reflectance of that dark pixel is estimated and subtracted from every pixel in the image as follows:

$$L_t = (L_{sat} - L_{hase}) \tag{5.2}$$

Where

L_t = Apparent surface radiance corrected for scattering $W\,m^{-2}\,sr^{-1}\,\mu m^{-1}$.

L_{sat} = Apparent at-satellite radiance $W\,m^{-2}\,sr^{-1}\,\mu m^{-1}$

L_{hase} = Radiance of dark object $W\,m^{-2}\,sr^{-1}\,\mu m^{-1}$

The Chavez, 1996 image-based COST model has been used in this study for reducing the multiplicative effects.

$$L_T = L_t / \cos(z) \tag{5.3}$$

Where

L_T = Apparent surface radiance corrected for scattering and transmission $W\,m^{-2}\,sr^{-1}\,\mu m^{-1}$,

L_t = Apparent surface radiance corrected for scattering $W\,m^{-2}\,sr^{-1}\,\mu m^{-1}$,

$\cos(z)$ = Cosine of the solar zenith angle (angle of the sun from vertical in degrees).

5.2.2.3 Topographic correction

Land cover classification in rugged terrain using satellite imagery is a difficult task as the apparent radiance measured by remote sensing systems is affected by the influence of topography on solar irradiance and by the atmospheric effects. Thus, to classify and map land cover from remotely sensed data, these effects have to be assessed and corrected. In areas of rugged topography, variable illumination angles and reflection geometry produced by different slope angles and orientations cause surfaces to receive differing levels of irradiance. Variation in illumination of similar cover types caused only by difference in slope and aspect is problematic for image classification. An often-used method to circumvent this problem is a classification of objects within smaller or broader illumination classes. Then training and test samples are taken in each illumination class separately and also the classifying is done individually. Only afterwards object classes are merged together. Another approach corrects the illumination variation as a preprocessing step. This second method was used in the present study.

A topographic correction converts the reflectance of scene elements on inclined topography to the reflectance of a horizontal element by making assumptions about surface properties. A perfectly diffuse surface that reflects radiation equally in all angles is referred to as a Lambertian surface. In an image of an unforested area, normally, scene elements are often assumed to be Lambertian, and a cosine correction is used to estimate surface reflectance. In the next section the Lambertian model, which has been applied in the present study, will be outlined.

5.2.2.3.1 Lambertian model

The cosine correction is often applied in flat terrain to equalize illumination differences due to the different solar positions. It is a strongly trigonometric approach based on a basic physical law assuming a Lambertian reflection characteristic of objects. The cosine law, however, only takes the Sun's position into account in the form of the solar zenith angle, assuming the solar constant and the distance between Sun and Earth to be constant for all scenes.

The following equation was used for topographic correction (Colby 1991; Smith *et al.*, 1980)

$$L_H = L_T / \cos i \qquad (5.4)$$

Where

L_H = corrected terrain surface radiance of flat surface at 90 degrees to the Sun $W\,m^{-2}\,sr^{-1}\,\mu m^{-1}$,

L_T = uncorrected terrain surface radiance $W\,m^{-2}\,sr^{-1}\,\mu m^{-1}$,

$\cos i$ = incidence angle, i (the angle between the solar rays and the normal to the surface in degrees).

The incidence angle is defined from the following equation

$$\cos i = \cos(90-\theta_s)\cos\theta_n + \sin(90-\theta_s)\sin\theta_n\cos(\phi_s-\phi_n) \qquad (5.5)$$

Where

i = the angle between the solar rays and the normal to the surface

θ_s = the elevation of the sun in degrees,

ϕ_s = the azimuth of the sun in degrees,

θ_n = the slope of each element in degrees,

ϕ_n = the aspect of each surface element in degrees.

The slope (θ_n) and aspect (ϕ_n) angles were calculated for the whole image from the DEM, while the azimuth and the elevation of the Sun, which are taken from the image header file, are 120.93° and 51.67°, respectively.

After applying this correction method to the image using the topographic normalized model of Erdas Imagine, it was found that the Lambertian correction was unsatisfactory, as it overcorrected the darker slopes and undercorrected the

brighter ones (Figure 5.4). Clearly, the assumption that solar radiation is scattered equally in all directions does not hold true for the study area and consequently the application of the non-Lambertian model becomes mandatory.

72	56	58	62	64	38	39	36	41
76	67	51	60	44	46	34	1636	43
60	62	56	57	24	27	27	0	40
59	63	57	37	19	51	0	0	50
60	69	36	626	26	28	42	44	54
42	20	28	0	24	39	64	84	56
32	26	0	0	32	78	90	84	77
20	0	0	27	65	88	84	72	70
423	0	0	77	73	73	67	65	63

Figure 5.4 Subset of the TM image after applying the cosine correction method. The brighter cells with high radiance values located in the shade western side while the darker ones with 0 values located in the sun facing side.

5.2.2.3.2 Non-Lambertian model (Minnaert)

Because of the finding that the cosine correction (Lambertian) is inappropriate in the studying area, the non-Lambertian correction method has been used instead. Minnaert (1941) proposed that the surface does not reflect incident solar energy uniformly in all directions. Instead he formulated the non-Lambertian model which takes into account variations in the terrain. This method allows the surface to favour certain directions of scattering over others, unlike the perfectly diffuse reflector assumed by the Lambertian correction. A common way to allow for non-Lambertian behaviour is to modify the cosine model to include a Minnaert constant (k). As in the following equation (Smith *et al* 1980, Colby 1991):

$$L_H = \frac{L_T \cos e}{\cos^k i \cos^k e} \qquad (5.6)$$

Where

L_H = Corrected terrain surface radiance $W\,m^{-2}\,sr^{-1}\,\mu m^{-1}$,

L_T = Uncorrected terrain surface radiance $W\,m^{-2}\,sr^{-1}\,\mu m^{-1}$,

$\cos i$ = Cosine of incidence angle in degrees,

$\cos e$ = Cosine of the exitance angle in degrees,

k = The empirically derived Minnaert constant.

Parameter k has become known as the Minnaert constant and is considered to be a measure of the extent to which a surface is Lambertian. The value of k varies between 0 and 1 when the k = 1 the surface is Lambertian. The smaller the value of k, the weaker is the influence of the quotient in equation (5.6), especially in areas with a cos i near 0, k increases the denominator and prevents a division by small values. Thus one can counteract to an overcorrection as obtained in the common cosine correction. The Minnaert constant k was found by using the empirical regression method. A log-linearised form of the equation is used to represent a $y = ax + b$ regression equation (Hodgson and Shelley 1993):

$$\log(L_H \cos e) = \log L_T + k \log(\cos i \cos e) \qquad (5.7)$$

Where,

L_H = Corrected terrain surface radiance $W\,m^{-2}\,sr^{-1}\,\mu m^{-1}$,

L_T = Uncorrected terrain surface radiance $W\,m^{-2}\,sr^{-1}\,\mu m^{-1}$,

$\cos e$ = The cosine of the slope angle in degrees,

$\cos i$ = The cosine of the incident angle in degrees.

It might be necessary to stratify the image into regions of similar land cover type and k constant calculated and applied to each stratum. Mather 1999, however, pointed out that if the purpose of performing a terrain illumination correction is to improve land cover classification, the problem becomes circular. In addition, each land cover type must include a large range of incidence and exitance angles to obtain a valid k. The simple approach, as the case in the present study, is to calculate an average k value for the whole image.

Equation (5.7) is solved for k constant by producing two images to represent the variables of X and Y. Values of k obtained with this method for all bands (see Figure 5.5) have been used in the Imagine topographic normalised model. Applying the Minnaert correction method derived an image that is free of shade and at the same time devoid of the problems which were raised previously by using the cosine method (Figure 5.6)

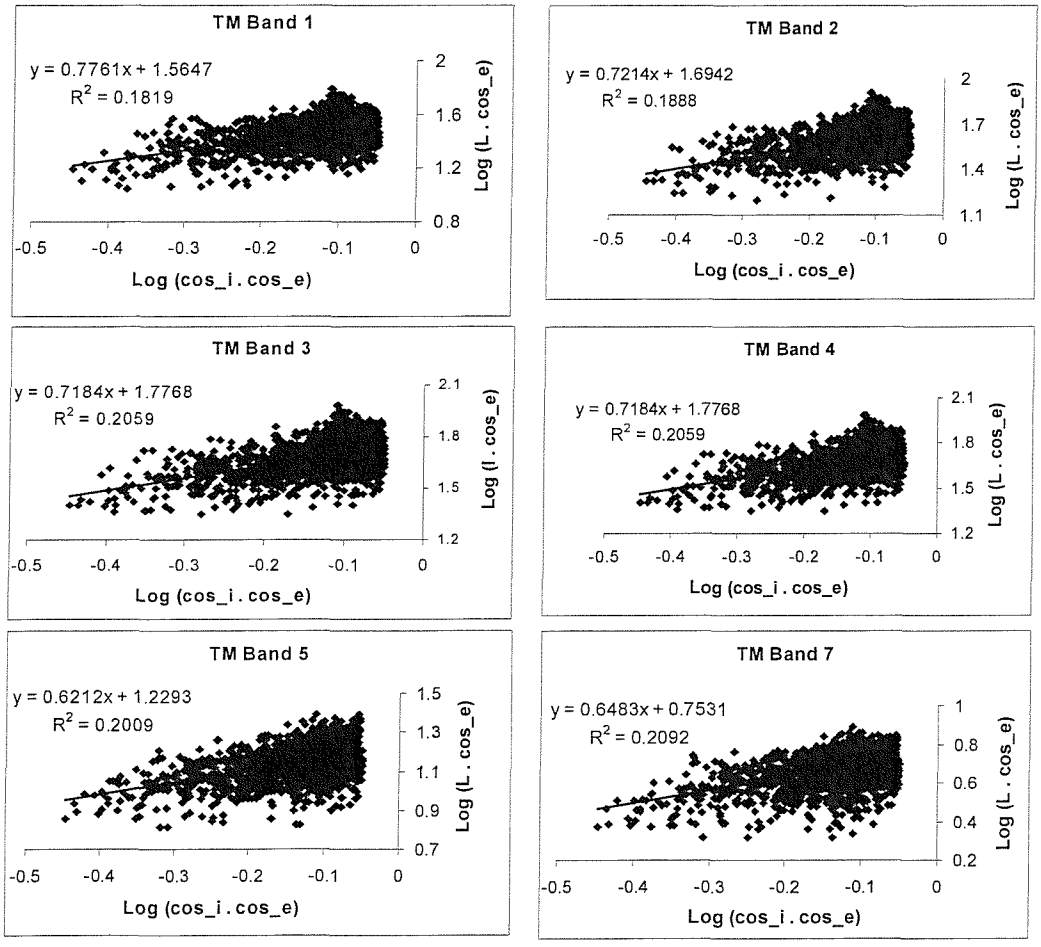

Figure 5.5 Linear regression for calculating k constant for Minnaert model.

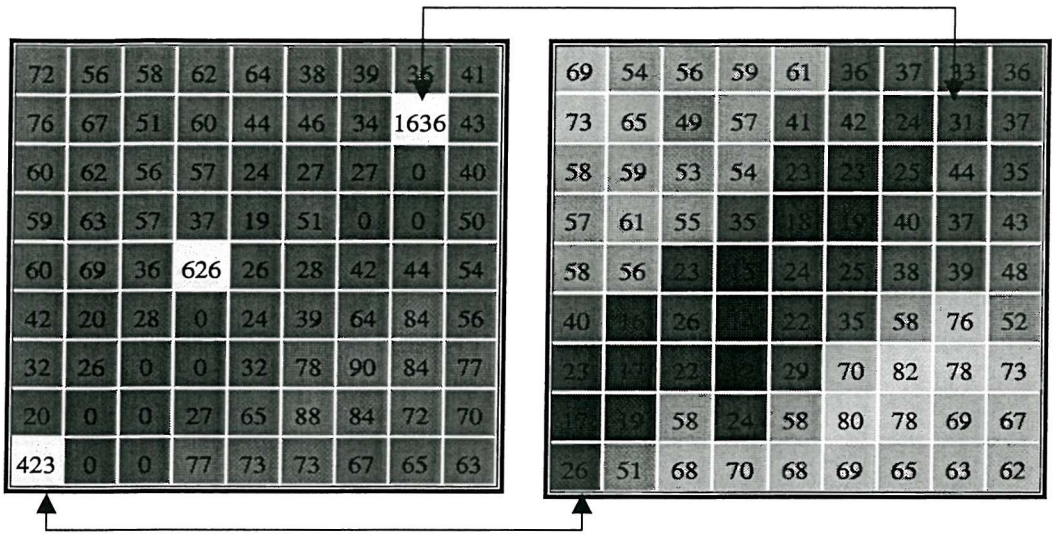

a- After the Cosine correction b-After the Minnaert correction

Figure 5.6 Cell values of band 3 after applying the two topographic correction methods. Cells of 0 value represent the eastern facing side, whereas, cells of very high values represent the western facing slope (shade side).

The results of applying the Minnaert method can be seen in Figure 5.7, which shows a reduction of the three-dimensional impression in the illumination corrected image. The effect of both the cosine and Minnaert methods on the spectral response is demonstrated in Figure 5.8, which showed a west east topographic profile (DEM) that runs parallel to the sun (in the eastern side). This Figure illustrates that the uncorrected radiance is too low on west-facing slope (shade side) and that the cosine method overcorrects these sides producing a reversed topographic effect (with value of 0) while it undercorrects the eastern facing side. The non-Lambertian model seems to perform better as it equalises the radiance on the two slope sides (see Figure 5.9).

TM topographic dependence can be evaluated by considering the correlation between the reflectance of a given band and the cosine of solar illumination angle (*i*), see Figure (5.9). Pearson's correlation coefficients before and after correction for all bands are given in Table (5.1). From this table, it becomes clear that the non-Lambertian Minnaert model is effective at removing the topographic effects on the remotely sensed response helping to ensure that the variation in image spectral

response observed was, as far as possible, a function only of land surface properties.

Table 5.1 Pearson's correlation coefficient for all bands before and after topographic correction using Minnaert constant *k*.

Band Numbers	Correlation Coefficients before correction	Correlation Coefficients after correction
Band 1	0.362	0.058
Band 2	0.384	0.058
Band 3	0.389	0.052
Band 4	0.382	0.026
Band 5	0.382	0.026
Band 7	0.393	0.020

5.2.3 Image Classification

Image classification is useful in digital image processing. It allows one to take a multitude of spectral band data and convert it to a value-added product that conveys the type of land cover in the study site. Land cover classes used in the present study were based on the LULC classification system (referred to as Anderson's land use land cover system) which is developed by Anderson *et al.,* (1976) for use with remotely sensed data in a variety of environmental applications. This system used a hierarchical structure with up to 4 levels. The broadest level, level I, divides land use into nine categories, whereas level II subdivides each category of level I into more descriptive land uses. For the purpose of this study, level II of the Anderson classification has been adopted (Table 5.2). Satellite TM images with aerial photographs have been reported (Floyd, 1987) as a suitable data source for producing the Anderson level I and II land use/cover classification map

There are many approaches to classify remotely sensed data. They all fall under two main topics: supervised and unsupervised classification. Supervised classification can be defined as the process of using samples of known identity to classify pixels of unknown identity (Campbell, 1996). In this process the user teaches the system how to recognize each class. It requires some input that may

derived from fieldwork, Air photo, maps and reports are obtained by the user before the chosen algorithm is applied (Mather, 1999).

Table 5.2 Land-use and land-cover classification system. (Source: Anderson *et al.*, 1976)

LEVEL I	LEVEL II
1. Urban or Built-up Land	11. Residential. 12. Commercial and Services. 13. Industrial. 14. Transportation, Communications and Utilities. 15. Industrial and Commercial Complexes. 16. Mixed Urban or Built-up Land. 17. Other Urban or Built-up Land
2. Agricultural Land	21. Cropland and Pasture. 22. Orchards, Groves, Vineyards, Nurseries and Ornamental Horticultural Areas. 23. Confined Feeding Operations. 24. Other Agricultural Land.
3. Rangeland	31. Herbaceous Rangeland. 32. Shrub and Brush Rangeland. 33. Mixed Rangeland.
4. Forest Land	41. Deciduous Forest Land. 42. Evergreen Forest Land. 43. Mixed Forestland.
5. Water	51. Streams and Canals. 52. Lakes. 53. Reservoirs. 54. Bays and Estuaries.
6. Wetland	61. Forested Wetland. 62. Non-forested Wetland.
7. Barren land	71. Dry Salt Flats. 72. Beaches. 73. Sandy and gravel other than Beaches. 74. Bare Exposed Rock. 75. Strip Mines, Quarries and Gravel Pits. 76. Transitional Areas. 77. Mixed Barren Land.
8. Tundra	81. Shrub and Brush Tundra. 82. Herbaceous Tundra. 83. Bare Ground. 84. Wet Tundra. 85. Mixed Tundra.
9. Perennial Snow or Ice	91. Perennial Snowfields. 92. Glaciers.

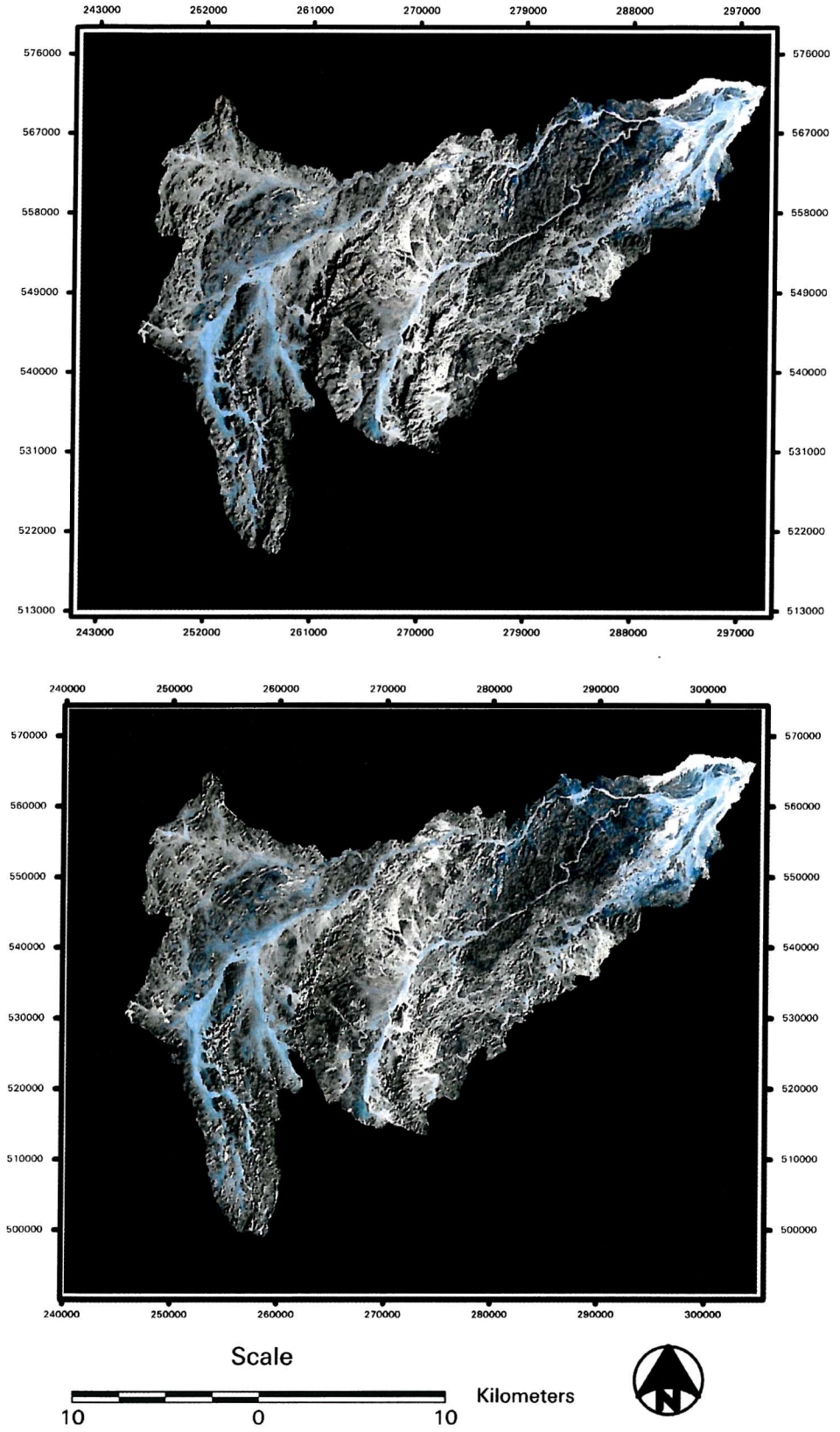

Figure 5.7 False color composite image (RGB = bands 2,3,4) of Wadi El-Alam before and after the Minnaert correction.

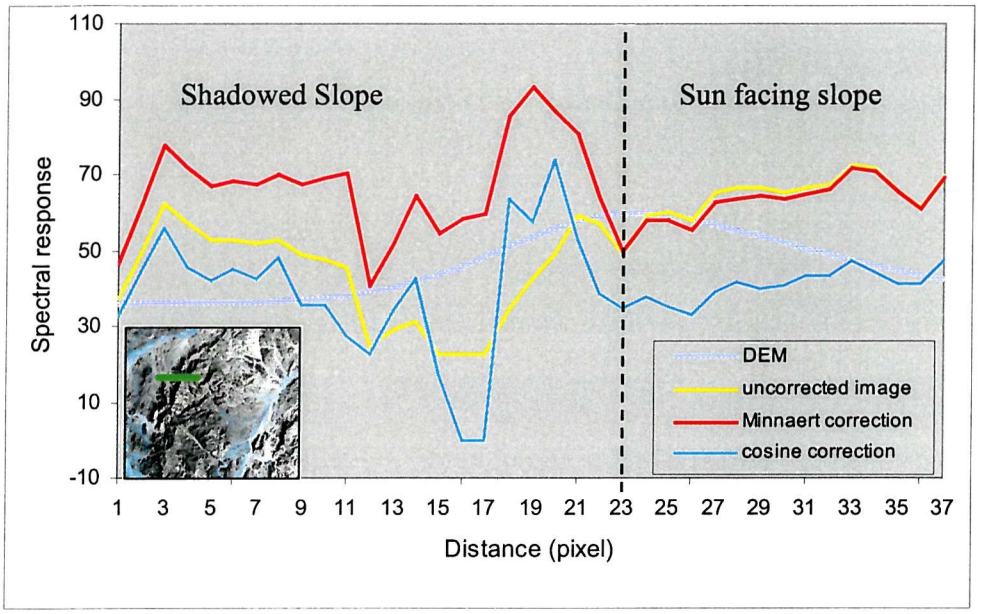

Figure 5.8 Effect of Lambertian and Non-lambertian topographic correction along a DEM profile parallel to the sun, TM (band 4). Profile location shown in green line.

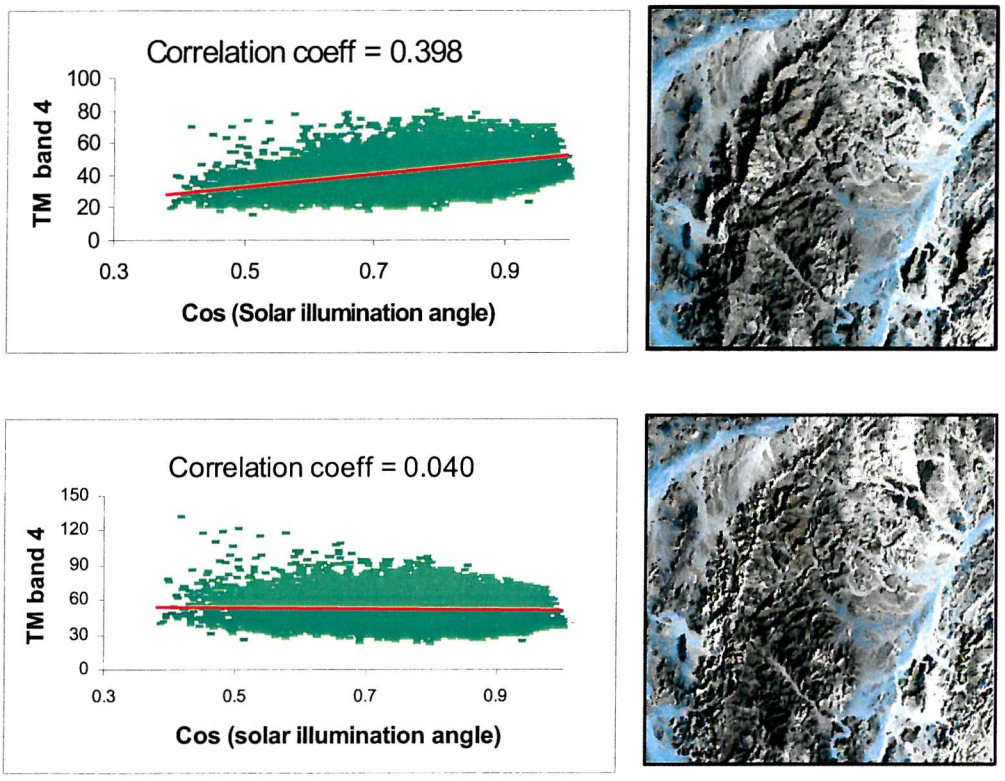

Figure 5.9 Correlation coefficient between TM band 4 and the cosine of solar illumination angle before and after Minnaert correction method.

One gives some characteristic examples of each class to the system. Then the system has to extract the spectral signature of each class from these examples, and to perform the classification on the whole image. Unsupervised classification, on the other hand, is the process of automatically segmenting an image into spectral classes based on natural groupings found in the data. This type of process does not rely on any help from the user. The system has to find by itself the spectral signature of each class, and to perform a classification. Usually, the only information provided by the user is the number of classes to look for.

From the aerial photographs of the basin under study, it is possible to distinguish easily four different land covers that might affect the runoff generation in Wadi El-Alam Basin: Firstly the old basement rocks (Igneous and Metamorphic), which cover a huge area of the basin; secondly the recent sediment rocks class which located in a small area along the coastal zone of the Red Sea; thirdly, desert pavements, which cover different area of the basin, are almost devoid of vegetation cover, and were generated on the gently sloping surface of old terraces, talus, pediment and parts of alluvial fans; and fourthly, channel networks, which dissect the basin surface and covers with poor desert shrubs. It was noted, during the fieldwork in February 1999, that these classes are separated into two different classes according to the nature of its top surface deposits. One of these two classes is covered with loose coarse deposits while the other is covered with less coarse but compacted materials. Apart from the above classes, it was observed during the fieldwork that some woody desert shrubs are sparsely distributed along some parts of the channel networks and this might be considered, so to speak, as a separate class of marginal effect from the runoff point of view.

Before performing a supervised classification on the image, a simple unsupervised classification was applied first using the ISODATA classification algorithm (Duda and Hary, 1973), which is the standard algorithm, found in virtually all image-processing packages. The key point of using the unsupervised method is to determine which classes could be best determined, for later use in the supervised classification. After several trials, it was found that 5 classes yielded information goes in line with that extracted from the aerial photographs. These 5 classes were

completed in 12 iterations at a 0.95 convergence level. The unsupervised classification image was, also, used as a preliminary guide in the fieldwork study.

To know about this rough grouping (classification) of the above land covers, the spectral reflectance for the different cover types that most prevail in the Alam basin, with the exception of the mountain classes, have been recorded by a hand-held Multiband Radiometer (Milton, 1980) during the fieldwork. The distribution of the measured spectral signatures of the different cover types can be visually inspected by making use of the three-dimensional feature space graph (Figure 5.10). In this graph, four cover types/classes can be easily identified. One of them that represents the woody desert shrubs is completely separated from the rest of the classes. The remaining three classes overlapping with each other. These overlapped classes, which are an indication of three different depositional surface covers in Wadi El-Alam basin, represents the desert pavements, unconsolidated wadi deposits and consolidated wadi deposits.

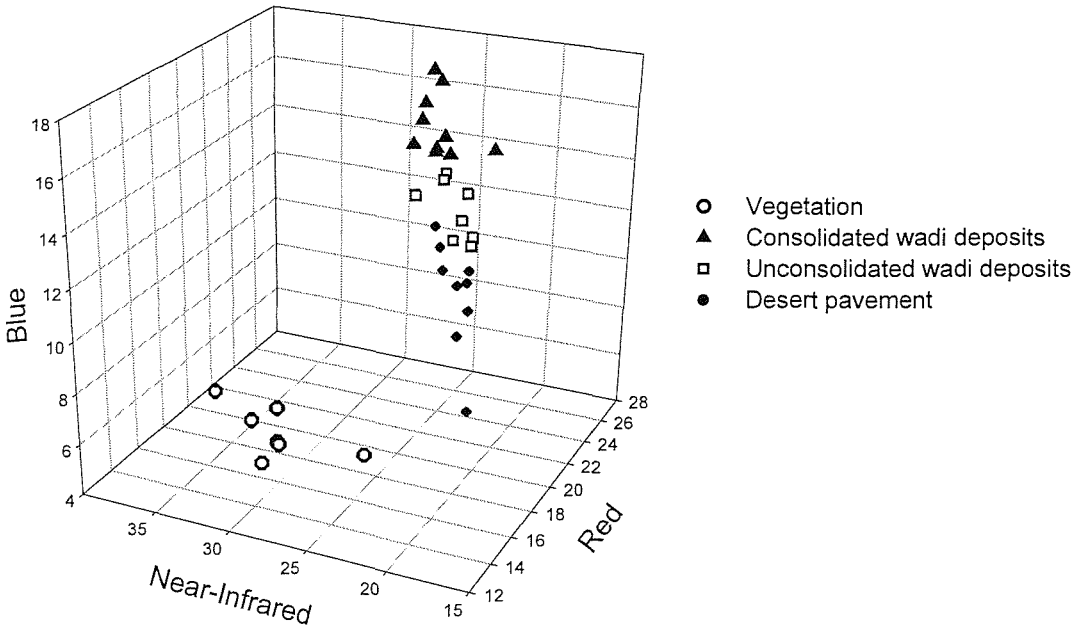

Figure 5.10 Distribution of the spectral reflectance of the surface classes in 3D Feature Space.

5.2.3.1 Supervised Classification

In order to classify an image into categories of interest, the classification algorithm needs to be trained to distinguish those categories. A total of 5 training sites were defined for each surface class. High quality training data are essential for accurate land cover classification of any sort. Extensive field reconnaissance throughout the entire area has been made in the winter of 1999 and 2001. As many training sites as possible were visited in each cover type as defined by a modified Anderson Level II categorization (Anderson *et al.,* 1976). The Global Positioning System (GPS) has been used to correctly match the location of the training sites to the corresponding points in the TM image data. These points were entered to the Arc/Info as a point cover using the GENERATE ARC function and transformed from Longitude/Latitude coordinate system to the transverse Mercator (TM) projection.

The training sites were chosen on the basis of visual interpretation of both the aerial photography and the TM image, aided by a good knowledge of the area, plus field data. Polygons for each surface class, with size of 30 pixels per each polygon, were digitised on screen over the TM image using site coordinates generated from the GIS. Once training sites have been carefully defined and are in spatially corrected polygons, spectral signatures are developed for each site. Site signatures were evaluated using a combination of signature separability and scatterplot methods. Signature separability, which is a statistical measure of distance between two signatures, can be calculated for any combination of bands that is used in the classification, enabling one to rule out any bands that are not useful in the results of the classification. This method has been performed on the training data to estimate the expected error in the classification for various feature combinations. The scatterplot that visually graphs the spectral distribution of signature by band can be described as a simplification of a two-dimensional histogram, where the data file values of one band have been plotted against the data file values of another band. It evaluates the overlap of signature based on standard deviation of the signature means. Then, similar signatures were grouped into one cover type. On the basis of observed inter- waveband correlation the data acquired in TM bands 3, 4, 5 and 7 only were selected for use. Image classification was carried out using the maximum likelihood algorithm. The likelihood method takes variability of classes into account by using the covariance matrix of the signature. In this method it assumes

that the statistics for each class in each band are normally distributed and calculates the probability that a given pixel belongs to a specific class. Unless a probability threshold is selected, all pixels are classified. Each pixel is assigned to the class that has the highest probability. The supervised classification resulted in five different cover type classes (Figure 5.11) of excellent average separability, which exceeded 1981. These are the classes that defined earlier during the fieldwork. These classes are unconsolidated deposits, desert pavements, consolidated deposits, sediment and basement Mountains. Although the woody desert shrubs do exist in the area under study, it was not possible to get them represented by a separate class in the supervised classified image. This may due to its low density and sparseness. The basin is mainly covered by desert pavements and basement rock mountains, which constitute 46.8% and 36.4 % respectively, of the total basin area (Figure 5.12).

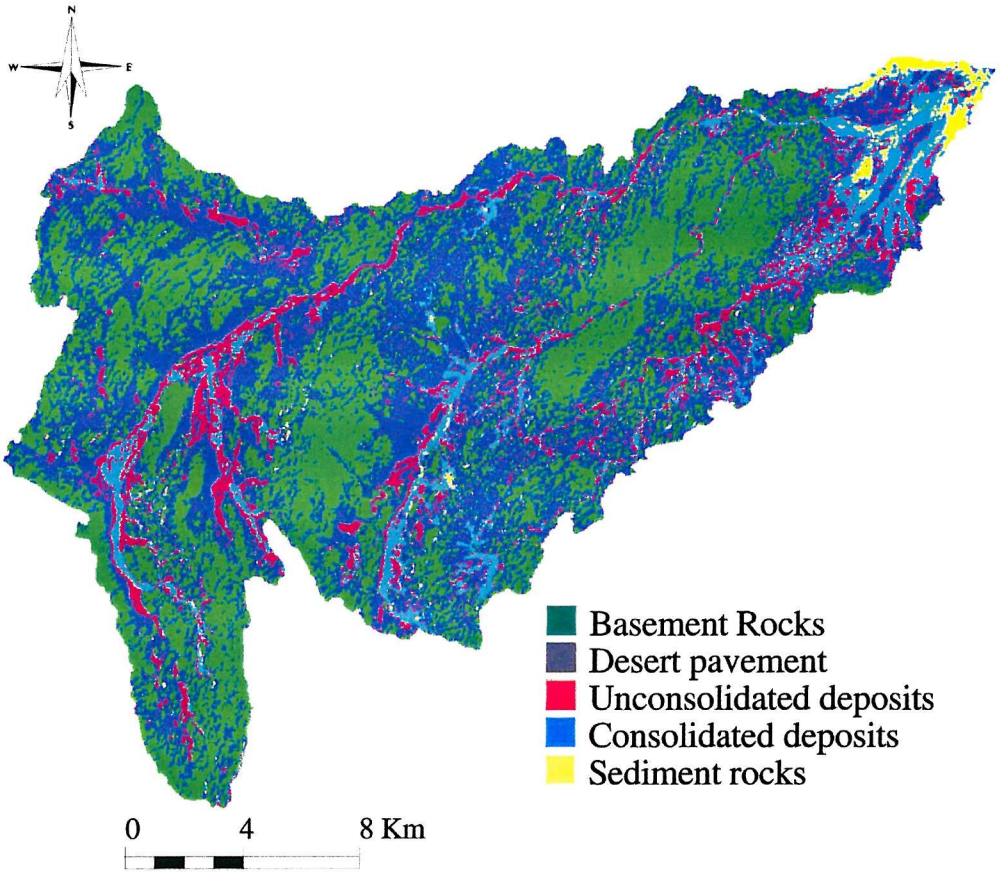

Figure 5.11 Landsat TM classified image of Wadi El-Alam basin.

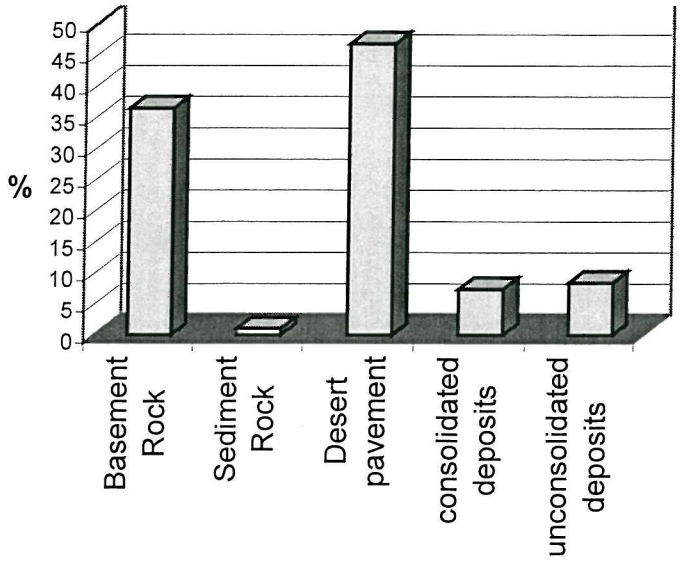

Figure 5.12 Percent of land cover classes of Wadi Alam basin

Before dwelling upon the different classes that emerged from the classification process, it is necessary to shed light upon the accuracy assessment to know how reliable the classification result is.

5.2.3.2 Accuracy assessment

Classifications derived from remotely sensed images are subject to error and uncertainty. In classifying an image, the spectral response of a pixel, representing a fixed area on the ground defined by the spatial resolution of the sensor, is used to assign it to one of a number of classes using various classification techniques. To assess classification accuracy, reference (ground data) data are needed for a number of sample locations for each class. Accuracy is defined in terms of misclassifications, where a pixel is assigned to the wrong class. Accuracy measures the agreement between a standard assumed to be correct and a classified image of known quality (Campbell, J B, 1996).

In this study an error matrix was used to calculate the classification accuracy, which represents the degree of agreement between the classified land cover and observed land cover. It is usually not practical to test every pixel of a classified image therefore, a set of reference pixels is usually used. Reference pixels are points on the classified image for which actual data are known. When reference

pixels are selected by the analyst, it is often tempting to select the same pixels for testing the classification that were used in the training samples. This biases the test, since the training samples are the basis of the classification. By allowing the reference pixels to be selected at random, the possibility of bias is lessened or eliminated (Congalton, 1991).

The accuracy of this thematic map was assessed from a random sample of 229 pixels, whose actual class was derived from 1:40 000 scale aerial photographs acquired in 1989; the nature of the environment dictates that (aside from short lived vegetal changes) surface cover is highly intransigent and so the ~1 year difference in the date of data acquisition was unimportant.

The original TM image was used to place the random points while the raster attribute editor for each supervised classification image was used for the reference class data. Each individual class on the TM image was assigned a reference number corresponding to the attribute editor. After each pixel was assigned a class, an accuracy assessment report was generated. The error matrix, which shows the user's, producer's and overall accuracy results for the land cover map of Wadi El-Alam Basin, has been tabulated in Table 5.3.

Table 5.3 Classification accuracy error matrix for the produced land cover map.

Class name	Unconsolidated deposits	Consolidated deposits	Sedimentary rocks	Desert pavement	Basement rocks	Total	Producer's Accuracy
Unconsolidated deposits	43	1	_	3	1	48	89.6%
consolidated deposits	2	19	_	_	_	21	90.5%
Sedimentary rocks	_	2	17	_	1	20	85.0%
Desert pavement	3	_	_	44	3	50	88.0%
Basement rocks	3	_	_	5	82	90	91.1%
Total	51	22	17	52	87	229	overall accuracy
User's accuracy	84.3%	86.4%	100%	84.6%	94.3%		**89.5**

The producer's accuracy, which is computed by dividing the total number of correct in a category by the total in that category as derived from the reference data,

is important measure of the omission error. This accuracy measure indicates the probability of a reference pixel being correctly classified (Congalton, 1991). While the user's accuracy (or reliability), which is computed by dividing the total number of correct in a category by the total that was classified in that category, is an important measure of commission error. It is indicative of the probability that a pixel classified on the map/image actually represents that category on the ground. (Story and Congalton, 1986). The producer's and user's accuracy of the classified image of Wadi El-Alam have good results for all classes. Sedimentary rocks, for example, has a high producer's accuracy of 100% which means that area classified as Sedimentary rocks match up well with the area determined to be Sedimentary rocks in the reference data. The user's accuracy showed similar results as the producer's accuracy. 86.3% of the desert pavement that was identified was actually desert pavement on the ground. The accuracy of the image classification was estimated to be 89.13%, above the commonly specified target accuracy for many thematic maps (Foody, 2002), which indicates the reliability of the image classification. The characteristics of these 5 land covers will be outlined in the following section (5.3).

5.3 WADI ALAM LAND COVER

Wadi El-Alam is non-urbanized area, except for the Wadi mouth where the town of Marsa Alam is located. This Wadi is characterized by its homogeneity as most of its area is covered by bar rock mountains, desert pavements and dry channel network. Land cover of this Wadi is discussed in the following sections:

5.3.1 Bed rock

Mountains in Wadi El-Alam basin are, in general, characterised by complex terrain. Some of them are sufficient high to receive more than the normal desert rainfall. Mountains of metamorphic rocks cover most of the basin area and display a marked schistosity and have parallel structure such as relict bedding. Drainage channels in these rocks are usually steep-sided and sharp cuts, contrasting with channels in igneous rocks (e.g. granite) which are characterised by dentritic shape and

relatively uniform courses. Weathered superficial material in the metamorphic rock mountains is characterised by sharp, angular fragment (flakes, chips, slabs), while it tends to be large but rounded blocks in the igneous rocks. Sedimentary rocks, which exist close to the coastal zone are distinguish by narrow channels (about 1.5 metres) with very steep-sides, and its surfaces are covered by a thin layer of loose, weathered sand grains (field observation).

5.3.2 Wadis (Channel course)

The general sparseness of rainfall and its torrential nature in arid regions cause most of the stream to be intermittent or ephemeral. The stream courses contain water during and shortly after heavy rainstorms, and are dry for the remainder of the time. These dry drainage channels are one of the most characteristic physiographic features of arid regions. The bed of a dry Wadi exhibits little relief. It is a flat, almost smooth surface broken only here and there by small depressions gentle rises (field observation). They are bounded in the study area by nearly vertical cliffs, which are the most pronounced relief feature associated with desert wadis. The slope of dry wadis varies widely along its length. At its head in the mountain areas the wadis have slopes that approach that of the mountain area while when it crosses the bordering fans the slope drops abruptly to an avenge of two or three degrees.

Wadi bed deposits can be separated in El-Alam basin into two classes according to the nature of its surface materials. The surface of the first class is made up largely of very coarse sediments. These sediments range in size from large gravel to large boulders in channels of the uplands and steeply sloping areas in the upstream parts of the study basin (Figure 5.13), while smaller gravel sizes may be found on channel bed further downstream. The difference in grain sizes is the result of variations in slope and hence flow velocity. Although sediment sorts by distance, there is no vertical sorting of wadi bed sediment due to the turbulent flood nature. Wadi courses in this class are floored by unconsolidated coarse air-dry loose material (Figure 5.14) with a small proportion of fines and a high void ratio.

The second class of wadi bed is also made up of coarse sediment but it is characterised by compacted material. It consists of a thick mixture of fine and coarse material. This compacted grained mixture is found in different locations along the Wadi bed where the channels have a gradient of one degree or less. In other words it can be found where the flood velocities reach their minimum values in dead zones. This type of sediment is found along the wide downstream plain delta of Wadi El-Alam, and in many flat parts of El-Sukkari and Khirayjah. Figure 5.15 shows site of Wadi Sukkari surface that consists of compacted grained mixture covered in some parts by fine material due to very low gradient of the Wadi surface. This kind of deposits are called 'slack-water deposition' (Baker, 1987). In contrast to the surface of the first wadi bed class, it has been noticed during the field study that the surface of this type is covered in some parts with poor desert vegetation, which may indicates the ability of this surface to trap some water during rain events.

Figure 5.13 Upstream channel bed covered with large boulders.

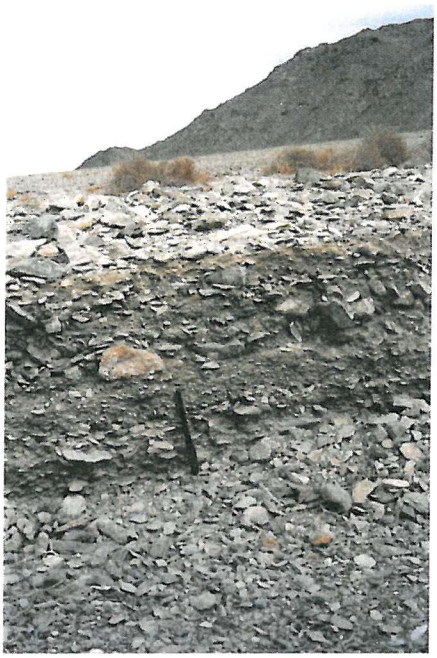

Figure 5.14 Wadi unconsolidated deposits.

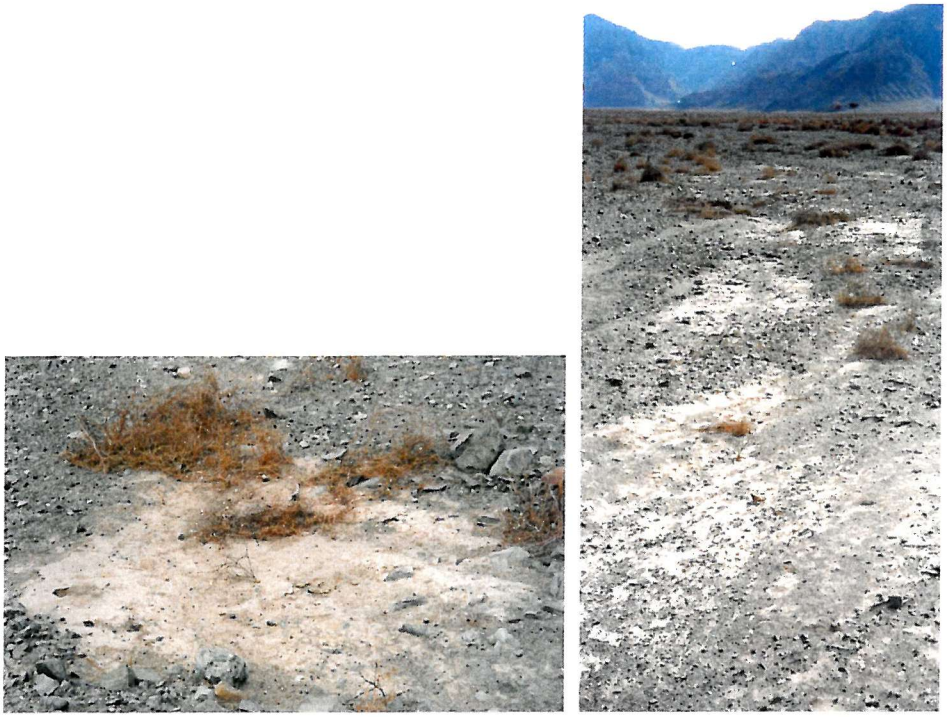

Figure 5.15 Wadi consolidated deposits.

5.3.3 Desert pavements

Desert pavement is a stony armoured surface generally composed of a layer of angular or sub-rounded gravel, usually only one or two stones thick sitting on a finer material comprising varying mixtures of sand, silt or clay (Abrahams and Parasons, 1994), see Figure 5.16. This desert pavement normally forms on the gently sloping surface of desert alluvial fans and wadi terraces as a result of rainbeat, overland flow and deflation that are active for a long period. These processes remove fine particles, leaving coarser, heavier materials behind (Strahler and Strahler 1996). This surface phenomenon is known as Hamada and Reg in the Old World. Hamada consists of extensive surfaces of large angular rock fragments and derives its name from the Arabic word meaning 'unfruitful' (Mabbutt, 1977), while Reg consists of smaller size gravel and derived its name also from the Arabic word meaning 'becoming smaller' (Amit and Gerson, 1986). The stone surface of the pavement acts as an armour that effectively protects the finer particles from rapid removal by overland flow and deflation. A fairly common feature of many soils beneath this stone surface is the absence of coarse material in the upper part of the profile. Often, there is a vesicular A horizon of mainly silt-clay-size particles. This vesicularity is probably due to trapped air that expands as soils dry out in rapidly rising temperature following desert rainstorms (Evenari *et al.,* 1974, McFadden *et al.,* 1987). Musick (1975) showed that these surfaces have relatively high salinity, high exchangeable sodium percentage (e.g. high alkalinity) and low infiltration capacity, which is partly because of their high ESP that aids deflocculation of soil colloids. In a study on Yuma County, Arizona, it has been reported that the desert pavement has a low infiltration capacity in the range of 8.4 mm hr^{-1} (Musick, 1975).

The development of desert pavements is generally attributed to one of a number of stone-concentrating processes. Deflation is perhaps the most commonly invoked process. Some workers such as Dan *et al.,* (1982) related the concentration of the top stone cover to the removal of fine-grained material from the desert surface by wind, leaving the stone cover behind as a lag deposit. A second mechanism for stone concentration is the winnowing of fines by surface wash (Sharon, 1962). The third and perhaps most widely accepted explanation, which is called the upward

umigration of stones (Abrahams and Parasons, 1994), is the progressive upward migration of coarse particles through the underlying finer material. This may relate to the alternate wetting and drying and associated swelling and shrinking of the fine-grained sub-pavement material. As the fine debris swells, coarse fragments are forced upward. When shrinkage occurs the coarse fragments fail to return to its former position, which are occupied by fine-grains.

Repetition of this process causes the coarse fragment slowly to make its way to the top surface, (Cooke, 1970b, Dan *et al.,* 1982, Jessup, 1960). Mubbutt, (1977) suggested that aeolian dust is trapped by the rough surface of the pavement and that there is a consequent upward displacement of the pavement as dust accumulation proceeds. He also suggested a fifth process called differential weathering. He argued that moisture conditions are more favourable for rock weathering in the subsoil than at the desiccated surface, leading to the more rapid breakdown of coarse debris. The result of this enhancement of weathering at depth is a layer of relatively fine materials with a lack of coarse debris.

Desert pavement surface is often coated with glossy brown to black, iron and /or manganese-rich patinas is termed desert varnish. Most desert varnish films are less than 300 um in depth. Rarity of well-developed rock varnish on Holocene surfaces suggests that in most desert surfaces the formation of continuous black varnish coatings requires at least, 10,000 years. (Abrahams and Parasons, 1994). The major determinations of rock varnish physical characteristics are the relative contents of clay minerals (commonly 60 to 80 %). Tricart and Cailleux, (1960) believed desert varnishing to be a physicochemical process, associated with the high Eh (dry, oxidizing) and pH (unleached, alkaline) conditions in deserts. The occasional in coherence of the underlying rock suggested to some that iron and manganese had been drawn in solution from the rock beneath and precipitated by evaporation. Later studies such as Dorm (1989a) suggested that the varnishing process relating to dust. In this new biological model, microcolonial lichens and bacteria are adsorbed to the surface of clay dust that settles on rock surfaces and they obtain energy by oxidizing incoming manganese, when occasionally activated during brief

wet periods. The manganese is then strongly adsorbed to the clay minerals. The varnish then protects bacteria from the harsh conditions at the desert surface.

Desert pavement covers a large area of the study basin (Figure 5.17). Most of this surface forms on old terraces, talus, inactive alluvial fans and pediment surfaces. It is characterized by a very coarse fragment surface with lots of boulders and cobbles. Some of these surfaces extend in length to 6 km as the case of the downstream area (close to the wadi mouth). It also can be recognised in flat parts of El-Sukkari and Khirayjah Sub-basins. The desert pavements are dissected by drainage channels that produce an irregular pattern in the aerial photographs. This irregular dissected pattern of the desert pavements helps to distinguish them from the active channels in the TM image. The coating of the desert pavements with the desert varnish of low DN (dark signature) facilitated the identification of the desert pavements in the TM image as previously outlined by Floyd (1987).

5.3.4 Settlement and road network

Wadi Alam is non-urbanized except for the coastal zone at its outlet. On the Wadi fan Marsa Alam town lies (Figure 5.18). The construction of Alam airport is expected to help in the expansion of this small town. Part of the town is building along the Wadi main trunk and consequently subjected to flash flood hazards. The town has in its northern side a small tree field (> 100 m^{-2}) which has been noticed during the fieldwork. There is also the small El-Sukkari settlement, which is built inside the Wadi, close to El- Sukkari gold mining. The basin includes a sector of both the Red Sea coastal highway, which crossing the Wadi alluvial fan, and the Idfu-Marsa Alam road, which is constructed for most of its length on the floor of the main drainage course. This is in addition to some desert tracks, which are linking the different parts of the Wadi.

5.4 LAND COVER MAP OF EL-ALAM BASIN

The above section reveals that Wadi El-Alam consists of five land cover types, which are the bare rocks, the wadi bed with its two types and the desert pavement,

in addition to the settlements (Marsa Alam town, and El-Sukkari mining settlement) and the road network (asphalt and desert tracks). Only three types of these five land cover types have been mapped earlier in this chapter using the remote sensing tools.

Figure 5.16 Stony surface underlain by fine grain size in desert pavement.

Figure 5.17 Large area covered by desert pavements dissected with small channels.

In order to produce a complete land cover map for the study area it was necessary to add the two remaining land cover types that consists of the settlements (with the tree field) and the road network to the classified map. This has been accomplished by digitising the Marsa Alam town from recent topographic/urban map of 1: 5000 scale produced in 1999 by the Marsa Alam city council (personal communication). Whereas the mining settlement, asphaltic roads and the desert tracks have been digitised from the 1: 50 000 scale topographic maps (Egyptian Military Survey, 1989).

In order to represent the road and tracks in their real size they have been converted from line to polygon feature by using the BUFFER ARC command with buffer distance of 15 meters for the asphalt roads and 10 meters for the desert tracks. This produced road-track polygon cover is then has been overlaid with the settlement polygon cover (Figure 5.19). The land cover map that generated from the supervised classification (section 5.2.4.1) was imported to Arc/Info and converted to polygons using the GRIDPOLY GRID command. Finally, the complete land cover map for the study basin was generated by the overlying classified land cover map with the digitised land cover one using the UNION ARC function (Figure 5.20). In this way, the land cover map of the Wadi El-Alam needed as one of the required parameters for determining the runoff curve number is now becoming ready.

Figure 5.18 Part of Marsa Alam town.

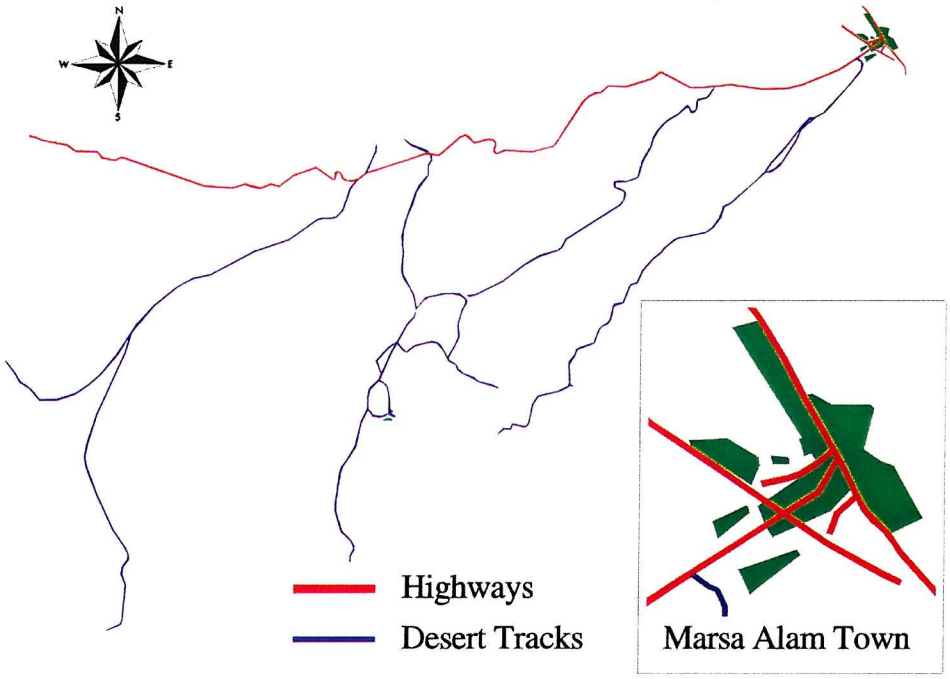

Figure 5.19 Digitised town, roads and desert tracks.

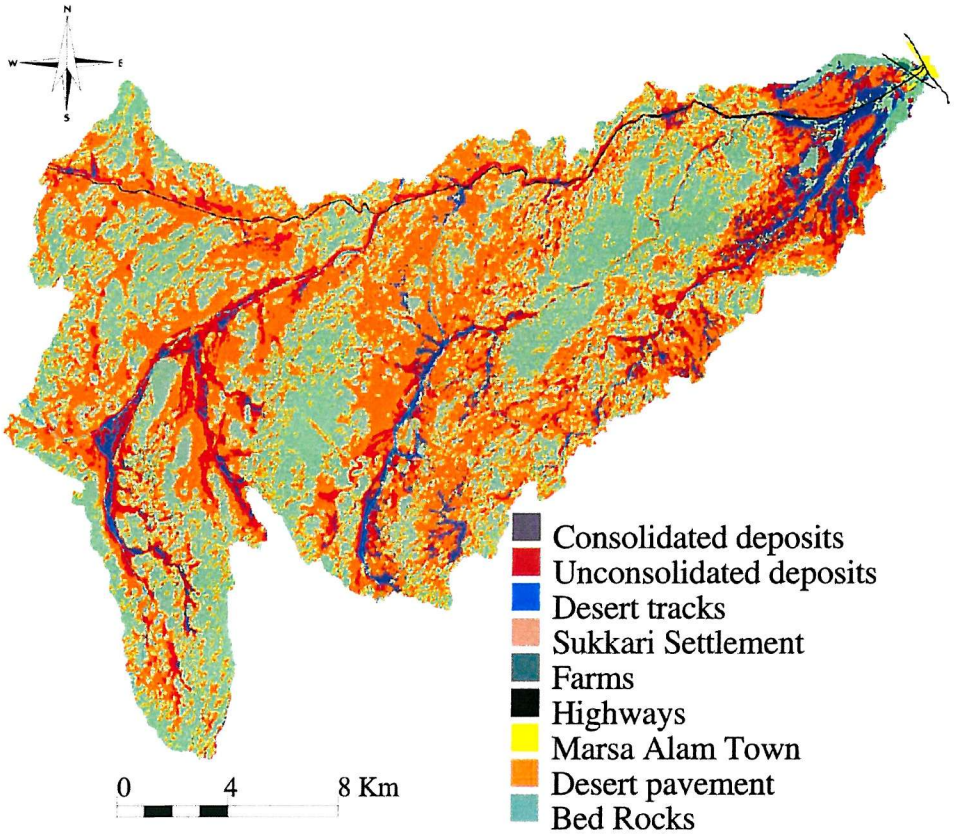

Figure 5.20 Land cover map of El-Alam basin.

5.5 SUMMARY

Information on land cover required for the hydrological modelling was derived with the aid of a supervised classification of Landsat TM imagery of the Wadi El-Alam. This analysis aimed to derive a thematic classification from the imagery in which the land cover classes mapped differed in terms of their hydrological properties. The TM data were rigorously pre-processed prior to the classification, through the application of geometric, radiometric and atmospheric corrections. Moreover, a topographic correction was made to compensate for the effects of variable surface illumination due to elevation variation.

The bedrock outcrops (basement and sediment), desert pavement, consolidated and unconsolidated wadi bed deposits, which were observed during the fieldwork, have been derived from the TM imagery. The accuracy of the derived classification image was estimated to be 89.5%, which was considered sufficiently accurate for using in representing the land cover map. The digitised settlement and road network were added to the derived map with the result of a final land cover map of seven classes.

CHAPTER 6

Application and sensitivity analysis of a hydrological model

6.1 INTRODUCTION

Rainfall runoff modelling and flood discharge estimation have always been important tasks of hydrologic sciences and engineering. Flood flow estimation, in particular, has been given special attention because of the impact that accurate forecasts have in the management of flood related emergency programmes. Probably more than other concerns in hydrology, estimation of flood discharges is oriented toward saving human lives and protecting people's properties.

The hydrologic modelling of any natural system is concerned essentially with the relationships between the amount of precipitation falling on a land surface and the quantity of runoff generated from that storm event, how the runoff becomes channelled flow, and how that flow proceeds to the outlet of a watershed. Hydrological models could be considered as the theoretical tie between geomorphology and hydrology. The geomorphology-based instantaneous unit hydrograph (GIUH) of Rodriguez-Iturbe and Valdes (1979) is an example of such a model, which finds the hydrological response of the watershed, given its geomorphological characteristics. Depending on whether the functions that relate the input, output and the state of system being modelled are functions of time and space, the hydrological models could be classified as either lumped or distributed. Lumped models do not account unequivocally for the spatial variability of the hydrological process, whereas the distributed models do. The input, output, and parameter values of lumped models are spatially averaged. Apart from the intensive computational demands of spatially distributed models, the lack of spatially distributed hydrological data remains a constraint. The analysis and input data of the distributed models could be handled on a grid basis. The raster-based

geographic information system (GIS) constitutes a powerful tool in this respect that not only eases the acquisition of data but also helps analyse the results in different scenarios.

6.2 THE HYDROLOGICAL MODELLING SYSTEM

By a model is meant the mathematical procedures that relate the known input of something to its unknown output. In the current context, the something is the hydrological system, e.g. a basin or a watershed, and its known input is the rainfall (or the upper stream flow) and its unknown output is the runoff (or the downstream flow). In this study the watershed-oriented Hydrological Modelling System (HMS) model (Peters, 1998), developed by the Hydrologic Engineering Centre (HEC) of the US Army Corps of Engineers (USACE), has been utilised to model the rainfall runoff processes in the Wadi El-Alam. Before dwelling elaborately upon the underlying concepts and modules of this model, the definition of the hydrological system (element) that will be acted upon by the model has first to be clarified. Chow *et al.* (1988) defined the hydrological system (element) as a volume in space delimited by a boundary that receives water and other inputs, works on them and produces them as output. In this way, the hydrological system is considered as a control volume of an output driven by the input through a response function. Within the framework of HMS model, basin reaches (stream channels) and their associated sub-basins (watersheds), junctions and diversions are considered as typical control volumes each of its own response function. To link these control volumes, HMS assumes that they are connected in series in such a way that the flow is passed on from an upper stream control volume to a next downstream one and so forth until ultimately the accumulated flow arrives the outlet (sink) of the last control volume in the system. This sequential connectivity is a sort of simplicity that technically rules out the side flow into the reach which needs the usage of a fully distributed model to be completely specified. However, it allows the basin to be modelled in a vector environment. Under this condition, the HMS model is considered as a partially distributed approach that allows parameters within hydrologic elements to be lumped while defining different responses and

parameters for each element. The routing procedures and modules of HMS model will be outlined in the following sections.

6.2.1 HMS Model Components

The HMS routing model, is essentially a collection of three components (models); the basin component, the precipitation component and the control component. The input data for these components are very tedious if prepared manually. Fortunately, the ArcView-based preprocessor, CRWR-PrePro, made the extraction of the topographic, topologic and hydrologic information from digital elevation model (DEM) of the basin to be modelled, a routine job. CRWR-PrePro has been developed at the Centre for Research in Water Resources (CRWR) of the University of Texas at Austin. Olivera and Maidment (2000), presented an excellent review on this HMS preprocessor.

HMS specifies the hydrologic elements, (control volumes) within a hydrologic system as subbasins, reaches, junctions, diversions, sources and sinks based on the types of the physical processes (inflow, outflow and storage), that might take place in such kind of elements. These hydrological elements are the basic building blocks of the basin model. A sub-basin is an element that usually has no inflow and only one outflow. A reach is an element with one or more inflow and only one outflow. Inflow comes from other elements in the basin; usually sub-basins. If there is more than one inflow, all inflow is added together before computing the outflow. A junction is an element with one or more inflow and only one outflow. All inflow is added together to produce the outflow by assuming zero storage at the junction. A diversion is an element (of zero storage) with two outflows, main and diverted, and one or more inflow. If there is more than one inflow, all inflow is added together before computing the outflow. Diverted outflow can be assigned to an element that is computationally downstream. All flow that not diverted becomes main outflow. A sink is an element with one or more inflows but no outflow. Sinks represent the lowest point (main outlet) of an interior drainage area of the basin. Source is an element with no inflow, one outflow and is one of only two ways to produce flow

in the basin. Figure 6.1 shows the symbols used to represent these hydrologic elements in HMS.

Figure 6.1 The symbols of the hydrological elements in HMS model.

For the sake of brevity, the process of generating the input data for the HMS basin model by CRWR-PrePro could be conceptually divided into six modules: (a) raster-based terrain analysis; (b) raster-based sub-basin and reach network delineation; (c) vectorization of sub-basin and reach segments; (d) computation of hydrologic parameters of sub-basins and reaches; (e) extraction of hydrological subsystem (if necessary); (f) topologic analysis and finally preparation of the basin file (in ASCII format). This file, once it is opened by HEC-HMS, automatically creates a topographically correct schematic network of connected sub-basins and reaches attributed with hydrologic parameters; see Figure 6.2.

At this point, a technical tip has to be made clear. Occasionally, an error was encountered during the import stage of the basin model into HMS or when the imported basin model is used to perform a simulation. This type of error is associated with those erroneously created sources which crop up owing to the presence of small polygons (known by sliver polygons) in the watersheds coverage. They are often not visible straight away but they are identified by CRWR-PrePro as sources not attached to an outlet. The presence of such sliver polygons is easy to detect when HMS is run because they result in sources with no associated outflow. These small closed polygons can be removed by using the ARC ELIMINATE function, or can be removed by deleting these sources from the basin file along with the reaches that link them to the next downstream element.

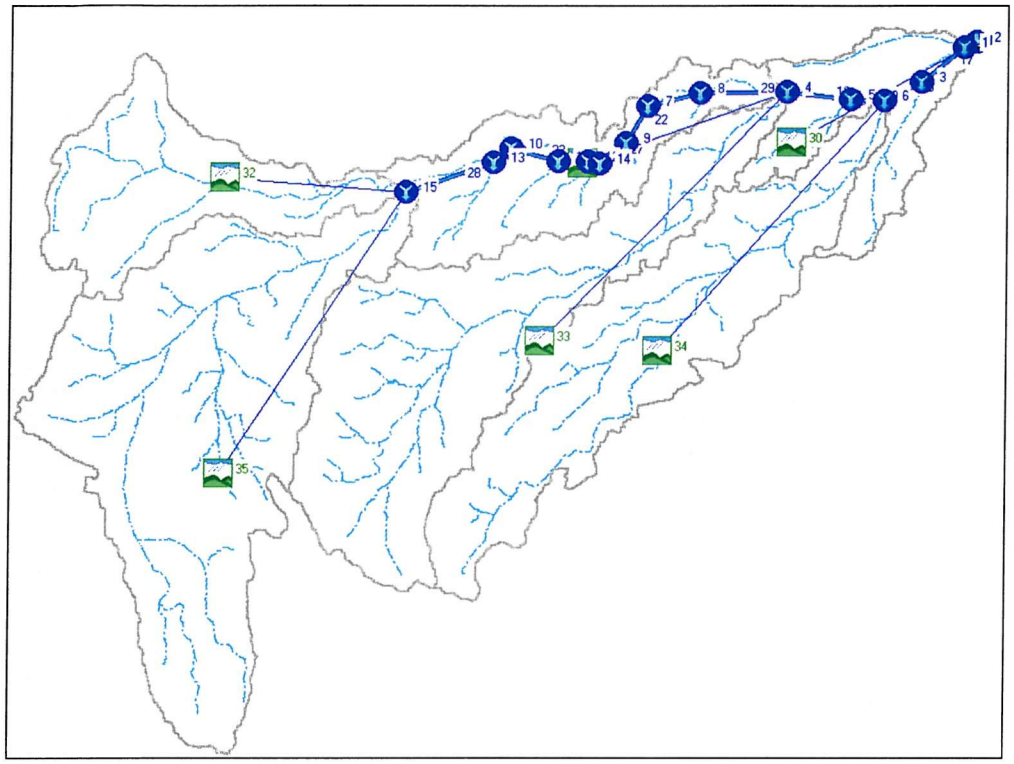

Figure 6.2 HMS schematics of Marsa Alam Basin.

The precipitation model describes the rainstorm that drives the response of the basin. Precipitation specification options might describe an observed precipitation event; a frequency based hypothetical precipitation event, or an event that represents the upper limit of precipitation possible at a given sub-basin. As the Wadi under investigation is an ungauged basin, precipitation has been described by a hypothetical rainstorm that covers the basin uniformly in space and time for two hours with a total rainfall depth of 60 mm.

The control model is the last component needed for commencing the simulation. It specifies the starting and ending date and time of a run, in addition to the time (routing) interval. The time interval (computation step) determines the resolution of model results computed during the run. The available intervals in HMS include 1, 2, 3, 4, 5, 6, 10, 15, 20 and 30 minutes in addition to 1, 2, 3, 4, 6, 8, 12 and 24 hours. In the current study a time step of 30 minutes has been used.

From the foregoing discussions, it becomes clear that HMS is a model flexible in its modularity and options. Besides, it is widely used, accepted and popular in the community of hydrology and more importantly the availability of the robust preprocessor CRWR-PrePro made, to a very large extent, the generation of its input data an easy process. All these features justify the usage of the HMS model in this research. The method of computing the runoff volume using HMS along with the adopted routing methods is described in the following section.

6.3 COMPUTING RAINFALL LOSSES

As precipitation moves over the surface of the basin, it incurs infiltration (losses). HMS offers the most common methods for calculating losses:
The initial and constant rate loss model;
The Green and Ampt loss model;
The deficit and constant rate model; and
The SCS curve number (CN) loss model (composite or gridded).

The Soil Conservation Service (SCS) developed (1985) curve number (composite) method has been opted for this research for the following reasons. Firstly, it is one of the method that the HMS preprocessor, CWCR-PrePro, can handle which means that a lot of manual effort for parameterizing the hydrological elements of the basin has now been set aside. Secondly, it uses the land cover of the basin, which has been already derived in chapter 5 from the Landsat TM satellite imagery of the Wadi. Thirdly, the method is suited for semi-arid and arid (SCS, 1985; Tables 2(a)-(d)) conditions and has been successfully applied to (ephemeral) watersheds in southwestern US and quite recently to arid wadis in Eastern Desert of Egypt (Gheith and Sultan, 2002). In principle, the SCS curve number method is an empirical model that estimates runoff as a function of cumulative precipitation, soil cover, land use forms, and watershed antecedent moisture, using the following equation:

$$P_e = \frac{(P - I_a)^2}{P - I_a + S} \tag{6.1}$$

Where P_e= accumulated precipitation excess (mm) at time t, P= accumulated rainfall depth (mm) at time t, I_a= the initial abstraction or loss (mm) and S= maximum potential retention (storage) in mm (a measure of the ability of a watershed to abstract and retain storm precipitation excess). Until the accumulated rainfall exceeds the initial abstraction, the precipitation excess, and consequently, the runoff will be zero. From studying the results from many small experimental watersheds, the SCS developed an empirical relationship of I_a and S:

$$I_a = 0.2S \tag{6.2}$$

Therefore, the cumulative excess at time t is:

$$P_e = \frac{(P - 0.2S)^2}{P + 0.8S} \tag{6.3}$$

The parameter S (mm) is related to soil and cover conditions of the watershed through an intermediate parameter, the curve number (CN) as follows:

$$S = \frac{25400}{CN} - 254 \tag{6.4}$$

where CN (curve number) is a hydrologic parameter used to describe the storm water runoff potential for drainage area (Ponce and Hawkins, 1996). The manual calculation of curve numbers for large areas or many drainage basins can be cumbersome and time consuming, therefore the GIS is an appropriate tool to use for such an application. The curve number of each watershed in the El-Alam basin can be estimated as a function of land use, soil type, and antecedent watershed moisture condition (AMC) using the tables compiled by the SCS (SCS, technical report TR-55, 1986) as it will be detailed in section 6.5. With the average CN

value for each watershed, precipitation loss is found for each computation time step and is taken away from the rainfall depth map for that step. The remaining depth is called precipitation excess, which is assumed to be uniformly distributed over a watershed area so it represents a volume of runoff ready to be routed to the outlet of the watershed.

6.4 HMS ROUTING METHODOLOGY

Routing is technically, the derivation of a downstream hydrograph from an upper stream one. The adopted HMS routing procedures in this study for sub-basins and reaches are described in the following section.

6.4.1 Sub-basin runoff transformation

Precipitation that does not infiltrate, becomes excess precipitation, capable of moving down-gradient on the surface of the watershed to become channelled flow or transformed into direct runoff. HMS includes the most common methods that allow modelling of the direct runoff within a sub-basin such as the kinematic wave model and empirical unit hydrograph (UH) techniques: Clark, Snyder, SCS and user specified. Given the absence of flood records for the investigated basin, the SCS UH method (SCS, 1985) has been used in this study. This method suggests that the UH peak (U_p) and time of UH peak (T_p) are related by:

$$U_p = c\frac{A}{T_p} \tag{6.5}$$

where A = Watershed area (km^2) and c = Conversion constant (2.08 in SI unit). The time of peak (T_p) is related to the duration of the unit of excess precipitation as:

$$T_p = \frac{\Delta t}{2} + t_{lag} \tag{6.6}$$

where Δt = the excess precipitation duration and t_{lag} = the basin lag (defined as the time difference between the centre of mass of rainfall and the peak of the UH). When the lag time is specified, HEC-HMS solves equation 6.6 to find the time of UH peak, and equation 6.5 to find the UH peak. With U_p and T_p known, the UH can be found from the dimensionless form, which is included in HEC-HMS, by multiplication. The determination of the lag time in addition to other hydrological parameters of watersheds will be discussed in section 6.4.3.1.

6.4.2 Channel (reach) routing

When the flow comes out of a sub-basin outlet and enters a channel, the flowing water is attenuated by friction and channel storage as it passes through the channel. The process of calculating the travel time and attenuation of water flowing in the channel is called routing. The travel time is a function of parameters such as length, slope, friction and flow path. Attenuation is dependent upon friction and channel storage. HMS provides six routing methods (HMS user's manual, 2000). Among them is the Muskingum method (Chow *et al.* 1988), which has been adopted in this research. This method has been selected, as it is the most commonly used hydrologic method for handling a variable discharge-storage relationship. The Muskingum method models the storage as the sum of prism and wedge storage, see Figure 6.3. During the advance of the flood wave, inflow exceeds outflow producing a wedge of storage. During the recession, outflow exceeds inflow resulting in a negative wedge. In addition, there is a prism of storage, which is formed by a volume of a constant cross section along the length of prismatic channel. The volume of prism storage is the outflow (O) multiplied by the travel time (K) through the channel. The volume of wedge storage is a weighted difference between the inflow (I) and outflow (O), $x[I(t)-O(t)]$, multiplied by the travel time (K). Thus the Muskingum method defines the storage as:

$$\begin{aligned} S(t) &= KO(t) + Kx[I(t) - O(t)] \\ &= K[xI(t) + (1-x)O(t)] \end{aligned} \qquad (6.7)$$

where x is a dimensionless weight ranging from 0 to 0.5 and represents the relative importance of the effect of inflow rate on defining the storage in the channel. The

quantity $xI(t)+(1-x)O(t)$ is a weighted discharge. Therefore, to know the channel storage as a function of time, the travel time (K) through the channel (reach) has to be determined, This will be explained in detail in section 6.4.3.2.

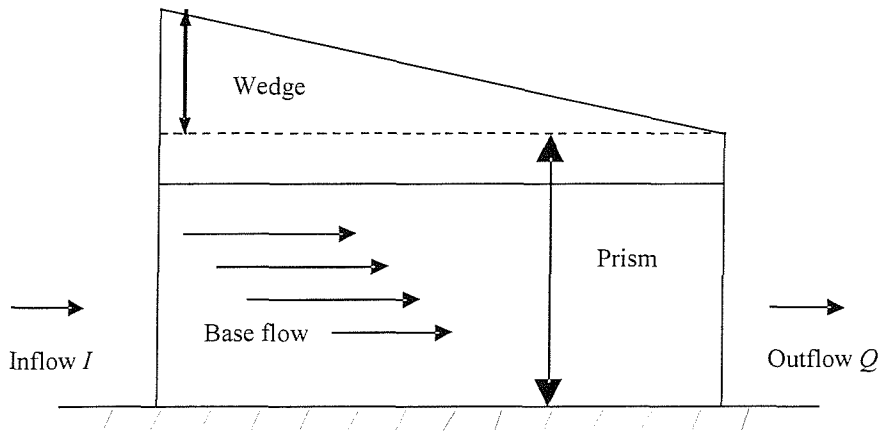

Figure 6.3 Prism and wedge storage in Muskungum routing.

6.4.3 GIS-based hydrologic parameter extraction

In this section the procedures followed by CRWR-PrePro preprocessor to extract the hydrological parameter of the sub-basins and their associated reaches will be discussed.

6.4.3.1 Extraction of hydrologic parameters of sub-basins

For each sub-basin CRWR-PrePro calculates the area, lag time and average curve number. Other parameters needed for estimating the lag time such as length and slope of the longest flow path are also calculated and stored in the sub-basin attribute file. The calculation of lag time might depend completely on spatial data (i.e. DEM, land cover, soils) or might require externally supplied input. Usually, it can be computed from the SCS formula (Chow *et al.* 1988) which is given by:

$$t_{lag} = \frac{L_w^{0.8} \times [(1000/CN)-9]^{0.7}}{31.67 S^{0.5}} \qquad (6.8)$$

where t_{lag} (min) is the sub-basin lag time measured from the centroid of the hyetograph to the peak time of the hydrograph, L_w (feet) is the length of the longest flow path, S (%) is the slope of the longest flow path, and CN is the average curve

number of the sub-basin derived from its land cover/use and soil data, see section 6.5. On account of the constraint imposed by HMS on the analysis time-step (Δt) which has to satisfy the condition of being smaller than 0.29 times the lag time of the basin (HEC 1990), the lag time is taken as the value given above or 3.5 times the analysis time-step, whichever is greater. Therefore, the lag time is redefined as:

$$t_{lag} = \max\left(\frac{L_w^{0.8} \times \left[(1000/CN) - 9\right]^{0.7}}{31.67 S^{0.5}}, 3.5\Delta t\right) \tag{6.9}$$

In connection with the longest flow path, Figure 6.4, its length is calculated by CRWR-PrePro as the distance from the centroid of the furthest cell in the watershed to the outlet of the sub-basin and its slope, as the elevation drop between two arbitrarily defined points of the flow path divided by their distance along the channel.

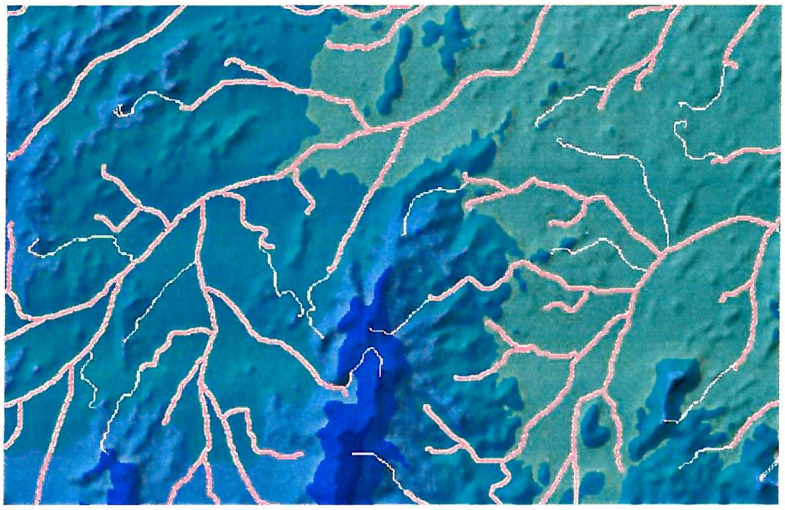

Figure 6.4 The longest flow path (white lines) as calculated by CRWR-PrePro. The pink lines are the digitised channel network.

6.4.3.2 Extraction of hydrologic parameters of reaches

For each reach, CRWR-PrePro calculates the length, the routing method (either Muskingum or pure lag), the in-reach flow travel time (K) and the number of sub-reaches into which the reach is subdivided if Muskingum is used for routing, and the flow time in case pure lag is used for routing. Other reach parameters like the

flow velocity and the Muskingum x cannot be computed from spatial data and must be externally supplied.

The reach length (m) is determined automatically in the process of reach vectorization. The Muskingum method is used for routing in reaches long enough not to present numerical instability problems. In short reaches in which the flow time is shorter than the time-step, the pure lag method of routing is used instead. In very long reaches, each reach is further subdivided into shorter reaches, again, to avoid numerical instability in such a way that the flow time in each of them (k) satisfies the condition (HEC, 1990):

$$2xk < \Delta t < k \tag{6.10}$$

where x is a parameter of the Muskingum method and k (min) is the flow time in the sub-reach calculated by CRWR-PrePro as follows:

$$k = \frac{60K}{i} = \frac{L/(60v)}{i} \tag{6.11}$$

where K (hrs) is the flow time in the reach of length L (m), v (m s^{-1}) is the reach flow velocity and i is the number of sub-reaches into which the reach should be subdivided and is given by:

$$i = \text{int}\left(2x\frac{L/(60v)}{\Delta t}\right)+1 \tag{6.12}$$

In the case of using the pure lag method, the lag time is given by:

$$T_{lag}(\text{min}) = \frac{L}{60v} \tag{6.13}$$

The calculation of the in-reach flow time (K) requires the estimation of the reach flow velocity (v). The variability of this flow velocity could be modelled by the following empirical formula of Manning:

$$v = \frac{1}{n} \times s^{\frac{1}{2}} \times y^{\frac{2}{3}} \qquad (6.14)$$

where v ($m.s^{-1}$) is the average flow velocity, y (m) is the hydraulic radius of the reach (flow area divided by the wetted perimeter) of a slope s ($m.m^{-1}$) and n is the Manning's coefficient that measures the effect of the channel roughness on the flow and depends on the land use. The value of Manning's coefficient (n) is ranges from 0.015 to 0.05 in the natural desert landscape (Prasuhn 1992, Bedient & Huber 1992, Roberson & Crowe 1996). In the current study, n is set equal to 0.025 according to the nature of the investigated basin. On the assumption that the reach is of a width much larger than its depth, the hydraulic radius in the present study is taken as unity. By making use of equation (6.14) and the average slope of every reach, it is possible to calculate the flow velocity in each of them. But, HMS does not allow the in-reach flow velocities (v) to be varied in space and time as it needs them to be represented by an average value. Therefore, the flow velocity (v) has to be estimated on a probability basis. This can be done by equating this velocity (v) to the most probable flow velocity along the main channel which links the watersheds. In the current study, the main channel is of order 7. To know not only about the flow velocity distribution along the main channel but also, at the same time, about the dependence of the flow velocity upon the channel order, a grid for the distribution of flow velocity along the channel network of the entire basin has been derived by applying equation (6.14) on the slope grid which is already derived in chapter 4. On overlapping this grid with that of the channels orders, a resultant grid is produced reflecting the dependence of the velocity of the flow upon the order of the channel. The frequency of cells of a certain flow velocity and a channel order is graphically presented in Figure 6.5. From this figure, it has been revealed that the velocity of the flow is in the range of 1-12 $m.s^{-1}$ and of a maximum value of 3 $m.s^{-1}$ irrespective of the channel order. This finding completely matches the in-field measured values (Sudia Arabia and Palestine), which were between 2 and 3 m s^{-1} (Allam and Balkhair; 1987Reid *et al.,* 1998). On feeding this maximum flow

velocity (3 $m.s^{-1}$) in to equation (6.11), the time of flow in each reach, and consequently each sub-reach, could be calculated.

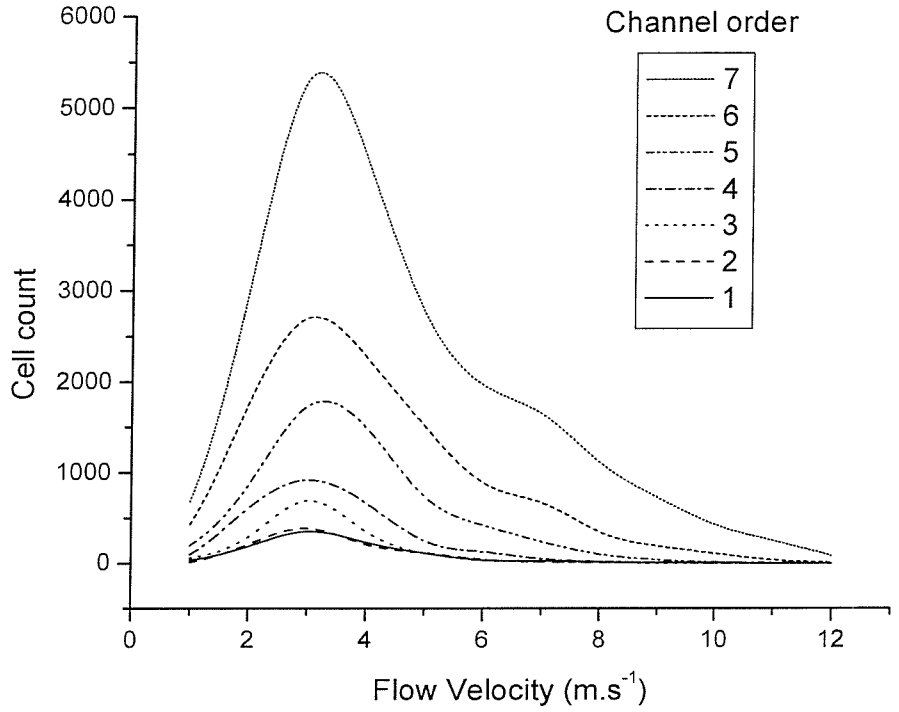

Figure 6.5 The distribution of the flow velocity as function of the channel order.

To start applying HMS on the basin of concern to predict its response to rainfall, one factor still remains to be determined. This is the curve number, which will be dealt with in the following sections.

6.5 EXTRACTION OF THE RUNOFF CURVE NUMBER

The SCS Runoff Curve Number method, which has been discussed in section 6.3, is used in the present study to predict the amount of water that freely flows over the top of the land (excess rainfall) versus the amount of water that is absorbed or trapped on the soil surface (losses or abstraction). This method needs the curve numbers of the basin land cover which themselves are functions of three factors: the antecedent moisture condition, the land cover/use, and the soil group. The antecedent moisture condition which measures the soil wetness is a function of the

total rainfall in the 5 days period antecedent to the storm (McCuen, 1982). The SCS methodology classifies the AMC into three levels as follows:

- AMC I conditions represent dry soil with a dormant season rainfall (5-day) of less than 12.7 mm and a growing season rainfall (5 day) of less than 35.6 mm.

- AMC II conditions represent average soil moisture conditions with dormant season rainfall averaging from 12.7 to 27.9 mm and growing season rainfall from 35.6 to 53.3 mm.

- AMC III conditions represent saturated soil with dormant season rainfall of over 27.9 mm and growing season rainfall over 53.3 mm.

Because of the hyper aridity of the study area of year-apart rainfall events, antecedent moisture condition of the basin is considered to be very low (level I), (Gheith and Sultan, 2002). The land cover has been previously derived in chapter 5 in which the catchment has been classified through satellite image processing and aerial photographs interpretation into homogeneous patches (classes) of land. The assignment of the resulting land classes to soil groups, see Table 6.1, necessitates the determination of their soil types (texture and structure). Therefore, in the following section, the physical characteristics of the soil of the entire basin will be considered.

6.5.1 Identifying the hydrological soil group

The determination of the soil groups of the basin is a key factor required for specifying its runoff curve numbers. The objective of this section is to distinguish among the different types (covers) of soil that are present in the basin under consideration. By understanding the physical characteristics of the main soil types and their infiltration properties, it might be possible to specify to which soil group, see Table 6.1, does the field-collected soil sample belong.

During the fieldwork, it has been observed that three different classes of soil types are prevailing in the basin. The first class of soil, the consolidated bed deposits, is

of a low gravel content deposited over most of the wide channel courses of very low gradient. The second class is the unconsolidated bed deposits of a relatively high gravel content covering most of the narrow steep channel courses. The third class, the desert pavement (or stone pavement), represents a soil cover, which is surficially consisting of stony particles of very dark colour and is of a higher content of fine grains. The rest of the catchment is covered mostly with impervious rocky mountainous formations (assignable to the soil group D; Table 6.1).

Table 6.1 SCS soil groups and infiltration rates (US Soil Conservation Service, 1986).

Soil Group	Description	Final infiltration rate (mm/h)
A	Lowest runoff potential. Coarse texture includes deep sand or gravel with very little silt and clay also deep rapidly permeable loess.	> 8
B	Moderately low runoff potential. Moderately fine to moderately coarse textures. Mostly sandy soil less deep or less aggregated than A.	4 - 8
C	Moderately high runoff potential. Moderately fine to fine texture comprises shallow solid and soil containing considerable clay and colloids. Though less than of those of group D.	1 -4
D	Highest runoff potential includes mostly clays of high swelling percent, but the group also includes some shallow soils with nearly impermeable sub-horizons near the surface	0 - 1

Sixteen soil samples, each approximately 500 g, have been collected, during the fieldwork, at depths in the range of 30-50 cm from various locations across the catchment from its source to its outlet. These soil samples have been mechanically analysed, in line with Wentworth methodology (Wentworth, 1922), in the laboratory by dry sieving to separate the particles of the same texture and size down to < 0.063 mm in diameter. With respect to the samples of desert pavement, they were first dispersed by washing by water, then dried and sieved. The fraction retained on each sieve was weighed and its percent was computed and represented graphically on the soil texture triangle as in Figure (6.6). A visual inspection of this figure reveals that the land cover of the Wadi El-Alam is composed of three different types of soil. The soil of the desert pavement is muddy sandy gravel.

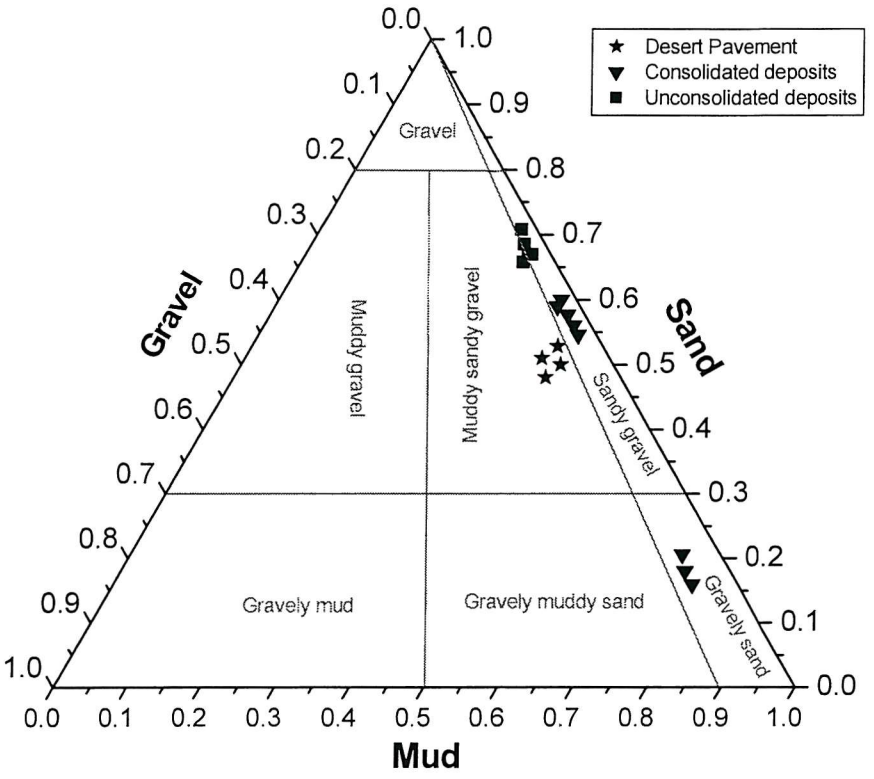

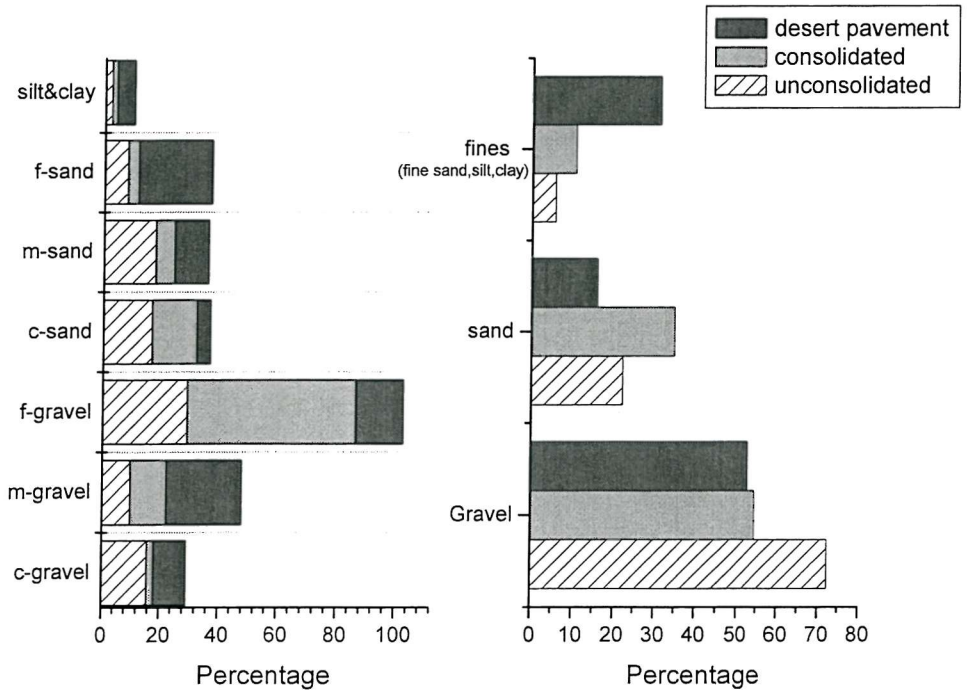

Figure 6.6 Soil texture triangle (above) and soil fragment size percentage (below) of Wadi El-Alam deposits.

The unconsolidated bed deposits are found to be mainly sandy gravel. The consolidated bed deposits are of the types of both the gravely sand and the sandy gravel, see Figure 6.6. The genesis of these soil types will be discussed in detail in the following section. In accordance with Table 6.1 and being of gravely nature, these three types of soil, altogether, could be assigned to the hydrological soil group A, which is characterised by the highest infiltration rate of a value > 8 mm. hr^{-1}. Therefore, from the soil texture point of view, the land cover of the Wadi is made up of two groups of soils A (the surface deposits) and D (the rocky mountains).

To further assert the result of the soil texture analysis, infiltration capacity measurements have been conducted in few localities (due to the difficulty of getting enough water in this arid region) of the three soil types by one or two hour infiltration tests. The field procedure was carried out using one ring infiltrometer. The ring was inserted to a depth of 15 cm in the deposits by gentle hammer blows to prevent any disturbance to the soil structure. In most situations the rate of infiltration is highest when water first enters the soil, and gradually decreases with time to a final constant value (infiltration capacity), which is mainly dependent on soil type. The change of the measured vertical Infiltration (I) as a function of time, Figure 6.7, follows the Philip's one-dimension infiltration model (Philip, 1957) given by:

$$I = St^{\frac{1}{2}} + At \qquad (6.15)$$

where I (mm) is the cumulative infiltration, t (min) is the time of infiltration since water application, S ($mm/min^{1/2}$) is the sorptivity of soil and A (mm/min) is a parameter dependent upon the soil properties and related to the hydraulic conductivity of saturated soil. On differentiating the above equation with respect to time, the infiltration rate (i), in $mm.min^{-1}$, is given by:

$$i = \frac{dI}{dt} = \frac{1}{2} St^{-\frac{1}{2}} + A$$

With the progress of the time, the infiltration rate asymptotically approaches the infiltration capacity of the soil (given by the value of the parameter *A*). The infiltration capacities for the unconsolidated, consolidated bed deposits, and desert pavement are 14.01, 9.70, and 0.072 $cm.hr^{-1}$, respectively, see Figure 6.7.

Thus, in the light of the results of the infiltration measurements, the surface deposits of the land cover of the basin could be assigned to the hydrological soil groups A and D, see Table 6.1, and not only to group A as revealed previously by the soil texture analysis above. It is the way in which the soil has been laid (structure) that has been reflected in the infiltration measurements and subsequently subdivided the soil groups of the surface deposits into two, see below. To conclude, the overall land cover of the basin can be assigned to two groups of soil. The first group is the soil group A of low runoff potential and includes both the unconsolidated and consolidated bed deposits. The second group is the surface runoff boosting soil group D, which incorporates mutually the mountains and desert pavement.

6.5.2 Characteristics of Wadi El-Alam surface deposits

The characteristics of the sediments that dominate Wadi El-Alam under consideration will be outlined in the following section.

6.5.2.1 The unconsolidated bed deposits

This type of sediment covers 8.4% of the total basin area. It is usually found on the channel bed in steep parts of the sub-watersheds as a result of transport and deposition by flash flood water movement in the main channels. Soil texture analysis revealed that the bed is composed of air-dry loose grains that it is made up of sandy gravel according to Folk classification (1980); Figure (6.6).

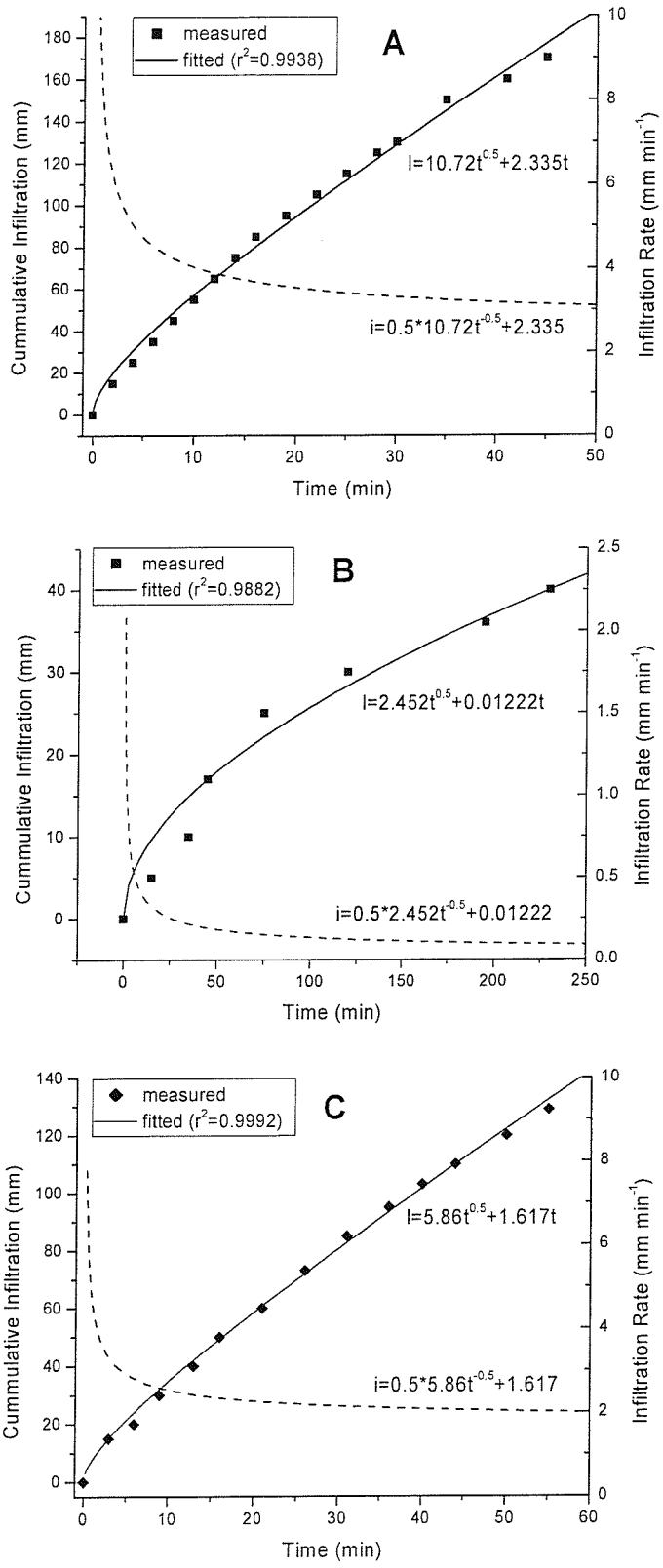

Figure 6.7 Infiltration capacities for the unconsolidated bed (a), the desert pavement (b), and consolidated bed (c).

The loose nature of the sediment grains is suggested to be related to the high velocity of flash flood water along the steeply channels, that mixed different fragment sizes together while moving fine particles as a bed or suspended load further downstream to get deposited in the wide parts of the channels leaving permeable coarse fragments dry and loose upstream. This rationalization explains the high gravel content (70% by weight) of such a kind of deposit; see Figure (6.6). The low content (30% by weight) of the fine materials of the sand, silt and clay is not sufficient at all to fill in the voids among the coarse grains in the sediment. This property made this type of deposit the most permeable one present in the basin with minimum infiltration rate as high as 14.01 $cm.hr^{-1}$. This may explain the growth of the Acacia trees (Figure 6.8) in some places, especially of subsurface faults and cracks, covered by this type of sediment. Large quantities of flash flood water can infiltrate to perhaps few metres into such a deep permeable texture and get protection from evaporation to the atmosphere. This will aid the growth of the desert plants that have a deep root system such as the acacia trees. These trees are, therefore, good indicators of year-round water supply existing the below ground surface.

6.5.2.2 The consolidated deposits

This type of sediment covers about 7.4% of the overall basin area, and is found laying on the flat channels with gentle slope of less than 2°. Soil texture analysis revealed that it is made up of gravelly sand and sandy gravel of moderate gravel content (45%) in comparison to its unconsolidated counterpart; (Figure 6.6). The bed is formed in a way different from that of the unconsolidated wadi bed; it is a bit compact. The low velocity of the flow in the flat areas of such a kind of deposit helps the large particles to get deposited first followed by the smaller and finer particles that fill in the voids resulting in a formation of a lower porosity. This feature is reflected in the infiltration capacity of this surface formation, which is lowered by 30% with respect to that of the unconsolidated wadi bed; see above. This helps to keep some water close to the surface for some time and hence afford different dense and contracted vegetation types, especially those of shallow root system (Figure 6.9). This type of surface formation exits in the very downstream area (wadi mouth) and along the wide flat channels of Sukkari sub-basin where the

surface slope is less than 2° and hence flood velocities reach their minimum values in these nearly dead zone areas.

6.5.2.3 Desert pavement

Desert pavements in Wadi El-Alam are ranging in size from a few square metres to several kilometres. It covers 191 km^2 (46.8%) of the total basin area, and is common in regions of gently sloping surfaces between wadi channels and mountains fronts. It is completely devoid of any vegetation whatsoever. This might be ascribed to its low infiltration capacity (0.072 $cm.hr^{-1}$) that keeps flash flood water near to the surface where it does little good to plants. It does promote the surface runoff to a very high degree. The nearly zero infiltration rate of this type of bed is related to the arrangement of its layers (Figure 6.10). The top layer is of stony particles covering the pavement surface and is of a negligible absorption capacity responding rapidly to rainfall. The underlying layer is composed of a mixture of compacted fine-grained materials that have very small pore spaces and create confining layer in the subsurface. As the pore spaces fill with water, the colloids and very fine soil particles in this underlying layer swell and increase in size. These fine particles clog the underlying layer to form an almost impenetrable crust, although the lower layers may be dry, this impermeable surface layer greatly reduces infiltration. The sealed surface also prevents the air in the voids of the lower layers from escaping through the surface and so causes a compression of entrapped air, which further tends to retard infiltration. Soil texture analysis has shown that the bed is of a rich content (ca. 50%) of sand and fines (fine sand, silt and clay).

6.6 CURVE NUMBER LOOKUP TABLE

From the foregoing discussion, results have shown that the surface deposits of the basin under study are belonging to two different soil groups. Based on the soil analysis along with the infiltration measurements, the desert pavements are assigned to soil group D, which has the lowest infiltration capacity; Table (6.1). Also, this group of soil D includes the mountainous cover of different rock origins (whether igneous, metamorphic or sedimentary). The rest of the wadi deposits are

assigned to soil group A, which has the highest infiltration capacity. In the basin, there are other forms of land use have to be taken into consideration. These are the asphalt road network, residential areas (Marsa Alam town and Sukkari mining settlement), a little farm (< 100 m^2) and desert tracks. With these all forms of land cover/use represented in a grid, each polygon in the grid has been assigned a runoff curve number (RCN) after looking up the SCS curve number tables. Although, the desert pavements are in the same soil group as the mountains and both have to be assigned the same curve number of the bare soil of value 98, the curve number values of desert pavements have been reduced by 10% to allow for their marginal infiltration capacities (20 mm/day). A curve number of value 88 has been assigned by Colombo and Sarfatti (http://www.fao.org/docrep/W7320B/w7320b22.htm) to soil formations (terraces) similar to those of the desert pavements. These derived RCN values are for the antecedent moisture condition II (AMC II). To adapt these values, *CN(II)*, to the antecedent moisture condition I, *CN(I)*, the following equation has been used:

$$CN(I) = \frac{4.2 \times CN(II)}{10 - 0.058 \times CN(II)} \qquad (6.17)$$

Since it is very common that the drainage area may have more than one type of land cover, and consequently, different CN values, the RCN of the area is taken as the sum of the different CN values weighted by their corresponding fractions of coverage in the area. For the six watersheds of the concerned basin, their average curve number values are given in Table 6.2.

Table 6.2 The average curve number values for the six watersheds of Wadi El-Alam.

Watershed	Average Curve Number
Sukkari	79.68
Khirayjah	78.86
Aswad	81.07
MB2	77.86
MB1	69.49
Alam	75.29

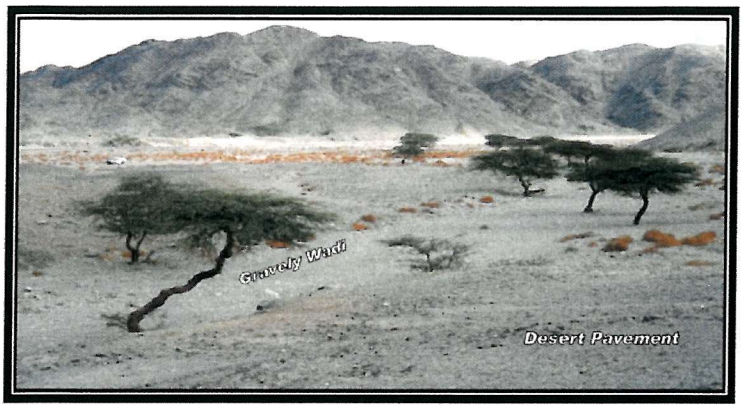

Figure 6.8 unconsolidated wadi bed deposits with acacia trees.

Figure 6.9 Wide wadi channel near the outlet covered with shrubs

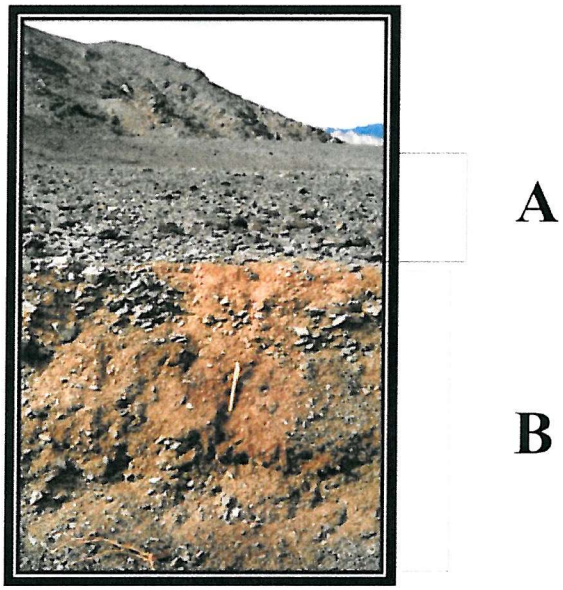

Figure 6.10 Section of desert pavement. (A) Shows the varnish stony surface overlying mixture of fine material (B).

6.7 SENSITIVITY ANALYSIS

Before estimating and analysing the basin's hydrograph, especially after having prepared all the parameters that are needed for running the HMS model, the effects of the spatial and time resolutions on the basin response have first to be considered.

The spatial resolution manifests itself in the resolution of the drainage network of the basin. In the preparatory stage of the basin module for the HMS modeller, the preprocessor CRWR-PrePro delineates a raster based stream network (which later gets vectorized) based on the flow accumulation grid and the user input of the minimum number of cells that contribute flow to a certain point in the DEM (channel threshold). This channel threshold (CT) technically sets the number of upstream cells after which the flow is considered to have the characteristics of channel flow. It also affects the number of sub-basins during the delineation process. The smaller the channel threshold, the greater the number of sub-basins and in turn the greater the number of reaches that link them. At a given number of sub-basins, the smaller the channel threshold the denser the stream network within each sub-basin. Figure 6.17 depicts the response of the basin delineated with three different channel flow thresholds. The smaller the CT the higher is the peak flow. This behaviour could be understood on the basis that at a lower delineation threshold without a restriction on the number of sub-basins (Figure 6.11a), the response of the basin is more rapid as there are more reaches with higher flow velocity. In contrast, at a higher delineation threshold and at a given number of sub-basins (Figure 6.11b), the drainage density is lower and in turn the sub-basin's throughput is slower as the runoff spends more time on the land surface with the same set (number) of routing reaches. Since the finer stream network is desirable and six sub-basins are sought, the channel threshold is fixed to the lowest HMS allowable limit (in this study) of 500 cells (each 30 by 30 m) throughout the rest of this research.

The routing interval, or the time step (Δt), defines the time resolution of the basin response. The time step also affects the lag time of the sub-basin that has been restricted by HMS modeller not to fall below the specified minimum of 3.5 times

the time step. To comply with this restriction on the sub-basin lag time and at the same time get a reasonably resolved basin response, the time has been assigned the value of 30 min. In addition to the routing interval, the basin response might be influenced by the values of two routing parameters namely the Muskingum x parameter and the routing velocity of the flow within the channels.

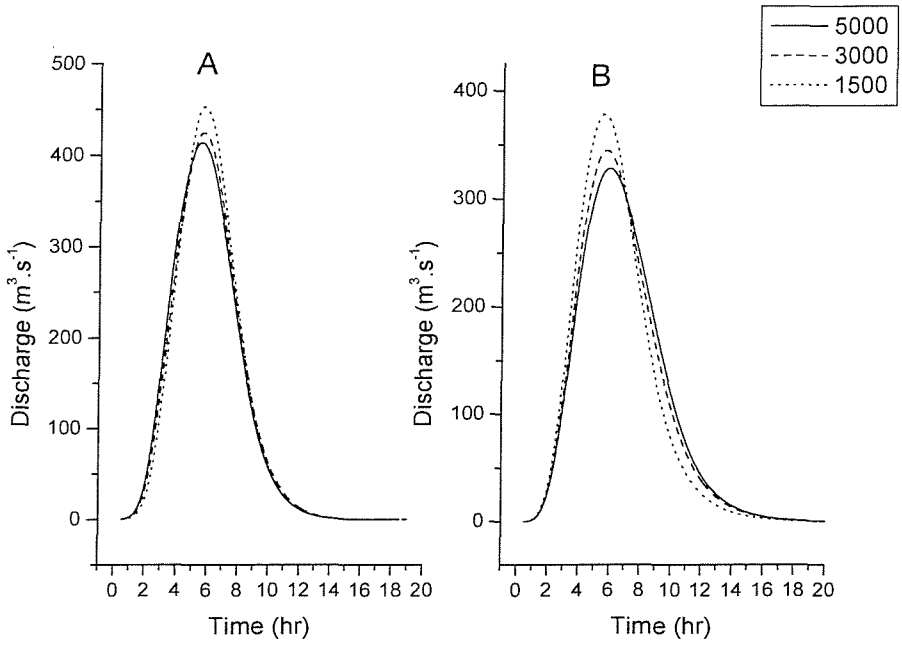

Figure 6.11 The effect of the channel threshold (number of cells required before channels are formed) on the basin response. (A) with and (B) without restricting the numbers of subbasins during the delineation process.

Figure 6.12 depicts the basin response at different values of Muskingum x. Obviously, the Muskingum x, exerts a marginal effect on the basin response. For this reason, the most widely used value of 0.2 for the Muskingum x in the literature has been adopted in this study.

In contrast, the effect of the channel flow velocity is significant, Figure 6.13. The variation of channel velocity affects the time to peak, the peak flow and the overall shape of the hydrograph. At lower channel velocity, the hydrograph is double peaked indicating more pronounced effect of the distance on flow peak timing. The flow from the furthest part of the catchment arrives after flow from the nearest parts of the catchment have began to recede. The higher the channel velocity, the lower the cumulative travel time and eventually the lower the time to peak. Noticeably, at

velocities higher than or equal to 3 $m.s^{-1}$, the shape and peak discharge of the hydrograph start to level off justifying the conclusion that has been already arrived at in section 6.3.5.2 that the routing velocity in the channel could be legitimately assigned the value of the most probable flow velocity (3 $m.s^{-1}$).

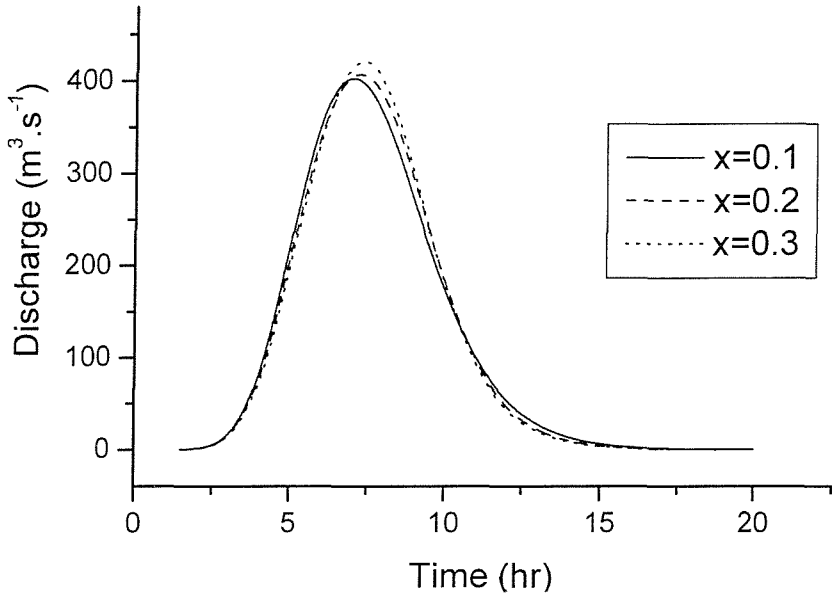

Figure 6.12 The effect of the Muskingum *x* parameter on the basin response.

6.8 THE HYDROGRAPH OF WADI EL-ALAM

The absence of rain gauges within the Wadi El-Alam, is the main reason behind the usage of a synthetic rainstorm in the present study. There are two recording meteorological stations around the study area lying along the Red Sea coastline. The first station is located in Ras Benas south of Wadi El-Alam, whereas the second is located in El-Quasier north of it. Both stations are far from Wadi El-Alam by around 70 km. The inspection of archival precipitation data of these stations over a period of 30 years, Figure 1.7, indicates that in extreme events of rainfall the area experiences rainstorms of total rainfall depth in the range of 60-70 mm. Since the study area is of a hyperarid nature, it means that this amount of rainfall had been precipitated in a short period of time. The rainstorms in the Eastern Desert are typically short, lasting on the average two hours (Naim, 1995). Thus, the

assumption that will be made during the running of the HMS model that Wadi El-Alam *similarly* is uniformly (in time and space) covered by a rainstorm of an intensity of 30 $mm.hr^{-1}$ for two hours becomes justifiable.

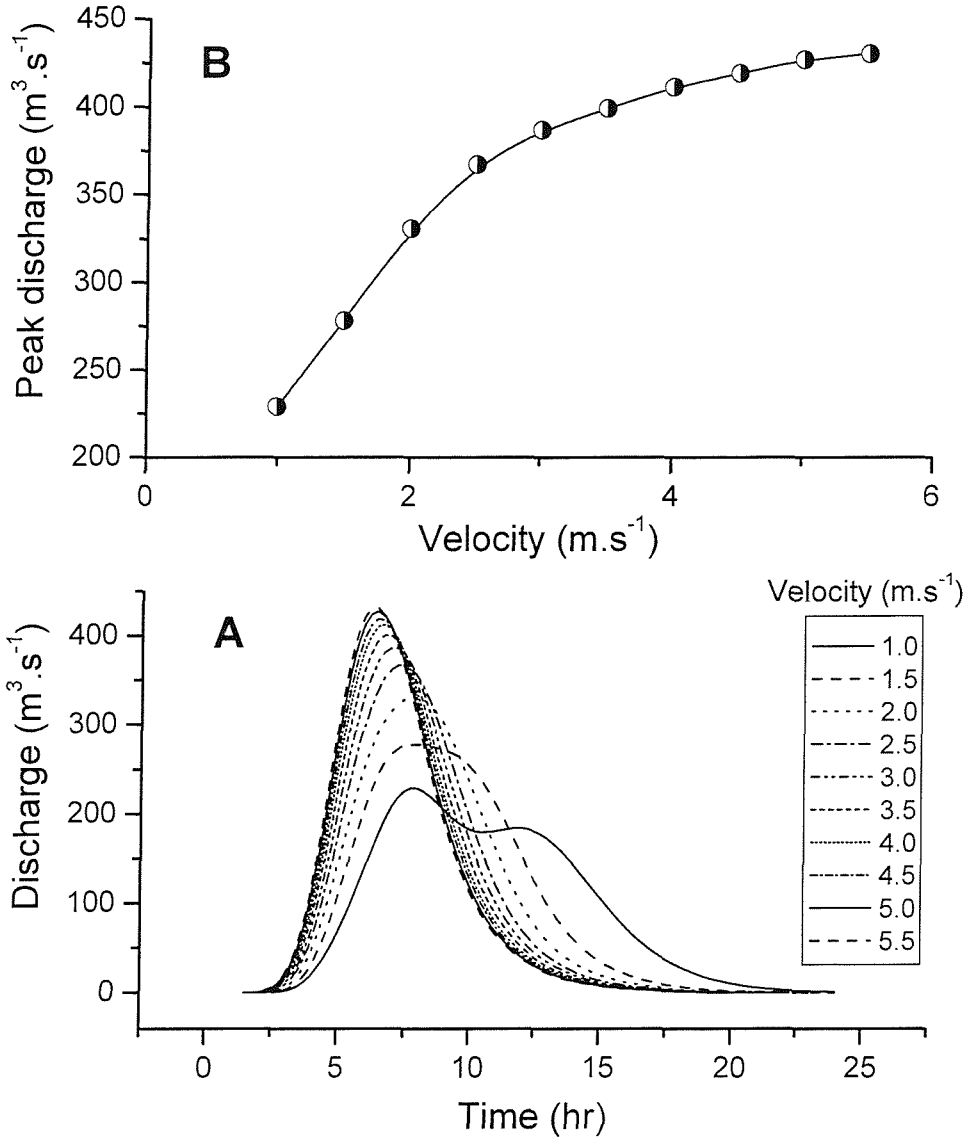

Figure 6.13 The effect of the routing velocity on the basin response (A) and the peak discharge (B).

Figure 6.14 shows the calculated hydrograph at each sub-basin's outlet and at the main outlet of the basin. Examination of this figure reveals that the total hydrograph of Wadi El-Alam is a single peak, which indicates that the peak discharge of at least the main sub-basins arrive the main outlet more or less at the same time. The discharge starts after 1.5 hours, reaches a peak after 6 hours with peak discharge of 393 $m^3.s^{-1}$ and subsides completely after 16 hours. Out of the total precipitation just 30% appears as discharge at the main outlet. This amount of discharge is equivalent to 17.8 mm (out of 60 mm) total excess precipitation (runoff) if the rainfall is uniformly distributed over the total basin area (406.89 km^2), the rest of the rainfall infiltrates into the subsurface.

The discharge of each sub-basin is influenced, among others, by the curve number of the sub-basin's land cover. The area normalised discharge might be taken as an indicator of the sub-basin's throughput (or rainfall that does not infiltrate), which is scalable by its area as shown in Figure 6.15. The higher the curve number, the higher the throughput of the sub-basin. The effect of the morphometric parameters of the basin on its discharge will be discussed in the next chapter.

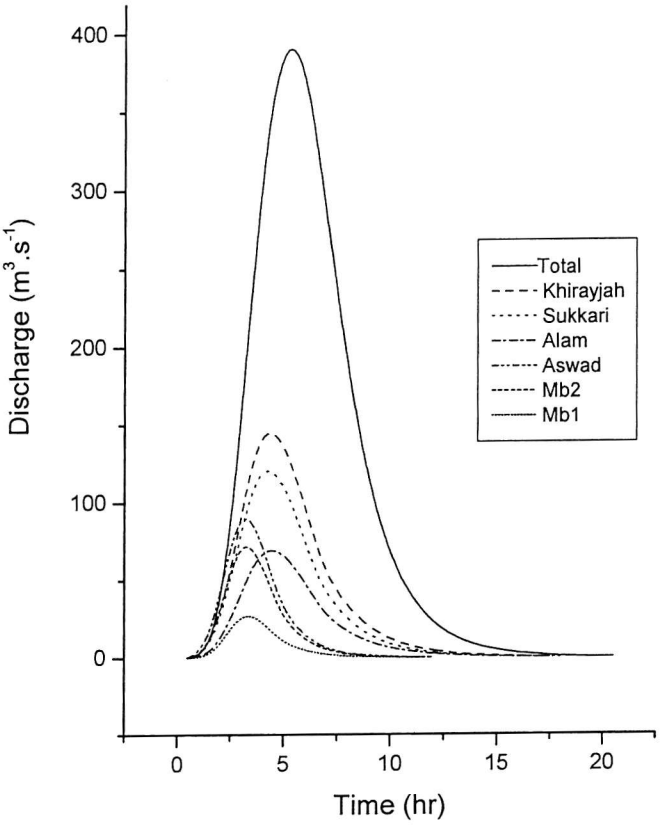

Figure 6.14 The calculated hydrograph of Wadi El-Alam as a response to rainfall event covers it uniformly for two hours with total precipitation of 60 mm.

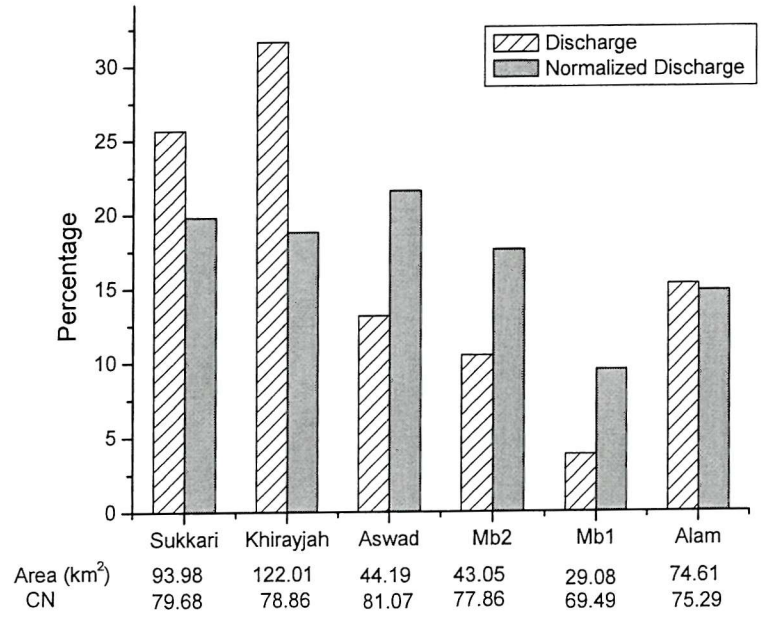

Figure 6.15 The percentage of discharge of each sub basin's along with its area normalized discharge.

6.9 SUMMARY

This chapter presents an integrated approach to simulating the rainfall-runoff processes in Wadi El-Alam within the quasi-distributed framework of the Hydrological Modelling System (HMS). With this model, the Wadi was viewed as a series of hydrologic elements (sub-basins, junctions, reaches and sinks) sequentially linked in such a way that the runoff was routed from one element to another until the main outlet was reached. With the aid of the GIS based CRWR-PrePro pre-processor, the hydrologic elements and their hydrologic parameters were derived from the basin's DEM and saved in ASCII file readable by HMS model. Precipitation excess due to a synthetic rainstorm of 60 mm total rainfall depth in two hours was accounted for in the model by means of the SCS method. This method estimates the excess rainfall as a function of the cumulative rainfall, initial losses and the maximum potential retention, which is dependent on the empirical curve number. The curve number reflects the infiltration properties of the basin land cover. Information on the land cover was derived from the remotely sensed imagery of the basin, soil texture analysis and in-field conducted infiltration capacities. From this information and through looking up the curve number tables of the SCS, the weighted curve number values for each sub-basin were extracted and in turn the runoff as a function of time was calculated. The routing of runoff within the sub-basins and channels was respectively modelled using the unit hydrograph and Muskingum methods. After deciding upon the optimum values of the user input parameters, the model was run to simulate the hydrographs at the main Wadi outlet and at each sub-basin's outlet. The total hydrograph of Wadi El-Alam is of a single peak indicating that the peak discharge of the main sub-basins arrive the main outlet more or less at the same time. The total discharge represents just 30% of the total precipitation; the rest of the rainfall infiltrates. Within 1.5 hour from the commence of the rainfall, the discharge starts to appear at the main outlet, reaches a peak after 6 hours with peak discharge of 393 $m^3.s^{-1}$ and subsides completely after 16 hours.

Chapter 7

Flash flood risk assessment for Wadi El-Alam basin

7. 1 INTRODUCTION

The increasing number of studies on the damages of the desert flash floods, especially in the last few decades, reflects the role played by the human intervention in exaggerating the destructive effects of these floods. Most of the newly built towns in deserts and their serving networks of roads intercept, in some way or the other, the flow of the floods. Therefore, in any flood risk assessment study, one has to be concerned not only with the flood itself as hazardous source but also with its receptors and pathways. By the receptors is meant the target elements, mostly man-made constructions that get affected by the risk of the flood. The pathways are the channel networks, i.e. conveyors, which transport the hazard of the flood to the targets. It is the combination of these three factors that determines how significant a risk would be.

In this chapter, an overview of the flood hazard in the area of Wadi El-Alam will be presented. The risk to Mara Alam – Idfu road and the factors affecting flood risk at the town of Marsa Alam will be examined.

7.2 EXPOSURE TO THE FLOOD HAZARD IN WADI EL-ALAM

The town of Marsa Alam was established on the Wadi El-Alam fan (outlet) and hence experiences flash floods from time to time. The topography of the area at the Wadi's outlet increases the flood problem to the town. There are two sedimentary rock hills located on the Wadi's outlet that reduce the Wadi channel width from about 1200 meters before the entrance of the hill zone to approximately 100 meters (Figure 7.1). This narrow width causes a concentration of the floodwater that increases the damaging ability of the flow. Part of the contemporary Marsa El-

Alam is spreading over the Wadi floor and, as a result, is open to flood hazards. In spite of these flood risks, the residential quarters continue to be built and the town is still expanding along this risky part of the Wadi. The extremely arid climate and the long floodless years encouraged the locals to forget the flood damage shortly after its occurrence, leading to more building in this part. The recent urban developments in the town have been constructed on the top of the two sediment rock hills to avoid flood risk. These two hills themselves were liable to the lateral erosion of the floodwater, which may threaten the existence of such urban settlements. Locals of the town are using now some local rock blocks to strengthen the hillsides (Figure 7.2).

The basin under study also includes sectors of both the Red Sea coastal highway and the Idfu-Marsa Alam road. The highway is constructed close to the Red Sea shore crossing the El-Alam alluvial fan and consequently subjects to flash flood hazards. Until the recent past, the coastal highway and the railways in the Red Sea region of Egypt were always severely damaged by flash floods. In general, the highway was unprotected on most of its parts while protected in others with poorly functioned mechanisms (constructions). Recently, several bridgeless crossings have been constructed along the coastal highway (Figure 7.3) while huge box culverts have been built along the coastal railway (Figure 7.4). These constructions have somewhat reduced the impact of the flash floods on both routes. The sector of the coastal highway that crosses Wadi El-Alam fan (outlet) experiences little appreciable damage probably because it was being constructed at exactly the same level of the Wadi floor. In the flood event, it becomes covered with sediments that merely need removal after the flood to reuse the highway again. Beside this road and parallel to it, a pedestrian road has been constructed near to the sea, but at a level 1 meter high from the Wadi floor. Although, it has been protected by two circle culverts (Figure 7.5), they were of so low hydraulic capacities that they got plugged with coarse wadi deposits and woody debris to a degree enabled the floodwater in the flash event of 1996 to wash the road away and surge it in the direction of the sea (Figure 7.6).

The eastern part of the Idfu-Marsa Alam road has been mostly constructed on the floor of the main drainage course of the Wadi El-Alam and its east-west tributary El-Aswad with a total length of approximately 36-km. The road is crossing a series of alluvial fans, which develop at the outlets of some sub-basins within the studied basin. These sub-basins are draining towards the main trunk of Wadi El-Alam from both sides giving rise to many problems such as the destruction and erosion of some parts of this road and covering it with a large amount of sediments.

It seems that this roadway has been constructed with the consideration of keeping it at a constant elevation noticeable from its curves or meandering shape. It runs close to the mountains fronts in its inter-fan segments while runs far from them on the fans themselves. This was to protect it from the floodwater at the sub-basins outlets. The curvatures along the road are relatively dense, because of the high drainage density characteristics of the arid mountain blocks. It has been reported by Schick (1974, 1979) that the spacing between neighbouring outlets of drainage basins at the mountain front will mostly be on the order of 1 km or less which is quite impossible for modern traffic.

Available evidences (Schick 1974,1979) indicate that exposure to flood damage increases on those parts of the road that have been constructed at the base of the fan than those that are close to the fan apex. This may be explained by the nature of the fan. The channel density is much higher at the base of the fan rather than its apex where there is only one well defined channel. This means that the road might be hit at one point at the apex of the fan but at many at its base. Local wadi bed deposits have been used as aprons to shield the road segments that have been attacked by the flood. The aprons that are made of the local deposits of the Wadi have been found ineffective as they shortly collapse after the flood occurrence. They even might feed the flood water with more wadi deposits that help in the erosion of the road. At the end of the nineties and on the urgent demand for joining the Nile valley with the Red Sea coastal zone via good and safe road networks, the Idfu-Marsa Alam road has been recently renewed with some parts reconstructed on the old road. As a technical improvement, the road planners in this time have taken into their considerations the modern standards that specify large horizontal radii of curvature

needed for the fast modern traffic (Figure 7.7). The deposit aprons have been replaced with concrete ones to create a bridgeless crossing in the front of the large sub-basins outlets expecting to reduce the damaging effects of the coming floods (the new road does not so far experience any flood).

7.3 HAZARD ASSESSMENT FOR THE IDFU-ALAM ROAD

7.3.1 Introduction

To identify the flood liable sites along the Idfu-Alam road, the crossing points (outlets) of the channel network with the road have been interactively located into a grid. On feeding this grid together with those of the channel network and the flow direction (both were already generated in chapter 3) into the WATERSHED grid function of the Grid module of Arc/info, it was possible to delineate, in the raster domain, the total area that leads to stream flow at each pour point (outlet) and consequently the boundaries of the sub-basins that drain directly to the road. A vectorization process is then applied by making use of the raster to vector conversion function of the Grid module of the Arc/info. This delineation process produced 55 sub-basins. After the exclusion of sub-basins of areas less than 1 km, 25 sub-basins have been left. 32 percent of them are located on the northern side of the road and the rest are on its southern side (see Figure 7.8).

The longest flow path and its length and slope for each delineated sub-basin have been computed using the CRWR-PrePro ArcView extension. On using these lengths and slopes with the curve number (CN) grid, that was already generated in chapter 5, the lag time for each sub-basin was calculated. From the data sets of both the channel and the sub-basins, the topology of the hydrologic system has been extracted and saved in ASCII file readable by HEC-HMS program. This file contains the type (e.g. channel, sub-basin, junction and sink), the hydrological parameters and downstream element of each hydrologic element of the system.

Figure 7.1 The narrow outlet of Wadi El-Alam

Figure 7.2 People using some local rock blocks to strengthen the hillside of the Wadi outlet

Figure 7.3 Bridgeless crossing along the Red Sea coastal road.

Figure 7.4 Large box culverts along the railway line.

Figure 7.5 Small culvert for passing the flood water under the pedestrian road.

Figure 7.6 Part of the pedestrian walkway damaged by a flood in 1996 due to the small size of the culvert that constructed under it. The line annotated runs along the length of the walkway and shows the general vertical profile after the flood damage in the bottom photo.

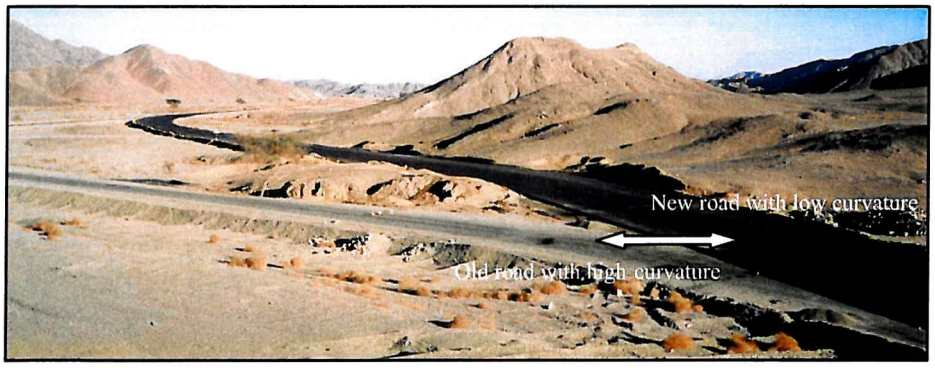

Figure 7.7 Oblique view of the Idfu-Marsa Alam road crossing through the Wadi El Alam. Note the low culvert of the new Idfu-Marsa Alam road that suits fast modern traffic.

Figure 7-8 The derived Sub-basins that are draining directly toward Idfu-Alam road.

A rainstorm of intensity 60 mm for 2 hours has been used in the precipitation model of the HEC-HMS with the assumption that the rainstorm uniformly and exclusively covers one sub-basin at a time. By executing the HMS model, the peak flow for each sub-basin has been evaluated (see Figure 7.9). At this point, it has to be emphasised that the peak discharge for a certain sub-basin is intimately related to its morphometric parameters. Therefore, the variation in the derived peak discharge values has to be accounted for on the basis of the morphometric parameters that have strong impact on the strength of the discharge of the concerned sub-basins.

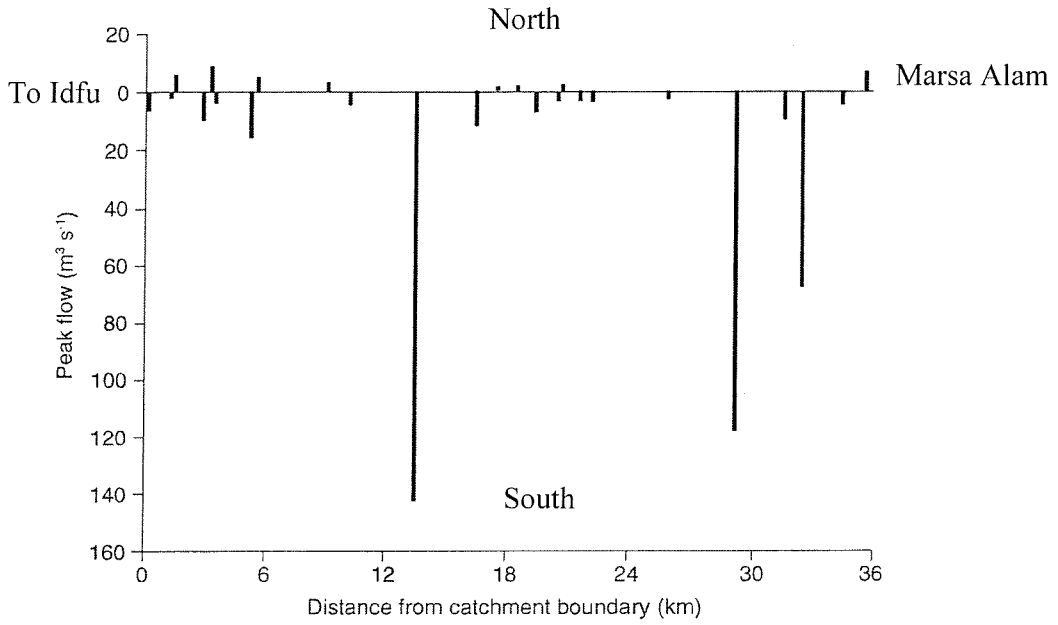

Figure 7.9 Predicted peak flow from the 25 sub-basins. For presentational reasons the horizontal line represents the road so that the flows from basins draining from the north and south may be discriminated.

Among these morphometric parameters are the drainage density, the ruggedness number, the elongation ratio, the main channel slope, the relief ratio and the average basin slope. These parameters have been computed for each sub-basin and tabulated in Table (7.1). This is in addition to the Curve Number parameter, which reflects the land cover and soil type of the sub-basins. As becomes clear from table 7.1, these sub-basins have diverse topographic features that are reflected in their calculated morphometric parameters which vary from one sub-basin to the other

(Figure 7.10), in a way making them affect the Idfu-Alam road differently. In general, there are a large number of these sub-basins of channel gradient so high as 3.5% that they induce floods of short time to peak. Basin shape (elongation ratio) for many sub-basins are also of high values up to 0.80; giving rise to high peak flows of short time of concentration. With reference to Figure 7.9, it can be seen that the highest peak flows are mostly produced from sub-basins on the southern side of the Idfu-Alam road. This is in addition to few northern sub-basins that are near to the western end of the road.

Table 7.1 Morphometric parameters of the sub-basins that are draining toward the road.

BASIN ID	CURVE NUMBER	AVERAGE BASIN SLOPE (°)	MAIN CHANNEL SLOPE (%)	RUGGEDNESS NUMBER	ELONGATION RATIO	AREA (km^2)	PEAK FLOW ($m^3.s^{-1}$)
1	71.69	2.15	0.65	0.64	0.41	6.25	6.70
2	63.37	2.35	0.60	0.89	0.48	9.29	4.81
3	75.29	6.94	0.20	2.52	0.42	74.61	68.01
4	79.68	8.72	0.19	2.94	0.50	93.98	118.30
5	78.86	8.79	0.20	3.46	0.59	122.01	142.12
6	82.03	14.12	0.89	0.71	0.51	5.16	10.44
7	82.85	8.44	1.93	0.58	0.58	1.47	3.10
8	84.90	9.04	1.78	0.52	0.64	1.61	3.76
9	76.00	7.01	1.55	0.42	0.59	2.44	3.50
10	77.02	8.09	1.23	0.54	0.52	2.43	3.70
11	81.56	6.63	1.08	0.46	0.51	3.83	7.56
12	76.16	4.57	0.94	0.64	0.70	8.58	12.42
13	75.42	3.93	1.04	0.41	0.51	3.55	4.89
14	83.05	8.25	0.81	0.77	0.52	7.57	16.15
15	83.45	8.57	1.72	0.47	0.56	1.69	3.70
16	82.95	8.70	1.00	0.81	0.60	4.86	10.32
17	82.39	6.12	0.05	0.56	0.51	1.22	2.46
18	81.28	9.00	0.95	0.66	0.46	3.30	6.10
19	83.04	11.39	1.25	1.70	0.49	2.77	5.91
20	84.82	12.48	1.25	1.53	0.56	3.66	8.54
21	83.01	10.09	1.38	0.91	0.55	2.51	5.34
22	82.89	6.90	2.00	0.70	0.79	1.28	2.72
23	76.30	4.59	0.04	0.44	0.76	1.02	1.47
24	79.31	6.74	2.75	0.35	0.81	1.01	1.76
25	81.05	8.57	2.43	0.35	0.70	1.19	2.10

The southern sub-basins; namely, Khirayjah (*id* 5), Sukkari (*id* 4) and Alam (*id* 3) are of high ruggedness number. The rather high peak flows from the northern basins — such as sub-basins of *id* numbers 19, 20 and 21 — can be correlated

mainly with their high relief ratio, high average basin slopes, and their high main channel slopes which help in reducing their basin lag times. Being of high curve number (CN), these northern sub-basins are of reduced water loss and increased surface runoff. Thus, with the reliance on the morphometric characteristics of all sub-basins one might be able to arrive at risk map for the Idfu-Alam road as outlined in the next section.

7.3.2 Risk classes

The mapping and topography of the sub-basins (watersheds) that drain directly on Idfu-Alam road have been explored in the previous section. Before digressing into the issue of rating these watersheds from the flood hazard point of view, a question begs itself. Is there some sort of similarity among these watersheds as far as the morphometric parameters are concerned? The notion behind this question is that watersheds of comparable topographies, land covers, soil types and areas, expectedly, will respond to a certain rainstorm similarly; subsequently, their classifications into different hazard zones get possible. Ahead of answering this question, the significance of hazard in the present context has to be clarified. According to its definition "hazard" means the probability of occurrence within a specified period of time and within a given area of potentially damaging phenomena (Vames, 1984). Since the area of interest is arid, the hazard in such kind of environments has to be *relatively* measured by the damage of *any* flood occurrence in the area. Undoubtedly, the damage of a flood is in direct relationship with its *peak discharge* not with its total amount of discharge.

Back to our question, the resemblance among the sub-basins can be explored by using the cluster (segmentation) analysis. Cluster analysis is a method of classification that places set of objects in groups, or clusters, in such a way that the profiles of objects in the same cluster are very similar and the profiles of objects in different clusters are quite distinct. Cluster techniques are either non-hierarchical (iterative) or hierarchical. Generally, the hierarchical methods are more widely used because they give greater insight into the overall structure.

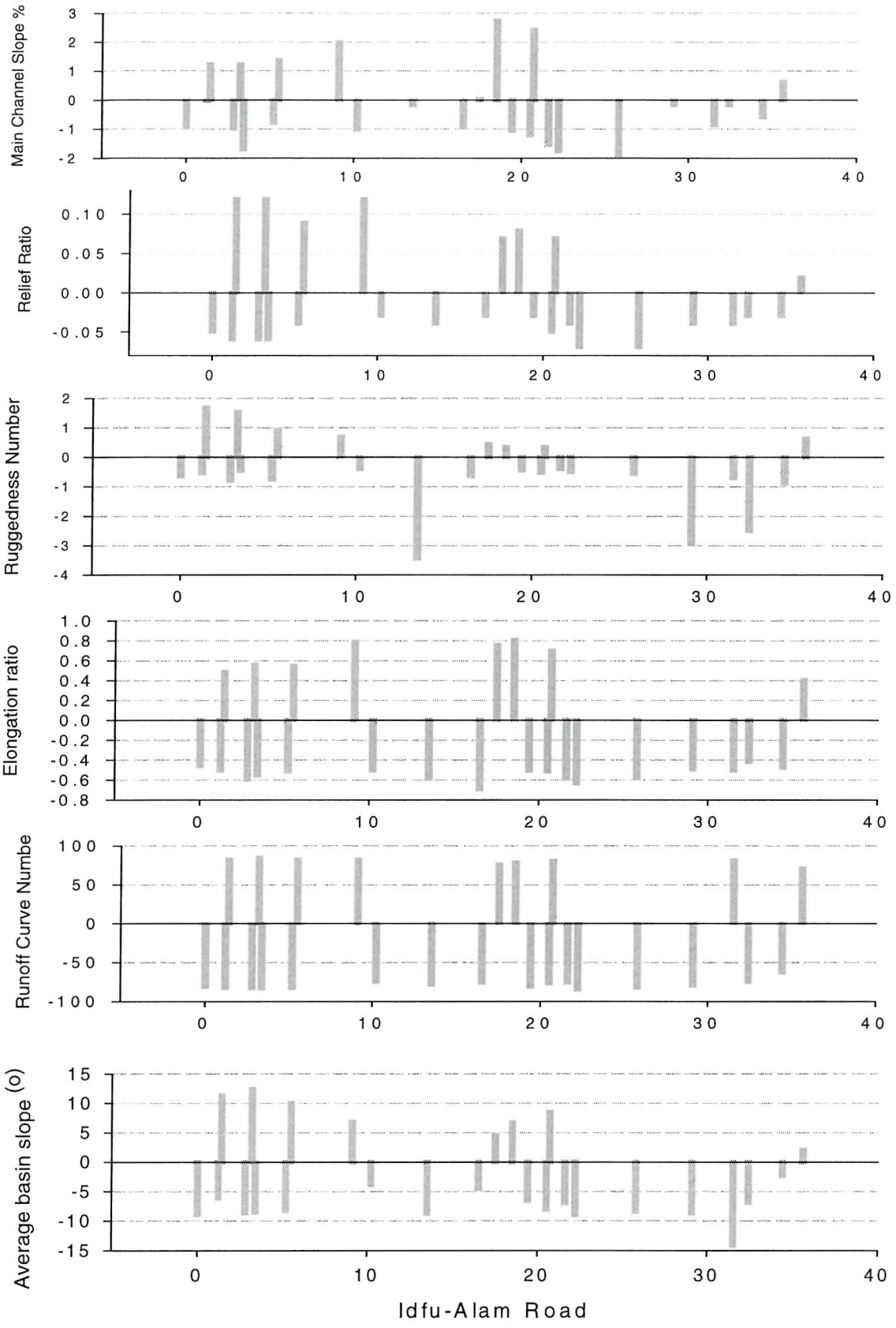

Figure 7.10 Morphometric parameters of the sub-basins that are draining toward the road. The negative signs are just for distinguishing the southern watersheds from the northern ones.

There are 2 ways of doing a hierarchical analysis - agglomeratively or divisively. The divisive method begins with all cases in one cluster. This cluster is gradually broken down into smaller and smaller clusters until some predetermined threshold is reached. That threshold might be determined by group size or relationships among group members. Agglomerative methods begin with each object representing a cluster, joining the two most similar, and then repeatedly joining new clusters together. Practically, the complete process of this type of hierarchical clustering can be summarised as follows:

1. Standardise the variables. Since the characteristics (variables) of objects differ in magnitude (mean value) and dispersion (standard deviation) one has to standardize them first. Standardization is the process of making variables comparable in magnitude and dispersion, i.e. unit-free: one subtracts the mean from each variable and divides by its standard deviation, giving all variables a mean of 0 and a standard deviation of 1.

2. Find the similarity among objects. In this step, one measure the similarity in a form of distance (proximity), according to a certain metric, between every pair of objects in the data set. For data set made of m objects, there are $m.(m\text{-}1)/2$ pairs in the data sets.

3. Fuse (amalgamate), in line with a certain clustering algorithm, the two most similar objects and recalculate the distances.

4. Repeat step 3 until all objects are in one cluster.

Keeping in mind that the effect of single large distance differences (outliers) has to be dampened to large extent and finely separated clusters (of small size) are sought, it has been decided to use in the present study, among many others, the block (Manhattan) distance metric and the agglomerative Ward's clustering algorithm as implemented in the Minitab package (Minitab, 2001). With the curve number (CN), average basin slope (ABS), main channel slope (MCS), area (Area), ruggedness (Rugd) and elongation ratio (ER), as flood influential variables characterising the 25 delineated sub-basins (as objects) that drain directly on the Idfu-Alam road, the adopted clustering procedure produced a cluster tree (dendrogram) depicted graphically in Figure 7.11. Deciding upon the optimum

number of clusters (also called the final partition) is largely subjective, although looking at the level of similarity or distance at fusion versus number of clusters may help. There will be sudden jumps in the level of similarity as dissimilar objects are fused. Here, the similarity level decreases by increments of about 2 until it decreases by about 13 at the step from seven clusters to six. This indicates that seven clusters are reasonably sufficient for the final partition. On scrutinizing table 7.1, in particular its entry of peak discharge, taking into consideration that the principal objective of this clustering analysis is to classify the sub-basins into groups of similar response (measured by the peak discharge) in accordance with their morphometric parameters, it becomes justified that a final partition of four clusters is a good choice, Figure 7.11.

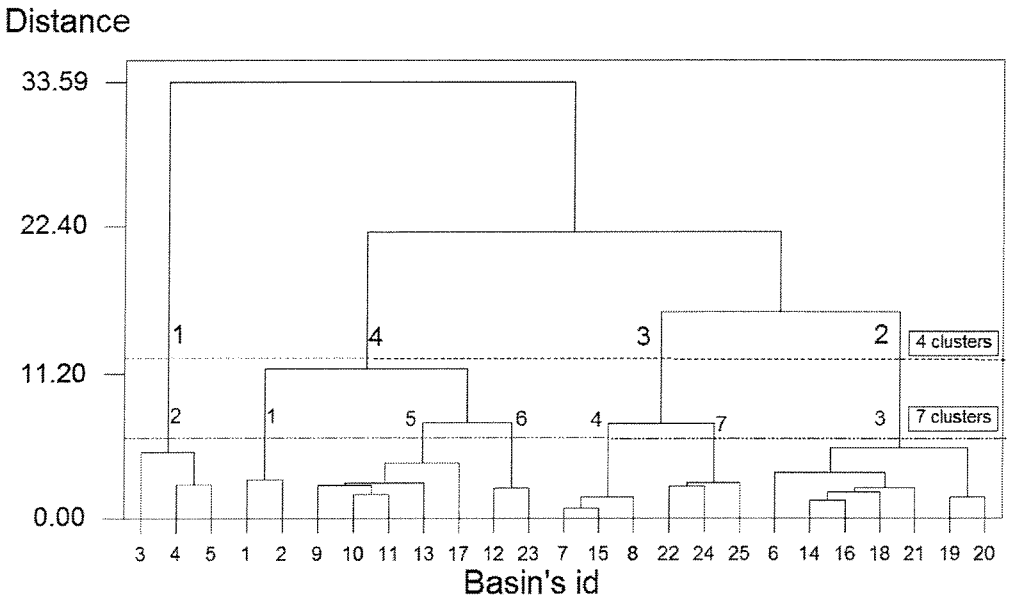

Figure 7.11 Dendrogram for the sub-basins that drain directly on the Idfu-Alam road using the ward's clustering method and the Manhattan distance metric.

These four clusters can be visualised in two dimensions if one attempts to extract the underlying (latent) variables, or the factors, that explain the pattern of correlations (covariances) within the data set of the concerned sub-basins, see Table 7.2. Factor analysis can be used to identify a small number of (uncorrelated) factors (which are themselves not directly observable) that explain most of the variability observed in a larger number of manifest variables. As revealed by the

principal component factor analysis, Table 7.2, the first two components explain 74% of the variability of the morphometric data and the communality values indicate that all the morphometric variables but elongation ratio (ER) are to far extent represented by these two factors (communalities are 0.34 for ER, 0.70-0.84 for other variables). Factor 1 has large positive loadings on Rugd (0.918), Area (0.891) and negative loadings on MCS (-0.752) and ER (-0.549). Factor 2 has large positive loadings on ABS (0.921) and CN (0.902) while the loadings on MCS (0.364), Rugd (0.228) and ER (0.194) are small. Given that one of the basin's dimensions, *viz.* relief (height), is contained in its ruggedness (Rugd) parameter and its other two dimensions in its area (Area) parameter, factor 1, which principally loads on Rugd and Area, might be interpreted as reflecting the morphometric dimensions of the basin. In view of its large positive loads on ABS (which controls the average velocity of the surface runoff) and CN (which defines the amount of the surface runoff), the second factor might be considered to be a "runoff" factor. Having reduced the number of factors needed to explain the variability of the data, the four clusters that have been mentioned above, and emerged also from the partitioning around medoids (S-Plus, 1998) as an alternative (confirmatory) clustering method, can now be projected into the bivariate space of factors 1 and 2, Figure 7.12. Should the Area be dropped as an observable, the pattern of clustering in Figure 7.12a should not change, see Figure 7.12b, as the Area and Ruggedness number are two variables moving in the same direction in factor 1; they are measuring the same driving principle governing the behaviour of the system.

At this point, one issue needs the light to be shed on. As the peak discharge (response) of a basin is a function of the intensity, duration, and location of the rainstorm, the peak discharge has to be used as a quantitative measure for the basin's response at a certain rainstorm to qualitatively classify the basins among themselves into hazard classes. Put another way, the limits of a certain response class have not to be set by the absolute values of the peak discharge that change with the rainstorm characteristics.

The six sub-basins in cluster 3, Figure 7.11, are of less than 5 m^3/s peak discharges (PD) and could be considered to be a group of sub-basins of response of a rank

slightly hazardous. Cluster 2 encompasses seven sub-basins of higher than 5 m^3/s and up to *ca.* 20 m^3/s peak discharges. Compared with the first group of sub-basins, these sub-basins of cluster 2 might be ranked as hazardous sub-basins. Although the nine sub-basins in cluster 4 are of peak discharges (6 sub-basins of PD < 5 m^3/s and 3 of PD > 5 m^3/s) overlapping with those in the last two clusters, this cluster is twice probable to be classified according to the rank of cluster 3 (slightly hazardous) rather than to that of cluster 2 (hazardous). Cluster 1 includes three sub-basins. A single sub-basin is of 68 m^3/s peak discharge and couples of sub-basins are of higher than 115 m^3/s peak discharge. Therefore, cluster 1 in itself has to be considered to be consisting of two groups of sub-basins and they might be ranked, accordingly, as highly hazardous and risky sub-basins. The splitting of cluster 1 into two groups, each includes 1 and 2 sub-basins, respectively, is quite evident when the dendrogram, Figure 7.10, gets trimmed at similarity level of approximately 65%.

In this way and on mathematical grounds it was possible to categorize the sub-basins that drain directly on the Idfu-Alam road into four different risk classes, as illustrated in Figure 7.12, with the complete reliance on the *interplay* of their morphometric parameters that has been quantified by their peak discharges. The average values for the morphometric parameters of each group of sub-basins in each risk class are tabulated in Table 7.3. Although, the sub-basins in the hazard class are of average basin slope (ABS) comparable to those in the risky class, they are on average of different basin fabrics (ruggedness) and dimensions reflected by the average values of their ruggedness and Area parameters. The same applies to the sub-basins that are in the slightly and highly hazard classes. Thus, in line with the interpretation of factor 1 and factor 2, see above, it may be concluded that factor 2 separates the sub-basins into two groups each of two different risk classes that are further get separated by factor 1 ultimately into 4 risk classes.

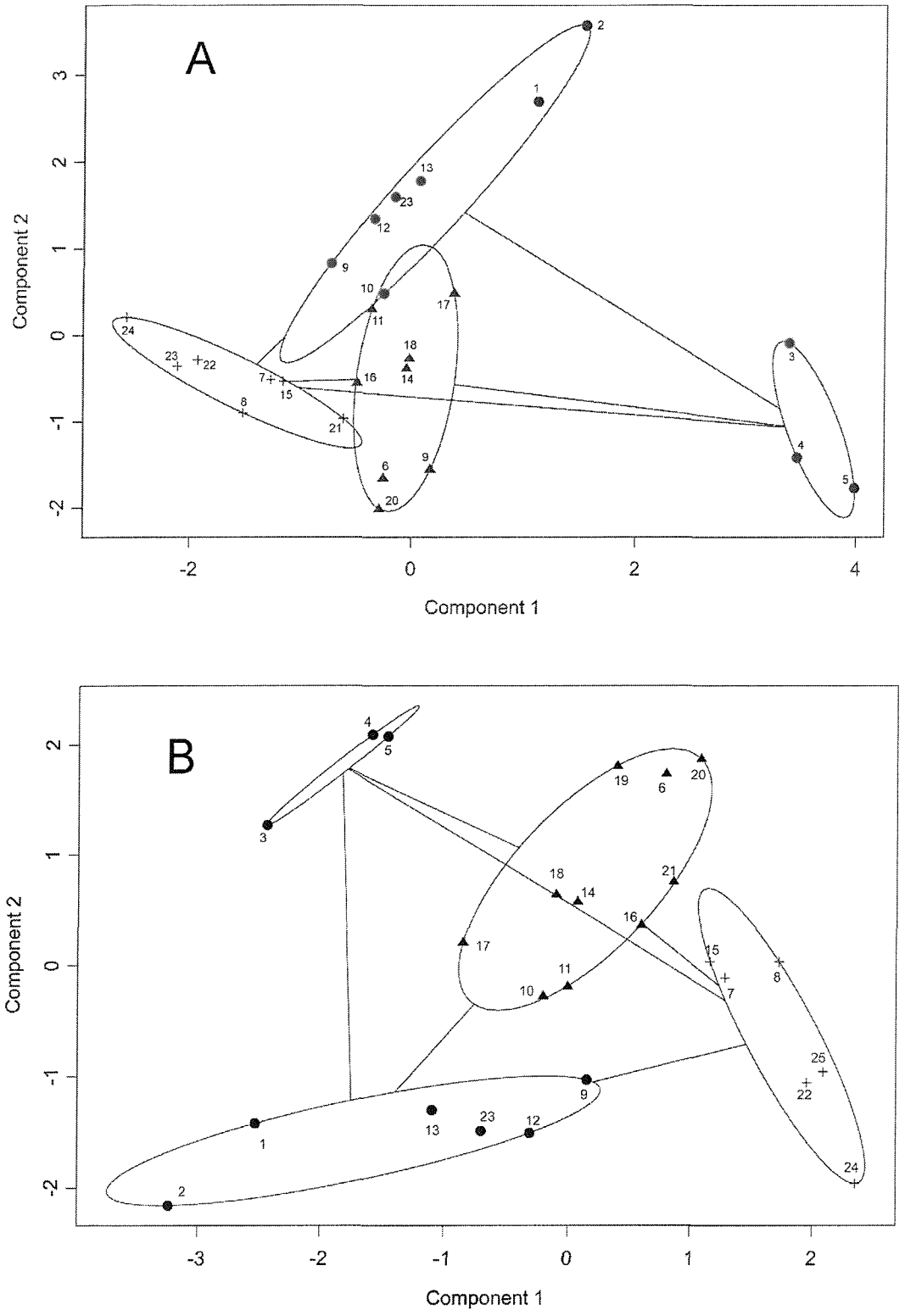

Figure 7.12 Cluster plot for the sub-basins that drain directly on the Idfu-Alam road with the area (A) and without the area (B) using the partition around the medoids and Manhattan metric. The two components explain 74% (A) and 75.53% (B) of the point variability.

Table 7.2 Factor analysis of the morphometric parameters of the sub-basins that drain on the Idfu-Alam road.

VARIABLE	*FACTOR 1*	*FACTOR 2*	*COMMUNALITY*
CN	-0.19	0.902	0.849
ABS	0.1	0.921	0.858
MCS	-0.752	0.364	0.698
Rugd	0.918	0.228	0.894
ER	-0.549	0.194	0.339
Area	0.891	0.086	0.802
% variance	42.5	31.5	74

Extraction method: principal component analysis.
Rotation method: Varimax.

Table 7.3 The average morphometric parameters for sub-basins in each risk classes.

RISK CLASS	*NO. OF BASINS*	*ABS (°)*	*MCS (%)*	*RUGD*	*AREA (km^2)*
Slightly hazard	12	6.70	1.43	0.52	2.35
Hazard	10	8.74	1.02	0.88	4.85
Highly Hazard	1	6.94	0.21	2.52	74.61
Risky	2	8.76	0.19	3.20	108.00

ABS is the average basin slope in degree, MCS is the main channel slope in percent. RUGD is the basin's ruggedness.

The relative risk classes of the sub-basins were found in one of the field visits consistent with the observations of the local Bedouins and residents of Alam town. Furthermore, in the flash event of 1991, two sites (among others) along Idfu-Alam road at 7 and 22.5 km, respectively, from the main basin's outlet were devastatingly ruined (El-Etr and Ashmawy, 1993). These two sites are located exactly at the outlets of the two sub-basins Sukkari and Khirayjah (basins no. 4 and 5), Figure 7.13, which have been classified, in the view of the present study, as risky, see above. The localisation of 6 (out of ten) of the hazardous sub-basins within the last ten kilometres of the road, especially they are distributed on both sides of the road and are so easily to be covered by any rainstorm of moderate size, renders this

area of the road of great danger. All these fact-matching outcomes confirm the reliability of the risk map that has been arrived at with the conclusion that the risk along the road is not simply related to sub-basin area as small, steep as highly rugged sub-basins are also dangerous locations.

7.3.3 Suggestions for flood hazard mitigation along the roadways in arid regions

Due to very long intervals between flood events little attention had been paid to these natural processes, resulting in a fallacious sense of security from destructive floods and in widespread settlement before newcomers to the desert are faced with the flooding problem. The extremely arid climate and long floodless years encourage the locals to forget the flood damage shortly after its occurrence, leading to an overall neglect in the maintenance of drainage ways, which have not been active for years (Tamir *et al.*, 2000).

One of the possibilities of reducing the flood hazard to transport lines in places where they cross desert wadis is to determine the route locally on the basis of flood experience correlative with geomorphic and vegetation feature (Schick, 1979). The road surface should stick to the original wadi floor as closely as possible. Schick (1974, 1979) declared from some evidence that road exposure to flood damage increases with vertical deviation of the road structure from the grade line. If the roadway is constructed below the Wadi level the road will be covered by sediment in even small flood events. A situation where the roadway is built above the Wadi bed level is usually tied to a channel crossing with a culvert. To keep a culvert clean from wadi deposits and woody debris it should be constructed with a suitable hydrologic capacity. Culverts are widely used in stream/road crossing sites in many places in the Egyptian desert. Some of these culverts are washed out or failed during flash flood events, and as a consequence failure of the culvert can cause erosion of the road system.

Culvert failure may have several causes of which hydraulic capacity is such one. Undersized culverts retard the passage of floating debris and wadi deposits, decreasing water flow velocity and the capacity for sediment transport, and

increasing the likelihood of plugging. A culvert's ability to transport sediment is based on a ratio between the slope of the culvert and the upslope channel; culverts set at a substantially lower gradient than the natural channel will tend to retard sediment transport and promote plugging. Where the culvert is not aligned with the channel, stream energy losses and reorientation of entrained floating debris are likely to lead to sediment deposition at the inlet. When large rocks, which are often moved downstream by rolling, encounter the edge of a culvert, rocks can lodge leading to plugging by sediment and debris. Culverts should be oriented with the natural wadi channel, and present no angular deviation from the natural channel platform. Moreover to keep the channel at grade and avoid sedimentation culverts should be set on the same or greater gradient as the natural stream channel to avoid accumulation of sediment at the inlet (Sckick 1997). Culverts as wide, or nearly as wide, as the stream channel minimising the cross-sectional change in the channel and are lest likely to plug, but at the same time, installation of a culvert that is larger than necessary results in needless expanse (Campbell and Sidle, 1984). Hydraulic capacity of culverts can be determined using some empirical culvert-sizing models (USGS 1977, Piehl *et al.,* 1988; Campbell and Sidle 1984), but these models need information on flood magnitudes. Culverts provide an inexpensive means of conveying water through the road prism. However, economic advantage is reduced if a culvert fails because of inadequate design and has to be replaced at a time interval much less than the useful life of the culvert (Piehl *et al.*, 1988).

Where the road surface is at or below, the channel grade line, the situation is more conducive to the construction of bridgeless crossings (a concrete apron designed to let the flood water pass over the road with minimal damage). Bridgeless crossings in general are preferable to culverts as they have as a whole none of the problems associated with culverts.

Some recent studies have proposed a new method for reducing the destructive effect of desert flash floods. Instead of constructing a large total flood protection system, with enormous cost and potential for total failure, the town itself with its framework (streets and road network, parking lots, playgrounds, parks etc.) can serve as drainage conveyors during the flood events (Schick *et al.*, 1995,1997 and

Tamir *et al.,* 2000). Presumed total protection from flash flood is both costly and, based on uncertain areal differentiation of flood frequencies, may lead to huge loss of life and properties. Contrary to expectations, a comprehensive study conducted in the city of Elat, Negev desert, confirms the viability of the concept of regarding urban facilities as an integral part of the flood control system. The existence of urban framework such as streets, parking etc. causes flood energy reduction and local sedimentation. Despite the small storage volume of these elements, they considerably reduce peak flows over a very short distance (Tamir *et al.*, 2000).

7.4 HAZARD ASSESMENT FOR MARSA ALAM TOWN

The risk map for Idfu-Alam road has been concerned with in section (7.3.2). A visual inspection of this map, Figure 7.13, unearths that the risky and highly hazardous sub-basins constitute a substantial amount of the total area of the El-Alam basin and they are the real sources of danger that threaten the road not only at the points of their outlets but also at the very eastern end of the road where the town of Marsa Alam is located.

During the derivation of the simulated hydrograph in the previous chapter 6 it has been assumed that the rainstorm of a certain intensity covers the concerned sub-basin completely whatever its area. In reality, this condition is seldom to be found fulfilled. To simulate the real situations, it is necessary to consider the dependence of the flood hazard at a certain location upon factors such as the size, the location and the duration of the rainstorm. The impact of these rainstorm characteristics upon the flooding event at the main basin's outlet will be considered in the following sections using the HEC-HMS model. The main basin's outlet has been selected to make this study of economic value as at this outlet the town of Marsa Alam lies, which is mostly populated by the residents of this area.

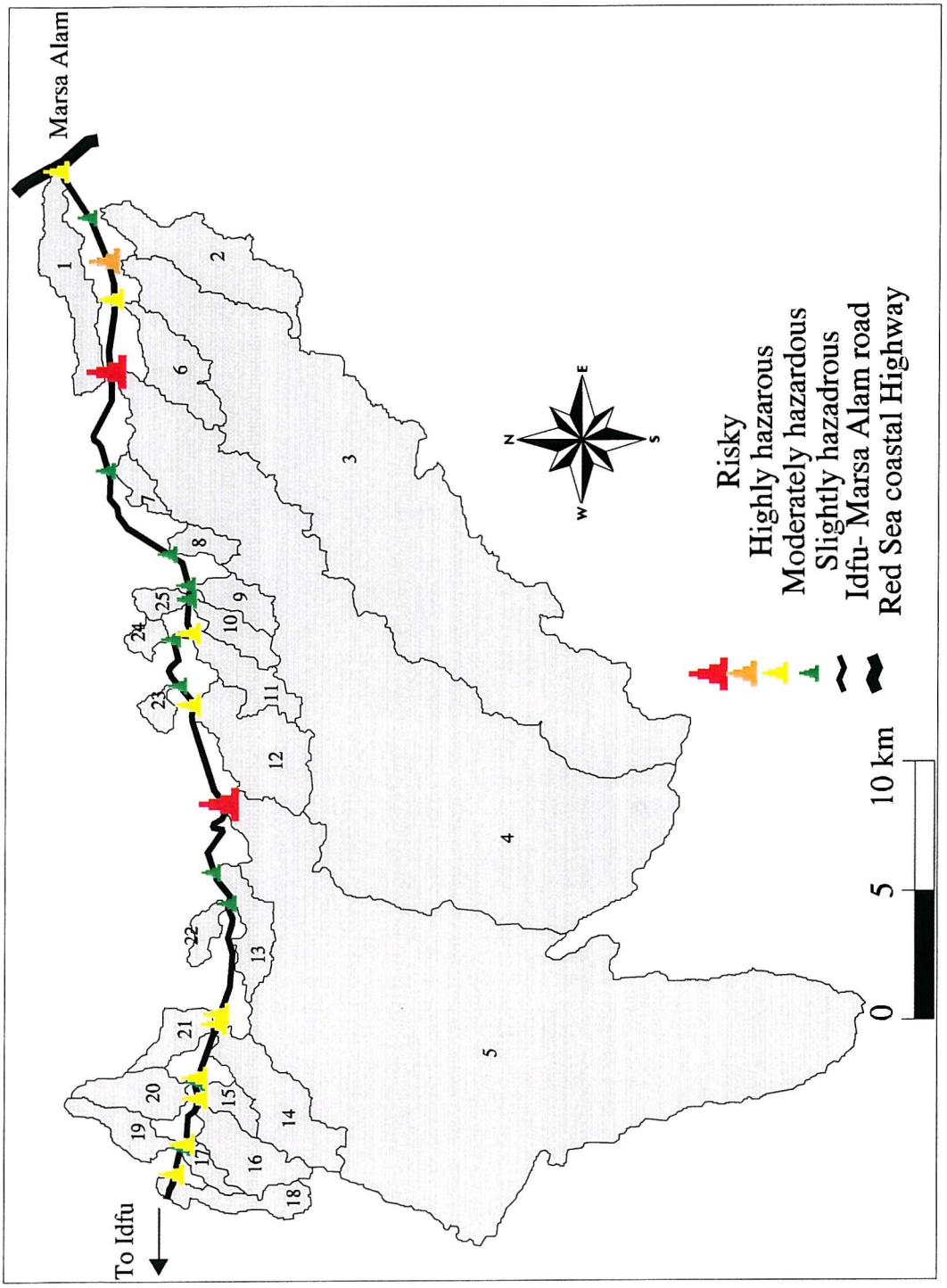

Figure 7.13 Flash floods vulnerable sites along Idfu-Alam road.

7.4.1 Assessment of the influence of various rainfall depths on the runoff hydrograph

In this study, the Wadi has been assumed to be wholly covered by a two-hour rainstorm of varying rainfall depth (10-100 *mm*). The values of the flood peaks resulted from applying these rainstorms are graphed in Figure 7.14. An inspection of this figure reveals that the precipitated rain gets absorbed by the soil with no surface runoff in case of covering the Wadi with 2-hour rainstorm of 10 mm rainfall depth. At rainfall depths (*rf*) >= 40 *mm*, the dependence of the flood peak (*PD*) in $m^3.s^{-1}$ upon the rainfall (*rf*) depth in *mm* could be approximated by the following linear relationship:

$$PD = 12.04(rf - 40) + 127.50 \qquad (r^2=0.992) \qquad (7.1)$$

The intercept here is the value of the flood peak at rainfall of 40 *mm*.

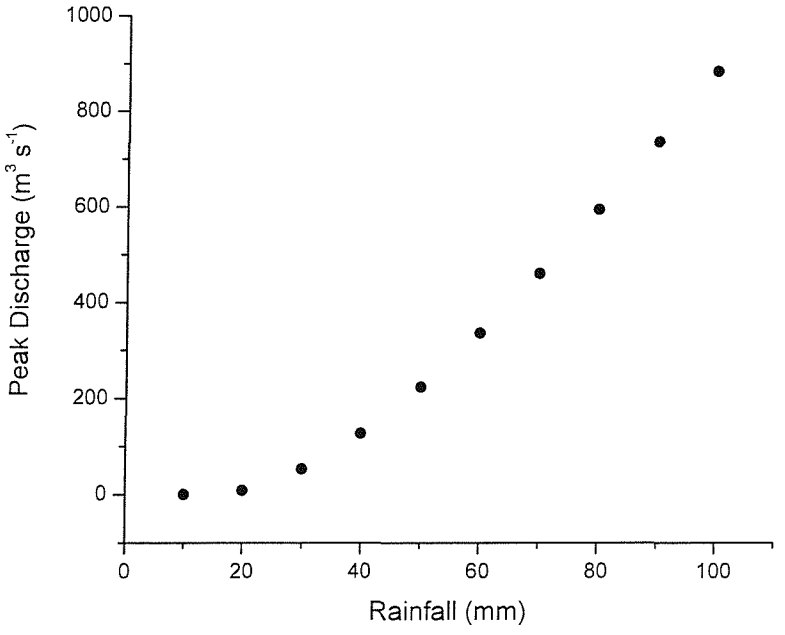

Figure 7.14 Flash flood peak calculated at different rainfall depths.

7.4.2 Assessment of the influence of rainstorms covering different sub-basins on the runoff hydrograph

Due to the nature of rainstorms in arid regions, which are characterised by localised convective cell (Sharon, 1972; Zeller, 1990 and Blood and Humphrey, 1990) that may cover only small area of the watershed, it is important to observe the shape of the hydrograph that results from rainstorms localized over different sub-basins of the El-Alam Wadi. In this section it has been assumed that the 2-h rainstorm of 60 *mm* rainfall depth exclusively covers one sub-basin each time the model runs. Under these conditions, the flooding responses (hydrographs) of the sub-basins at the main outlet of the El-Alam basin have been computed and the results have been represented pictorially in Figure 7.15.

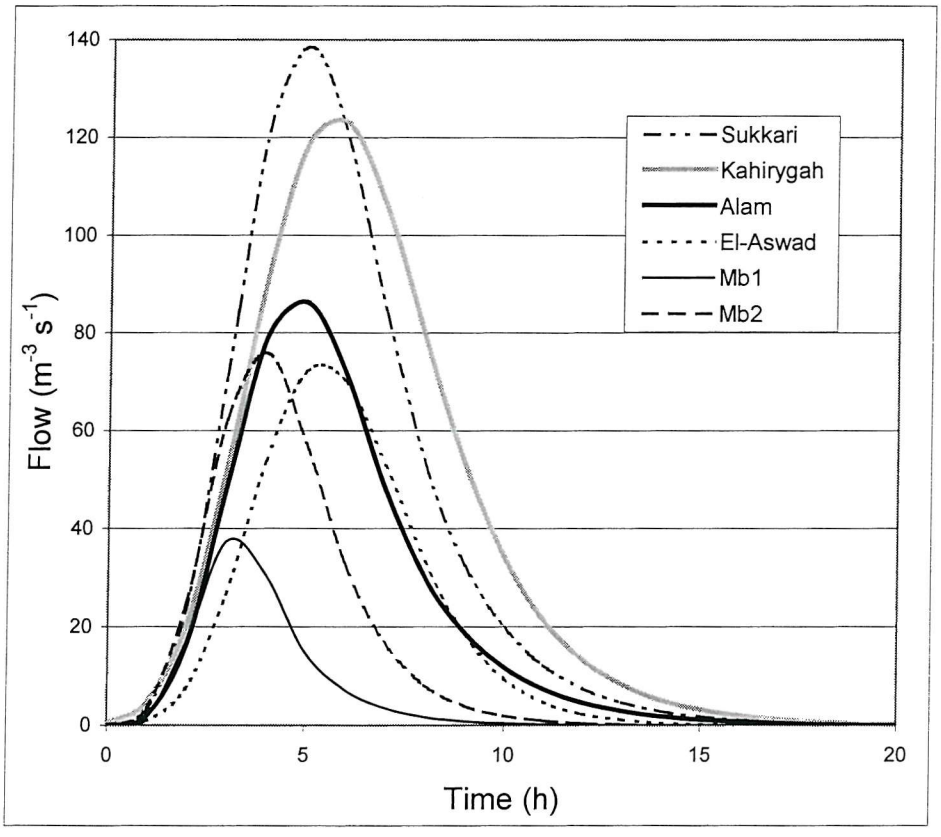

Figure 7.15 Hydrographs calculated at Wadi El-Alam's outlet with the assumption that the rainstorm exclusively covers one sub-basin at a time.

At first glance, two observations could be drawn from Figure 7.15. Firstly, the time to peak is influenced by the location of the sub-basin with respect to the main outlet of the Wadi. Secondly, the start of the surface runoff of each sub-basin at the main outlet of the Wadi is not strongly dependent upon the location of the sub-basin. This observation could be technically exploited through the placement of a flood warning gauge somewhere along the flow path near to the main basin outlet to signal the flooding in any sub-basin. The explanation of these observations is so intricate as more than one (compensating) factor comes into play. But, the incipient appearance of the surface runoff within a narrow time slot at the main outlet might be expounded on the permeability of the land cover, elevation (slope), and location (distance) of the sub-basin. It is the compensating effect of the slope that makes the surface runoff of a distant sub-basin of less permeable land cover initially appears, more or less at the same time of one nearer to the main outlet and of more permeable land cover. The relative shapes of the hydrographs might be explained in terms of the areas, shapes, and more importantly the locations of the sub-basins with respect to the main outlet.

7.4.3 Assessment of the effect of rain-cell location on the runoff hydrograph

This section investigates the sensitivity of the Wadi hydrological response to rainfall distribution. The model is used to calculate the time to peak and the peak discharge of the flood at the Wadi mouth due to several simulated rainstorms of varying locations. It has been assumed that the basin has been affected by a small rainstorm covering an area of 5.5 km^2 (which is the average size of raincell in the arid regions, Sharon, 1972) and lasts for 2 hours with 60 *mm* rainfall depth; these values for the duration and the rainfall depth are the typical values of the rainstorm of the flash flood event of 1996. This rainstorm has been localized 5 times over different sites across the Wadi. These sites were chosen randomly between the basin outlet and the basin water-divide line. The calculated hydrographs at the main basin outlet are displayed in Figure 7.16a. From this figure, it emerges that the location of the rainstorm has an important effect on the shape of the final hydrograph. The flood starts and hence peaks earlier if it is generated from a rainstorm of centre nearer to the main outlet. That is, the water of downstream

flood has to travel shorter distance than that of the upstream one to reach the Wadi mouth. Also, it has been noted that the upstream flood (e.g. site 4) is of a magnitude and a peak higher than those for downstream ones (e.g. site 1). This observation might be attributable to the fact that the downstream land cover is mainly coarse deposits (e.g. site 1) in contrast to the upstream one which is mostly basement rocks plus low porosity desert pavement (e.g. site 4).

To widen the scope of the present study, the rainfall depth of the applied rainstorm has been varied to cover the range from 40 *mm* to 120 *mm*, Figure 7.16b. On referring to this figure, it becomes clear that the flood peak is linearly dependent upon the rainfall depth. On calculating the slope and intercept that characterizes the flooding response of each site at the Wadi mouth and then evaluating the dispersions (standard deviations) around the averages of these slopes and intercepts (at 40 mm), one finds that the dispersion of the slope is about 10% of the slope's average while that of the intercepts around the average is about 60%. This result has qualitative and quantitative implications. The qualitative aspect is that the response (reflected by the slope) at the Wadi mouth due to the change in the rainfall by unity is, to far extent, the same wherever the rainstorm is localized. But quantitatively, the localization of the rainstorm (the site) is reflected in the intercept. That is, the behaviour of the site is contained in the slope and quantified through the intercept of its flooding response versus the rainfall depth. To free the flooding response of the site at the Wadi mouth from the dependence upon its location, one has to average the flooding peaks of all sites at each rainfall depth. The least square linear fitting of these averages as a function of the rainfall depth is depicted graphically in Figure 7.17. If the individual flooding response of each site is plotted on the same graph, the conclusion would be that the flooding behaviours of the sites are within the 95% prediction interval (band) of their average response. One could exploit this average relation, in particular after normalization by the area of the rain cell, in the prediction of the average flood peak at the Wadi mouth due to the localization of a rainstorm over the unit area somewhere in the Wadi. However, statistically, it is better to use the relation that describes the overall flooding response of the whole basin when it is covered completely by rainstorm of large cell size, *viz.* equation 7.1, as it reflects the ultimate average for the all

features of the basin and hence its sub-basins. Thus after normalising equation 7.1 by the area of the basin of 406.89 km^2 (which also the size of the rain cell in this case), one arrives at an approximate equation for calculating the average peak (APD) of a flood at the main basin outlet as a function of the rainfall depth (*rf*) of a 2-h rainstorm:

$$APD(m^3.s^{-1}) = rc \times [0.03 \times (rf - 40) + 0.313] \quad \text{for} \quad rf >= 40\ mm \qquad (7.2)$$

where *rc* is the area of the rain cell in km^2; the projected surface area of the rainstorm. To what extent this equation is reliable could be checked if the already calculated average flood peak due to a rainstorm of 2-hour duration and rain cell of 5.5 km^2, see Figure 7.16, has compared to that predicated by this equation as in Figure 7.17. Although the calculated average flood response is of modest averaging nature, the predicated response is within its 99% predication level confirming the trustworthy nature of equation (7.2).

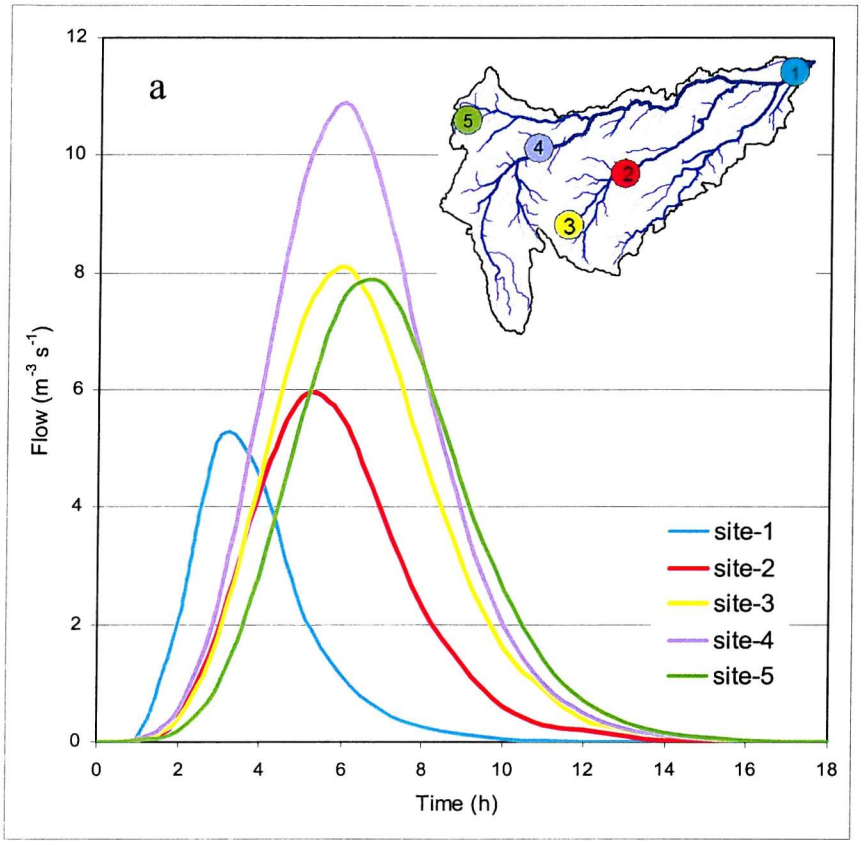

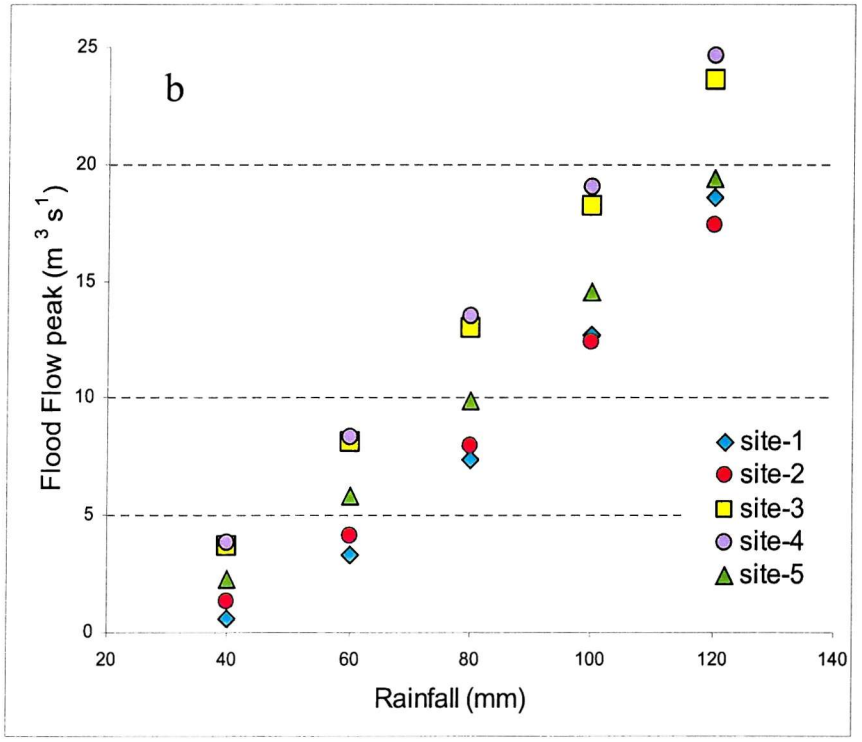

Figure 7.16 (a) Hydrographs and (b) flow peaks due to 5.5 km^2 raincells across Wadi El-Alam.

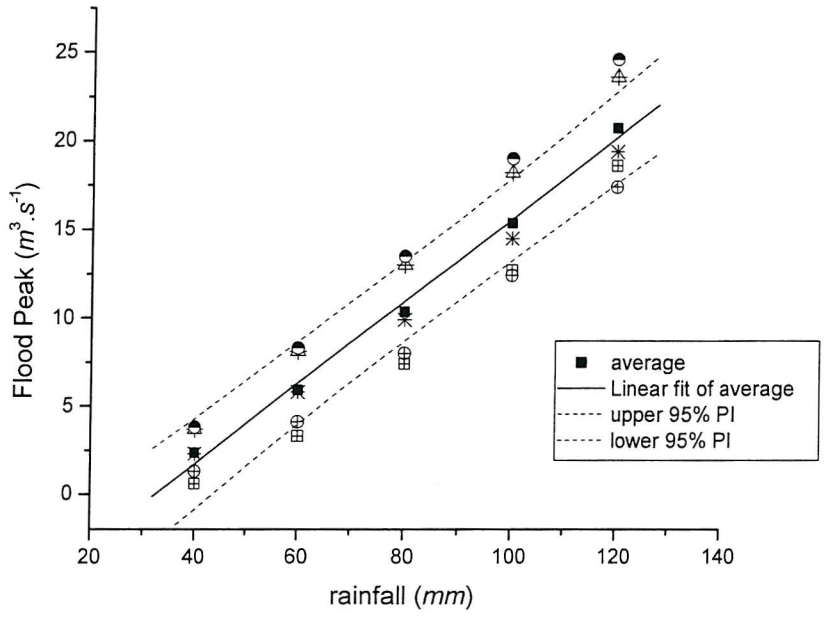

Figure 7.17 The least square linear fit of the calculated average flood peaks for 5 sites, each of area of 5.5 km^2, across the El-Alam basin.

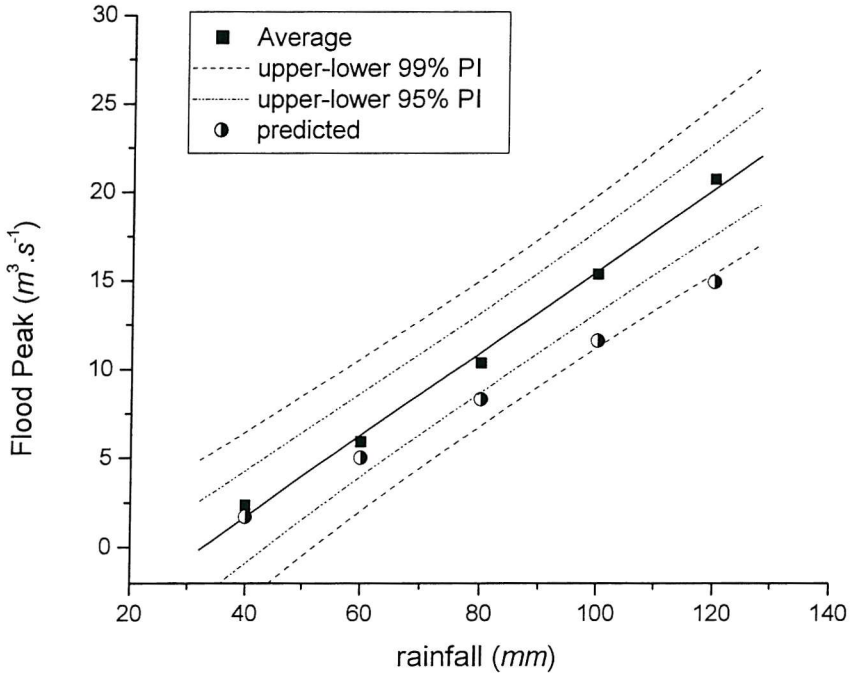

Figure 7.18 The calculated and predicted average flood peaks for 5 sites, each of area of 5.5 km^2, across the El-Alam basin as a function of the rainfall depth.

7.5 SUMMARY

The town of Marsa Alam is located at the main outlet of Wadi El-Alam. Marsa Alam is connected to the town of Idfu by a road. Around 36 km of this road has been constructed on the floor of the Wadi crossing the alluvial fans of 25 sub-basins. In order to locate the flood vulnerable sites along the road, the flood related morphometric parameters (such as area, ruggedness, main channel slope, elongation ratio and average basin slope) of these sub-basins along with their average curve numbers have been calculated and analysed. With the help of these parameters and through segmentation (cluster) analysis, it was possible to classify these sub-basins into 4 groups. Each group represented a risk class defined by the magnitude of the peak of discharge in each sub-basin due to a synthetic rainstorm. From these results, it has been found that the risk along the road is not simply related to the area of the sub-basin as small, steep and highly rugged sub-basins are also found to be dangerous locations. The sites ranked to have the highest flood hazard along the road were exactly the sites of the highest damage in the 1991 flood.

With regards to Marsa Alam, it has been found that the magnitude and timing of the flood peak are functions of the location, size and duration of the rainstorm. However, the surface runoff in each sub-basin initially appears at the main outlet of the Wadi within a narrow time slot. Technically, this point could be exploited through the placement of a flooding warning system along the flow path near to the town to signal the flooding in any sub-basin. It also found that certain amount of rain does not always produce the same flood; it depends on where it falls in the basin.

CHAPTER 8

Summary, conclusions and recommendations

8.1 SUMMARY AND CONCLUSION

There is no doubt that flash flooding in arid regions is a double-edged natural phenomenon; it is both a blessing and a curse at the same time. It is a blessing as it is the only source in arid regions for recharging ground water. It is a curse as the tremendous power of the water flow is able to cause devastation along its pathway.

This natural phenomenon, flash flooding, has been found to be real obstacle threatening and hampering the development along the Egyptian desert coast, and specifically in the town of Marsa Alam and its surrounding area. Severe floods have happened three times in the last few years (1991, 1994, 1996). The town of Marsa Alam is exactly at the main outlet of an arid basin, Wadi El-Alam, which spans around 407 km^2 between longitudes 34°33′-34°53′ and latitudes 24°50′-25°04′. Part of the highway that connects between the Marsa Alam town and the Nile valley runs on the floor of this Wadi. Both the town and the highway are seriously affected by any flooding events in Wadi El-Alam.

In order to take necessary measures against the flood risk, it is necessary first to locate the sites that are vulnerable to flash flooding and second to estimate the timing and amount of water of any discharge at these sites.

This study has developed a procedure for estimating flood risk in desert environments, using data for the Wadi El-Alam. The first step was the construction of a Digital Elevation Model (DEM) which was derived in the raster domain (of cell size 30 m by 30 m) by interpolating contours *manually* digitized (at intervals of 20 m) from 1:50 000 topographic maps for Wadi El-Alam. After removing artefact pits in the initial DEM (by filling), calculations performed on the resulting DEM determined the stream network and drainage sub-basins boundaries. The corrected

DEM, stream network and their associated sub-basins altogether constituted the first digital database for Wadi El-Alam as an outcome of this study. From this dataset, it was possible to quantitatively extract sets of geomorphometric properties specifying the linear, areal and relief characteristics of the entire basin. Information on the land cover/soil types of the basin was derived with the aid of a supervised classification of geometrically, radiometrically atmospherically, and topographically corrected Landsat TM imagery of Wadi El-Alam.

The flood hazard has to be estimated not only on the basis of its location but also on the basis of the amount and timing of its discharge. This necessitates taking into account the excitation factor (rainfall) which derived the basin in its flooding events via the hydrological modelling given the absence of the flooding records as the case in the current study. The response of Wadi El-Alam to a synthetic rainfall event (of 60 mm total precipitation in two hours) was approximated within the quasi-distributed framework of the Hydrological Modelling System (HMS) model. With this model, the Wadi El-Alam was considered as a series of hydrological elements linked sequentially in such a way that the water was routed from one element to another until the main basin's outlet was reached.

The curve number data needed for running this model were extracted from field measurements (infiltration rate and soil texture) conducted during two field visits, each for two weeks, undertaken in February 1999 and January 2001. After accounting for precipitation losses with the help of the land cover information, adopting the unit hydrograph and Muskingum methods as models for routing the flow within the sub-basins and channels, respectively, and with the assumption that the rainstorm uniformly covers the basin, the running of the HMS model gave rise to hydrographs at the main basin's outlet and at each outlet of every sub-basin intersecting the highway that runs through Wadi El-Alam. From these results the flash vulnerable sites were located. These sites corresponded with those known to have suffer prime damage. For example, the two sites along Idfu-Alam road judged to have the highest flood hazard were the sites damaged in the 1991 flash flood.

The key observations and conclusions made throughout this research could be summarised as:

- It has to be noted that the only available topographic maps of Wadi El-Alam are of the scale 1:50 000 and these maps were used right through the digitisation processes of the contour lines from which the digital elevation model (DEM) of the Wadi was derived.

- During the construction of the digital elevation model (DEM), the burn-in methodology was proved to be effective in correcting the errors introduced by the intermittent channel network and unclear drainage pattern in the flat regions.

- The sharp junctions that characterise the arid areas presented difficulties to standard interpolation procedures, which assume smooth transitions.

- Morphometric parameters can give preliminary indications on the flooding possibilities in the drainage basin. The relationships between the bifurcation ratio, channel density and channel frequency were useful in this respect.

- The topographic correction of remotely sensed imageries of the highly rugged terrains is crucial to compensate for the effects of variable surface illumination due to topographic variation (including shade).

- Remotely sensed images are very useful data sources for extracting information on the land cover/soil types of the arid regions, especially in inaccessible mountainous areas, where field observations are relatively rare and difficult.

- The soil texture analyses, alone, are not enough to identify the soil groups of the alluvial deposits and have to be coupled with infiltration measurements taken in the field to get the correct values of the curve numbers used in runoff modelling.

- Care has to be given to the spatial resolution of the drainage network (cell threshold) before applying the hydrological model.

- The routing velocity of the flow in the channels can be inferred from the velocity distribution grid.

- The hydrological response of the watershed to a rainfall is governed intrinsically by its geomorphometry and land cover, and its area is just a scaling factor for its response.

- The response of the watershed is very sensitive to the size, location and intensity of the rainstorm.

- Rainstorms with total rainfall depth less than 20 mm do not induce discharging events at all in Wadi El-Alam.

- Around one third of the total precipitation (60 mm) over Wadi El-Alam appears as a discharge at its main outlet and the remaining two-third contribute in recharging the ground water.

- The sites predicted to be vulnerable to flash flood damage corresponded to the sites destroyed in real flash flood events, indicating the usefulness of applying a hydrological modelling for flash flood hazard assessment studies.

- In principle, the approach developed in the present study could be applied to any mountainous wadi, in particular, those of the Eastern Desert and Sinai Peninsula in Egypt. The wadis in these areas are similar in their surface cover and terrain characteristics to those of Wadi El-Alam. These wadis also often have settlements located near their outlets and may be traversed by road in a similar fashion to that observed at Wadi El-Alam. Moreover, as most of these wadis are void of rainfall and flow gauges, an approach such as that presented in this thesis may be the only practical method for predicting flood hazards associated with such wadis.

8.2 RECOMMENDATIONS FOR FUTURE WORK

- Essentially, the combination of gentle gradient with a 30 m DEM worked together to make modelling the Wadi El-Alam difficult. Using a terrain model of finer spatial resolution (derived from, e.g., Satellite images of fine resolution) will undoubtedly assist greatly in giving accurate results.

- More extensive data about the channel cross section and roughness coefficient should be obtained from field, so that assumption made about these factors in this research could be replaced by measured and observed data.

- Improvement could also be achieved in the application of the rainfall-runoff model through the use of real rainfall event profiles, which was not available for the current study.

- The derived hydrological data in the research have not been tested against real or verified flow data - because none exist. However, information from just one event would help validate and refine the model.

- Due to the fact that the hydrological and climatological data are unlikely to be available for arid regions, it is important to rely on other source of data for model calibration in such areas. Historical floods may be considered to be one of the important data sources in this respect. They can be reconstructed by implementing the palaeoflood hydrology approach, using deposits from past floods and inferring velocity and discharge from sediment characteristics.

To conclude, the success of any study is measured by the extent to which the research objectives have been fulfilled. From the forgoing discussions, it is apparent that the objectives of the thesis have been met. In particular, it was possible to build a digital database (comprising DEM, watershed and stream network, geomorphometric parameters, and land cover/soil types) for the basin of interest and to locate the sites vulnerable to flooding together with their risk classes.

REFERENCE

Abdulrazzak, M.J., Sorman, A.U, and Alhames, A.S., 1989. Water balance approach under extreme arid conditions: A case study of Tabalah basin, Saudi Arabia. *Hydrological Processes*; 3 (2): 107-122.

Abrahams, A.D., 1977. The factor of relief in the evolution of channel networks in mature drainage basins. *American Journal of Science*; 277: 626-645.

Abrahams, A.D., 1984. Channel network: a geomorphological perspective. *Water Resources Research*; 20: 161-168.

Abrahams, A.D and Parsons, A.J., 1994. *Geomorphology of Desert Environments*. Chapman & Hall, London.

Abu–Hassen, A.S., 1994. *The effect of the Red Sea Trough in the Jordan climate during the spring and autumn*. MSc thesis, Geography Department Jordan University, (in Arabic).

Agnew, C. and Anderson E., 1992. *Water resources in the arid realm*, Routledge.

Allam, M.N and Balkhair, S.K., 1987. Case study evaluation of the geomorphologic instantaneous unit hydrograph. *Water Resources Management*; 1: 267-291.

Amit, R. and Gerson, R., 1986. The evolution of Holocene reg (gravelly) soils in deserts – an example from the Dead Sea region. *Catena*; 13: 59-79.

Anderson, J.R., Hardy, E.E., Roach, J.T. and Witmer, R.E., 1976. *A Land Use and Land Cover Classification System for Use with Remote Sensor Data*. U.S. Geological Survey, Professional Paper 964: 28.

Arnell, N., 2002. *Hydrology and Global Environmental Change*. Prentice Hall, Pearson Education Ltd, London.

Ashmawy, M.H and Nassim, A.S., 1999. Hydrological impact and assessment of morphometric aspects of wadi Al-Asyuti basin, Eastern Desert, Egypt. *The Egyptian Journal of Remote Sensing and Space Sciences*; 1 (1): 207-232.

Atia, A.H., 1999. *Geo-Environmental study in Marsa Alam.* MSc thesis, Department of Geology, Ain Shams University, Cairo, 113.

Baker, V R., 1977. Stream-channel response to floods, with examples from central Texas. *Geological Society of America, Bulletin*; 88: 1057-1071.

Baker, V.R., 1987: Palaeoflood hydrology and extraordinary flood events. *Journal of Hydrology*; 96: 79-99.

Bedient, P.B. and Huber, W. C., 1992. *Hydrology and Floodplain Analysis*, 2nd ed., Addison-Wesley, Reading.

Benson, M.A., 1962. Factors influencing the occurrence of floods in a humid region of diverse terrain. U.S. Geological Survey. *Water Supply Paper*; 1580-b: 1-64.

Benson, M.A., 1964. Factors affecting the occurrence of floods in the Southwest: U.S. Geological Survey. *Water Supply Paper*; 1580-d: 72.

Ben-Zvi, A. and Shentsis, I., 2000. Runoff events in the Negev, Israel. The Hydrology –Geomorphology Interface: Rainfall, Floods, Sedimentation, Land Use (ed. M Hassan, O. Slaymaker & S. Berkowicz), Jerusalem Conf, May 1999. *IAHS Publ*; 261: 53-71.

Blood, W.H and Humphrey, J.H., 1990. Design cloudburst and flash flood methodology for the western Mojave Desert, California. In *Hydraulics/ hydrology of aridlands (H^2AL),* French R H. The American Society of Civil Engineers: 561-566.

Briggs, D., 1977. *Soils, sources and methods in geography.* Butterworths.

Brunsden, D., Jones, D., Downey, J. and Richards, K., 1982. *The wadi Dhamad geomorphological survey*. Govt. of Saudi Arabia and Sir William HalCrow and Partners.

Burkham, D.E., 1966. Hydrology of Cornfield Wash area and effects of land-treatment practices, Sandoval County, New Mexico, 1951- 60. U.S. Geological Survey. *Water Supply Paper*; 1831: 1-87.

Byers, H.R., 1959. *General Meteorology*. Mc-Craw Hill Book Comp, New York, 3rd ed: 458-479.

Campbell, A.J. and Sidle, R.C., 1984. Prediction of Peak Flows on Small Watersheds in Oregon for Use in Culvert Design. American Water Resources Association. *Water Resources Bulletin*; 20 (1): 9-14.

Campbell, J.B.,1996. *Introduction to Remote Sensing*, 2nd edition. Guilford Press, New York.

Carlston, C.W., 1963. *Drainage density and streamflow*. U.S. Geological Survey, Professional Paper; 422 (C): 1-8.

Cairns, M.C., 1997. A flash flooding event in the high Atlas Mountains of Morocco. *Geography*: 85-90.

Chorley, R.J., 1957. Climate and morphometry. *Journal of Geology*; 65: 628-668.

Chorley, R.J., 1969. *Introduction to physical hydrology*. Methuen, London.

Chow, V.T., Maidment, D.R. and Mays, L.W., 1988. *Applied Hydrology*, McGraw-Hill, Inc., NY.

Congalton, R., 1991. A review of assessing the accuracy of classification of remotely sensed data. *Remote Sensing of Environment*; 37: 35-46.

Cooke, R.U., 1970b. Stone pavements in deserts. *Annals of the Association of American Geographers*; 60: 560-577.

Cooke, R.U., Brunsden, D., Doornkamp, J.C. and Jones, D.K.C., 1982. *Urban geomorphology in drylands*. New York: Oxford University Press.

Cooke, R.U., Brunsden, D., Doornkamp, J.C. and Jones, D.K.C., 1985. Geomorphological dimensions of land development in deserts- with special reference to Saudi Arabia; *Nottingham monographs in applied geography*; 4: 54-71.

Colby, J.D. 1991. Topographic Normalization in Rugged Terrain. *Photogrammetric Engineering & Remote Sensing*; 57 (5): 531-537.

Colombo, R. and Sarfatti, P. *Hydrological analysis of two sub-catchments of the Mareb River (Eritrea)*. Istituto Agronomico per l'Oltremare, Firenze, Italy. http://www.fao.org /docrep/W7320B/w7320b22.htm.

Cordery, I., Pilgrim, D.H and Doran, D.G., 1983. *Some hydrological characteristics of arid western New South Wales*. Hydrology and Water Resources Symposium. Institution of Engineers. Australia, National Conference Publ; 38 (13): 287-292.

Costa, J E., 1987. Hydraulics and basin morphometry of the largest flash floods in the conterminous United States. *Journal of Hydrology*; 93: 313-338.

Dan, J., Yaalon, D.H., Moshe, R. and Nissim, S., 1982. Evolution of reg soil in southern Israel and Sinai. *Geoderma*; 28: 173-202.

Dorn, R.I., 1989. Cation- ratio dating of rock varnish: a geographic assessment. *Progress in Physical Geography*; 13: 559-596.

Duda, R.O. and Hary, P.E., 1973. *Pattern classification and scene analysis*. Wiley, New York.

Dunne, T. and Leopold, L.B., 1978. *Water in environmental planning*. W, H. Freeman and Company, San Francisco.

Each, D.A., 1994. A Geographic Information System procedure to quantify drainage basin characteristics. *Water Resources Bulletin*; 30: 1-8.

Egyptian Geological Survey Authority., 1994. *The flash flood of November 1994: Red Sea*, (in Arabic).

Egyptian Military Survey., 1989. Egyptian map series 1: 150 000. Cairo, Egypt.

Eissa, M., Abas, A., Abd El Aziz, A. and El-Sharquawy, H., 1999. *Utilizing geographical information system technique in a flood assessment model for Sinai watersheds*. The Forth conference, Meteorology and Sustainable Development to 21St Century, March 1999; 368-378.

El-Etr, H.A and Ashmawy, M.H., 1993. *Flash flood vulnerability and mitigation of the Red Sea basins between latitudes 24°41' and 25°26'N, Egypt*. Proc. International. Conference. 30 Years Cooper., Geological Survey, Egypt, Cairo; 335-351.

El-Hames, A.S. and Richards, K.S., 1998. An integrated, physically based model for arid region flash flood prediction capable of simulating dynamic transmission loss. *Hydrological Processes*; 12: 1219-1232.

El-Shamy, I. Z, 1992c. *Towards the water management in Sinai Penninsula*. Proc. 3rd Conference. Geol, Sinai Develop., Ismailia; 63-70.

Emmett, W.W., 1970. *The hydraulics of overland flow on hillslopes*. U. S Geological Survey, Professional Paper 662 (A).

Environmental Systems Research Institute (ESRI)., 1993, *ARC/INFO Users' Guide*. Redlands, California.

Evenari, M., Shanan, L. and Tadmor, N., 1968. Runoff farming in the desert: 1. Experimental layout, *Agron Journal*; 60: 29-32.

Evenari, M., Shanan, L. and Tadmor, N., 1971. *The Negev, the challenge of a desert.* Harvard University press.

Evenari, M., Yaalon, D.H and Gutterman, Y., 1974. Note on soils with vesicular structure in deserts. *Zeitschrift fur geomorphologie*; 18 (2): 162-172.

Floyd, S.F., 1987. *Remote sensing: principles and interpretation*, New York, Freeman.

Folk, R.C., 1980. *Petrology of Sedimentary Rocks.* Hemphill Publishing Company.

Foody, G.M., 2002. Status of land cover classification accuracy assessment. *Remote sensing of environment*; 80: 185-201.

Garbrecht, J., Martz, L., 1993. Network and subwatershed parameters extracted from Digital elevation models- the Bills Creek Experience. *Water Resource Bulletin*; 29: 909-916.

Gheith, H and Sultan, M., 2002. Construction of a hydrologic model for estimating Wadi runoff and groundwater recharge in the Eastern Desert, Egypt. *Journal of hydrology*; 263: 36-55.

Ghoneim, E.M., 1995. *Wadi Umm Gheig: a geomorphological study.* MSc thesis, Geography department, Faculty of Arts, Tanta Universty, Tanta, Egypt.

Ghoneim, E.M., Arnell, N. and Foody, G., 2002. Characterizing the flash flood hazards potential along the Red Sea coast of Egypt. The Extremes of the Extremes: Extraordinary Floods. Reykjavik, Iceland, Conf July. *IAHS Publ*; 271: 211-216.

Ghosh, A.K & Scheidegger, A.E., 1970. Dependence of stream order. *Water Resources Research*; 6: 336-340.

Graf, W.L., 1988. *Fluvial processes in dryland rivers*, Springer-Verlag, Berlin.

Greenbaum, N., Margalit A., Schick, A.B. and Backer, V.R., 1998. A high magnitude storm and flood in a hyperarid catchment, Nahal Zin, Negev Desert, Israel. *Hydrological Processes*; 12: 1-23.

Grodek, T., Lekach, J. and Schick, A.P., 2000. Urbanizing alluvial fans as flood-conveying and flood-reducing systems: lessons from the October 1997 Eilat flood. In: The Hydrology-Geomorphology Interface: Rainfall, Floods, Sedimentation, Land Use. Proc. Jerusalem Conference, May. *IAHS Publ*; 261:229-250.

Hassan, M.A., 1990. Short communications observations of desert flood bores. *Earth Surface Processes and Landforms*; 15: 481-485.

HEC., 1990. HEC-1 Flood Hydrograph Package. *HEC-1 User's Manual*, Hydrologic Engineering Center, U.S. Army Corps of Engineers, Davis, CA.

HEC-HMS (Hydrologic Modeling System)., 2000. *HEC-HMS User manual*, version 2. US Army Corps of Engineers Hydrologic Engineering Center. http://www.hec.usace.army.mil/publications/pubs_distrib/hec-hms/user/hms_user.pdf.

Hickok, R.B., Keppel, R.Y. and Rafferty, B.R., 1959. Hydrograph synthesis for small arid land watershed. *Agricultural Engineering*; 40: 608-615.

Hillel, D. and Tadmoor, M., 1962. Water regime and vegetation in the central Negev Highlands of Israel. *Ecology*; 43: 33-41.

Hjalmarson, H.W., 1984. Flash flood in Tanque Verde Creek, Tucson, Arizona. *Journal of Hydraulic Engineering*; 110 (12): 1841-1852.

Hodges, W.K., 1982. Hydraulic characteristics of a badland pseudo-pediment slope system during simulated rainstorm experiments. *In badlands geomorphology and piping*, Norwich: Geo Books.

Hogg, J., McCormack, J.E., Roberts, S.A., Gahegan, M.N. and Hoyle, B.S., 1993. Automated derivation of stream-channel networks and selected catchment characteristics from digital elevation models. In *Geographic Information Handling - Research and Applications.* John Wiley and Sons, New York.

Horton, R.E., 1932. Drainage basin characteristics. *American Geophysical Union Transactions*; 13: 350-361.

Horton, R.E., 1945. Erosional development of streams and their drainage basins: hydrophysical approach to quantitative morphology. *Geological Society of America, Bulletin*; 56: 275-370.

Huggins, L.F. and Burney, J.R., 1982. Surface runoff, storage and routing. In *Hydrologic modeling of small watersheds.* ASAE Monograph n°5, St Joseph Michigan.

Hutchinson, M., 1989. A new procedure for gridding elevation and stream line data with automatic removal of spurious pits. *Journal of Hydrology*; 106: 211-232.

Jessup, R.W., 1960. The stony Tableland soils of the southeastern portion of the Australian arid zone and their evolution history. *Journal of Soil Science*; 11: 188-196.

Jenson, S.K. and Domingue, J.O., 1988. Extracting topographic structure from digital elevation data for Geographical Information System analysis. *Photogrammetric Engineering and Remote Sensing*; 54 (11): 1593-1600.

Kincaid, D.R., Gardner, J.L. and Schreiber, H.A., 1964. *Soil and vegetation parameters affecting infiltration under semiarid conditions. IAHS Publ*; 65: 440-53.

Knighton, D., 1998. *Fluvial forms and processes, a new prespective.* Arnold, London.

Koon, J.L., Hendrick, J.G. and Hermanson, R.E., 1970. Some effects of surface cover geometry on infiltration rate. *Water Resources Research*, 6: 246-253.

Langbein, W.B., 1947. Topographic characteristics of drainage basins, U.S. Geological Survey. *Water Supply Paper*, 968 (C): 125-157.

Lange, J., Leibundgut, C.H. and Schick, A.P., 2000. The importance of single events in arid zone rainfall-runoff modelling. *Physical, Chemical and Earth Sciences*, 25(7-8): 673-677.

Laronne, J.B., Outhet, D.N., Carling, P.A. and McCabe, T.J., 1994a. Scour chain employment in gravel bed rivers. *Catena*, 22: 299-306.

Laronne, J.B., Reid, I., Yitshak, Y. and Frostick, L E., 1994b. The non-layering of gravel streambeds under ephemeral flood regimes, *Journal of Hydrology*, 159: 353-363.

Lavee, H. and Poesen, J.W., 1991. Overland flow generation and continuity on stone-covered soil surfaces. *Hydrological Processes*, 5: 345-360.

Lekach, J., Amit, R., Grodek, T. and Schick, A., 1998. Fluvio-pedogenic processes in an ephemeral stream channel, Nahal Yael, Southern Negev, Israel. *Geomorphology*, 23: 353-369

Leopold, L.B. and Maddock, T., 1953. *The hydraulic geometry of stream channels and some physiographic implications*. US Geological Survey, Professional Paper; 252.

Leopold, L.B. and Miller, G.P., 1956. *Ephemeral streams, hydraulic factors and their relation to the drainage net*. U.S. Geological Survey, Professional Paper; 282-A.

Linsley, R.K., Kohler, M.A. and Paulhus, J.L.B., 1949. *Applied hydrology*. McGraw-Hill, New York.

Lyford, F.P. and Qashu, H.K., 1969. Infiltration rates as affected by desert vegetation. *Water Resources Research*, 5: 1373-1376.

Mabbutt, J.A., 1977. *Desert landforms. Cambridge*, MIT press, Massachusetts.

Maguire, D.J. and Dangermond, J., 1991. The functionality of GIS. In *Geographical information systems: Principles and Applications*, edited by D. J. Maguire, M. F. Goodchild and D. Rhind, London, Longman.

Martinez-Goytre, J., House, P.K. and Baker, V.R., 1994. Spatial variability of small-basin paleoflood magnitudes for a southern Arizona mountain range. *Water Resource Research*, 30: 1491-1501.

Mather, P.M., 1999. *Computer processing of remotely-sensed images: an introduction.* 2nd ed. Chichester, John Wiley.

McCuen, R.H., 1982. *A guide to hydrologic analysis using SCS methods*, Prentice-Hall, Inc., Englewood Cliffs, New Jersey.

McFadden, L.D., Wells, S.G. and Jercinovich, M. J., 1987. Influence of eolian and pedogenic processes on the origin and evolution of desert pavements: *Geology*, 15: 504-508.

Melton, M.A., 1957. An analysis of the relations among elements of climate, surface properties and geomorphology, Office of Naval Research, Geography Branch, Technical Report 11.

Miller, C.L. and Laflamme, R.A.., 1958. The digital elevation model - theory and application, *Photogrammetric Engineering*, 24: 433.

Milton, E.J., 1980. A portable multiband radiometer for ground data collection in remote sensing. *International Journal of Remote Sensing*, 1: 153-165.

Minitab software, version 13.1, 2001. Minitab Inc, PA, USA.

Minnaert, M., 1941. The reciprocity principle in lunar photometry. *Astrophysical Journal*, 93: 403-410.

Montgomery, D.R. and Dietrich, W.E, 1989. Channel initiation, drainage density and slope, *Water Resources Research*, 25 (8): 1907-1918.

Moore, I.D., Grayson, R.B. and Ladson, A.R., 1991. Digital terrain modelling: a review of hydrological, geomorphological and biological applications. *Hydrological Processes*, 5 (1): 3-30.

Moran, M.S., Jackson, R.D., Clarke, T.R., Qi, J., Cabot, F., Thome, K. J., and Markham, B. L., 1995. Reflectance factor retrieval from LANDSAT TM and SPOT HRV data for bright and dark targets. *Remote Sensing of Environment*, 52: 218– 230.

Morisawa, M.E., 1962. Quantitative geomorphology of some watersheds in the Appalachian Plateau, *Geological Society of America, Bulletin*, 73: 1025-1046.

Morisawa, M.E., 1968. *Streams, their dynamics and morphology*. McGraw-Hill, New York.

Musick, H.B., 1975. Barrenness of desert pavement in Yuma County, Arizona, *Journal of the Arizona Academy of Sciences*, 10: 24-28.

Naim, G., 1995. *Flood of upper Egypt governorates*. Egyptian Geological survey and Mining Authority, Cairo, Egypt.

National Authority for Remote Sensing and Space Science (NARSS), 1997. *Hazard assessment and mitigating measures of flash flooding on the Red Sea towns*. Cairo, Egypt.

Nouh, M., 1990. Flood hydrograph estimation from arid catchment morphology. *Hydrological Processes*, 4: 103-120.

O'Callaghan, J.F. and Mark, D.M., 1984. The extraction of drainage networks from digital elevation data. *Computer Vision and Graphics in Image Processing*, 28 (3): 323-344.

Olivera, F., 1996. *Spatial Hydrology of the Urubamba River System in Peru Using Geographic Information Systems (GIS).* http://www.ce.utexas.edu/prof/olivera/peru/peru.htm.

Olivera, F. and Maidment, D.R., 2000. *GIS tools for HMS Modeling Support.* Chapter 5 in Hydrologic and Hydraulic Modeling Support, eds. D.R. Maidment and D. Djokic, ESRI Press, Redlands, CA.

Osborn, H.B., 1983. Timing and duration of high rainfall rates in the Southwestern United States. *Water Resources Research*, 19: 1036-1042.

Parker, R.S., 1977. *Experimental study of drainage basin evolution and its hydrologic implications.* Hydrological Paper, 90. Colorado states University, Fort Collins.

Patton, P.C., 1988. Drainage basin morphometry and floods. Baker, V.R., Kochel, R.C., and Patton, P.C., eds, 1988, *Flood Geomorphology*: New York, John Wiley, 503p.

Patton, P.C. and Baker, V.R., 1976. Morphometry and floods in small basins subject to diverse hydro-geomorphic controls. *Water Resources Research*, 12: 941-952.

Peters, J.C., 1998. *HEC-HMS, Hydrologic Modeling System.* US Army Corps of Engineers, Hydrologic Engineering Center, Davis, CA.

Philip, J.R., 1957. The theory of infiltration: 4. Sorptivity and algebraic infiltration equations. *Soil Science*, 84: 257-264.

Piehl, B.T.,. Beschta, R.L. and Pyles, M.R., 1988. Ditch-relief Culverts and Low-volume Forest Roads in the Oregon Coast Range. *Northwest Science*, 62 (3): 91-98.

Pilgrim, D.H., Chapman, T.G. and Doran, D.G., 1988. Problem of rainfall-runoff modelling in arid and semiarid regions. *Journal of Hydrological Sciences*, 33 (4): 379-400.

Poesen, J., Ingelmo-Sanchez, F. and Műcher, H., 1990. The hydrological response of soil surfaces to rainfall as affected by cover and position of rock fragments in the top layer. *Earth Surface Processes and Landforms*, 15: 653-671.

Ponce, V.M. and Hawkins, R.H., 1996. *Journal of Hydrologic Engineering*, ASCE, 1(1): 11-19.

Prasuhn, A.L., 1992. *Fundamentals of Hydraulic Engineering*. Oxford University Press, New York, NY.

Quinn, P., Beven, K., Chevallier, P. and Planchon, O, 1993. The prediction of hillslope flow paths for distributed hydrological modelling using digital terrain models. In: Terrain analysis and distributed modelling in hydrology John Wiley & Sons, Chichester, 63-83.

Reid, I., Laronne, J.B., Powell, D.M. and Garcia, C., 1994. Flash floods in desert ephemeral rivers. EOS, American Geophysical Union Transaction, 75 (39): 452.

Reid, I., Laronne, J.B. and Powell M.D., 1998. Flash-flood and bedload dynamics of desert gravel-bed streams. *Hydrological Processes*, 12: 543-557.

Renard, K.J., 1969. Evaporation from an ephemeral streambed: discussion. *Journal of Hydraulics Division*, proceedings of the American Society of Civil Engineers, 95: 2200-2204.

Renard, K.J., 1970. *The hydrology of semiarid Rangeland watersheds*. U.S. Department of Agriculture. Research Service. Washington, Publ ARS: 41-162.

Renard, K.J., 1977. *Past, present and future water resources research in arid and semiarid areas in southwestern United States*. Hydrology Symposium, Institution of Engineers Australia, National conference Publ, 77 (5): 1-29.

Research Institute for Groundwater (RIGW), 1988. Hydrogeological map of Egypt, scale 1 2000,000, Cairo, Egypt.

Roberson, J.A. and Crowe, C.T., 1997. *Engineering Fluid Mechanics*. 6th ed. John Wiley, New York.

Roberts, M. C., 1978. Drainage density variations on the morainic landscapes of northeastern Indiana. *Zeitschrift für Geomorphologie*, 22: 462-471.

Rodriguez-Iturbe, I. and Valdes, J.B., 1979. The Geomorphologic Structure of Hydrologic Response. *Water Resources Research*, 15(6): 1409-1420.

Rostagno, C.M., Del valle, H.F. and Videla, L., 1991. The influence of shrubs on some Chemical and physical properties of an aridic soil in northeastern Patagonia, Argentina. Journal of Arid Environment, 20: 179-88.

Sabol, G.V. and Stevens, K.A., 1990. Comparison of design rainfall criteria for the Southwest. In *Hydraulics/ hydrology of aridlands (H^2AL)*, edited by French R H. American Society of Civil Engineers, 102-107.

Saleh, A.S., 1989. *Flash floods in deserts; a geomorphic study of desert wadis*. Institute of Arab Research, Special Studies Series, 51: 93, (in Arabic).

Schick, A.P., 1971. A desert flood: physical characteristics, effects on man: geomorphic significance, human adaptation. *Jerusalem Studies in Geography*, 2: 91-156.

Schick, A.P., 1974. Alluvial fans and desert roads - a problem in applied geomorphology. Abhandlungen der Akademie der Wissenschaften in Göttingen, Mathematische-Physikalische Klasse, 29: 418-425.

Schick, A.P., 1979. Fluvial processes and man in arid environments - applications to planning. *GeoJournal*, 3: 353-360.

Schick, A.P., 1988. Hydrologic aspects of floods in hyper-arid environments. In *Flood Geomorphology*, V.R. Baker, R.C. Kochel, P.C. Patton, editors, Wiley, New York, 12: 189-203.

Schick, A.P., 1995. Fluvial processes on an urbanizing alluvial fan: Eilat, Israel. In: *Natural and Anthropogenic Influences in Fluvial Geomorphology*, J.E. Costa *et al.*, eds., Geophysical Monograph (Am. Geoph. Union), 89: 209-219.

Schick, A.P., Grodek, T. and Lekach, J., 1997: Sediment management and flood protection of desert towns: effect of small catchments. In: Human Impact on Erosion and Sedimentation (Proc. Rabat Symp), *IAHS Publ.* 245: 183-189.

Schick, A.P. and Lekach, J., 1987. A high magnitude flood in the Sinai desert. In Mayer, L. and Nash, D.(Eds), *Catastrophic flooding*. Allen and Unwin, Winchester, 381-410.

Schick, A.P. Lekach, J. Hassan, M.A., 1987: Bedload transport in desert floods - observations in the Negev. In sediment transport in gravel-bed rivers, C.R. Thorne, J.C. Bathurst, R.D. Hey, editors, Wiley, Chichester, Ch. 20:617-642.

Schumm, S.A., 1956. Evolution of drainage systems and slopes in badlands at Perth Amboy, New Jersey. *Geological Society of America, Bulletin*, 67: 597-646.

SCS., 1985. *National Engineering Handbook.* Section 4, Hydrology, U.S. Department of Agriculture Soil Conservation Service.

Sharon, D., 1962. On the nature of hamadas in Israel. *Zeitschrift für geomorphologie*, 6: 129-147.

Sharon, D., 1972. The spottiness of rainfall in a desert area. *Journal of Hydrology*, 17: 161-175.

Sharon, D., 1974. The spatial pattern of convective rainfall in Sukumaland, Tanzania- a statistical analysis. *Arch. Meteor. Geophys. Bioklim*, 22 (13): 201-218.

Sharon, D., 1981. The distribution in space of local rainfall in the Namib Desert. *International Journal of Climatology*, 1: 69-75.

Sharon, D. and Kutiel, H., 1986. The distribution of rainfall intensity in Israel, its regional and seasonal variation and its climatological evaluation. *International Journalof Climatology*, 6: 277-291.

Smart, J.S., 1970b. Comment on dependence of stream link lengths and drainage areas on order, by Ghosh, A K and Scheidegger, A E. *Water Resources Research*, 6: 14-24.

Smith, D.J. and Stopp, P., 1978. *The river basin, an introduction to the study of hydrology*. Cambridge University Press.

Smith, J., Lin, T. and Ranson, K., 1980. The Lambertian Assumption and Landsat Data. *Photogrammetric Engineering and Remote Sensing*, 46 (9): 1183-1189.

Snyder, F.F., 1938. Synthetic unit hydrograph. EOS, *American Geophysical Union Transactions*, 19: 447-454.

Sorman, A.U, Abdulrazzak, M.J and Elhames, A.S., 1990. Rainfall-runoff modelling of a microcatchment in the western region of Saudi Arabia. Hydrology in Mountainous regions. 1 – Hydrological measurements; the Water cycle. *IAHS Publ*, 193: 655-659.

S-Plus software, version 4.5., 1998. Mathsoft Inc, Seattle, Washington

Stark, N., 1973. Nutrient cycling in a desert ecosystem. *Bulletin of the Ecological Society of America*, 54: 21-30.

Strahler, A.H. and Strahler, A.N., 1998. *Introducing Physical Geography*, 2nd ed, John Wiley & Sons.

Strahler, A.N., 1957. Quantitative analysis of watershed geomorphology. *American Geophysical Union Transaction*, 38: 913-920.

Strahler, A.N., 1958. Dimensional analysis applied to fluvially eroded landforms: *Bulletin of the Geological Society of America*, 69: 279-300.

Strahler, A.N., 1964. Quantitative geomorphology of drainage basins and channel networks. In: V.T.Chow (editor), *Handbook of applied hydrology*, McGraw-Hill, New York.

Story, M. and Congalton, R., 1986. Accuracy assessment: a user's perspective, *Photogrammetry Engineering of Remote Sensing*, 52 (3): 397-399.

Thome, K., Markham, B., Barker, J., Slater, P. and Biggar, S., 1997. Radiometric Calibration of Landsat. *Photogrammetric Engineering & Remote Sensing*, 63: 853-858.

Thornes, J.B., 1976. *Semi-arid erosional systems: Case studies from Spain.* London School of Economics, Geography Department. Paper, 7.

TR55., 1986. *Urban Hydrology for Small Watersheds.* Technical Report 55, U.S. Department of Agriculture Soil Conservation Service.

Tricart, J., and Cailleux, A., 1960. *Le modele des regions seches.* Paris: Le Cours de Sorbonne, Centre documentation universitaire.

Varnes, D.J., 1984. *Landslide hazard zonation: a review of principles and practice.* UNESCO, Paris.

Wang, X. and Yin, Z., 1998. A Comparison of Drainage Networks Derived from Digital Elevation Models at Two Scales. *Journal of Hydrology*; 210: 221-241.

Ward, R.C., 1975. *Principles of hydrology*. 2nd ed, McGraw-Hill.

Ward, R.C. and Robinson, M., 2000. *Principles of Hydrology*. 4th ed, McGraw-Hill.

Wentworth, C.K., 1922. A scale of grade and class terms for clastic sediments. *Journal of Geology*; 30: 377-392.

Yair, A., 1983. Hillslope hydrology, water harvesting and areal distribution of ancient agriculture fields in the northern Negev desert. *Journal of Arid Environments*; 6: 283-301.

Yair, A., 1987. Environmental effects of loess penetration into the northern Negev Desert. *Journal of Arid Environments*; 13: 9-24.

Yair, A., 1990. Runoff generation in a sandy area – the Nizzana sands, western Negev, Israel. *Earth Surface Processes and Landforms*; 15: 597-609.

Yair, A. and Lavee, H., 1976. Runoff generative process and runoff yield from arid talus mantled slopes. *Earth Surface Processes*; 1: 235-247.

Yair, A. and Lavee, H., 1985. Runoff generation in arid and semi-arid zones, in Hydrological forecasting. Edited by Anderson, M. G., and Burt, T. P., 220. John Wiley & Sons Ltd, Chapter 8, 182 .

Yair, A. and Shachak, M., 1987. Studies in watershed ecology of an arid area. In L. Berkofsky and M. G. Wurtele, eds. *Progress in Desert Research*. Rowman and Littlefield, Totawa, New Jersey; 145-193.

Yair, A., Sharon, D. and Lavee, H., 1980. Trends in runoff and erosion process over an arid limestone hillside, northern Negev, Israel. *Hydrological Science Bulletin*; 25 (3), 243-255.

Zeller, M.E., 1990. Precipitation on arid or semiarid regions of the southwestern United States: research needs from a consultant's perspective. In *Hydraulics/ hydrology of arid lands (H^2AL)*, edited by French, R H. The American Society of Civil Engineers, 525-529.